UNIVERSITY OF CALGARY

A methodology for studying tectonic subsidence variations: insights from the Fernie Formation of west-central Alberta

by

Tannis Maureen McCartney

A THESIS

SUBMITTED TO THE FACULTY OF GRADUATE STUDIES

IN PARTIAL FULFILMENT OF THE REQUIREMENTS FOR THE

DEGREE OF MASTER OF SCIENCE

DEPARTMENT OF GEOSCIENCE

CALGARY, ALBERTA

APRIL, 2012

UNIVERSITY OF
CALGARY

Abstract

Tectonic subsidence curves for over 300 subsurface wells in west-central Alberta indicate that the Western Canada Foreland Basin was initiated at the same time the lower units of the Fernie Formation were being deposited. This evidence is further supported by sedimentological data and fits with the timing of the onset of deformation in the Cordillera and the initiation of the foreland basin in Montana.

The volume of subsidence curves in this study required an innovative methodology. Subsidence calculations were performed using customized macros in a spreadsheet. The tectonic subsidence variations were displayed in a tectonic subsidence envelope, which showed the total variation in the subsidence curves, and three suites of maps: tectonic subsidence, tectonic subsidence residuals, and tectonic subsidence ratios. Collectively, the maps of the tectonic subsidence in the Fernie Formation show that there was a western influence on subsidence during deposition of the oldest members of the Fernie Formation.

Acknowledgements

There are so many people I want to thank for their support over the last two and a half years that it is almost impossible to know where to begin.

Thank you to my supervisor, Dr. Andrew Leier, for believing in me enough to let me take this project in a different direction than we'd originally planned. Thank you to the other professors in CABS (Centre for Applied Basin Studies) for their support and feedback over the years, especially Dr. Stephen Hubbard, Dr. Benoit Beauchamp, and Dr. Bernard Guest.

A huge thank you also goes to Dr. Terry Poulton, of the Geological Survey of Canada, for his feedback and support.

In my time as a graduate student at the University of Calgary, I have been incredibly lucky to have learned from Dr. Philip Simony and Dr. Ed Ghent—thank you both for your mentorship.

To my CABS colleagues, thank you for your support and discussions. In particular, thank you to Dallin Laycock for the Adobe tutorials, to Ross Kukulski and Julianne Fic for the brief but awesome time we spent together in the field, to Kevin Jackson and Erin Pemberton for all the feedback and moral support, and to Kate Zubin-Stathopoulos for teaching me so much, as my TA and in our "Beer and Tectonics Sessions." Ross, I cannot thank you enough for all of the additional help and discussions—I have learned a lot from you and you've been instrumental in helping me understand the Jurassic in west-central Alberta better.

In the last year or so I have become involved in the geoblogging and geotweeting community. I want to thank them for the support, suggestions, feedback, enthusiasm, and for the constant reminders that geology is really cool. #ThankYouGeoTweeps.

None of this would have been possible without the support of my family and friends—thank you for not telling me I was totally crazy to come back to school. In particular, I cannot thank Jennifer Unterschutz enough for the constant reminders that I was smart enough and strong enough to do this, even on the hardest days. And thank you for volunteering to read my thesis!

I was lucky enough to spend some time with friends overseas just before the final push to finish writing my thesis. Thank you to Janine and Ben, Annabel and Arend, Krista and Kris, Ailsa and Ray, Linda and Steve, the entire Woodley family, and Mick: the time I spent with you (and your families) was just what I needed.

To Andy Owens and Tony England: you are gone, but never forgotten. You believed in me, and gave me so much support while you were alive; I know you both would have been proud of me.

Last, but not least, thank you to the staff at the Last Defence Lounge, but especially Charley, for taking such good care of me at my other home. You kept me sane (and fed and watered).

Dedication

Toitū he whenua, whatungarongaro he tangata is a Maori proverb stating that man perishes, but the land remains. I dedicate this work to the people of New Zealand. It was in your land, in the raw landscapes of Aotearoa, that I became interested in geology. An earthquake in 1995 started me on this path. Over the last 18 months earthquakes have changed your country, and it nearly broke my heart because I wasn't prepared for how much so until I visited in late 2011.

Kia Kaha New Zealand

Table of Contents

List of Tables

List of Figures

List of Symbols, Abbreviations and Nomenclature

Symbol	Definition
b_1, b_2, b_3	Thickness of the crust in an Airy isostasy model
c	Compaction Coefficient
h_1, h_2, h_3	Topography in an Airy isostasy model
S*	Total decompacted thickness of entire sediment column
TeS	Tectonic subsidence
T_i	Decompacted thickness of sediment layer
Tn	Present Thickness
w	Water depth (paleobathymetry)
WCFB	Western Canada Foreland Basin
$y_{1,}$	Present top depth of layer
y_1	Top depth of the decompacted layer
$y_{2,}$	Present bottom depth of layer
y_2	Bottom depth of the decompacted layer
z	Amount of tectonic subsidence
ΔSL	Magnitude of sea level change
ρ_c	Density of crust
ρ_g	Density of entire sediment layer
ρ_m	Density of the mantle
ρ_s	Density of sediment grains within decompacted layer
ρ_{S*}	Density of entire sediment column
ρ_w	Density of water-filled pore space
ϕ	Porosity at depth
ϕ'	Decompacted porosity (at depth)
ϕ_0	Original porosity at deposition

Epigraph

No Geologist worth anything is permanently bound to a desk or laboratory, but the charming notion that true science can only be based on unbiased observation of nature in the raw is mythology. Creative work, in geology and anywhere else, is interaction and synthesis: half-baked ideas from a bar room, rocks in the field, chains of thought from lonely walks, numbers squeezed from rocks in a laboratory, numbers from a calculator riveted to a desk,... cheap equipment in the human cranium, arguments before a road cut.

Stephen Jay Gould, *An Urchin in the Storm*

Chapter One: **Introduction**

1.1 Western Canada Foreland Basin

The Western Canada Foreland Basin (WCFB) is part of a foreland basin system that extends more than 3000km from Texas to the Northwest Territories (Miall et al., 2009). The eastern portion of the WCFB, referred to as the Alberta Basin, is one of the three major depocenters in the Western Canada Sedimentary Basin (Figure 1-1); the other two depocenters are the Liard Basin in the north and the Williston Basin in the southeast. The WCFB extends west into the Cordillera, possibly as far as the western limit of the Western Canada Sedimentary Basin (Colpron and Price, 1995).

The WCFB is one of the most widely studied foreland basins in the world (Stockmal et al., 1992). The classic indicators of the initiation of the foreland basin (basin geometry, sedimentary facies, and provenance) suggest a Late Jurassic initiation of the WCFB (Poulton, 1989; Miall, 2009). The Upper Jurassic Green Beds are thought to contain the initial foredeep deposits (Poulton, 1989) although westerly-derived sediments have been found in the Middle Jurassic Pigeon Creek Member (Stronach, 1984). The youngest deposits in the foreland basin succession are those of the Palaeocene Paskapoo Formation, which makes up much of the bedrock immediately west of Calgary (Price and Monger, 2000).

The sediments of the foreland basin contain information about the Cordilleran orogenic system. A key to unravelling the evolution of the western margin of North America is to understand the evolution of the Cordillera; the initiation and evolution of the foreland basin are a record of this.

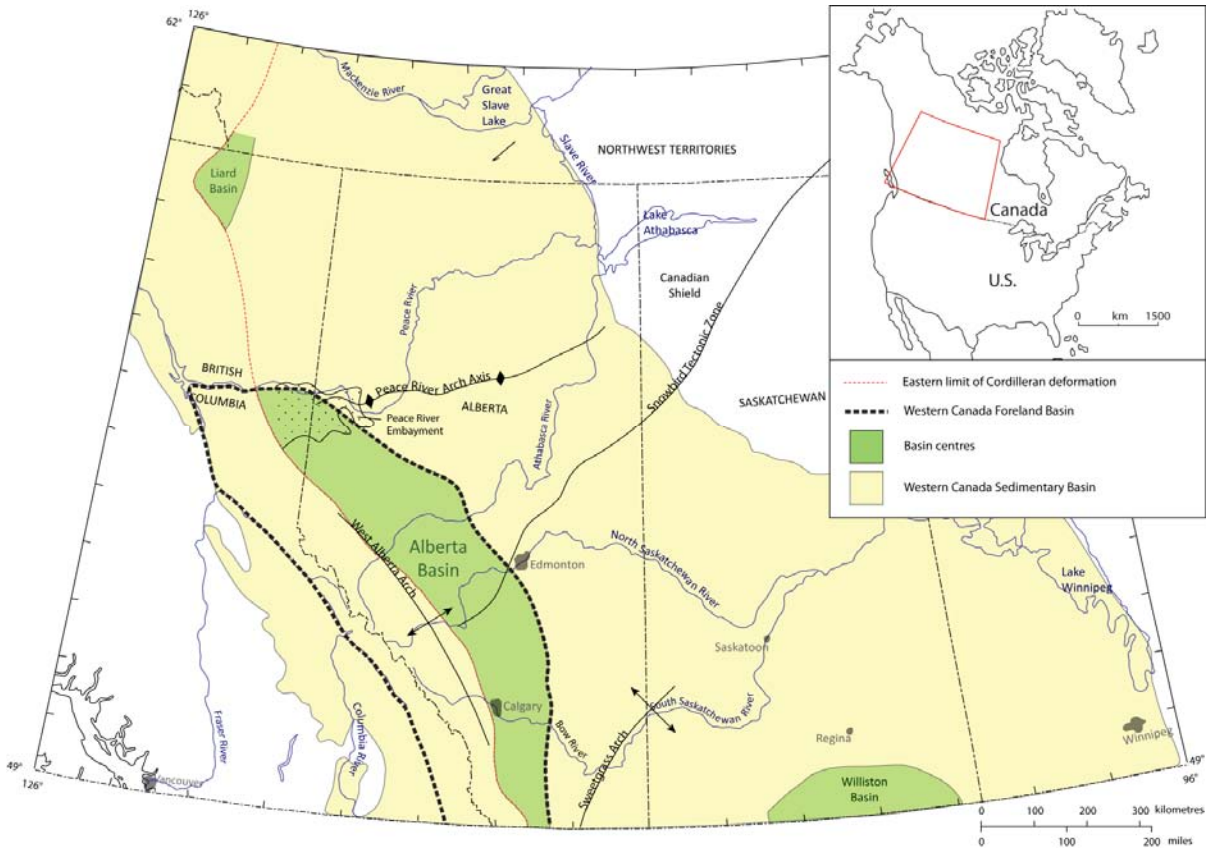

Figure 1-1: The Western Canada Sedimentary Basin

Map of the Western Canada Sedimentary Basin (modified from Wright et al., 1994). The eastern extent of the Western Canada Foreland Basin is based on the boundary of the Foreland Belt (Gabrielse et al., 1991)**.**

1.2 Timing Problem

There are two timing issues related to the current model for the initiation of the WCFB that are not satisfactorily resolved (Figure 1-2). The first is the large discrepancy in timing between initiation of the Cordilleran Orogeny and initiation of the foreland basin. The deformation that would ultimately result in the uplift of the Canadian Cordillera began with the development of an arc-trench system along the western margin of North America (Dickinson, 2004; Price and Monger, 2000). There is an approximately thirty million year gap between the onset of deformation in the Cordillera and the initiation of the WCFB.

The second timing discrepancy is between the initiations of the foreland basins throughout western North America. Published studies suggest upwards of a twenty million year difference between the initiation of the foreland basins in southwestern Canada and the northern United States. Gillespie & Heller (1995) used subsidence analysis to constrain the timing of the initiation of the foreland basin in Alberta ca. 150-145Ma and in Montana to ca. 100 Ma. A more recent study proposed a narrower time window between the initiation of the two foreland basins, with initiation in Montana occurring approximately 170 Ma (Fuentes et al., 2009). This interpretation proposed that the initial deposits of the foreland basin are preserved in the backbulge depozone, which is characterized by moderate subsidence changes and isopachs which show thinning toward both the forebulge and the craton. At the same time this study was published, there was a call for similar studies to be done in Canada (Miall, 2009).

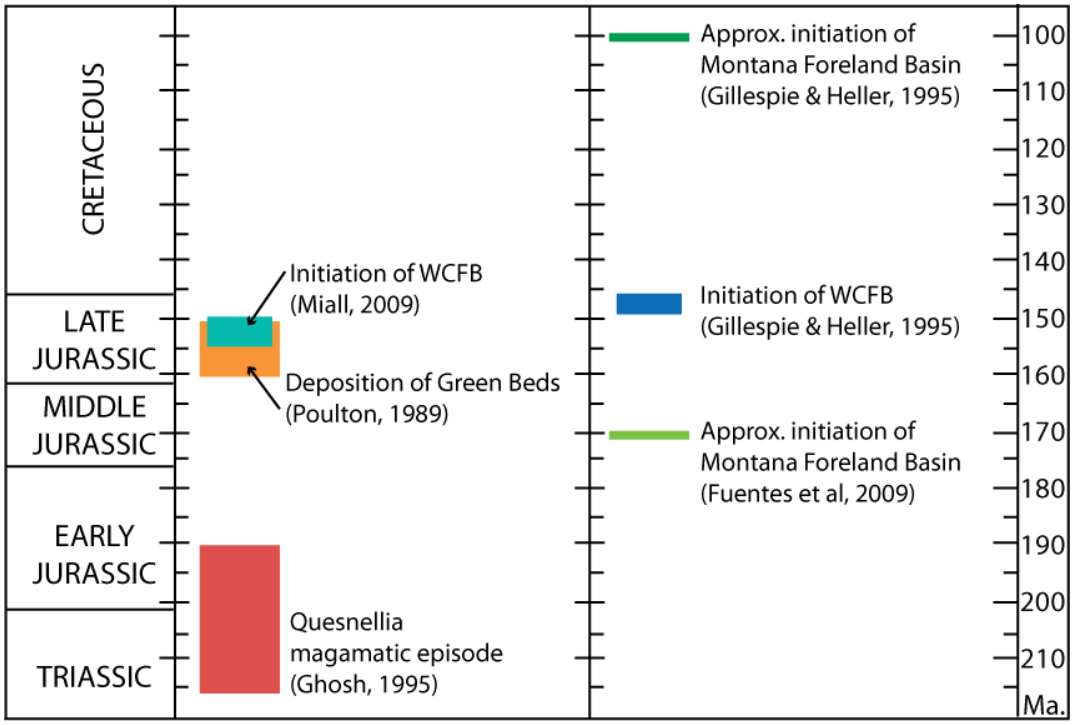

Figure 1-2: Chronological chart of timing discrepancies

The initiation of the Western Canada Foreland Basin with respect to Cordilleran Deformation is shown on the left and with respect to the initiation of the Montana Foreland Basin on the right. Both Miall (2009) and Poulton (1989) use the arrival of westerly-derived sediments as an indication of the initiation of the foreland basin. On the right, the nearly 50 million year difference in timing of the initiation of the foreland basins in Montana and Western Canada (according to Gillespie and Heller, 1995) is seen between the dark green and blue bars. Note that when the criteria for defining the initiation of the foreland basin changes, the resulting change in timing of initiation can be as much as 100 million years, as is the case when comparing the dates given by Gillespie and Heller (1995) and Fuentes et al (2009).

1.3 Preliminary Work

This study began with the generation of subsidence curves along the axis of the WCFB to tie to the subsidence studies in the western United States. The preliminary subsidence curves showed characteristics of an early Jurassic initiation of the foreland basin but they also revealed a new direction for the study. The profiles of the initial subsidence curves varies considerably, particularly related to the sub-Cretaceous unconformity (Figure 1-3).

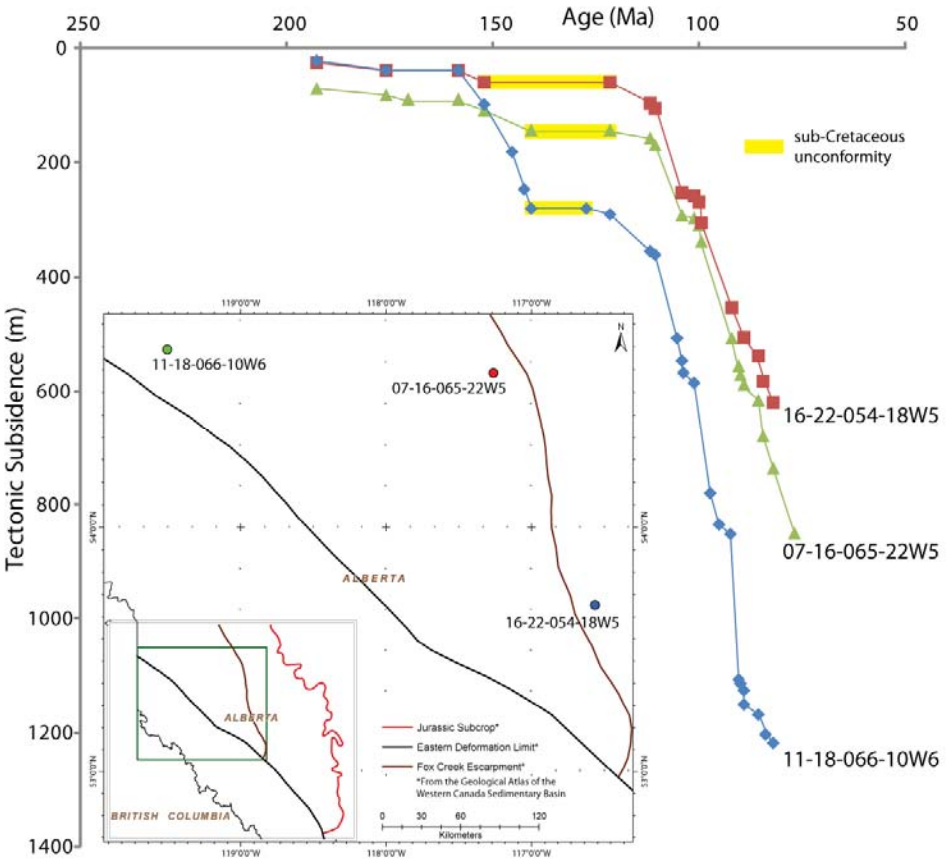

Figure 1-3: Initial subsidence curves in the study area

Three tectonic subsidence curves from subsurface wells in west-central Alberta which show the variation in tectonic subsidence within the Western Canada Foreland Basin.

1.4 Objectives

This study investigates two problems: the lack of subsidence analysis throughout the WCFB to tie with similar studies in the western United States, and the variation of tectonic subsidence profiles within the basin. These problems will be addressed by answering four questions:

1. How much does tectonic subsidence vary within the Jurassic of the WCFB?
2. How can these tectonic subsidence variations be displayed?
3. What can these tectonic subsidence variations tell us about regional and local tectonics?
4. What evidence is there for Early Jurassic initiation of the WCFB?

1.5 Study Area

The study area is in west-central Alberta, covering the central portion of the WCFB (Figure 1-4). It is between 51.5° and 55° north, and 114° and 120° west; bounded to the north by the southern limits of the Peace River Arch/Embayment, to the east and south by the Jurassic subcrop edge and to the west by the edge of the fold-thrust belt (Wright et al., 1994).

Over 300 subsurface wells were included in the study; the portion of the foreland basin extending into the fold-thrust belt has not been included because overthickening in faulted strata are difficult to identify in well logs and even more difficult to account for in subsidence calculations. Closer to the Jurassic subcrop edge, there are fewer wells that penetrate the entire Fernie Formation; in many of those wells that do penetrate deep enough, so much of the Fernie Formation has been removed by erosion that it is difficult

to determine which part of the Fernie Formation remains; these limitations are the reason for the change in density of well coverage from west to east.

The strata being studied are in the Fernie Formation; the base of the formation is the sub-Jurassic unconformity and the top of the succession is the top of the Upper Fernie shales. In the west these are overlain by the Nikanassin Formation or the Minnes Group. In the east they are truncated by the sub-Cretaceous unconformity.

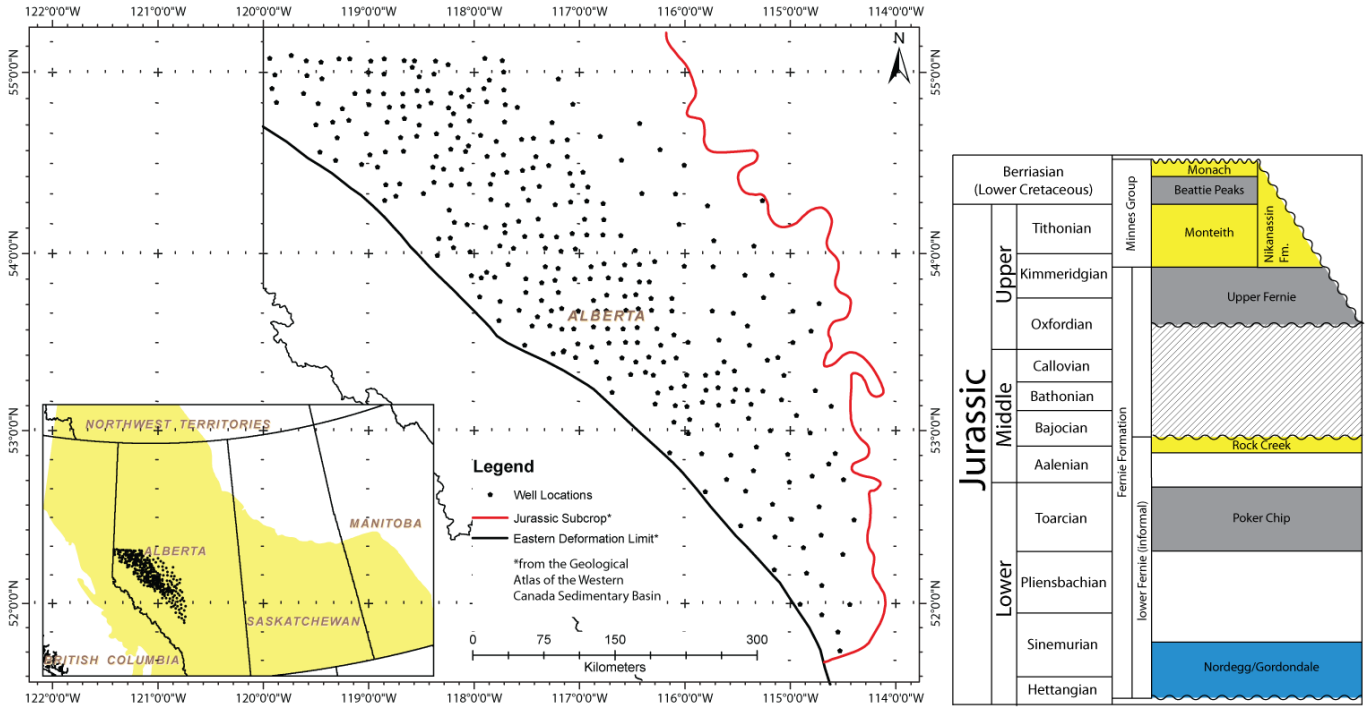

Figure 1-4*:* Study area in west-central Alberta and stratigraphic chart of study interval

The locations of over 300 wells used for subsidence analysis are shown *on the map*. Information for the analysis came from well logs. The Eastern deformation limit, Jurassic subcrop and Fox Creek Escarpment are modified from the Geological Atlas of the Western Canada Sedimentary Basin (Price, 1994). The stratigraphic chart of the Fernie Formation and the members identified in this study is based on an industry stratigraphic chart (Core Laboratories Geological Sciences Department).

Chapter Two: **Background**

2.1 Foreland Basin

Retroarc foreland basins (Figure 2-1) form during the collision of oceanic and continental lithosphere; additional flexure in these basins is caused by dynamic subsidence of the subducting slab (Beaumont, 1981). Peripheral foreland basins (Figure 2-1) form during continent-continent collisions with additional flexure coming from subduction loads (*ibid.*). While some authors claim there is nothing preserved in the basin sediments to classify the foreland basin as retroarc or peripheral (Dickinson, 1974), others suggest that the stratigraphy and subsidence histories of foreland basins forming on the overriding lithosphere of continent-continent and continent-oceanic lithosphere collisions may differ (Naylor and Sinclair, 2008). Recent work suggests that the subsidence rates within the foreland basins may be critical to differentiating the type of foreland basin from the sedimentary record (Sinclair and Naylor, 2011). The WCFB is a retroarc foreland basin.

In order to describe overall deformation in the southern Canadian Rockies, Price defined the foredeep trough in Western Canada as an “isostatically induced peripheral depression that developed in response to the load imposed on the lithosphere by the northeasterly flow of supracrustal rocks up on to the flank of the craton” (Price, 1973, p498).

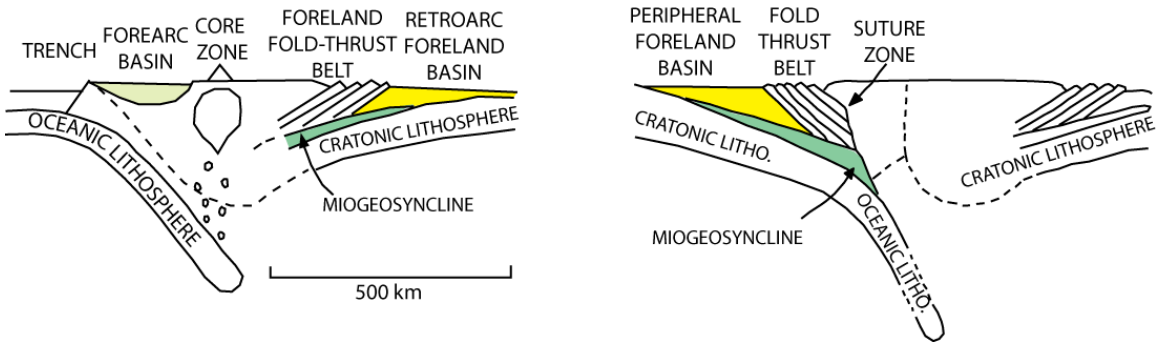

Figure 2-1: The two principal styles of foreland basin

Retroarc foreland basins (left) develop on the overriding slab at a subduction zone. Peripheral foreland basins (right) form on the downgoing slab during a continental collision (modified from Beaumont, 1981).

According to Beaumont (1981), the mechanism that forms foreland basins is the downward flexure of the lithosphere that is a result of passive loading during formation of a fold-thrust belt.

The wedge-shaped foreland basin is coupled with the adjacent fold-thrust belt and advances cratonward with it (Figure 2-2; Beaumont, 1981; Price, 1973). Leckie and Smith (1992) divide the wedge into five components (Figure 2-3). This model describes the zones of the foreland basin in terms of subsidence and sedimentation rates, recognizing that both decreased away from the orogen. Here, the maximum water depth in the WCFB is estimated to be 200-300m.

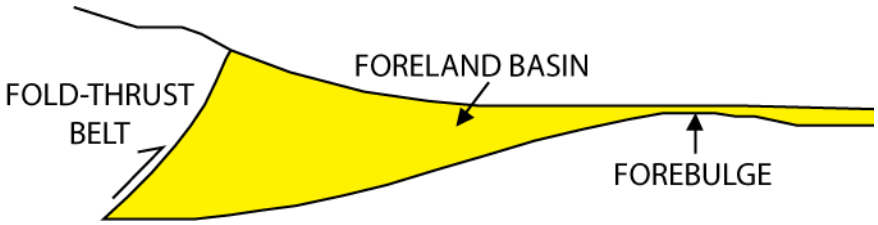

Figure 2-2: Wedge-shaped foreland basin

The foreland basin of classic models advances cratonward in front of the advancing fold-thrust belt (modified from DeCelles and Giles, 1996)

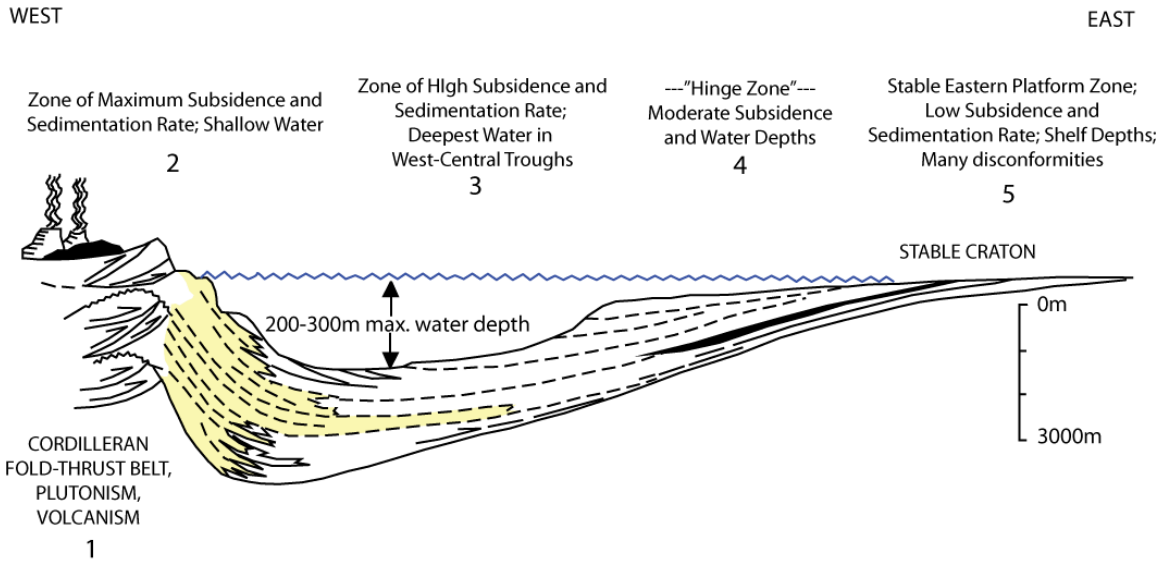

Figure 2-3: Five components of a foreland basin

The five zones of a foreland basin, with subsidence and sedimentation rate decreasing away from the fold-thrust belt (modified from Leckie and Smith, 1992).

More recently, DeCelles and Giles (1996) described a system consisting of four depozones: the wedge-top, foredeep, forebulge, and backbulge (Figure 2-4**)**. The wedge-top depozone, which sits on top of the edge of the thrust belt, has not been included in

previously published models of a foreland basin. In the case of the WCFB, the post-orogenic erosion that shaped the front ranges (Osborn et al., 2006) likely removed any remnants of the wedge-top depozone. The foredeep depozone is the "wedge" of previous authors (Price, 1973; Beaumont, 1981; Leckie and Smith, 1992). The forebulge depozone is a region of uplift caused by lithospheric flexure. The forebulge may be represented in the stratigraphic record by unconformities, particularly in the early stages of foreland basin development (Crampton and Allen, 1995). Sediments that accumulate between the forebulge and the craton are in the backbulge depozone. The backbulge deposits are a small component of the overall foreland basin, but they are critical to understanding its initiation (Sinclair and Naylor, 2011).

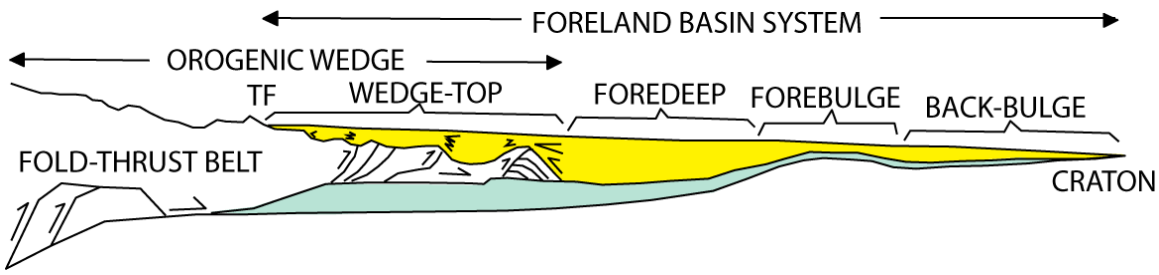

Figure 2-4: Four depozones of a foreland basin system

In this model, the orogenic wedge and the foreland basin overlap. The entire foreland basin system advances cratonward in front of the advancing fold-thrust belt (modified from DeCelles and Giles, 1996).

In both the wedge-shaped model and the foreland basin system model, subduction (and the associated plutonism, volcanism, and crustal shortening) is the major source of tectonic loading that leads to subsidence in the basin (Leckie and Smith, 1992). Foreland basins are "dynamic sedimentary systems that evolve in response to the interplay and

growth of the adjacent thrust-and-fold belt, climate, surface processes, properties of the underlying flexed lithosphere, and large-scale tectonic boundary conditions" (Ross et al., 2005, p748).

Traditionally the initiation of a foreland basin is defined using a combination of the following: the first appearance of orogen-derived sediments (Poulton, 1989; Leckie and Smith, 1992; Miall, 2009), the base of a flysch and molasse succession (Figure 2-5; Beaumont, 1981), and the development of narrow basin fill parallel to the axis of the thrust belt (Jordan, 1981).

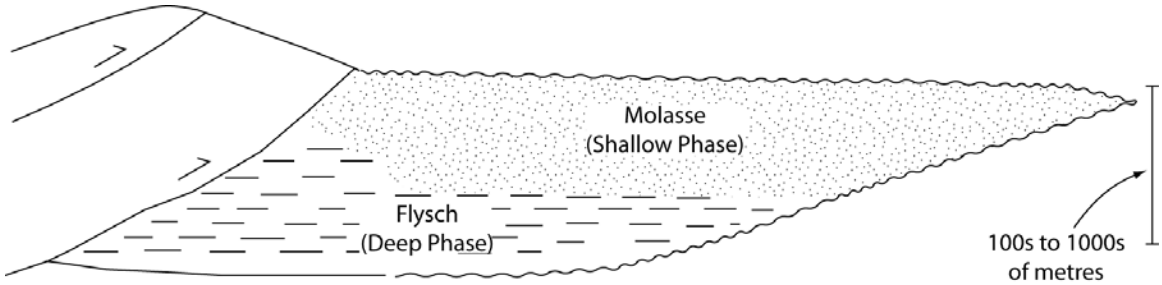

Figure 2-5: A flysch-molasse sequence in a foreland basin

A typical foreland basin is unconformity bounded and is filled by a coarsening- and shallowing-upward sequence (modified from Stockmal et al., 1992)

2.2 Subsidence Analysis

The primary controls on basin subsidence are deposition and erosion, local and/or global sea level fluctuations, changes in crustal thickness, and lithospheric flexure (Pigott and Sattayarak, 1993).

Tectonic subsidence measures the tectonically controlled vertical movement of a basin. As sediment begins accumulating, the weight of it pushes the basin down.

Continued sediment accumulation causes compaction of the earliest deposited sediments and results in significant downward movement of the base (Figure 2-6**)**. Tectonic subsidence analysis involves decompaction calculations that remove the effects of compaction and sediment loading, followed by backstripping calculations that calculate the vertical movement of the basin as if it were water-filled not sediment-filled (Xie and Heller, 2009). This step determines how much of the vertical movement of the basin is due to tectonics. Decompaction and backstripping will be discussed in more detail in subsequent sections; the full derivations of the equations are in Appendix A.

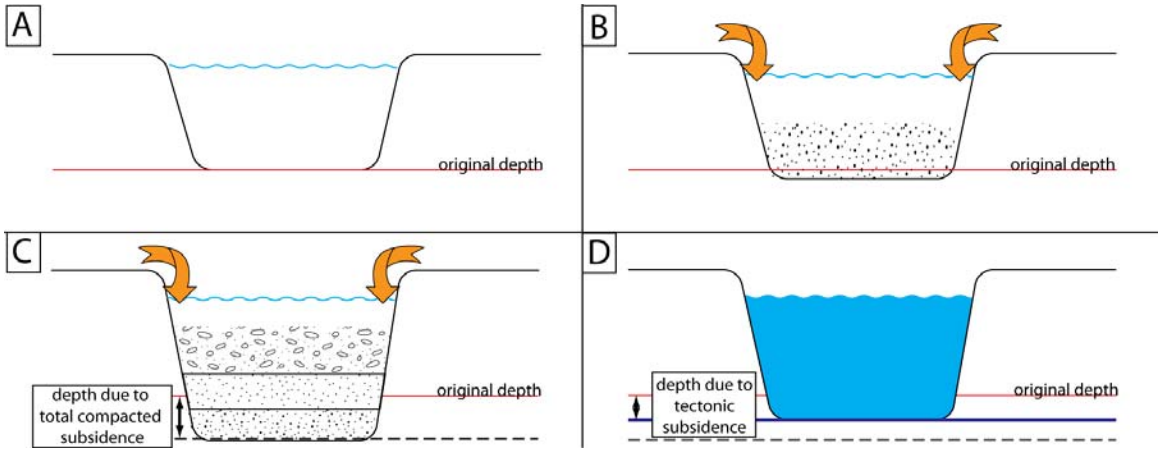

Figure 2-6: Vertical movement of a basin due to tectonic subsidence

(A**) Basin at its original depth. (B) Sediment begins accumulating in the basin, pushing it down below its original depth. (C) As the basin fills, the sediments are compacted and the basin continues to drop. (D) A water-filled basin does not subside as much as a sediment-filled basin; the primary mechanism for this difference is tectonics.**

In basin analysis, tectonic subsidence plotted on a depth vs. age chart is used to classify the type of basin the sediments were deposited in. Basins from different times

and geographic locations, but with similar tectonic controls, have been shown to have similarly shaped subsidence curves (Figure 2-7**;** Angevine et al., 1990; Xie and Heller, 2009).

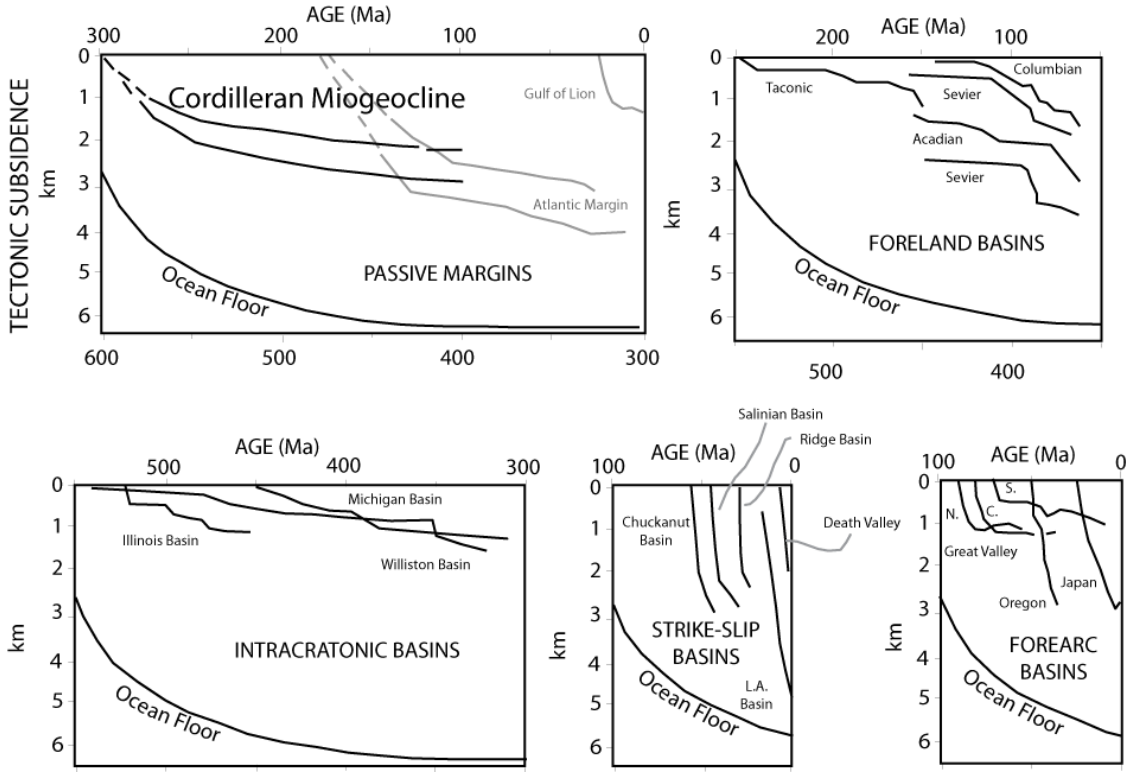

Figure 2-7: Basins around the world classified according to subsidence profile (from Angevine et al., 1990)

A foreland basin has a blocky, concave-down subsidence curve (Figure 2-9**)** with a low initial rate of subsidence followed by a rapid increase in subsidence (Angevine et al., 1990; Xie and Heller, 2009). Unconformities are typically shown as horizontal lines (or in some cases, gaps in the line between two points with the same depth).

Because the foreland basin migrates cratonward with the advancing orogen, a Walther's Law-type relationship between the depozones of the foreland basin system can

be expected (Figure 2-8**).** The most distal, or backbulge, deposits are expected to have low subsidence rates. Sediment accumulation in the foredeep is rapid, represented by the steepest gradient on a subsidence curve (Figure 2-9). Because of the Walther's Law-type relationship, the depozones represented on a subsidence curve reflect a vertical succession, not a synchronous, lateral one.

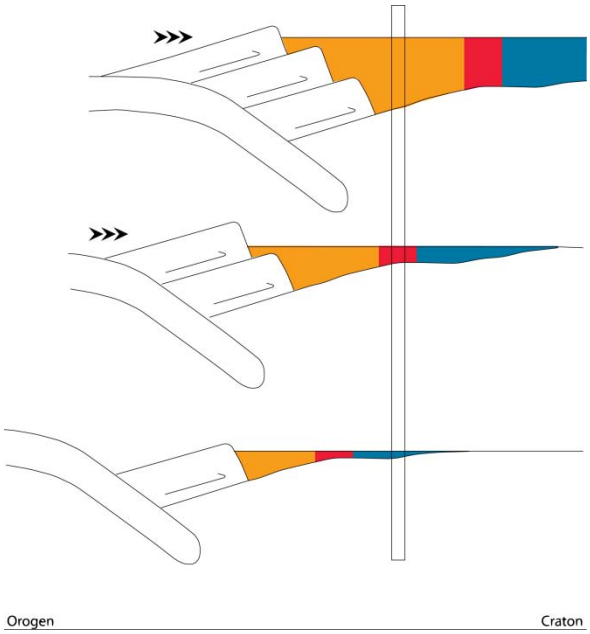

Figure 2-8: Walther's Law-type relationship in a foreland basin

At a single point in the basin, a vertical section (rectangle) will contain a sequence of deposits from a backbulge (blue), a younger forebulge (red), and an even younger foredeep (yellow).

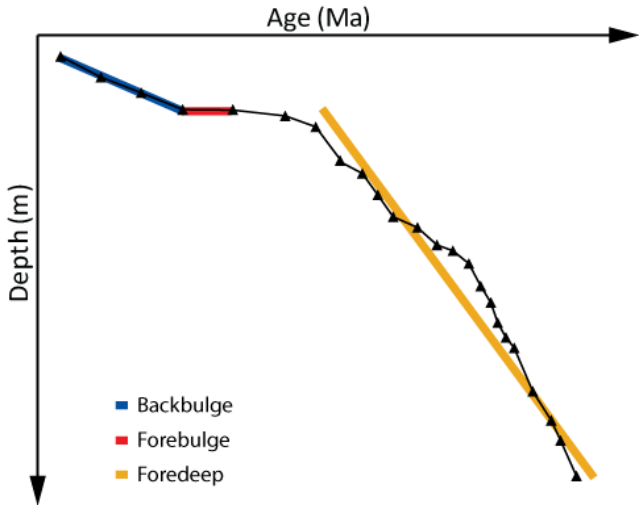

Figure 2-9: Generalized foreland basin subsidence curve.

The low rate of subsidence (blue) is found in the backbulge. The unconformity (red) signifies passage of the forebulge through the region. The steeply dipping segment of the curve (yellow) shows the rapid subsidence of a foredeep.

2.2.1 Airy Isostasy

In Airy compensation, (Figure 2-10**),** the thickness of the crust above a depth of compensation vary to balance changes in topography (Allen and Allen, 2005). Balancing layers of different densities above a depth of compensation is the foundation of the backstripping calculations (Angevine et al., 1990).

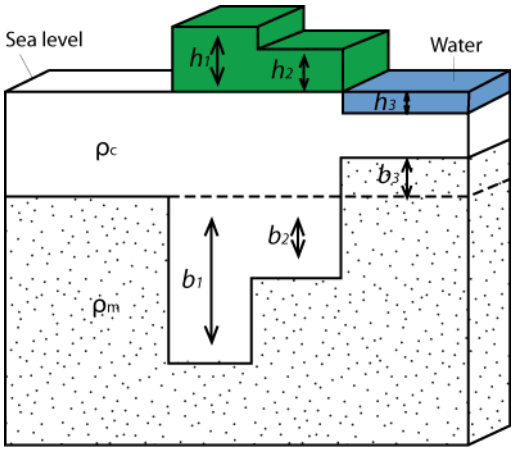

Figure 2-10: Airy isostasy

The thickness of the crust (b_1, b_2, b_3) compensates for the changing topography (h_1, h_2, h_3). The densities of the crust (ρ_c) and mantle (ρ_m) do not change (modified from Allen and Allen, 2005).

In reality the lithosphere acts as an elastic beam and its response to loading is controlled by the rheology and density of both the load and the lithosphere as well as the position and time of the loads (Beaumont, 1981). The geometry of the basin is controlled by the rigidity of the lithosphere (Angevine et al., 1990). Flexural backstripping, which assumes regional rather than local isostasy, is possible but difficult because the rheology of the crust, specifically its flexural rigidity, must be known for the calculations (Allen and Allen, 2005).

2.2.2 Decompaction

The purpose of decompaction is to find the total thickness of the unit before it was compacted by sediment burial. In order to estimate the amount of compaction, it is necessary to assume that sediment compaction is only caused by sediment loading and the subsequent closure of the pore spaces (Sclater and Christie, 1980). This requires that the volume of sediment grains in the layer does not change. The implications of this, and other assumptions, will be discussed in Chapter 4. A second assumption required for decompaction is that the porosity decreases exponentially with depth according to the following relationship:

$$\boldsymbol{\phi = \phi_0 e^{-cy}} \qquad \textbf{Equation 1}$$

where ϕ is the porosity at depth, ϕ_0 is the original porosity of the layer when it was deposited, *c* is the compaction coefficient, and *y* is the depth. The relationship in Equation 1, and the values commonly used for compaction coefficient and original porosity, are an estimated "best fit" from a compilation of subsurface data (Allen and Allen, 2005).

Compaction cannot be measured directly because the original volume of the sediments is not known (Athy, 1930). Because we assume that all changes in pore space are caused by compaction, we can estimate the amount of compaction from the porosity.

Porosity-depth functions can be generated using downhole porosity measurements but this should be done with caution as multiple sources of porosity values should not be mixed to create a single curve (Giles et al., 1998). The effectiveness of the porosity-depth relationship depends on the depth of the sedimentary unit—for depths up to 10km it is generally considered effective (Giles et al., 1998).

The decompaction equation (Equation 2; derived in Appendix A) is derived from the porosity-depth relationship:

Equation 2

$$\boldsymbol{y_2' - y_1' = y_2 - y_1 - \frac{\phi_0}{c}\{\exp(-cy_1) - \exp(-cy_2)\} + \frac{\phi_0}{c}\{\exp(-cy_1') + \exp(-cy_2')\}}$$

where $y_2'$and y_1' are the bottom and top depths of the decompacted layer, and y_2 and y_1 are the present bottom and top depths of the layer. Because y_2' and y_1' appear on both sides of the equation, Equation 2 must be solved iteratively.

2.2.3 Backstripping

Backstripping calculates the amount of basin subsidence that is driven by tectonics. Assuming Airy isostasy, the decompacted sediment is balanced with a water-filled column of the same height. In order to calculate the amount of tectonic subsidence the basin has undergone, the porosity and bulk density of each decompacted layer must be calculated for each time interval in the sediment column.

The decompacted porosity, ϕ', of a sediment layer is given by Equation 3:

$$\boldsymbol{\phi' = \frac{\phi_0}{c}\frac{\left(exp(-cy_1') - exp(-cy_2')\right)}{y_2' - y_1'}} \qquad \textbf{Equation 3}$$

The density of the sediment grains within the decompacted layer, ρ_s, is calculated using Equation 4 and assuming that the pore space is water-filled:

$$\boldsymbol{\rho_s = \phi'\rho_w + (1 - \phi')\rho_g} \qquad \textbf{Equation 4}$$

where ρ_w is the density of the water-filled pore space and ρ_g is the density of the entire layer.

The density of the sediment column, ρ_{S^*}, is calculated by multiplying the density of each layer by the ratio of that layer's thickness to the total column thickness, as in Equation 5:

$$\boldsymbol{\rho_{s^*} = \frac{\sum_1^i \{\rho_s T_i\}}{S^*}} \qquad \textbf{Equation 5}$$

where T_i is the decompacted thickness of each layer and S^* is the total decompacted thickness of the sediment column.

When the paleobathymetry and magnitude of sea level changes for each layer are known, the amount of tectonic subsidence, z, is calculated using Equation 6 (Angevine et al., 1990):

$$\boldsymbol{z = S^* \left(\frac{\rho_m - \rho_s}{\rho_m - \rho_w}\right) + w - \Delta SL\left(\frac{\rho_m}{\rho_m - \rho_w}\right)} \qquad \textbf{Equation 6}$$

where w is the water depth, $\Delta SL$is the magnitude of the sea level change and ρ_m is the density of the mantle. When paleobathymetry and sea level changes are not known, these two terms are omitted from the tectonic subsidence calculations; they are accounted for in the error estimates instead. The derivations of equations 2, 3, 4, 5 and 6 can be found in Appendix A.

2.3 Geological Framework

2.3.1 Western margin of North America

The evolution of the western margin of North America, although complex, can be summarized in four phases (Figure 2-11**)**. The margin was established with the breakup of Rodinia in the Neoproterozoic (Dickinson, 1976; Dickinson, 2009). Rifting in the Triassic, associated with the breakup of Pangea, brought about an end to approximately

500 million years of passive margin sedimentation that were punctuated by deposits associated with active tectonism along the western margin of North America (Colpron and Price, 1995; Root, 2001; Zubin-Stathopoulos, 2011). The Cordilleran Orogeny, which persisted through most of the Mesozoic and into the early Cenozoic, was a result of the establishment of an arc-trench system (Dickinson, 2004). Finally, the overall regime changed from compressional to extensional, with strike-slip faults developing along the margin in the mid-Cenozoic (Dickinson, 2004; Price and Monger, 2000).

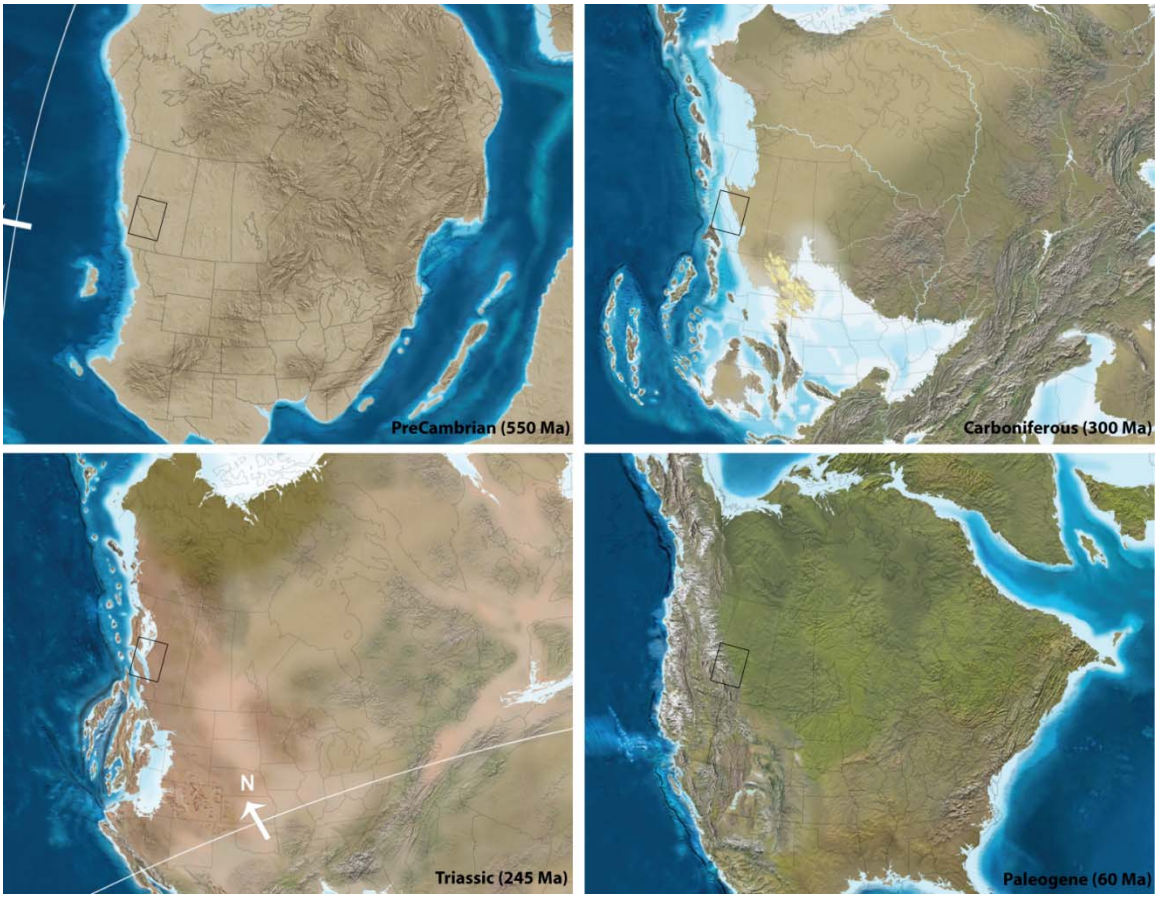

Figure 2-11: Paleogeography of the western margin of North America

North America in the Precambrian (top left), following the breakup of Rodinia. During the Palaeozoic (top right), sedimentary strata were deposited on the "passive" margin. The arc-trench system developed in the Early Mesozoic (bottom left). During the Palaeocene (bottom right) a large part of the margin became extensional.. The black rectangle on all maps is the study area (maps by Ron Blakey, Colorado Plateau Geosystems, Inc).

2.3.2 Cordilleran Tectonics

The Canadian Cordillera has been divided into five longitudinal geomorphological belts (Figure 2-12) which provide a useful framework for understanding the evolution of the Cordillera (Price and Monger, 2000). Of particular interest to this study are the Omineca and Intermontane Belts, where the earliest deformation took place, and where the pericratonic terranes are preserved (Figure 2-13).

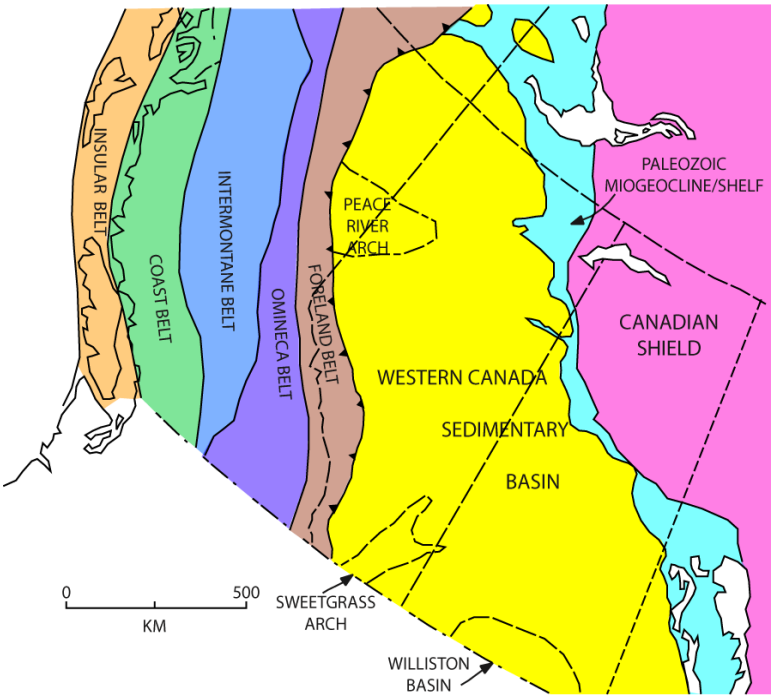

Figure 2-12: Geomorphological belts of the Canadian Cordillera

From east to west, the belts are: Foreland Belt, Omineca Belt, Intermontane Belt, Coast Belt, and Insular Belt. The Western Canada Foreland Basin includes both the westernmost portion of the Western Canada Sedimentary Basin and the Foreland Belt (modified from Stockmal et al., 1992).

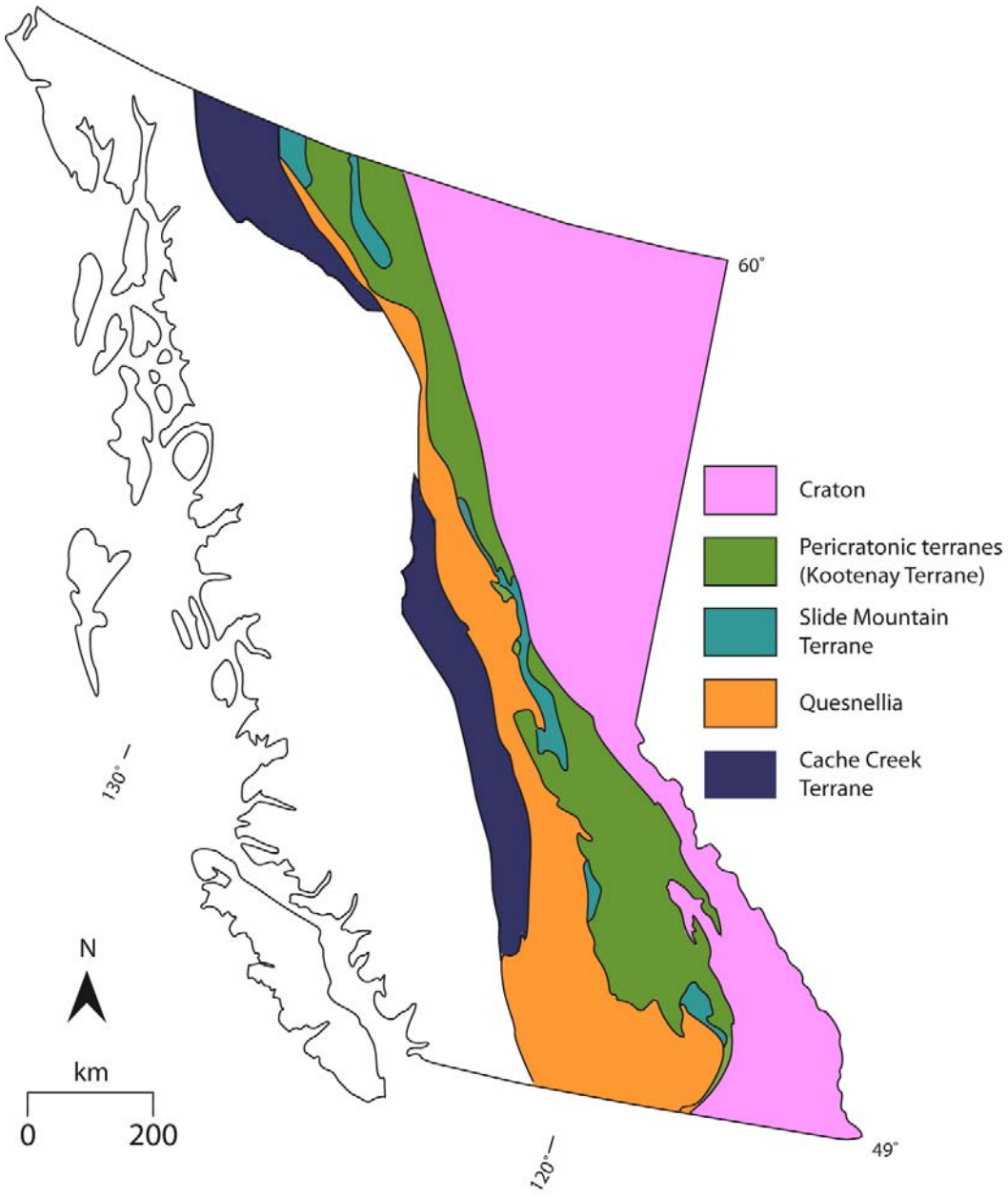

Figure 2-13: Pericratonic terranes in the Canadian Cordillera

These terranes record the earliest deformation in the Canadian Cordillera. There is evidence that these terranes have a North American affinity and were close enough to the craton when they were being deformed to create a flexural response (modified from Petersen et al., 2004).

The terranes are the building block of the Cordillera, and their relationship to ancestral North American crust is fundamental to establishing the timing of the initiation of the foreland basin. Many of the terranes, particularly the Intermontane terranes, are the remnants of magmatic arcs (Monger and Price, 2002).

The magmatic episode in Quesnellia occurred from 215-290 Ma as part of a continuous arc along the entire margin of North America (Ghosh, 1995; Höy and Dunne, 1998). While the exact timing of the amalgamation of terranes is still debated, there is a consensus that all of the Intermontane terranes had docked with North America by Mid-Jurassic at the latest (Ghosh, 1995; Murphy et al., 1995; Dickinson, 2009; Ricketts, 2009). The amalgamation process likely began in the Late Triassic (Dickinson, 2004; Ricketts, 2009).

Cordilleran-wide deformation occurred from Early to Mid-Jurassic, as a result of the crustal shortening caused by the terrane amalgamation. By Late Jurassic the fold-thrust belt was well established (Murphy et al., 1995; Colpron et al., 1998; Dickinson, 2004).

It is critical to this study to note that although the pericratonic terranes may have been offboard initially, they did have a North American affinity throughout the Mesozoic, and were likely formed on the distal edge of the craton (Höy and Dunne, 1998). The Lardeau Group of the Kootenay terrane has been shown to be deposited conformably with the underlying miogeocline (Colpron and Price, 1995). The composition of the sedimentary Quesnellian rocks in southern British Columbia and their geochemical signatures suggests that the arc was proximal to North America in the Triassic (Unterschutz et al., 2002).

2.3.3 Major structural features in west-central Alberta

The basement beneath the Western Canada Sedimentary Basin is an extension of the Precambrian Shield (Ross et al., 1994). Despite the thick sedimentary cover over it, geophysical investigations have been used to map the structure of the basement (*ibid*.). A relationship between basement structure and subsidence and facies patterns has been inferred (Ross, 1989 and references therein).

2.3.3.1 Snowbird Tectonic Zone

In the study area, the most significant tectonic domain is the Snowbird Tectonic Zone (Figure 2-14). The Snowbird Tectonic Zone is one of the largest, yet least-understood, blocks of Archean crust in existence (Jones et al., 2002). It has been interpreted as an intercontinental suture (Mahan and Williams, 2005 and references therein), intracontinental fault (*ibid.*), intracontinental strike-slip shear zone (*ibid.*), or an intracontinental rift within an older orogenic zone (Berman et al., 2007 and references therein). More recent interpretations suggest it contains lozenges that were part of a highly metamorphosed terrane within the Rae Domain (Mahan and Williams, 2005) or an early phase of the Hudsonian orogeny (Berman et al., 2007). Its origins remain enigmatic, but it is clear is that the Snowbird Tectonic Zone was involved in the major Paleoproterozoic tectonic events in what is now Western Canada (Jones et al., 2002). Furthermore, the Bouguer gravity anomaly associated with it coincides with the Devonian Rimbey-Leduc-Meadowbrook chain of reefs (Edwards et al., 1999).

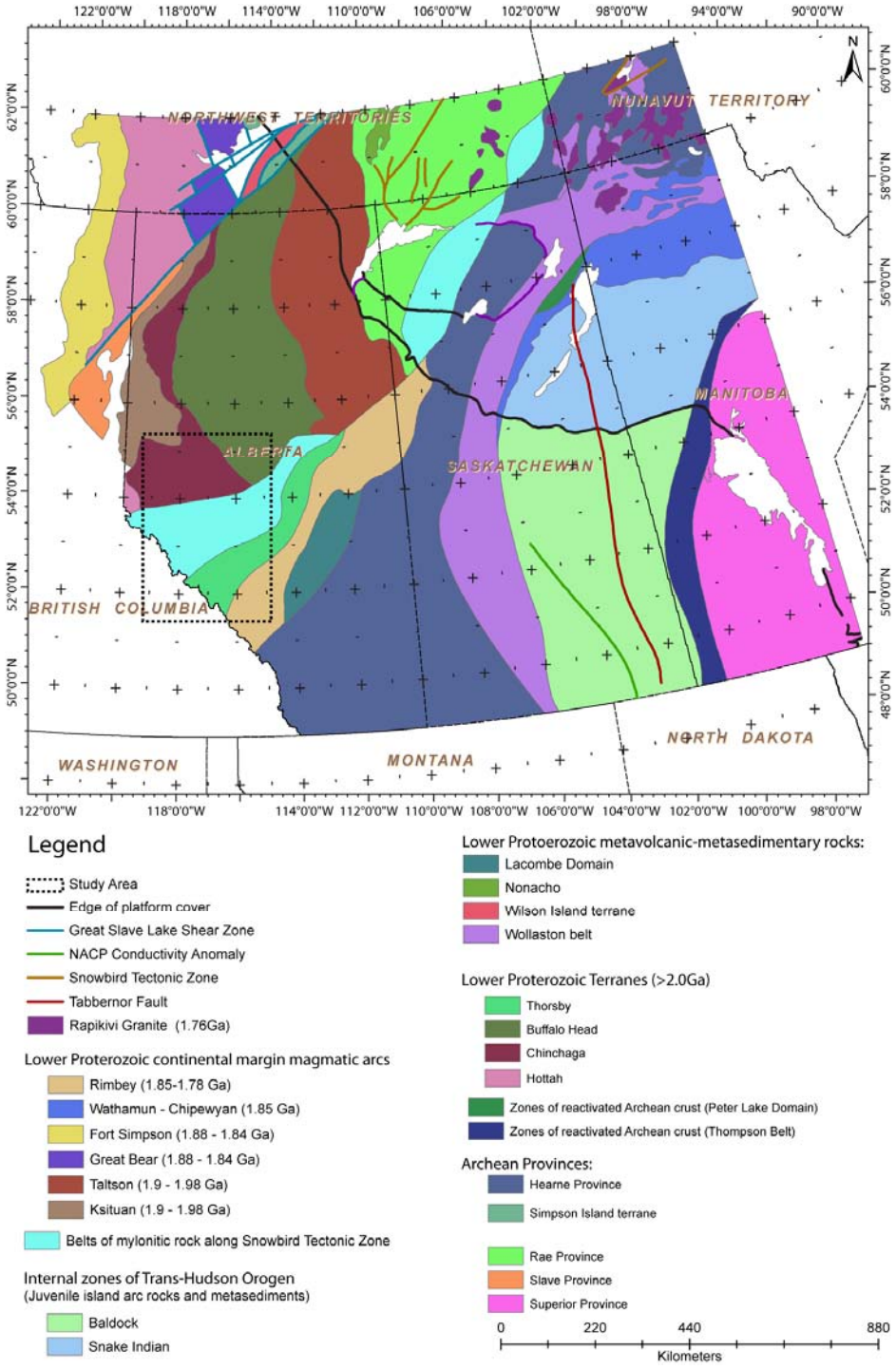

Figure 2-14: Basement domains of the Western Canada Sedimentary Basin Tectonic domains interpreted from potential field data and U-Pb geochronology of the basement (modified from Ross et al., 1994).

2.3.3.2 Fox Creek Escarpment

The southern end of the Fox Creek Escarpment runs approximately north-south through the study area (Figure 2-15). This escarpment formed the eastern boundary of the axial-flowing Spirit River Channel during the Cretaceous (McLean, 1977). In the Early Cretaceous, it was a high-relief feature that exposed the Jurassic sediments to erosion (Tittemore, 1991). There is an approximately 30-40, rise in pre-Cadomin relief that corresponds to the Fox Creek Escarpment (Losert, 1986). Its origin is not well studied, however north of the study area it is coincident with the boundary between the Ksituan and Chinchaga basement zones (O'Connell et al., 1990).

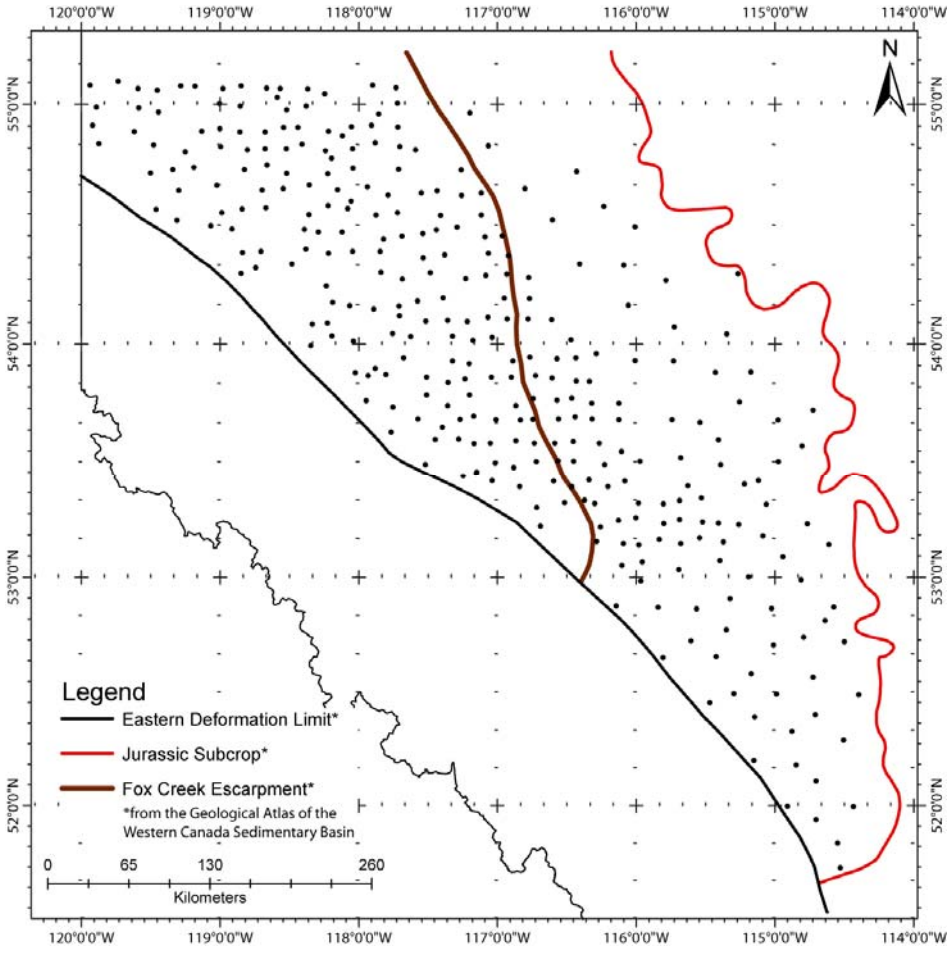

Figure 2-15: The Fox Creek Escarpment

2.3.4 Jurassic sediments of west-central Alberta

At the beginning of the Jurassic, west-central Alberta was between 45° and 70° North latitude, part of the stable craton that persisted from the Carboniferous through the Middle Jurassic (Poulton, 1989). The western interior of North America was covered by a shallow marine sea for most of the Jurassic (Marion, 1984).

The Jurassic strata of west-central Alberta are bounded by two regional angular unconformities. Most of the sediments in this interval are part of the Fernie Formation, however in the northwest corner of the study area the Nikanassin Formation and the Minnes Group were deposited above the Fernie but below the sub-Cretaceous unconformity. The primary focus of this study is the Fernie Formation, a thin, craton-derived marine sequence overlain by Cordilleran-derived sandstones (Rosenthal, 1989).

The Fernie Formation has been described at several locations in Alberta and British Columbia (Figure 2-16). There are several challenges to studying the Fernie Formation; correlations are difficult because of the poor distribution of well-preserved specimens; nomenclature has been applied to units based on lithostratigraphy and biostratigraphy (Stronach, 1984); and poor or incorrect correlations existed between outcrop and the subsurface (Riediger, 2002). The Fernie Formation contains many unconformities; in the past some of these were assigned because of “missing” fauna. Many of these so-called unconformities occurred in continuous sections that simply did not contain preserved fossils and therefore were not actual depositional hiatus’ (Hall, 1984). Recognition of the divergence of ammonite faunas in western North America from those used to define the Standard Zones in northwest Europe has been crucial to resolving some of these challenges (Hall, 1984). Many of these problems have been resolved;

however care must be taken to ensure that the most recent literature is being used regarding correlations and unconformities.

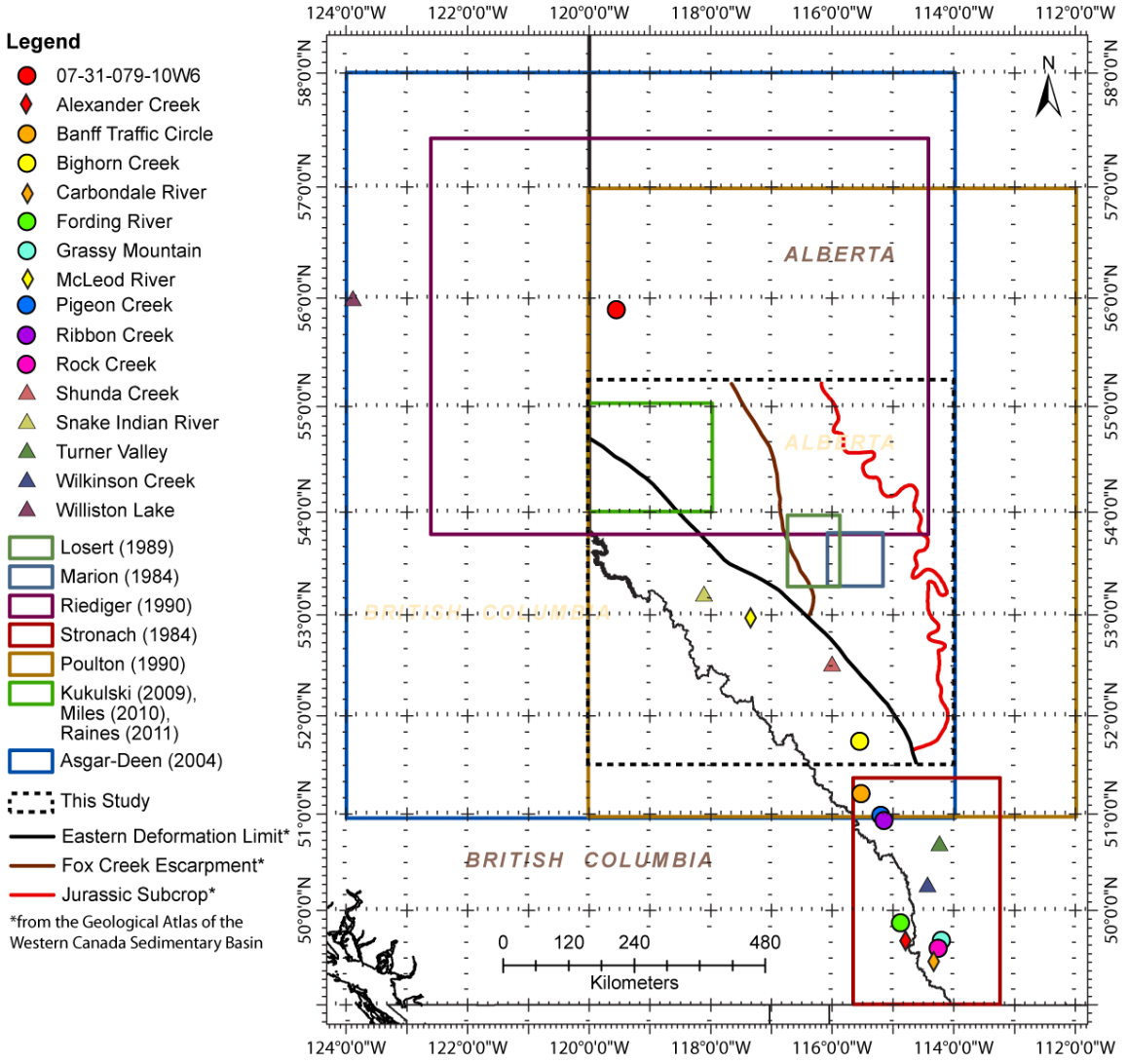

Figure 2-16: Type-section locations of described members of the Fernie Formation and the study areas of previous authors.

Previous work and descriptions of units within the Fernie Formation have been discussed in detail by Hall (1984) and more recently Asgar-Deen (2003). The lithostratigraphy of the Fernie Formation is summarized in Table 1. The Fernie

Formation is usually described separately in southern Alberta and British Columbia (Figure 2-17**)** and in west-central and northwest Alberta (Figure 2-18).

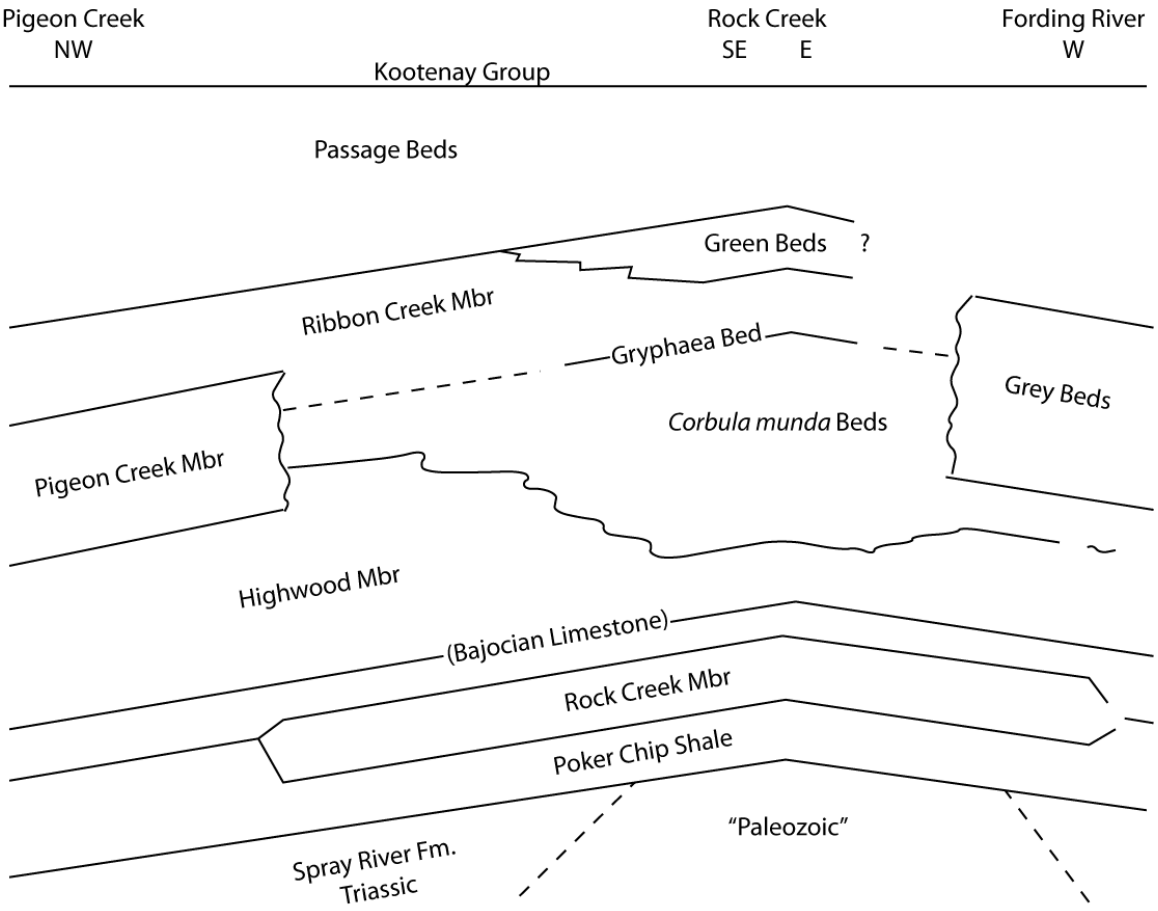

Figure 2-17: Stratigraphic relationships within the Fernie Formation in southern Alberta and British Columbia

Pigeon Creek, Rock Creek, and Fording River are shown in Figure 2-16 (modified from Stronach, 1982).

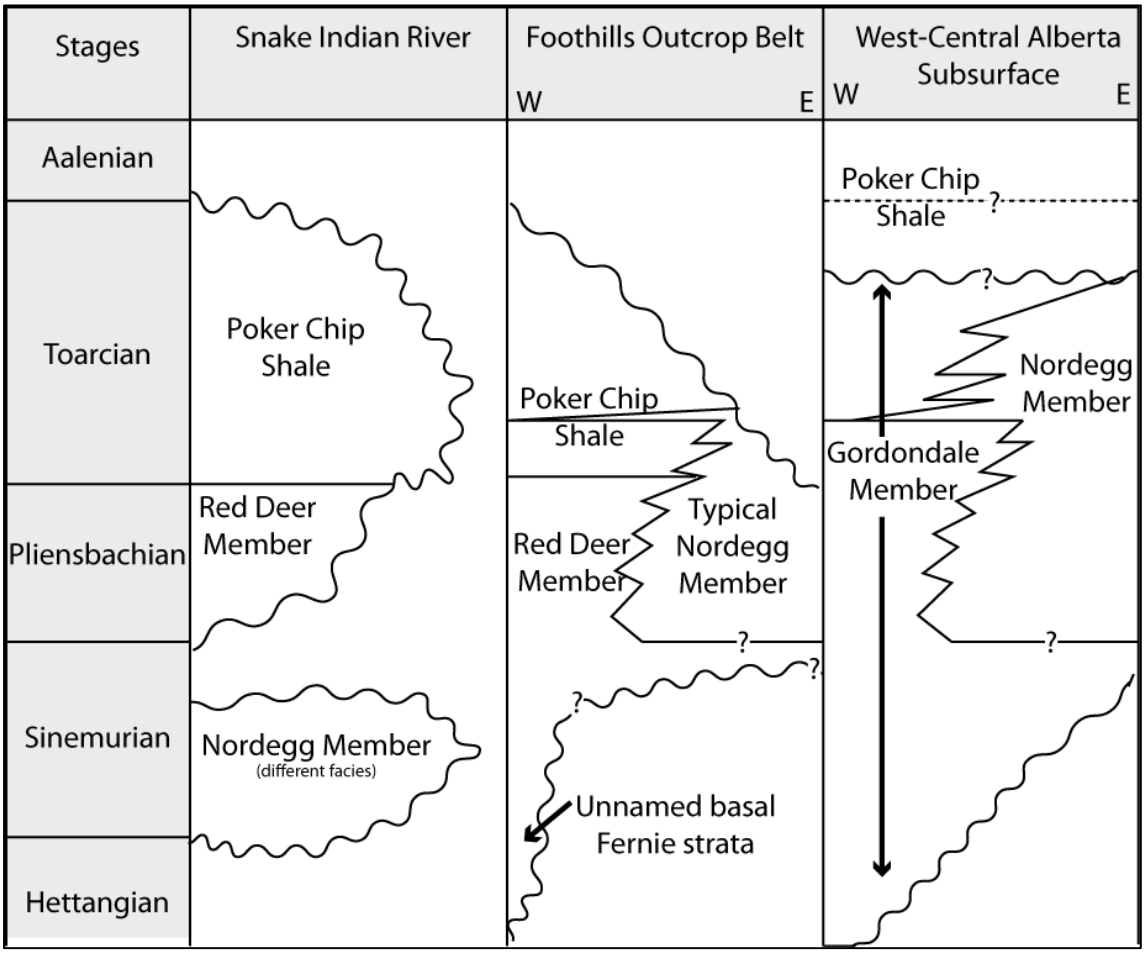

Figure 2-18: Lower Jurassic correlation chart for west-central and NW Alberta Snake Indian River is shown in Figure 2-16 (modified from Asgar-Deen et al., 2004).

Other Jurassic strata are preserved in Western Canada, however they are not considered here because they are deposited outside the study area. To the south are the Kootenay and Ellis Groups. The Jurassic deposits of the Williston Basin are separated from the foreland basin deposits by the Sweetgrass Arch (Poulton et al., 1994) and as such, are not considered foreland basin deposits.

2.3.5 Eustatic Sea Level Trends

Hallam (2001) summarized both the difficulty in determining global sea level trends during the Jurassic, and some of the different methods that have been used to generated sea level curves.

A compilation of sea level trends across four widely scattered regions (*ibid.*) revealed an overall pattern of sea level rise throughout the Jurassic. This gradual transgression was interrupted by periods of standstill (Figure 2-19).

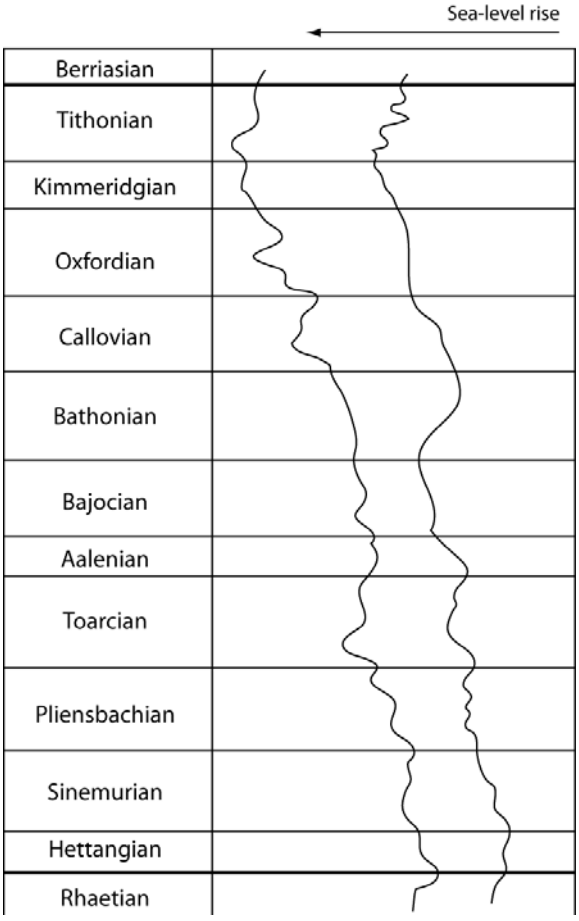

Figure 2-19: Global Jurassic sea level curves

Sea level curves modified from Hallam (2001) showing overall sea level rise during the Jurassic. The curve on the left is from Hallam (1988). The curve on the right is from Haq et al. (1987).

2.3.6 Depositional environments

The Nordegg Member in the subsurface is a massive chert and limestone unit that correlates to the outcropping Nordegg in the foothills and is interpreted to be carbonate platform deposits (Poulton et al., 1994). The Gordondale Member (sometimes referred to as the "Nordegg" Member) consists of highly radioactive fine-grained shales and limestones deposited north of the platform in a deeper portion of the basin with restricted circulation (Poulton et al., 1994; Asgar-Deen et al., 2004). The Red Deer Member, in the Red Deer River valley, and similar deposits identified elsewhere in west-central Alberta are presumed to represent the transition between the Nordegg and Gordondale Members (Figure 2-20; Asgar-Deen, 2003). The Red Deer Member and equivalent strata were deposited on a dysaerobic shelf with restricted circulation (Poulton et al., 1994).

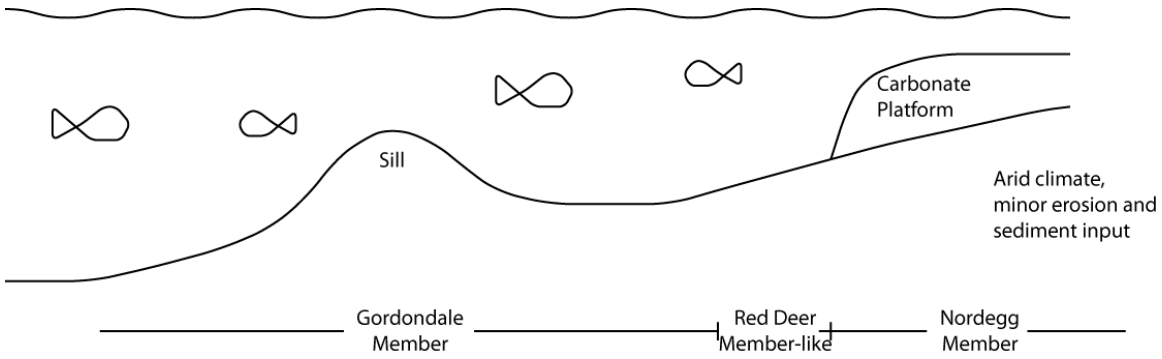

Figure 2-20: Depositional model for the Nordegg and Gordondale Members Depositional model showing the relationship between the basinal Gordondale Member, the transitional Red Deer Member-like units, and the Nordegg carbonate platform (modified from Asgar-Deen, 2003).

The organic-rich Poker Chip Shale is one of the most widespread units in the Fernie Formation (Hall, 1984). A model proposed for the British Toarcian Shale works

for the Poker Chip Shale (Stronach, 1984). In this model, the shale was deposited on a broad shallow shelf (Figure 2-21) during the worldwide Toarcian anoxic event and was abruptly overlain by the Rock Creek Member (Stronach, 1984). A recent model for the Posidonia Shale Formation in the Dutch Central Graben proposed that the shales were deposited in a shallow marine epicontinental sea with variable conditions (Trabucho-Alexandre et al., 2012). This is consistent with what is currently understood about the Poker Chip Shale.

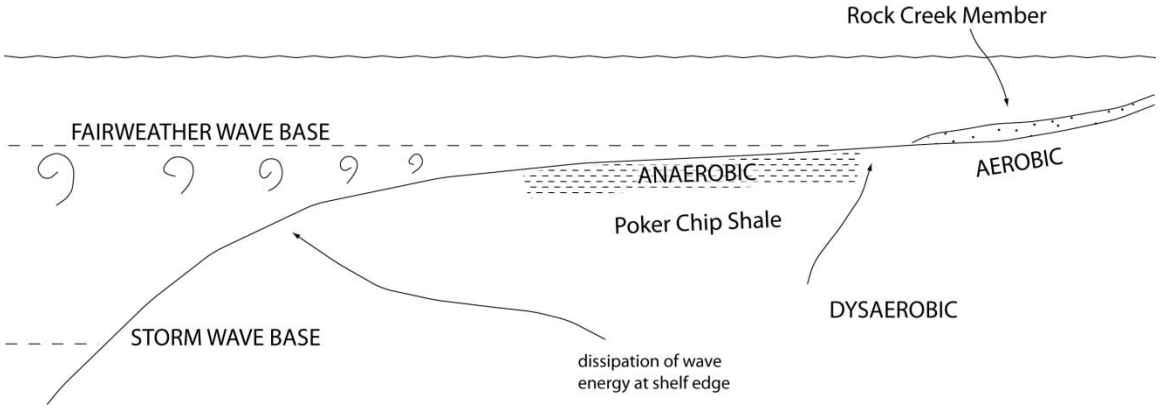

Figure 2-21: Depositional model for the Poker Chip Shale

Dissipation of wave energy at the shelf edge causes the anaerobic conditions that the Poker Chip Shale was deposited under (modified from Stronach, 1984).

In southern Alberta the contact between the Poker Chip Shale and the overlying Rock Creek Member is gradational (Stronach, 1984), whereas in the subsurface it is a sharp contact (Marion, 1984). This difference was considered to be a reflection of the depositional environment rather than an unconformity (Losert, 1986). Generally, sandstone content in these units increases to the west, suggesting an easterly-derived source (Marion, 1984). The Rock Creek Member consists of tidally-dominated sheet

sands deposited on a shallow shelf (Figure 2-22**;** Marion, 1984; Stronach, 1984; Putnam and Moore, 1994).

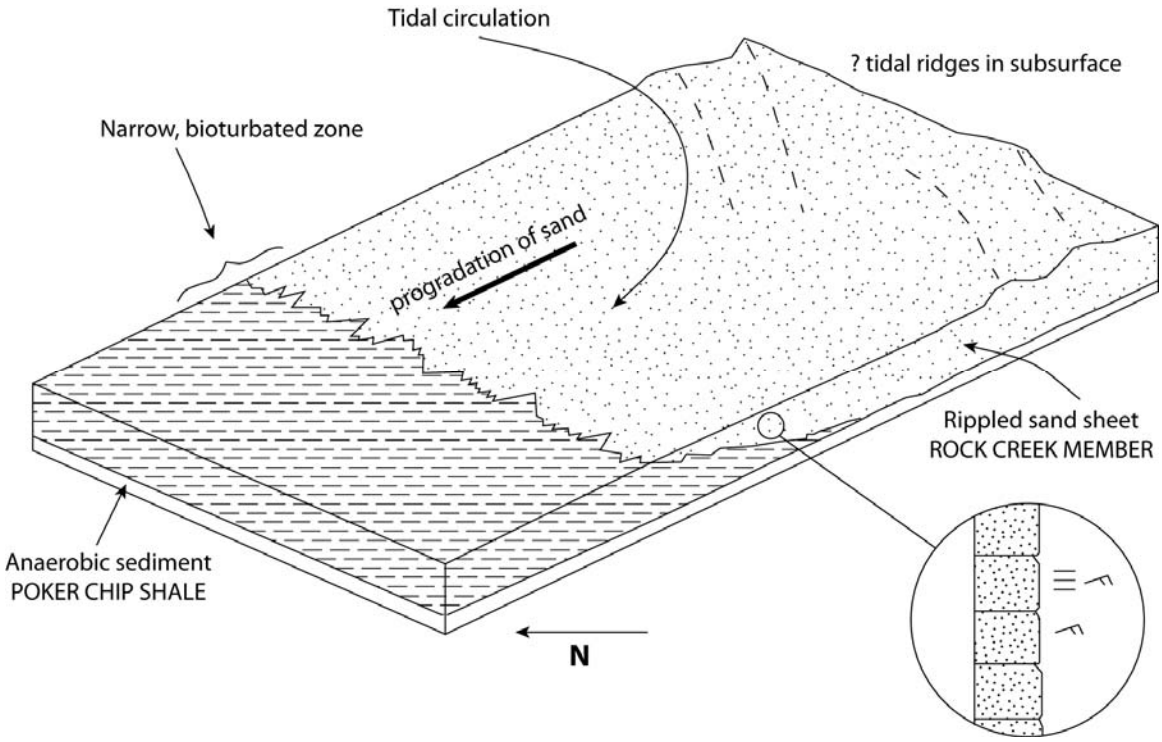

Figure 2-22: Depositional model for the Rock Creek

Rock Creek sands are deposited by tidal currents in shallow waters, prograding over the low relief Poker Chip shale (modified from Stronach, 1984)

In the study area, the Rock Creek Member (or Poker Chip Shale where the Rock Creek is not found) is unconformably overlain by the Upper Fernie marine shales. These shales, with some local sandstones, shallow- and coarsen- up as the foredeep is filled and transitions to a non-marine basin (Poulton et al., 1994).

Table 1: Described members of the Fernie Formation

Name	Description	Age	Original reference[1]	Distribution	Type location or reference section
Nordegg Member	Dark grey to black, hard, platy to medium bedded cherty and phosphatic limestone with minor amounts of dark platy to papery shales Usually capped by *Oxytoma* Bed (highly fossiliferous)	Sinemurian (at Snake Indian River only) Pliensbachian to Toarcian[2]	Warren (1934)	Outcrop in foothills of west-central Alberta; subsurface extends just south of the Clearwater River and T24-49, R3-21W5	Shunda Creek, near Nordegg
Gordondale Member[2]	Organic-rich, phosphatic, highly radioactive, fine-grained strata	Hettangian to Upper Toarcian	Asgar-Deen et al (2004)	Subsurface of west-central Alberta and Peace River Embayment, outcrops near Williston Lake and Black Bear Ridge	07-31-079-10W6
Nordegg Member Carbonate Platform Facies[3]	Grey, calcareous chert varying to cherty limestone characterized in the subsurface by blocky gamma logs	Not well dated	Poulton et al (1990)	Widespread throughout west-central Alberta	6-26-55-15W5, 14-8-56-19W5, outcrops at Snake Indian River bridge

Name	Description	Age	Original reference[1]	Distribution	Type location or reference section
Unnamed basal shale and coquina[4]	Contains phosphatic conglomerates, conglomeratic sandstones, or coarse, phosphatic, Bioclastic rudstones	Sinemurian	Hall (1984)	Bighorn Creek, Lodgepole Creek, Crowsnest, Fording River	
Red Deer Member	Thin resistant unit with dark grey to black platy shales and dark limestones	Pliensbachian	Frebold (1959)	Limited area north and south of the Red Deer River	Best exposed above the falls on Bighorn Creek
Poker Chip Shale	Black, fissile to papery shale	Toarcian	Spivak (1949)	One of the most extensive units in the Fernie	Wells near Turner Valley and Wildcat Hills
Rock Creek Member	Grey calcareous-cemented sandstones and siltstones, grey shales, black oolitic limestones, calcareous concretionary bands associated with belemnite “battlefields” and grey, rusty-weathering shales	Bajocian	Warren (1934) expanded by Frebold (1976)	Rock Creek, Daisy Creek, Livingstone Gap, Mount Gibraltar, Fording River, McLeod River, Fiddle River, Morris Creek, Snake Indian River	Rock Creek

Name	Description	Age	Original reference[1]	Distribution	Type location or reference section
Highwood Member	Dark grey, rusty-weathering shales, in some places black, papery and organic-rich with interbedded bands of calcareous concretions, bentonites and belemnites; includes the Bajocian Limestone, (black, oolitic, fossil-rich marker horizon)	Latest Early Bajocian	Stronach (1981, 1984)	Widespread throughout the area of Fernie outcrop	Wilkinson Creek
Lille Member	Calcareous grit and coquina	Possibly equivalent to Rock Creek Member	Frebold (1957)	Single outcrop	Foot of the south slope of Grassy Mountain
Pigeon Creek Member	Regularly interbedded hard, grey calcareous siltstones; light brown to pale grey weathering surfaces; grey finely laminated shales	Bathonian or Callovian	Crockford (1949)	Kananaskis-Banff area; thins rapidly to north and south of reference section	Headwaters of Pigeon Creek on Mount Allan
***Corbula munda* Beds**	Brownish-grey, silty shales with a greenish hue, interbedded with fine-grained, hard calcareous sandstones	Early Bathonian	McLearn (1927)	Blairmore region of SW Alberta and adjacent areas of British Columbia	Southern slope of Grassy Mountain
***Gryphaea* Bed**	Resistant, thin coquina composed of large oyster valves	Mid-Bathonian	McLearn (1927)	Blairmore region	Southern slope of Grassy Mountain

Name	Description	Age	Original reference[1]	Distribution	Type location or reference section
Grey Beds	Medium grey, calcareous, silty, non-bedded shales with blocky to conchoidal fractures	Lower and Middle Bathonian	Frebold (1957)	Southern Alberta	Alexander Creek, alternately west bank of Fording River
Ribbon Creek Member	Dark grey shale with large, ovoid, orange-weathering, sideritic concretions	Late Bathonian	Stronach (1981, 1984)	Ribbon Creek, Pigeon Creek, Rock Creek, Bighorn Creek, Willson Creek	Ribbon Creek
Green Beds	Dark to bright green, often friable, berthierine sandstone and siltstone; irregular interbeds of purplish-grey siltstone and yellow-brown-weathering calcareous concretions; occurrences of large belemnite guards and brown fossil wood	Late Oxfordian and Kimmeridgian	McLearn (1927)	Blairmore area, Willson Creek, Cadomin, Jasper	Best accessed along north bank of Carbondale River
Passage Beds	Dark grey, easily fractured shales interbedded with silty bands which thicken, increase, and become sandier upward	Late Oxfordian or Kimmeridgian	McLearn (1927)	Outcrop in central and southern Alberta	Most easily accessed at Banff "traffic circle"

[1] Unless otherwise noted, information in this table is from Hall, 1984
[2] Asgar-Deen et al., 2003; Asgar-Deen et al., 2004
[3] Poulton et al., 1990
[4] Collar, 1990

Chapter Three: **Data and Methods**

3.1 Data

The Fernie Formation members identified for this study are, from bottom to top, the Nordegg, Poker Chip Shale, the Rock Creek, and the Upper Fernie (Figure 3-1). Thicknesses at each location were determined from well logs. Gamma ray was the principle log used, however the neutron-density, density-porosity, and sonic logs were also used in some cases.

The tops of the Jurassic units were determined using published well logs as guidelines (Putnam and Moore, 1993; Putnam and Ward, 2001; Asgar-Deen et al., 2003; Asgar-Deen et al., 2004). Where the Minnes Group is present in the study area (Figure 3-2) a database from colleagues in the Center for Applied Basin Studies was used (Kukulski, 2009; Miles, 2010; Raines, 2011). The GeoScout system tops were used for the picks outside of this interval.

3.1.1 Units identified in this study

The units in this study have been picked from well logs, and where possible, correlated to well logs that have been tied to core in previously published studies. This work was done to supplement the subsidence analysis and is not intended to be a comprehensive sedimentological study.

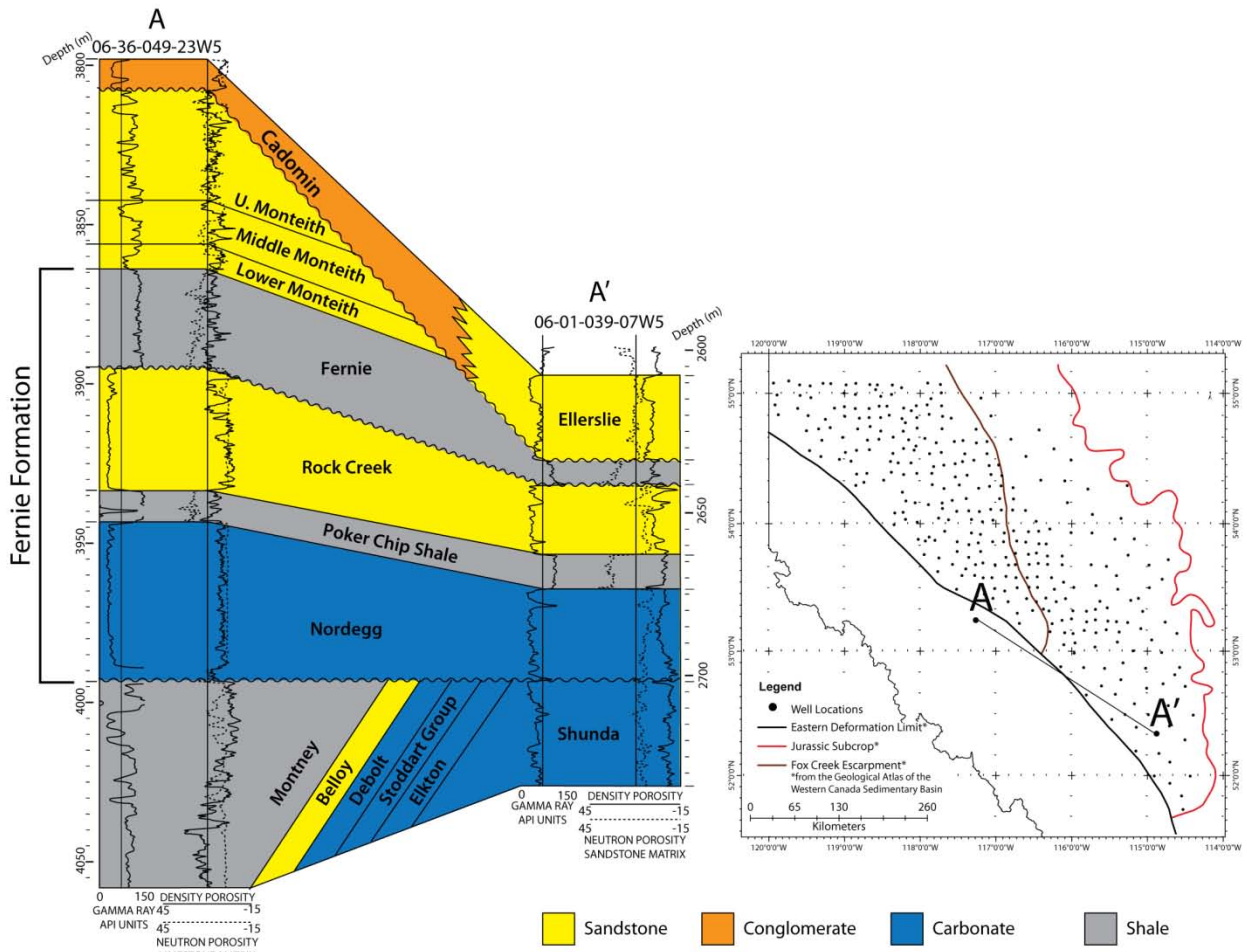

Figure 3-1: Fernie Formation stratigraphic column

Well logs showing the full Fernie Formation. The Fernie Formation was deposited above a regional unconformity. In the east (A'), the sub-Cretaceous unconformity cuts into the Fernie Formation. In the west the Minnes Group was deposited above the Fernie Formation.

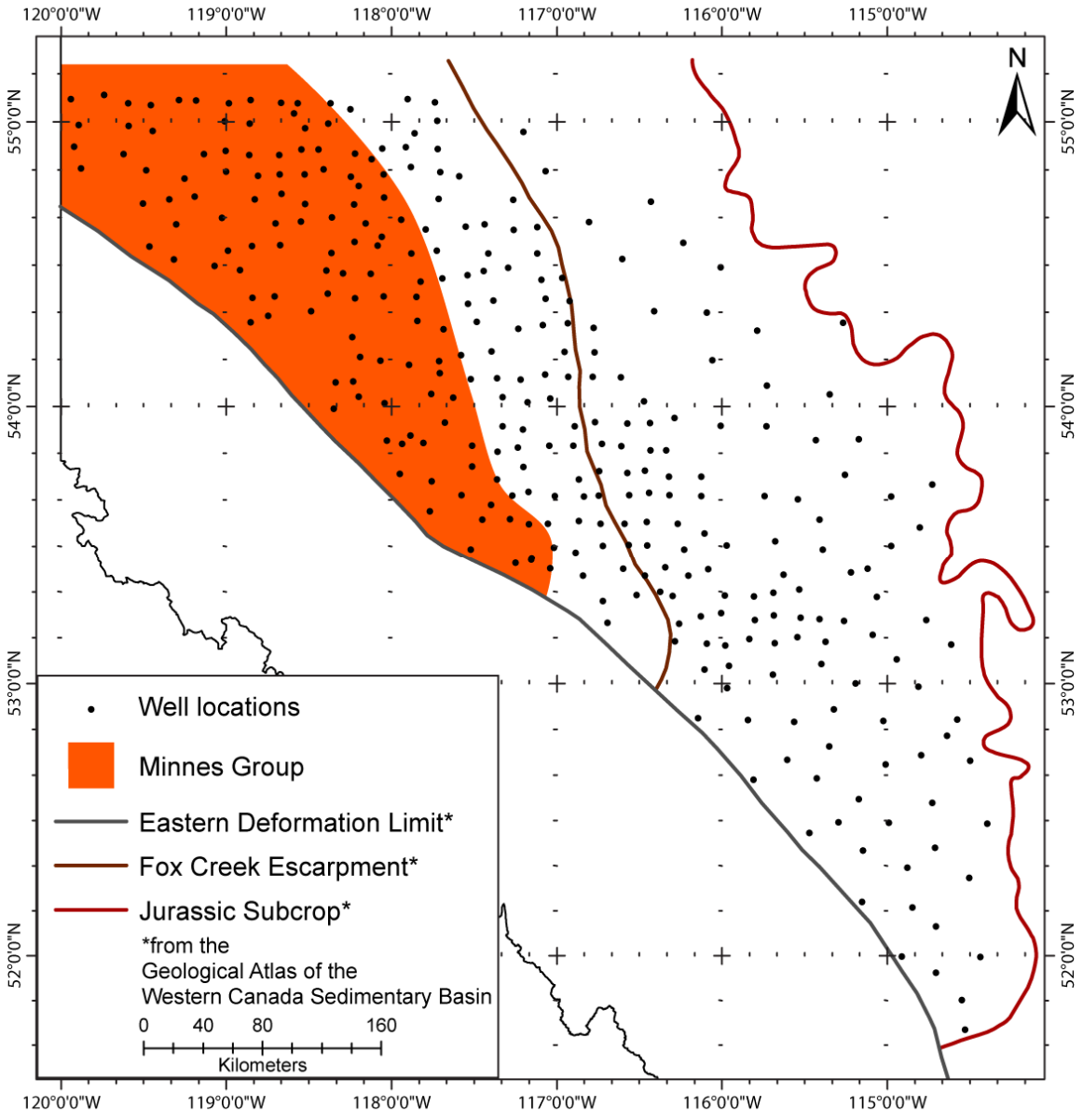

Figure 3-2: Minnes Group distribution

The Minnes Group is found in the northwest corner of the study area. Its southern and eastern boundary is the subcrop edge (orange).

3.1.1.1 Nordegg

The Nordegg defined here is the lowermost Jurassic unit and includes the Nordegg Member, the Gordondale Member and the Red Deer Member (and equivalents). The Nordegg extends throughout most of the study area (Figure 3-3) and overlies Triassic through Mississippian aged units. Its maximum thickness is 63.5m. The base of the Nordegg is identified in most of the study area by the strong gamma signature at the base of the unit.

In the center of the study area the Nordegg is significantly thicker than in the surrounding regions. A depocenter has been defined for this region (Figure 3-4), to enable a study of how the thick deposits in this area affected the layers deposited above it. The mean thickness of the Nordegg is 32.35m and the depocenter is defined as all thicknesses greater than 45.4 m. This value was chosen for visual and statistical reasons. The Nordegg thins away from the 45.4 m contour in all directions.

The histogram of the Nordegg isopach values (Figure 3-4) shows a nearly normal distribution when the data points are grouped according to equal intervals (the same intervals they are contoured at). 45.35 is the 3rd quartile; one-quarter of the isopach values are greater than 45.35m. The 45.41 – 51.44m contour interval contains the thickness that is one standard deviation away from the mean (46.772m).

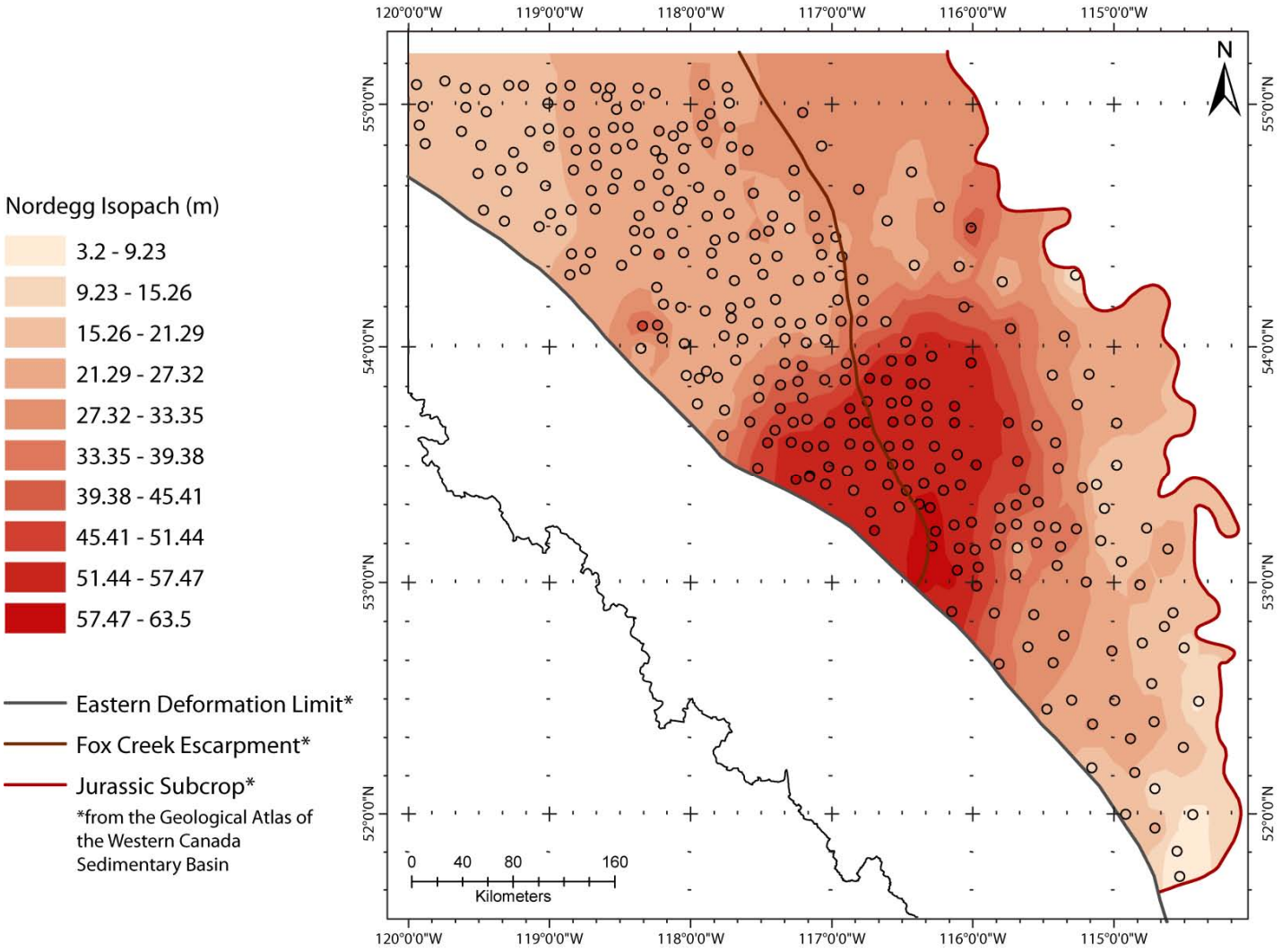

Figure 3-3: Nordegg isopach

The colour inside each data point corresponds to the actual thickness of the Nordegg at that point.

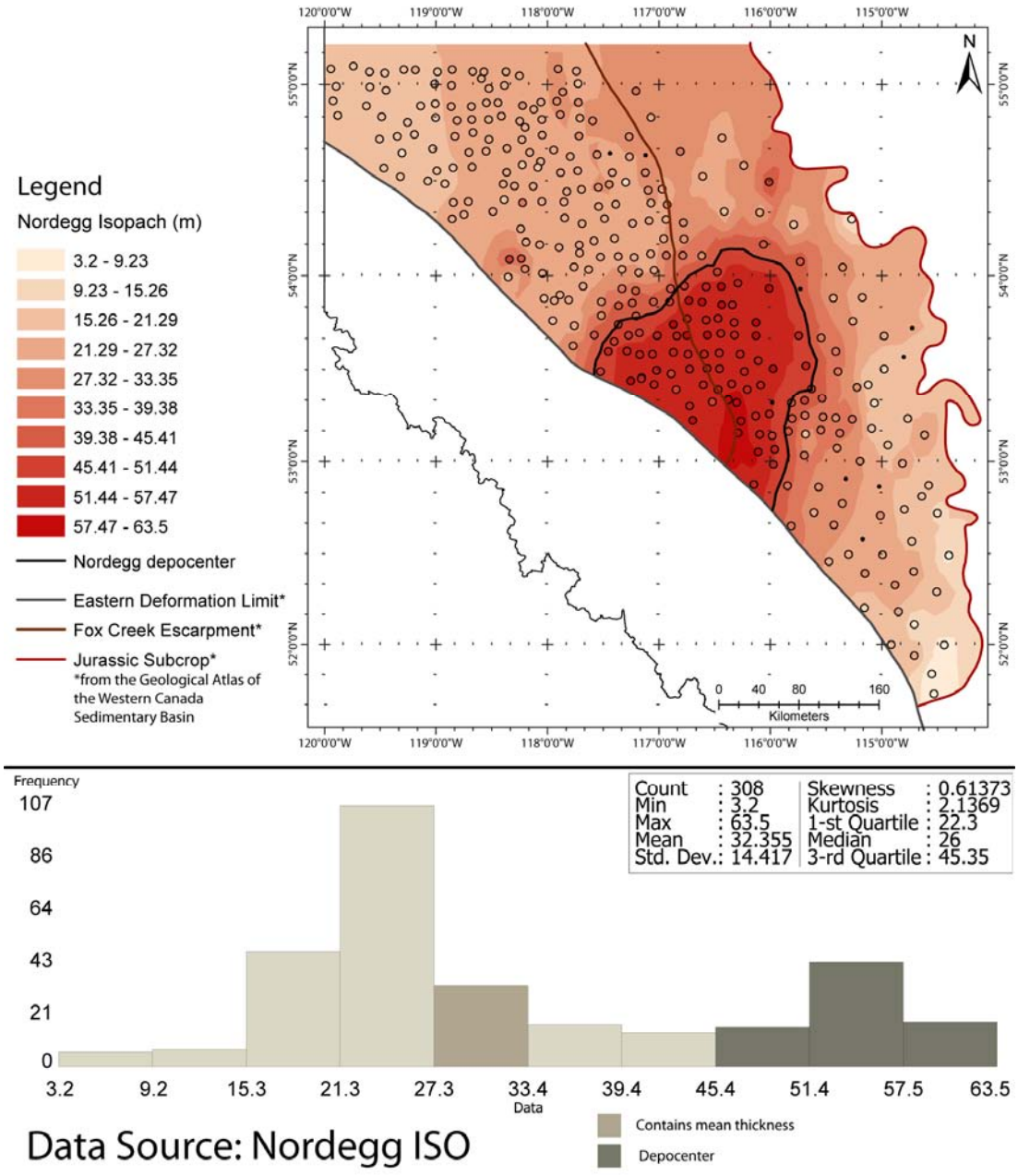

Figure 3-4: Nordegg depocenter – isopach and histogram

Map: the depocenter was defined as the thickest portion of the Nordegg (the isopach thins away from the depocenter boundary in all directions). Histogram: the depocenter boundary coincides with the 3rd quartile. The depocenter contains the thickness that is one standard deviation away from the mean.

3.1.1.2 Poker Chip Shale

The Poker Chip Shale extends throughout the study area and its maximum thickness is 44.9m. It thickens to the northwest (Figure 3-5).

The Poker Chip Shale is present immediately above the Nordegg Member. Where the overlying Rock Creek Member does not separate it from the Upper Fernie the Poker Chip Shale is picked based on a deflection in the gamma log and/or a change in the sonic log. In some wells in the northwest portion of the study area there was no discernible change from the Upper Fernie to the Poker Chip; in these wells the Poker Chip was not picked.

3.1.1.3 Rock Creek

The Rock Creek in this study is defined as any sandy sequence between the Upper Fernie and the Poker Chip Shale, as determined by gamma-ray logs and, in some cases, neutron-density logs. The Rock Creek is present in the southeast half of the study area only (Figure 3-6). Its maximum thickness is 33m. The thickest occurrence of the Rock Creek is in the south central part of the study area.

Overlying the Rock Creek sand in some parts of west-central Alberta is the Niton B sand (Putnam and Moore, 1993). This sand is equivalent to the Oxfordian Green Beds (Table 1**;** T. Poulton, pers. comm.). The Niton B is commonly included with the Rock Creek Member because it contains Rock Creek sands that have been reworked during transgression (Putnam and Moore, 1993). Although difficult to determine from well logs, the Niton B is characteristically glauconitic (Losert, 1986). In this study, the Niton B is included with the Rock Creek Member.

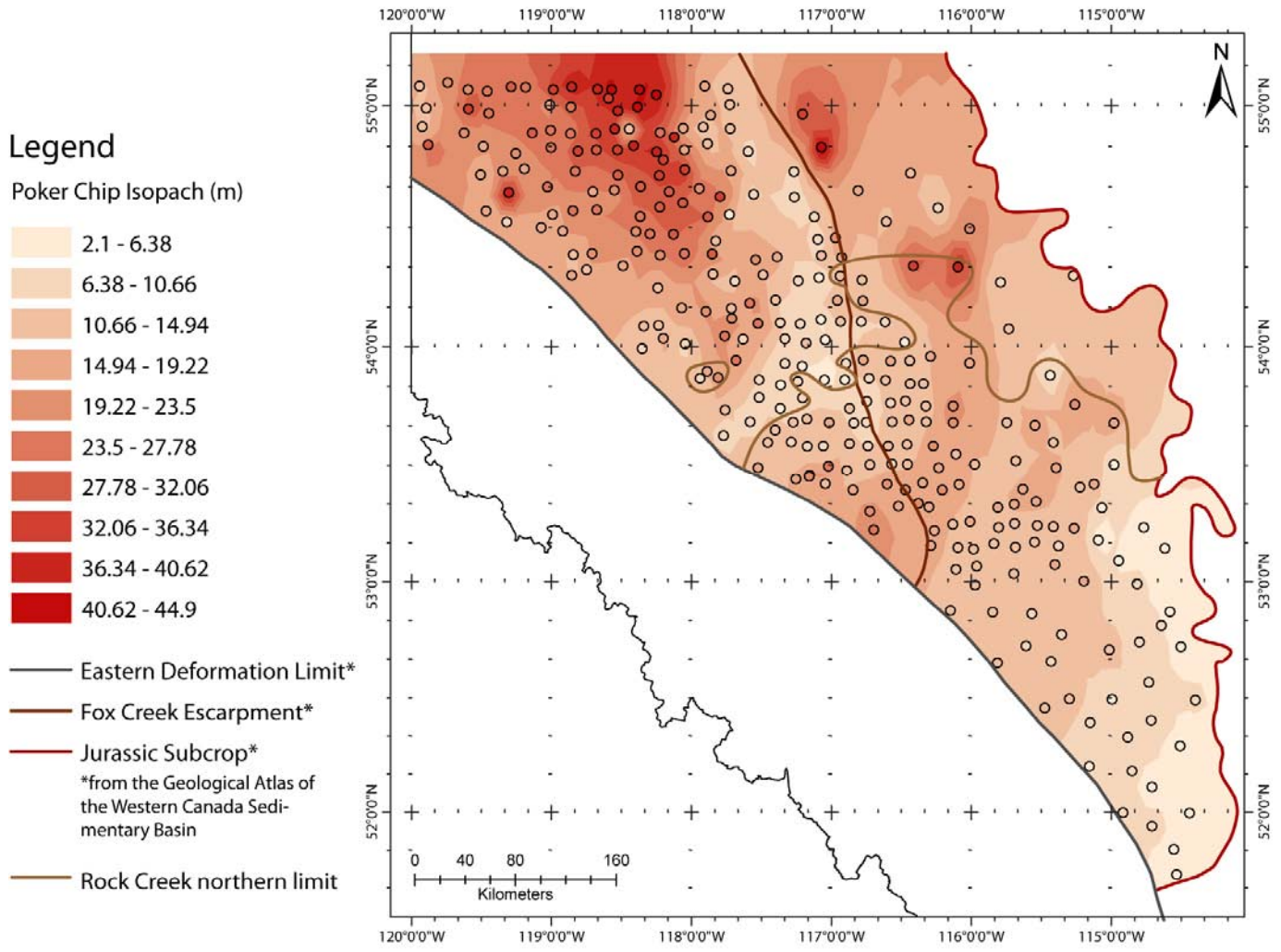

Figure 3-5: Poker Chip Shale isopach

The colour inside each data point corresponds to the actual thickness of the Poker Chip Shale at that point. North of the Rock Creek limit the Poker Chip Shale is difficult to differentiate from the Upper Fernie based on well logs alone.

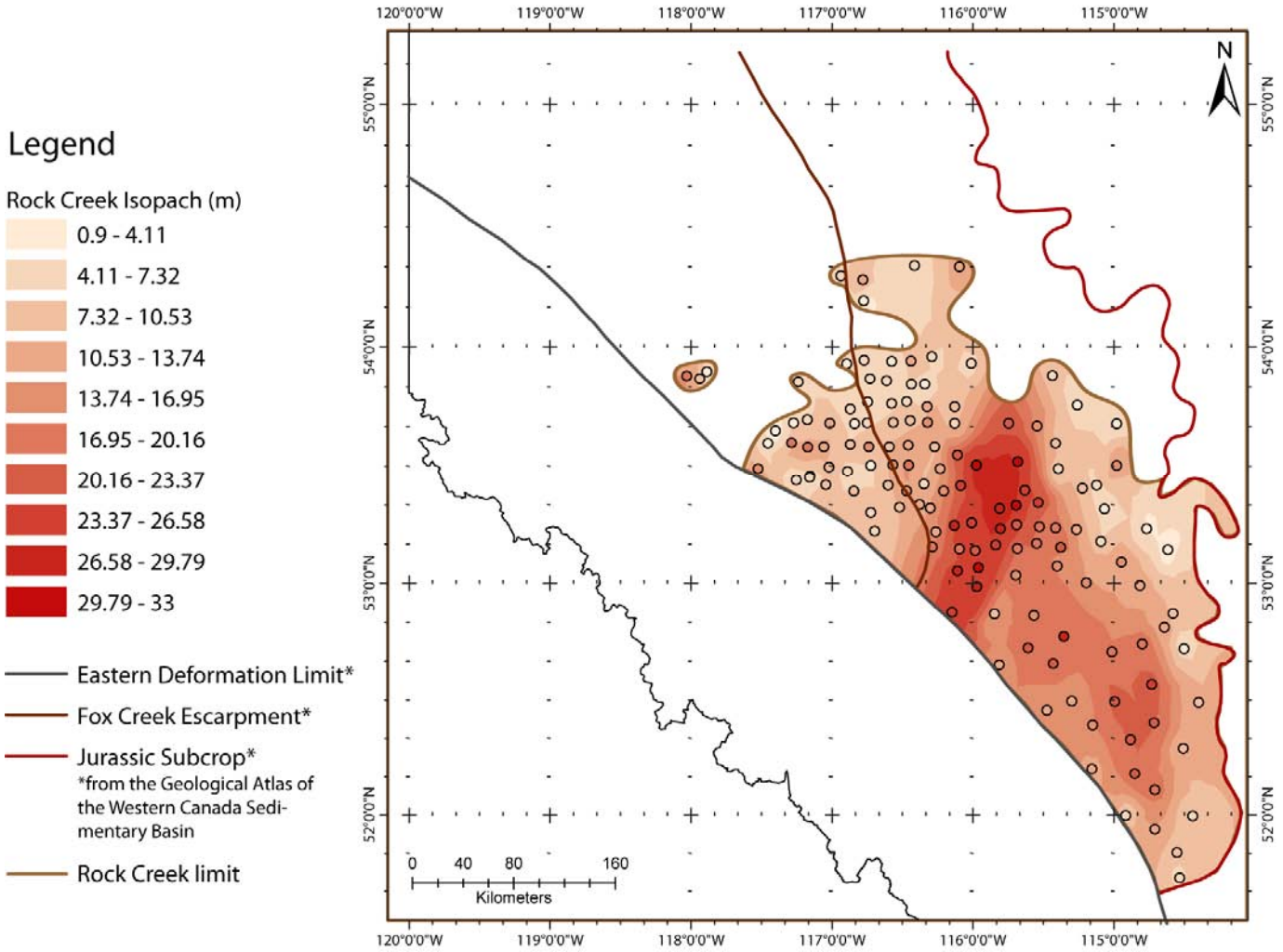

Figure 3-6: Rock Creek isopach The colour inside each data point corresponds to the actual thickness of the Rock Creek at that point. Only the sands of the Rock Creek Member are picked in this study.

3.1.1.4 Upper Fernie

The Upper Fernie is defined in the study area as the predominantly shaly package found above the Rock Creek (and/or the Poker Chip Shale). In the northwest portion of the study area, it is bounded at the top by the clastics of the Minnes Group or the Nikanassin Formation. Elsewhere, it is capped by the sub-Cretaceous unconformity. The Upper Fernie extends throughout the study area (Figure 3-7). Its maximum thickness is 73.9m. The Upper Fernie thickens to the west and northwest. East of the Minnes Group subcrop the isopach is partially controlled by erosion associated with the sub-Cretaceous unconformity.

As discussed in section 3.1.1.2, the Upper Fernie and Poker Chip Shale are difficult to distinguish where the Rock Creek is not present between them. This makes the thicknesses of the Upper Fernie less certain beyond the Rock Creek limits.

A thin channel-like feature runs approximately north-south through the study area, between the Minnes Group subcrop and the Fox Creek Escarpment. This is interpreted to be an erosional channel (Figure 3-8**)**, created by the Cretaceous Spirit River Channel (McLean, 1977). The Spirit River Channel was a northwestward flowing trunk stream, fed by alluvial fans and rivers originating in the west (*ibid***.**).

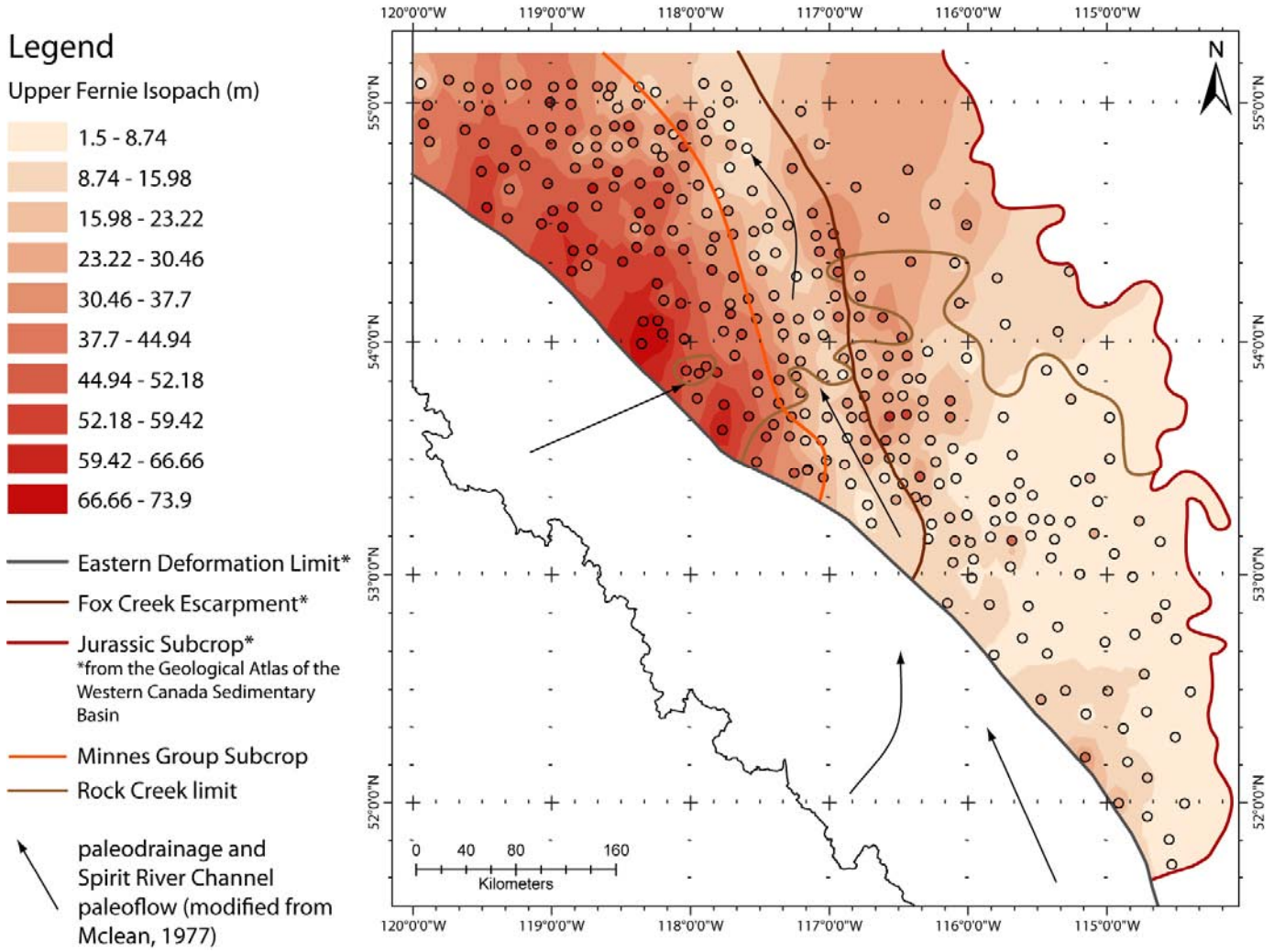

Figure 3-7: Upper Fernie isopach The colour inside each data point corresponds to the actual thickness of the Upper Fernie at that point.

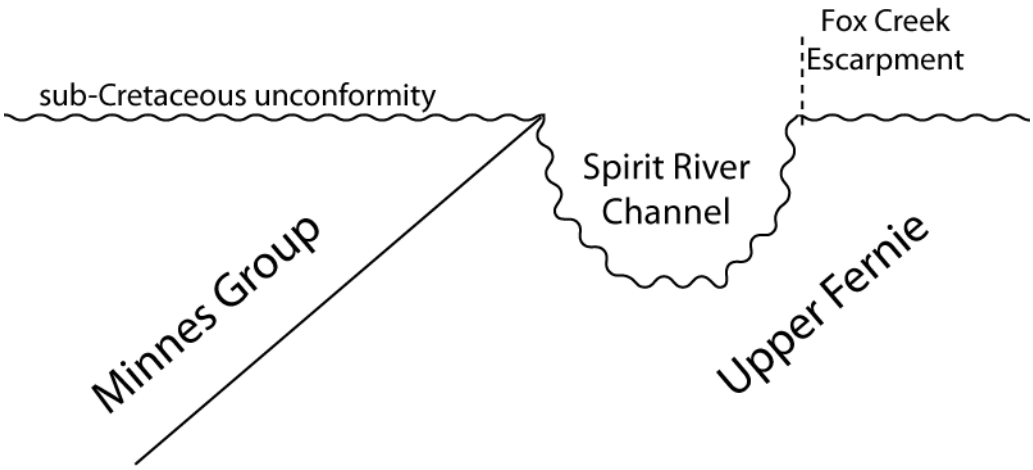

Figure 3-8: Schematic illustration of the Spirit River Channel cutting into the Upper Fernie

3.1.1.5 Uncertainty in thicknesses

The study area is stratigraphically complex, making confidence in picks difficult in some regions. The study area has been divided into four qualitative zones (Figure 3-9), ranked based on the confidence in the thicknesses of the units within the Fernie Formation. The confidence in the picked thicknesses of the Nordegg is 100% everywhere, because of the strong gamma signal at its base and the deflection in gamma at the top of the Nordegg/base of the Poker Chip Shale.

Zone 1 has the highest confidence. Here, the Rock Creek sand is present, separating the Poker Chip Shale from the Upper Fernie shales. Additionally, the Minnes Group and/or Nikanassin Formation overlie the Fernie Formation, so the full thickness of the Upper Fernie is preserved here.

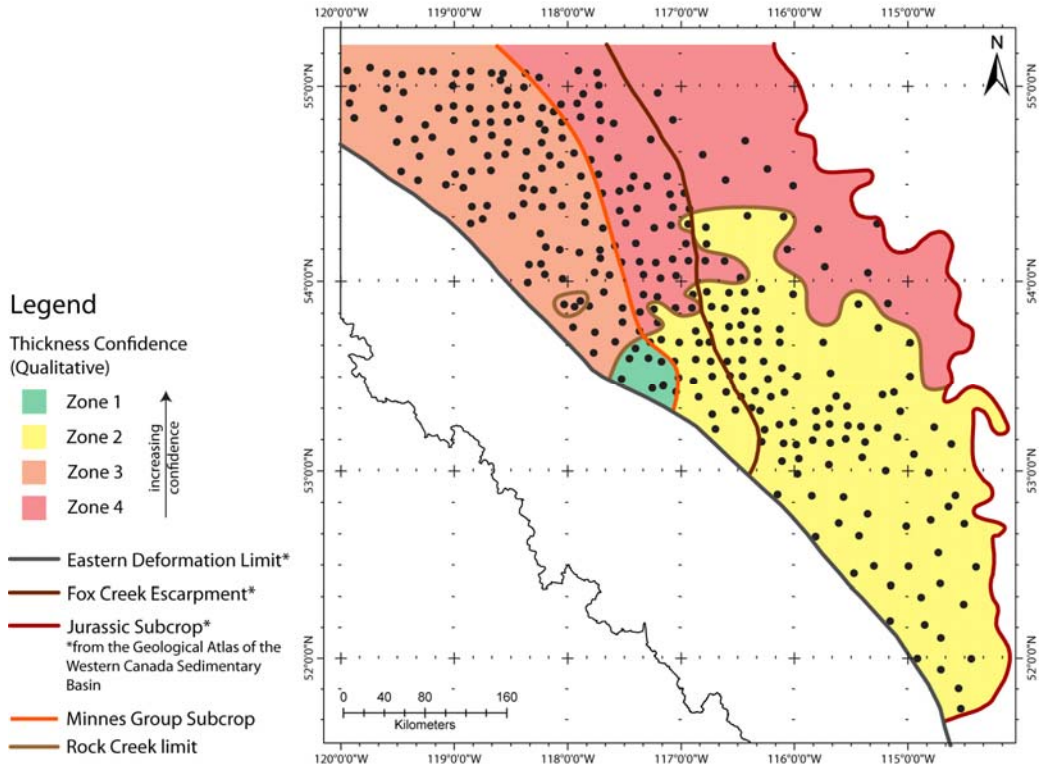

Figure 3-9: Qualitative confidence in the thicknesses of the Fernie Formation units The study area has been divided into four zones which have been labeled with increasing confidence in the thicknesses from 4 (least confidence) to 1 (most confidence). This is a qualitative measurement, and the zones are defined by the northern limit of the Rock Creek sand and by the Minnes Group subcrop.

In Zone 2, the Rock Creek sand is present, separating the Poker Chip Shale from the Upper Fernie. However, there is less confidence in the thickness of all the units because erosion associated with the sub-Cretaceous unconformity has removed increasingly more of the Fernie Formation from west to east. On the eastern edge of the study area, it possible that the Upper Fernie and Rock Creek have been removed completely, leaving only part of the Poker Chip Shale.

Zone 3 is west of the Minnes Group subcrop, so the full thickness of the Upper Fernie and the Poker Chip Shale are believed to be preserved. However, the Rock Creek sand is not present, making it difficult to differentiate between the two on well logs.

Confidence in the thicknesses is lowest in Zone 4. Like Zone 2, it is east of the Minnes Group subcrop which means that the Fernie Formation has been at least partially removed by erosion. Additionally, the Rock Creek sand is not present to separate the Upper Fernie and the Poker Chip Shale; they cannot always be differentiated on well logs.

3.1.2 Log Facies

Log facies have been identified in the Nordegg and Rock Creek members, based solely on the well log signatures. Some of these log facies can be correlated to facies described in published studies, however detailed lithology interpretations have not been made based on the well logs alone. Six log facies have been identified in the Nordegg and five in the Rock Creek.

3.1.2.1 Nordegg Facies

Nordegg Facies 1A (N1A; Figure 3-10A) is characterized by a single, significant gamma spike at the base of the Nordegg. This facies occurs at the base of the Nordegg in the northwest half of the study area. It is overlain by Facies N1B or Facies N2. N1A has been correlated with the base of the Gordondale Member (Figure 3-11A) but it extends further south beneath Facies N2 (Figure 3-12).

.

Nordegg Facies 1B (N1B; Figure 3-10B) is characterized by high gamma radiation with consistently separated neutron-density logs. It has been correlated with the upper portion of the Gordondale Member (Figure 3-11B). This facies has been described as the basinal equivalent of the carbonate platform facies (Asgar-Deen et al., 2004). It occurs in the northwest half of the study area only, with very little overlap of the carbonate platform facies (Figure 3-12).

Gamma of Nordegg Facies 2 (N2; Figure 3-10C) has a low-frequency and low-value gamma signature. Generally, the neutron log is lower frequency than the density logs. N2 has been correlated to the carbonate platform facies (Asgar-Deen et al., 2003; Asgar-Deen et al., 2004) and is found where the Nordegg is the thickest, in the central portion of the study area (Figure 3-12).

Nordegg Facies 3A (N3A; Figure 3-10D) has a gamma that decreases-up, while the gamma of Nordegg Facies 3B (N3B) increases up. Both have relatively little frequency variation in the gamma, and there are no discernible trends in the neutron-density logs. Both facies are randomly distributed throughout the study area; they do occasionally occur in the same log (Figure 3-13). A cross-section through the study area (Figure 3-14) suggests that N3B may represent the edges of the carbonate platform facies.

Nordegg Facies 4 (N4; Figure 3-10E) has an irregular, blocky gamma signature. It is found south of N2, the carbonate platform facies, but has not been correlated to any identified facies in literature. There is some overlap between its occurrence and the occurrence of N2 (Figure 3-12).

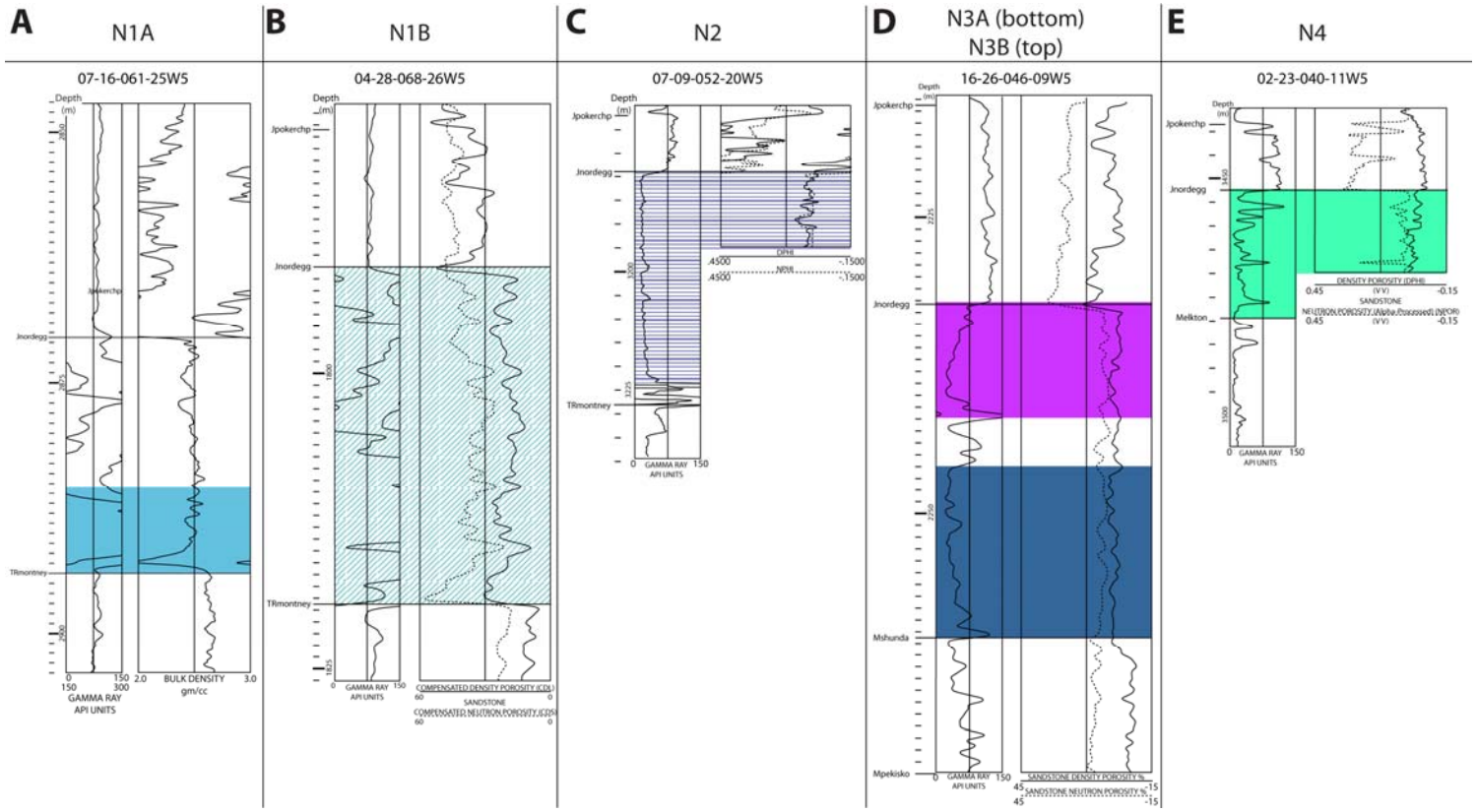

Figure 3-10: Well logs showing the five log facies identified within the Nordegg.

Each log facies is highlighted with colour on its respective well log. The same colours are used in Figure 3-12, 3-13, , and Figure 3-14. Well locations are shown in Figure 3-12 and 3-13. (A) N1A, (B) N1B, (C) N2, (D) N3A and N3B, (E) N4.

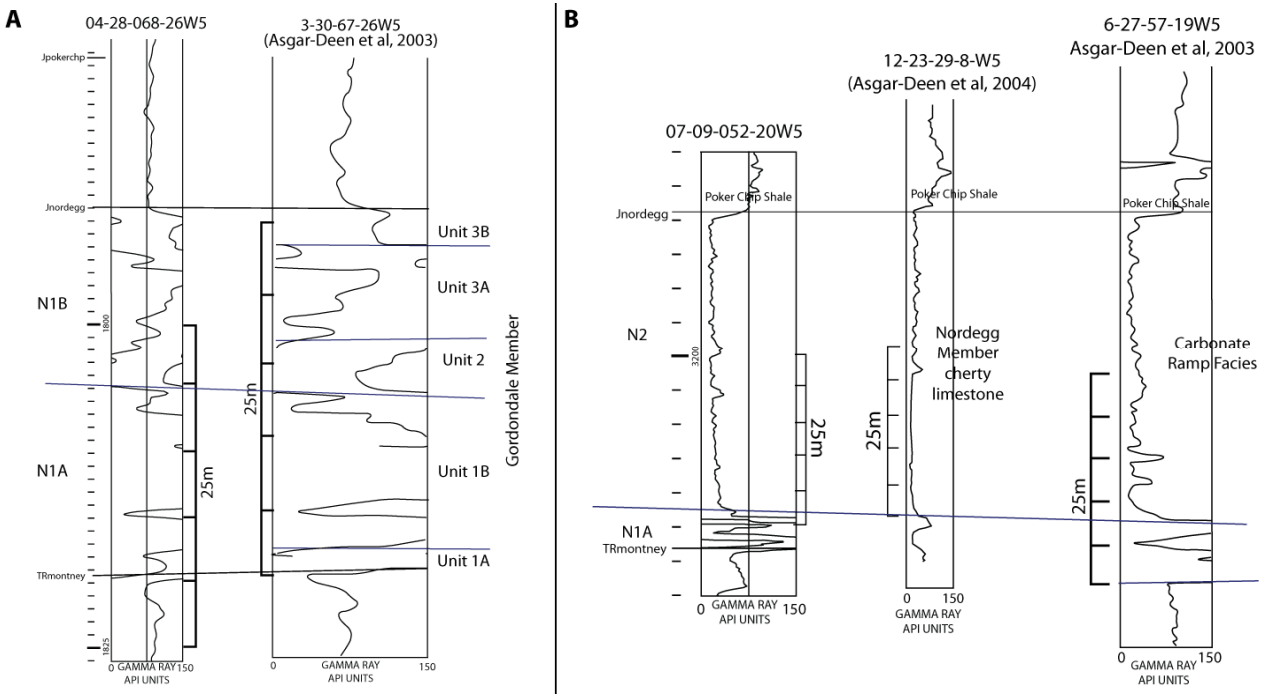

Figure 3-11: Correlation of Nordegg facies to published well logs

(A) Log from this study (left) compared to a well log from Asgar-Deen et al. (2003; right) showing the correlation of N1A and N1B to the Gordondale Member. (B) Log from this study (left) compared to well logs from Asgar-Deen et al. (2004; center) and Asgar-Deen et al. (2003; right) showing the correlation of N2 to the Nordegg Member cherty limestone and Carbonate Ramp facies of Asgar-Deen et al (2003; 2004).

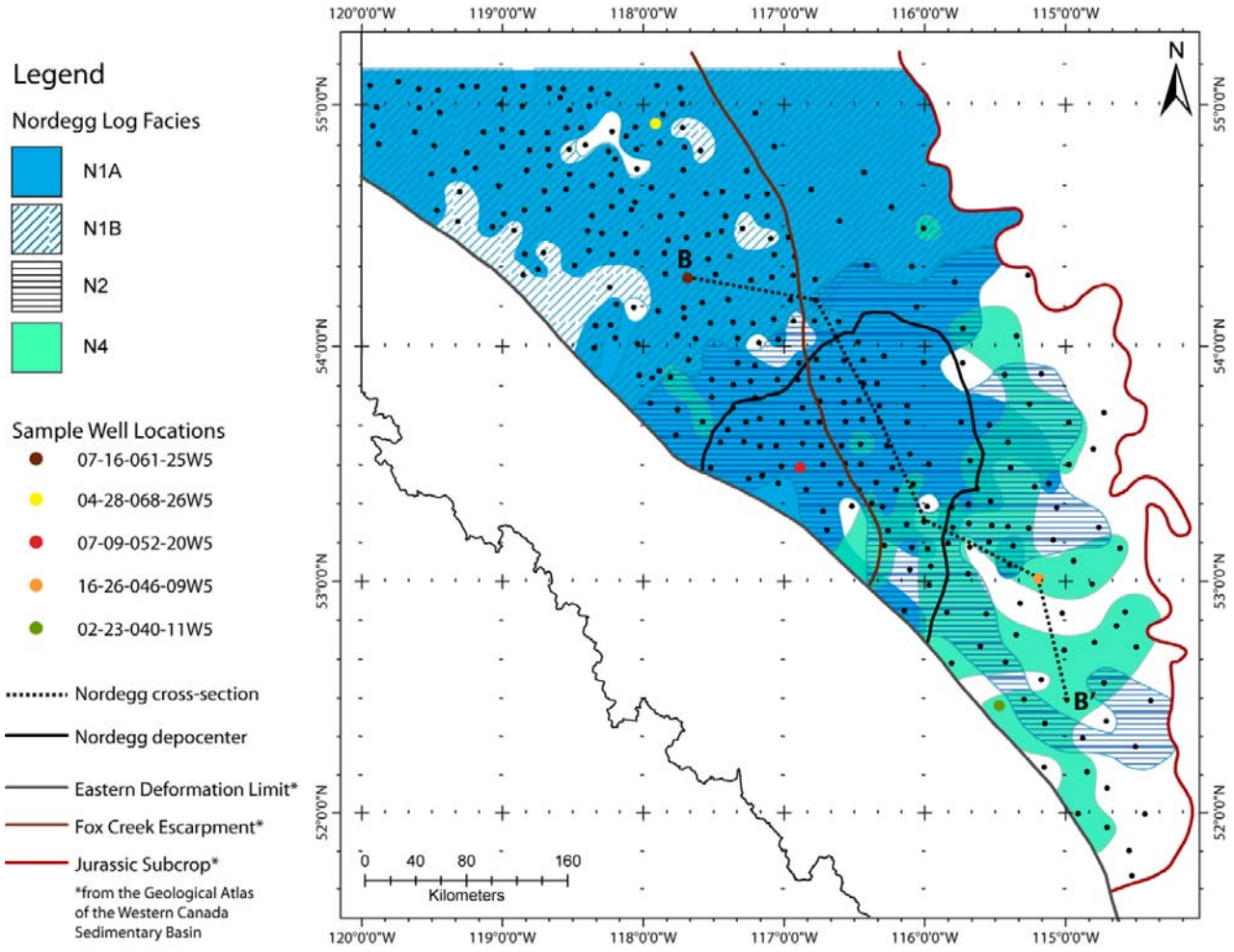

Figure 3-12: Distribution map of facies N1A, N1B, N2, and N4.

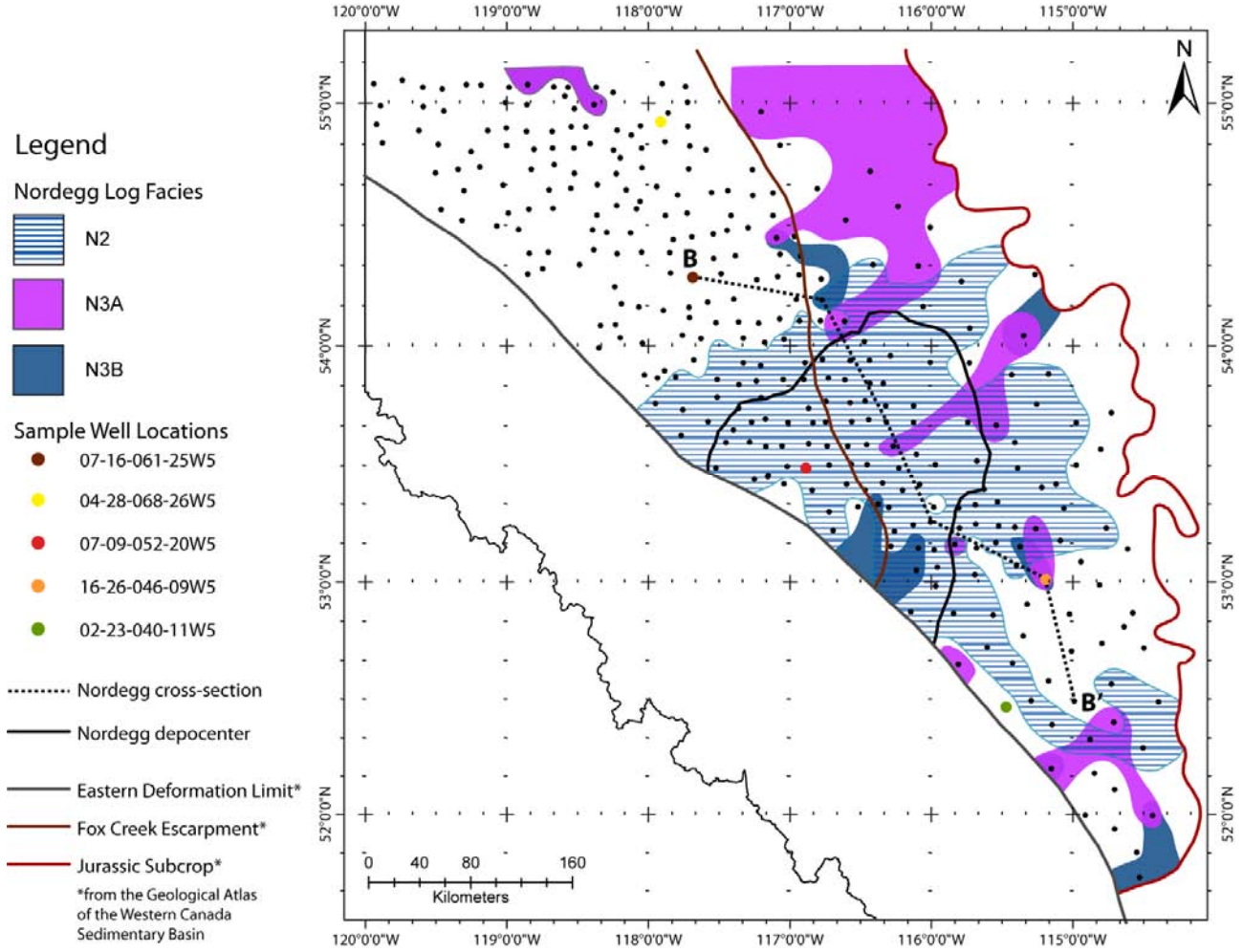

Figure 3-13: Distribution map of facies N2, N3A, N3B

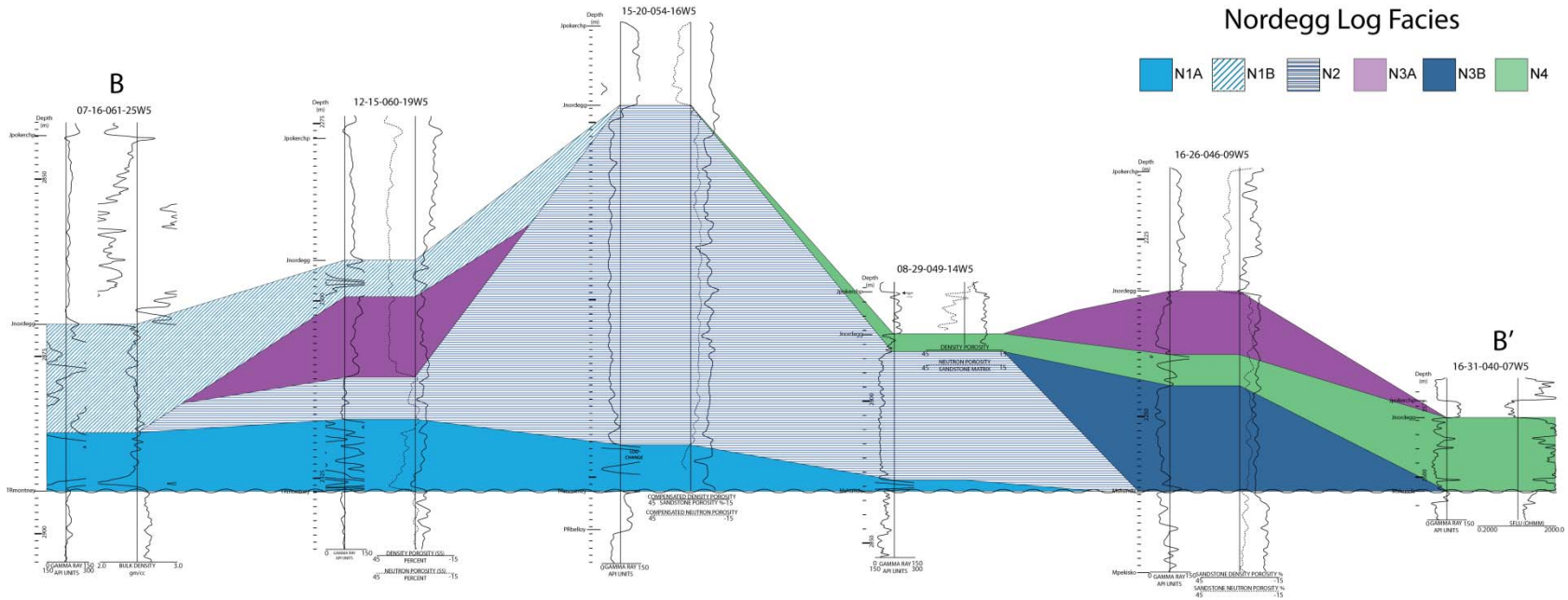

Figure 3-14: Cross-section through the study area showing the relationships of the Nordegg log facies

3.1.2.2 Rock Creek Facies

Rock Creek Facies 1 (RC1; Figure 3-15A) has an irregular gamma signature. This facies may actually represent the Niton B sandstone (T. Poulton, pers. comm.).

The gamma of Rock Creek Facies 2 (RC2; Figure 3-15B) increases-up rapidly from an abrupt base, and then decreases abruptly before increasing again. This is followed by a final decreasing-up pulse which is capped by an abrupt gamma increase. RC2 has been correlated to a quartzarenite (Figure 3-16; Putnam and Moore, 1993). The arenites are interpreted by Putnam and Moore (*ibid.*) to represent a tidally-dominated middle shoreface.

Rock Creek Facies 3 (RC3; Figure 3-15C) has a blocky, low-gamma signature. The neutron log shows less frequency variation than the density log. Like RC2, RC3 has been correlated to a quartzarenite (Figure 3-16), but has much less frequency variation than RC2. Core descriptions indicate that the interval correlated to RC2 contains more flasers and shale rip-ups than the interval correlated to RC3 (Putnam and Moore, 1993).

Rock Creek Facies 4 (RC4; Figure 3-15D) has a gamma signature that decreases-up, interpreted to reflect a coarsening-up grain-size trend. It has not been correlated to published logs/cores.

The gamma log for Rock Creek Facies 5 (RC5; Figure 3-15E) has three “sandy” (low-gamma) sequences with a neutron-density crossover in the middle pulse. RC5 can be correlated to a cored well (Figure 3-16; Putnam and Moore, 1993) that includes the “siltstone unit” identified by Marion (1984). The sequences in RC5 have the “boxy” gamma described by Losert (1986) as typical of marine shelf deposits.

A distribution map of the Rock Creek log facies reveals how complicated the distribution of the Rock Creek facies is (Figure 3-17). Correlating the log facies and determining the relationship between them is difficult because the log facies do not occur in any particular vertical order, and can occur more than once in the same log. Some generalizations can be made about where the facies tend to occur. RC1 occurs mainly in the western portion of the Rock Creek distribution area. RC2 is primarily found in the center of the Rock Creek distribution area. RC3 is found primarily in the central and western portions of the distribution area. RC4 is not widely distributed. RC5 is found where the Rock Creek is thickest, in the southwest portion of the Rock Creek distribution area.

What is apparent from Figure 3-17 is that the most commonly occurring facies in the Rock Creek are RC2, RC3, and RC5; the same three facies that were correlated with logs identified in previously published studies (Figure 3-16).

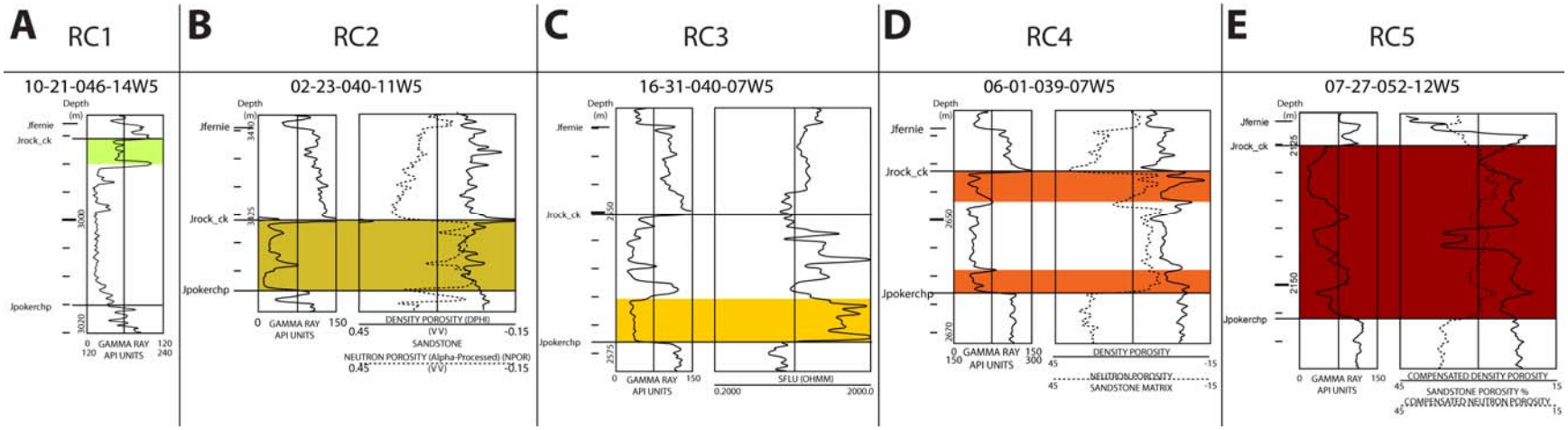

Figure 3-15: Well logs showing the five log facies identified within the Rock Creek.

Each log facies is highlighted with colour on its respective well log. The same colours are used in Figure 3-17. Well locations are shown in Figure 3-17. (A) RC1. (B) RC2. (C) RC3. (D) RC4. (E) RC5.

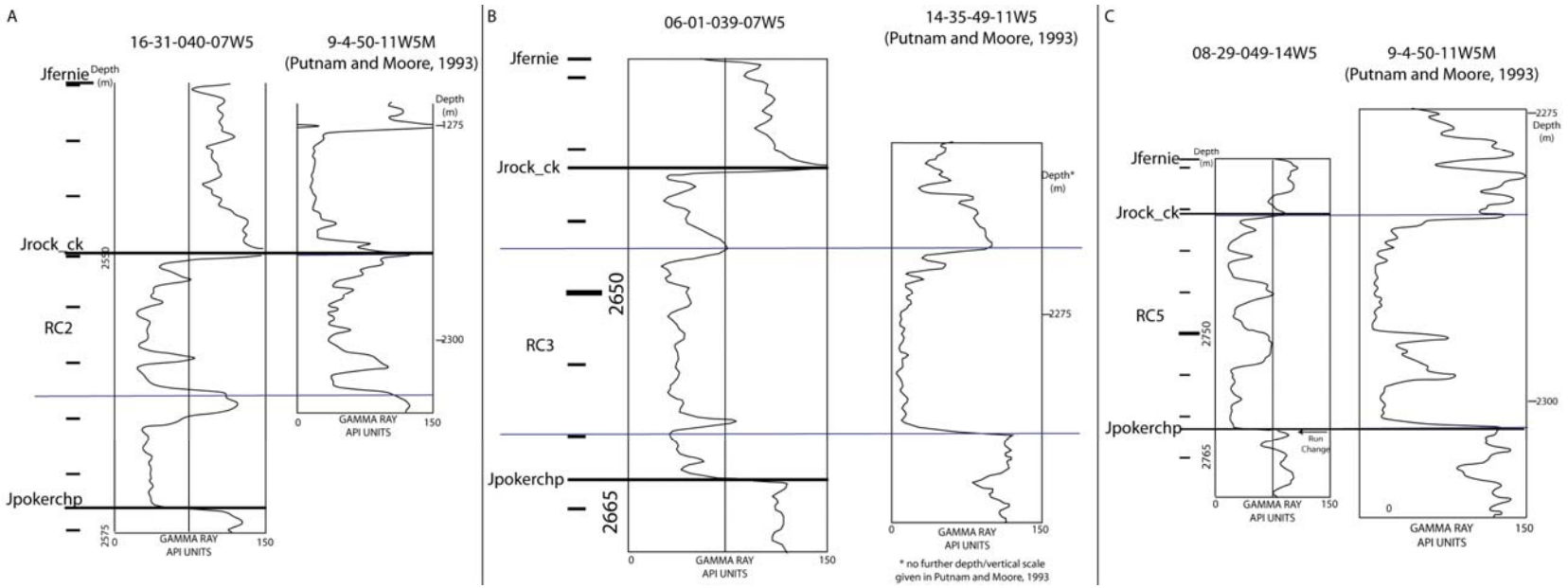

Figure 3-16: Correlation of Rock Creek facies to published well logs

(A) Log from this study (left) compared to a well log from Putnam and Moore (1994; right) showing the correlation of RC2 to a fractured quartzarenite. (B) Log from this study (left) compared to a well log from Putnam and Moore (1994; right) showing the correlation of RC3 to a quartzarenite. (C) Log from this study (left) compared to a well log from Putnam and Moore (1994; right) showing the correlation of RC5 to the quartzarenite. The central segment of RC5 represents the "siltstone unit" of Marion (1984).

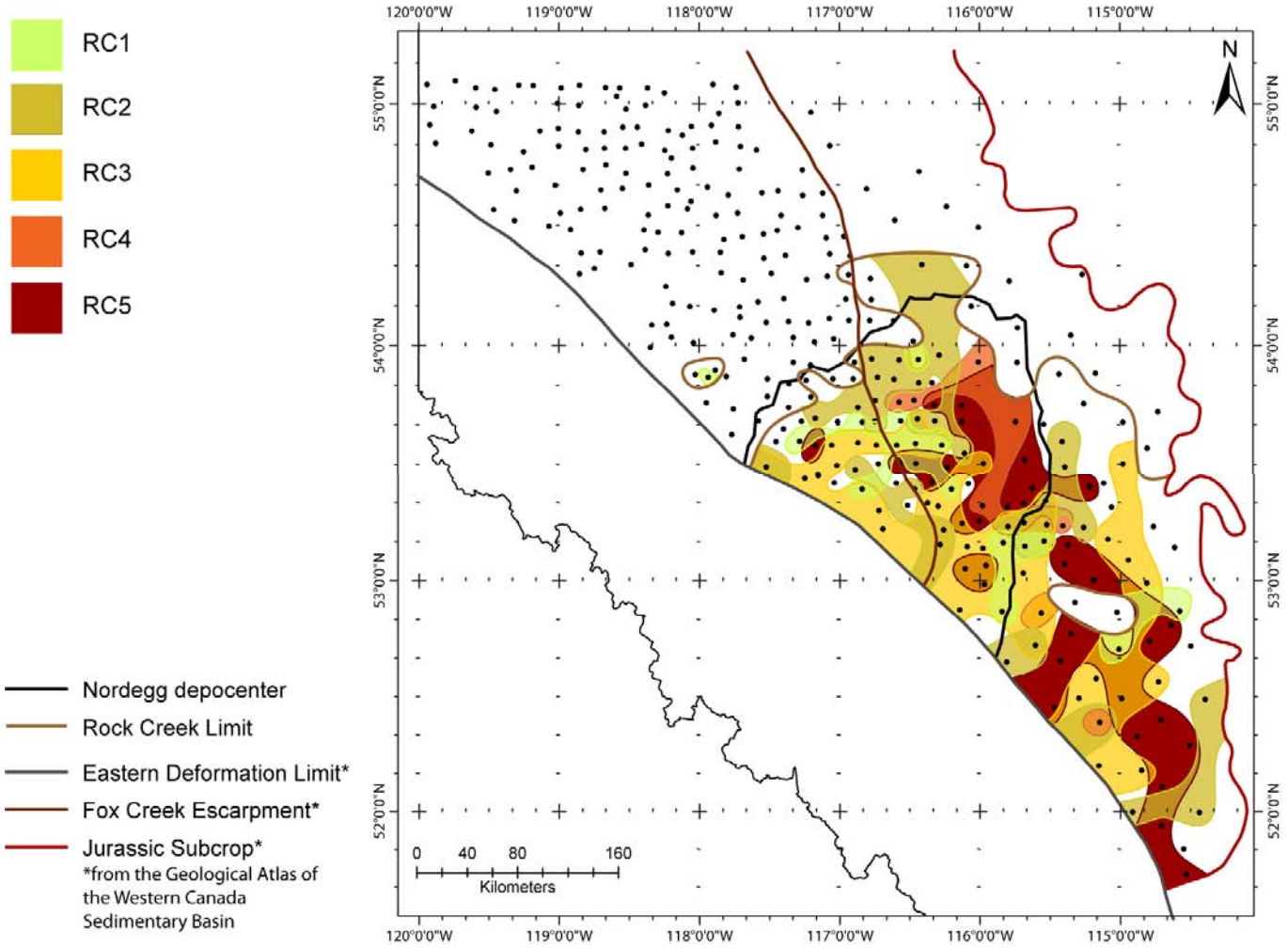

Figure 3-17: Distribution map of Rock Creek log facies.

3.1.3 Unconformities

Three regional unconformities are recognized in this study area (Figure 3-18**)**: the sub-Jurassic unconformity the sub-Cretaceous unconformity and the unconformity beneath the Upper Fernie.

The sub-Jurassic unconformity is an angular unconformity at the base of the Fernie Formation. In the northwest it overlies Triassic strata, while in the southeast it overlies Mississippian strata (Figure 3-19).

The Middle Jurassic of western Canada is recognized as containing many unconformities (Marion, 1984; Poulton, 1984; Stronach, 1984; Collar, 1990). In this study, these unconformities are represented by a single unconformity, here called the sub-Oxfordian unconformity, at the base of the Upper Fernie (Figure 3-20).

The Jurassic of west-central Alberta is bounded at the top by another angular unconformity, the sub-Cretaceous unconformity. It truncates the latest Jurassic-Earliest Cretaceous Minnes Group in the northwest and the Upper Fernie in the southeast and east (Figure 3-21**)**.

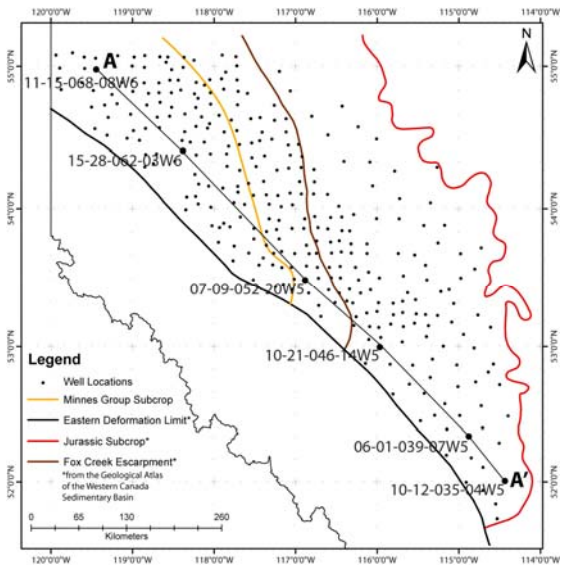

Figure 3-18: Index map for Figure 3-19, Figure 3-20, and Figure 3-21.

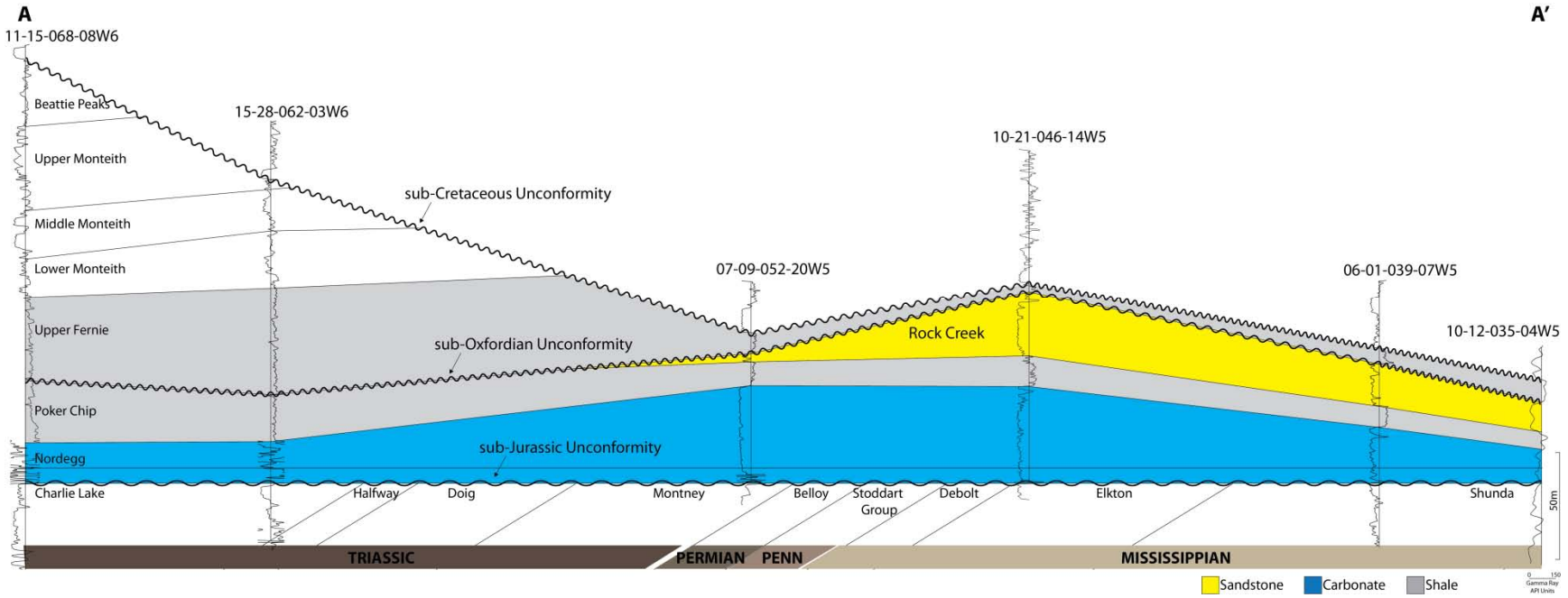

Figure 3-19: Axial cross-section through the study area flattened on the sub-Jurassic unconformity

This cross-section shows the angular truncation of Triassic (A) through Mississippian (A') strata below the sub-Jurassic unconformity. Index map is in Figure 3-18.

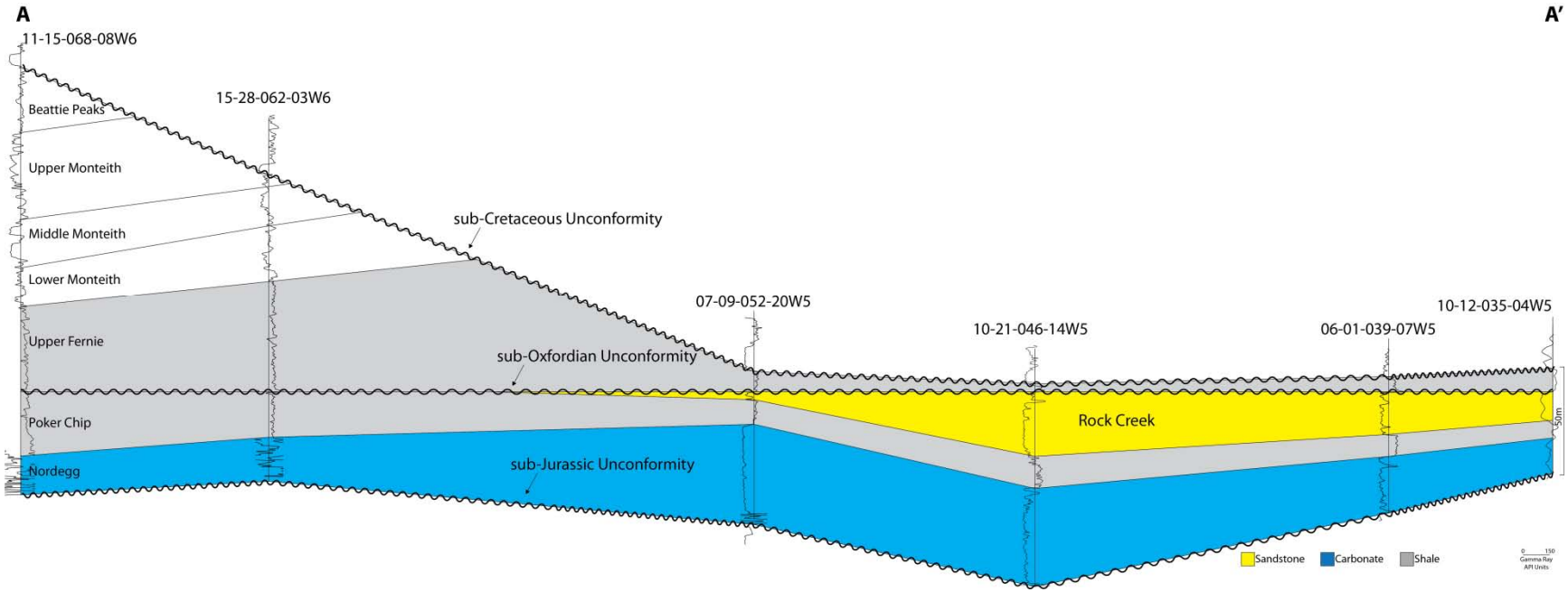

Figure 3-20: Axial cross-section through the study area flattened on the sub-Oxfordian unconformity

Index map is in Figure 3-18.

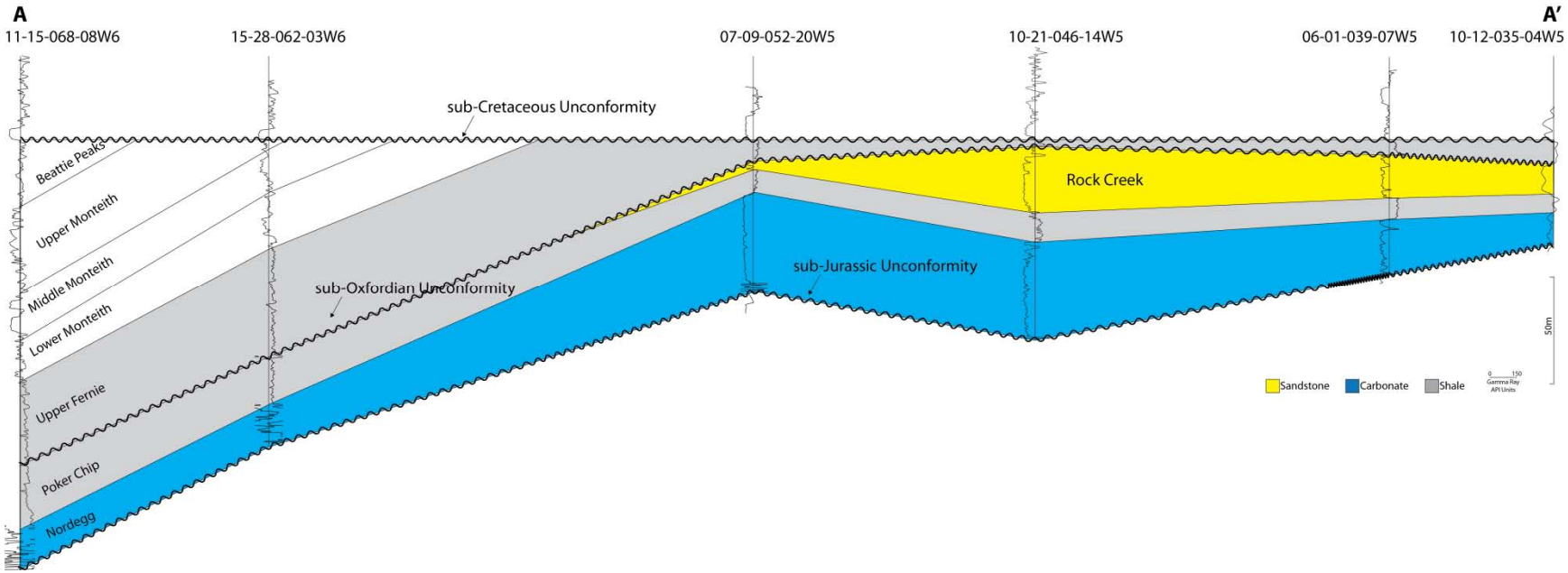

Figure 3-21: Axial cross-section through the study area flattened on the sub-Cretaceous unconformity

This cross-section shows the angular truncation of the Minnes Group (A) through the Upper Fernie (A') below the sub-Cretaceous unconformity. Index map is in Figure 3-18.

3.2 Methodology

Subsidence analysis quantifies and removes the effects of sediment accumulation, compaction, and paleobathymetry (Angevine et al., 1990) to yield a depth versus time curve that describes the tectonic subsidence history for a particular point in the basin (van Hinte, 1978; Xie and Heller, 2009).

Traditionally these calculations are performed either manually, in Microsoft Excel, or with a software package. The software available to produce subsidence curves is limited in both its ability to import the original data from a spreadsheet or text file and in the lack of user control over the input parameters, access to calculated values, and display of the final subsidence curve.

The number of calculations needed to produce a subsidence curve for a single sediment column makes it preferable to automate the calculations. For example, in a sediment column with 25 layers, 1848 calculations are performed and the lithologic constants are used 144 times. Automating and simplifying this process as much as possible reduces the likelihood of clerical errors.

Excel 2007 was chosen over Matlab for its simple handling of iterative calculations, flexibility in display options, and the ability to easily update the input data with immediate recalculation of the output data (Larrieu, 1995; Turer and Maynard, 2003). Excel graphs can be used to generate subsidence curves. Additionally, all of the calculated values are stored in the spreadsheet.

3.2.1 Spreadsheet setup

The horizons and their TVD depths were exported from GeoScout to text files in batches of 50 to 60 wells. Once opened in Microsoft Excel, the text files were rearranged and set up for running the subsidence analysis.

The spreadsheet must be saved as a macro-enabled spreadsheet. Iterative calculations must be enabled in the Excel options (Figure 3-22) and Relative References must be turned on in the Code section of the Developer tab (Figure 3-23).

For each new spreadsheet, the two modules storing the subsidence analysis macros must be added to the spreadsheet. This is done by importing modules in the Visual Basic Editor (accessed from the Developer tab).

In order to run, the spreadsheet must contain three worksheets: one for the input and output data, one for the table of formations, and one for the lithologic constants.

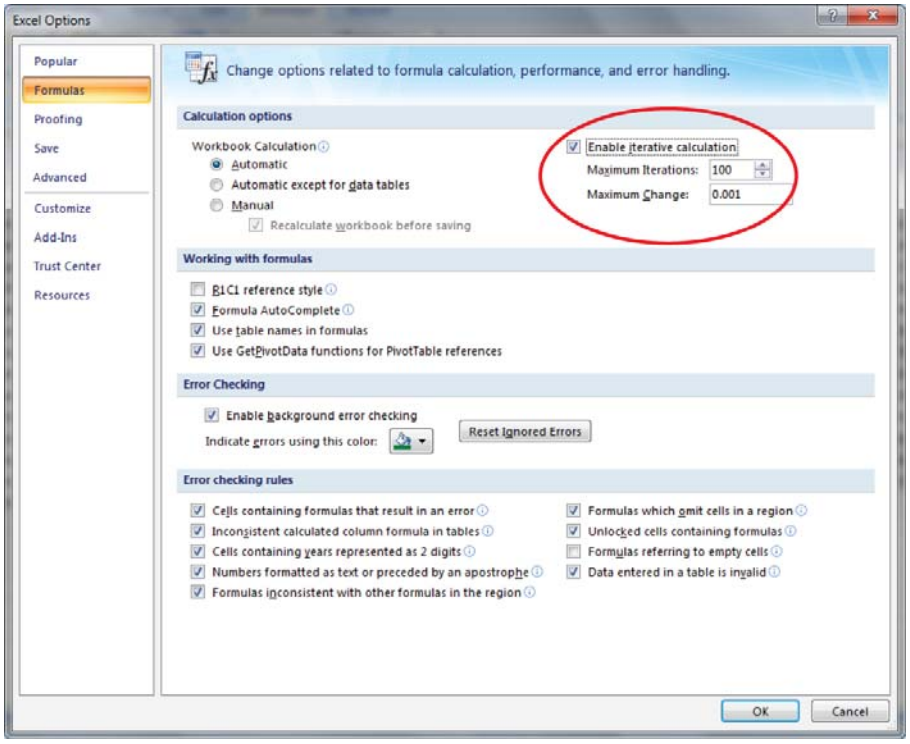

Figure 3-22: The Excel Options window (Excel 2007)

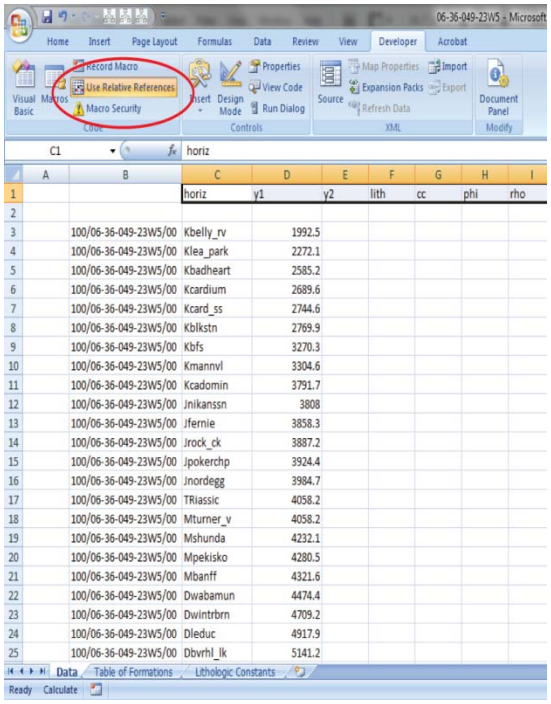

	A	B	C	D	E	F	G	H	I
1			horiz	y1	y2	lith	cc	phi	rho
2									
3		100/06-36-049-23W5/00	Kbelly_rv	1992.5					
4		100/06-36-049-23W5/00	Klea_park	2272.1					
5		100/06-36-049-23W5/00	Kbadheart	2585.2					
6		100/06-36-049-23W5/00	Kcardium	2689.6					
7		100/06-36-049-23W5/00	Kcard_ss	2744.6					
8		100/06-36-049-23W5/00	Kblkstn	2769.9					
9		100/06-36-049-23W5/00	Kbfs	3270.3					
10		100/06-36-049-23W5/00	Kmannvl	3304.6					
11		100/06-36-049-23W5/00	Kcadomin	3791.7					
12		100/06-36-049-23W5/00	Jnikanssn	3808					
13		100/06-36-049-23W5/00	Jfernie	3858.3					
14		100/06-36-049-23W5/00	Jrock_ck	3887.2					
15		100/06-36-049-23W5/00	Jpokerchp	3924.4					
16		100/06-36-049-23W5/00	Jnordegg	3984.7					
17		100/06-36-049-23W5/00	TRiassic	4058.2					
18		100/06-36-049-23W5/00	Mturner_v	4058.2					
19		100/06-36-049-23W5/00	Mshunda	4232.1					
20		100/06-36-049-23W5/00	Mpekisko	4280.5					
21		100/06-36-049-23W5/00	Mbanff	4321.6					
22		100/06-36-049-23W5/00	Dwabamun	4474.4					
23		100/06-36-049-23W5/00	Dwintrbrn	4709.2					
24		100/06-36-049-23W5/00	Dleduc	4917.9					
25		100/06-36-049-23W5/00	Dbvrhl_lk	5141.2					

Figure 3-23: The Developer tab (Excel 2007)

3.2.1.1 Data Worksheet

The first row of the Data worksheet should be blank (Figure 3-24); it will contain named variables that are used by the macros. Column A of the worksheet should also be blank; it will be used to number the layers in each sediment column. When subsidence analysis is being performed on multiple sediment columns in the same spreadsheet, there should be three blank rows between them; the named variables do not need to be repeated.

There are three columns of input data in the worksheet. Column B contains the identifier for each sediment column—in this study it is the Unique Well Identifier (UWI) for each well. The layer names are stored in Column C and the depths to the top of each layer are stored in Column D.

In addition to the layers in the sediment column, the macros require a “Surface” layer, the depth to which is zero. Unconformities should be added in the appropriate locations before the calculations are run. The depth to the top of each unconformity is the same as the depth to the top of the layer below it.

There are twelve named variables used by the macros to refer to values. These named variables are listed in Table 2, along with the columns that will be filled in during the calculations. The variables are defined in the Defined Names section of the Formulas tab in Excel (Figure 3-25).

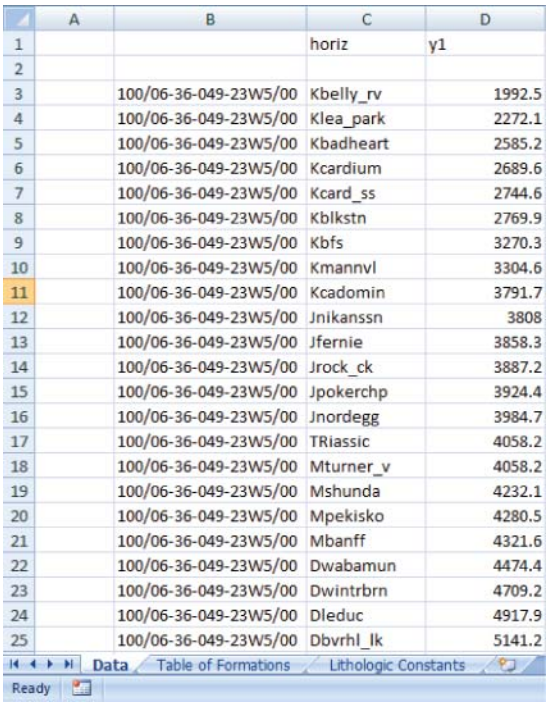

	A	B	C	D
1			horiz	y1
2				
3		100/06-36-049-23W5/00	Kbelly_rv	1992.5
4		100/06-36-049-23W5/00	Klea_park	2272.1
5		100/06-36-049-23W5/00	Kbadheart	2585.2
6		100/06-36-049-23W5/00	Kcardium	2689.6
7		100/06-36-049-23W5/00	Kcard_ss	2744.6
8		100/06-36-049-23W5/00	Kblkstn	2769.9
9		100/06-36-049-23W5/00	Kbfs	3270.3
10		100/06-36-049-23W5/00	Kmannvl	3304.6
11		100/06-36-049-23W5/00	Kcadomin	3791.7
12		100/06-36-049-23W5/00	Jnikanssn	3808
13		100/06-36-049-23W5/00	Jfernie	3858.3
14		100/06-36-049-23W5/00	Jrock_ck	3887.2
15		100/06-36-049-23W5/00	Jpokerchp	3924.4
16		100/06-36-049-23W5/00	Jnordegg	3984.7
17		100/06-36-049-23W5/00	TRiassic	4058.2
18		100/06-36-049-23W5/00	Mturner_v	4058.2
19		100/06-36-049-23W5/00	Mshunda	4232.1
20		100/06-36-049-23W5/00	Mpekisko	4280.5
21		100/06-36-049-23W5/00	Mbanff	4321.6
22		100/06-36-049-23W5/00	Dwabamun	4474.4
23		100/06-36-049-23W5/00	Dwintrbrn	4709.2
24		100/06-36-049-23W5/00	Dleduc	4917.9
25		100/06-36-049-23W5/00	Dbvrhl_lk	5141.2

Data | Table of Formations | Lithologic Constants

Ready

Figure 3-24: The Data worksheet

The first row contains named variables, the second row is blank, and the first column is blank. The location identifier (UWI in this study), horizon (layer name), and the depth to the top of the layer are required.

Table 2: Data Worksheet columns

Group	*Column No.*	*Header*	*Named Variable*	*Position from myCell*	*Subroutine Name*	*Equation*
Input Data	1	No.		0	Start	
	2	Well ID		1		
	3	Horizon Name	horiz	2		
	4	Present Upper Burial Depth	y1	3		
Autofilled Data	5	Present Lower Burial Depth	y2	4	pLBD	
	6	Lithology Type	lith	5	autoLith	
	7	Compaction Coefficient	cc	6	autoCC	
	8	Porosity	phi	7	autoPHI	
	9	Density	rho	8	autoRHO	
	10	Age		9	autoAGE	
Total Calculated Values	11	Total Thickness	ToT	10	tThick	
	12	Total Subsidence	ToS	11	tThick, ToSub	
	13	Tectonic Subsidence	TeS	12	TeSub	
	14	Total Column Density	TCD	13	propDens	
	15	Present Thickness	Tn	14	pThick	y_2-y_1
T=0Ma	16	Porosity		15	Time_0Ma	$\frac{\phi}{c}\frac{e^{-cy_1}-e^{-cy_2}}{y_2-y_1}$
	17	Density		16		$\rho_s = \phi\rho_w + (1-\phi)\rho_g$

Group	*Column No.*	*Header*	*Named Variable*	*Position from myCell*	*Subroutine Name*	*Equation*
	18	Proportional Density		17		$\rho_{S^*} = \frac{\rho_S y}{S^*}$
T=iMa	19	Depth to Top		18 + (6+i)	NewDepths	
	20	Depth to Bottom		19 + (6+i)		$y_2' = y + y_1' + \frac{\phi_0}{c}\{\exp(-cy_1') - \exp(-cy_2') - \exp(-cy_1) + \exp(-cy_2)\}$
	21	Decompacted Thickness		20 + (6+i)		$y' = y_2' - y_1'$
	22	Porosity		21 + (6+i)	NewDensity	$\phi' = \frac{\phi_0}{c}\frac{\left(exp(-cy_1') - exp(-cy_2')\right)}{y_2' - y_1'}$
	23	Density		22 + (6+i)		$\rho_s = \phi'\rho_w + (1-\phi')\rho_g$
	24	Proportional Density		23 + (6+i)	PropDens	$\rho_{S^*} = \frac{\rho_S y}{S^*}$

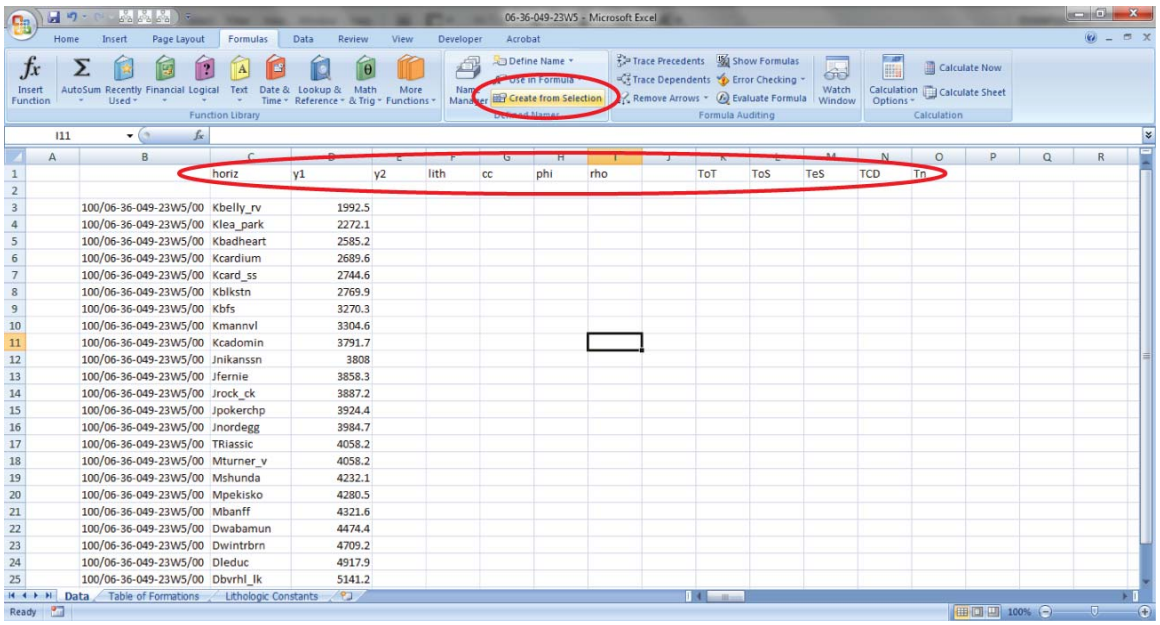

Figure 3-25: The Formulas tab (Excel 2007)

The entries in the first row must be typed in, exactly as shown, and then selected and set as named variables by "creating from selection."

3.2.1.2 Table of Formations worksheet

The Table of Formations contains four columns (Figure 3-26A). Column A contains the names of the layers in the sediment columns, including the Surface and Unconformity layers. Column B contains the lithologies assigned to the layers. Columns C and D contain the ages at the top and bottom of each layer, respectively.

3.2.1.3 Lithologic Constants worksheet

The Lithologic Constants worksheet contains four columns (Figure 3-26B). Column A contains each of the lithologies used in the Table of Formations. Column B, C, and D contain the compaction coefficient, initial porosity, and density for each lithology.

This worksheet also contains the densities of water and of the mantle used in the backstripping calculations. These two variables are named variables, like those found in the first row of the Data worksheet.

A

	A	B	C	D
1	Formation Name	Lithology	Age at Top (Ma)	Age at Base (Ma)
2	Unconformity	NA		
3	Surface	NA	0	
4				
5	Kbelly_rv	sandstone	77.05	82.21
6	Klea_park	shale	82.21	84.08
7	Kchinook	sandstone	84.08	84.65
8	Kcolorado	shale	84.65	90.56
9	Kbadheart	sandstone	85.8	89.3
10	Kmuskiki	shale	89.3	90.14
11	Kcardium	shale	89.3	90.14
12	Kcard_ss	sandstone	90.14	90.56
13	Kkaskapau	shale	90.56	95.33
14	K2nd_ws	shale	92.24	97.77
15	Kdoe_ck	sandstone	92.57	93.03
16	Kdunvegan	sandstone	95.33	97.47
17	Kshftbury	shale	97.47	100.19
18	Kbfs	shale	99.6	99.6
19	Kviking	shale	99.6	100.19
20	Kvik_ss	sandstone	100.19	101.37
21	Kcadotte	sandstone	101.37	103.98
22	Kjoli_fou	shale	101.37	102.55
23	Kharmon	shale	103.98	104.03

Data | Table of Formations | Lithologic Cc

Ready Calculate

B

	A	B	C	D	E
1		C	phi	rho	
2	shale	0.0005	0.5	2.72	
3	sandstone	0.0003	0.4	2.65	
4	dolostone	0.0007	0.5	2.71	
5	limestone	0.0007	0.5	2.71	
6	sandstone/limestone	0.0005	0.45	2.68	
7	limestone/shale	0.0006	0.5	2.715	
8	NA	0	0	0	
9					
10	rho_h2o	1.03			
11	rho_mantle	3.33			
12					
13					
14					
15					
16					
17					
18					
19					
20					
21					
22					
23					
24					
25					

Data | Table of Formations | Lithologic Constants

Ready Calculate

Figure 3-26: (A) Table of Formations and (B) Lithologic Constants worksheets The full tables can be found in Appendix D.

3.2.2 Macros

Initially the Excel VBA macros were written and tested using a sample dataset with a known solution (Angevine et al., 1990). The calculations were written as subroutines which are run sequentially by the “subsidence” macro (Table 3).

The final macros (Appendix B) were saved as modules which can be imported to any spreadsheet file. The columns in the Data Worksheet (Table 2) can be grouped together into five categories: Input Data, Autofilled Data, Total Calculated Values, T=0Ma, and T=iMa.

Table 3: Subroutines used in Excel macros for subsidence calculations

Subroutine Name	**Subroutine Function**
Subsidence	Calls the subroutines needed for complete subsidence analysis (listed below in the order they are called)
Start	Allows the user to set the reference cell and define the number of horizons for the sediment column. Fills in the column headers and the first column in the 'Data' worksheet, which numbers the horizons.
pLBD	Calculates the present Lower Burial Depth for each horizon, based on the Present Upper Burial Depth of the horizon below
autoLith	Autofills the lithology information for each horizon
autoCC	Autofills the compaction coefficient for each horizon
autoPHI	Autofills the surface porosity for each horizon
autoRHO	Autofills the surface density for each horizon
autoAge	Autofills the age at the top of each horizon
pThick	Calculates the present thickness of each horizon
tThick	Fills in the Total (uncorrected) Thickness at each interval
Time_0Ma	Calculates porosity, density, and proportional density at T=0Ma
D_TS_col	Sets up columns for Decompaction and Tectonic Subsidence calculations at each time interval
NewDepths	Calculates the decompacted depths and thicknesses at each time interval
NewDensity	Calculates the decompacted porosity and density at each time interval
ToSub	Fills in the Total (decompacted) Thickness at each interval
PropDens	Calculates the proportional densities and fills in the Total Column Density at each time interval
TeSub	Calculates the tectonic subsidence

3.2.2.1 Input data

This group of columns contain the well IDs, horizon names and tops (Present Upper Burial Depth) that were exported from GeoScout. Each row is numbered, beginning with one, for referencing. The first row of column A is set as the reference cell. All other columns and cells are referred to by their positions relative to the reference cell and to the total number of layers in the sediment column. The reference cell is called "myCell" in the macros and the number of layers is called "myNum."

3.2.2.2 Autofilled data

The present lower burial depth, or bottom, of each layer is filled in using the top of the next layer below it. When the layer is an unconformity the top and the bottom depth are the same. The remaining columns in this group are filled from the Table of Formations and Lithologic Constants worksheets. The Horizon Name is used to get the lithology type and age (at the top of the layer) from the Table of Formations Worksheet. The lithology is then used to get the Compaction Coefficient, Porosity, and Density from the Lithologic Constants worksheet.

3.2.2.3 Total Calculated values

This group of columns is filled in gradually, as calculations are performed for each time interval, with the exception of the Present Thickness, which is calculated using the present upper and lower burial depths. The Total Thickness, Total Subsidence, and Tectonic Subsidence are the three values commonly plotted on subsidence curves. The Total Column Density is used in the final tectonic subsidence calculations.

3.2.2.4 T=0Ma

For this group of columns, the Porosity, Density, and Proportional Density are calculated at the present time (T=0Ma).

3.2.2.5 T=iMa

This grouping represents the columns and calculations that are present for each time interval in the sediment column. Once the youngest layer has been "removed," the decompacted depths to the top and bottom of each layer are calculated first, followed by the decompacted porosity, density and proportional density for each layer.

3.2.3 ArcMap workflow

The maps in this study were generated using the Geostatistical Analyst in ArcMap. A single set of x-y coordinates was used and all data being mapped was linked to those coordinates using the UWIs.

The first step was to use a preliminary dataset, using a map exported directly from GeoScout, to generate hand-contoured maps. From these, the Upper Fernie isopach (Figure 3-27) was chosen as the reference map to use for determining the best methods to use in ArcMap. This map was chosen because the data showed the erosional feature discussed in Section 3.1.1.4. This feature was a useful marker for testing the accuracy of the available geostatistical methods in ArcMap.

When testing the built-in geostatistical methods, the Upper Fernie isopach value at each well location was displayed using the same colour bar that the final surface was displayed with. By doing this, the actual value could be compared to the surface value to

see how well the given geostatistical method honoured the data. The same method has been used for the final isopachs and tectonic subsidence maps generated.

Of the methods tested (Global Polynomial Interpolation, Inverse Distance Weighting, Kernel Smoothing, Kriging, Local Polynomial Interpolation and Radial Basis Functions), Inverse Distance Weighting was chosen for all subsequent mapping because it had the best combination of honouring the actual data values and honouring the erosional "channel" in the Upper Fernie isopach (Figure 3-28).

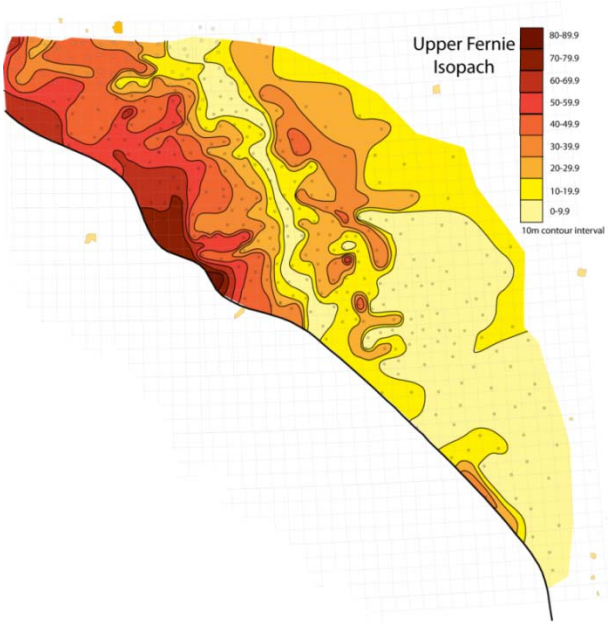

Figure 3-27: Preliminary hand-drawn (and digitized) isopach of the Upper Fernie unit

Figure 3-28 (next page): Upper Fernie isopach maps generated in ArcMap Isopach maps generated using different gridding methods available in ArcGIS. Top left – Global Polynomial Interpolation. Top right – Inverse Distance Weighting. Centre left – Kernel Smoothing. Centre right – Kriging. Bottom left – Local Polynomial Interpolation. Bottom right – Radial Basis Functions.

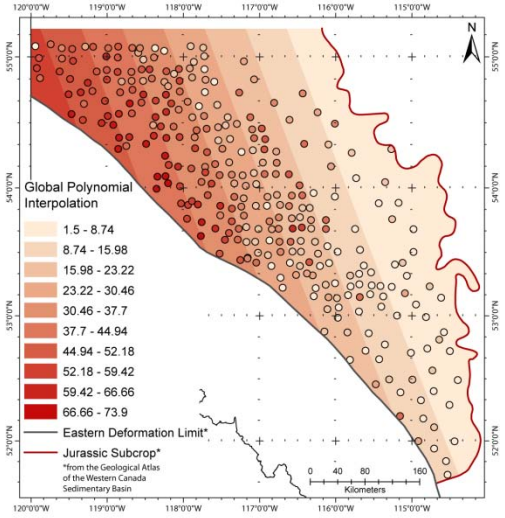
Global Polynomial Interpolation
1.5 - 8.74
8.74 - 15.98
15.98 - 23.22
23.22 - 30.46
30.46 - 37.7
37.7 - 44.94
44.94 - 52.18
52.18 - 59.42
59.42 - 66.66
66.66 - 73.9
Eastern Deformation Limit*
Jurassic Subcrop*
*from the Geological Atlas of the Western Canada Sedimentary Basin
0 40 80 160
Kilometers
N

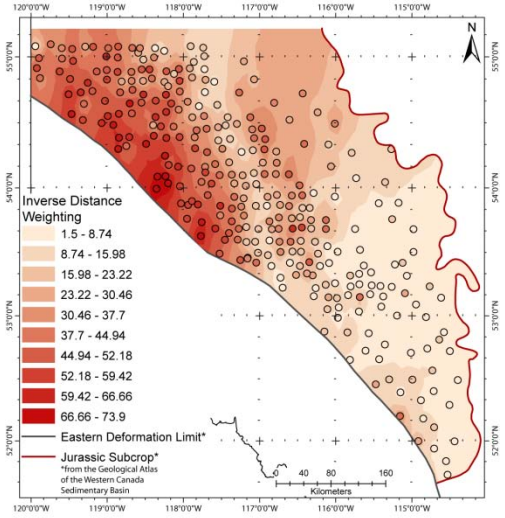
Inverse Distance Weighting
1.5 - 8.74
8.74 - 15.98
15.98 - 23.22
23.22 - 30.46
30.46 - 37.7
37.7 - 44.94
44.94 - 52.18
52.18 - 59.42
59.42 - 66.66
66.66 - 73.9
Eastern Deformation Limit*
Jurassic Subcrop*
*from the Geological Atlas of the Western Canada Sedimentary Basin
0 40 80 160
Kilometers
N

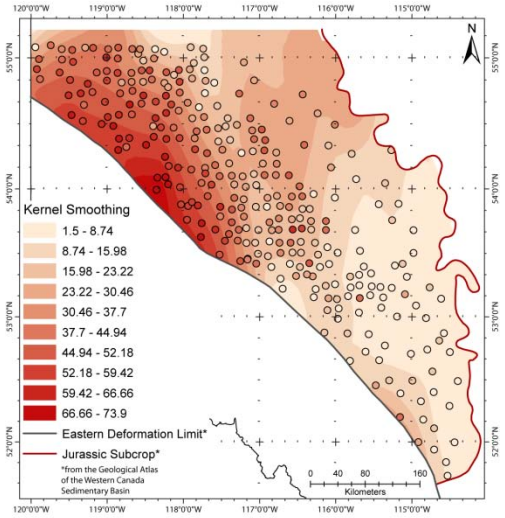
Kernel Smoothing
1.5 - 8.74
8.74 - 15.98
15.98 - 23.22
23.22 - 30.46
30.46 - 37.7
37.7 - 44.94
44.94 - 52.18
52.18 - 59.42
59.42 - 66.66
66.66 - 73.9
Eastern Deformation Limit*
Jurassic Subcrop*
*from the Geological Atlas of the Western Canada Sedimentary Basin
0 40 80 160
Kilometers
N

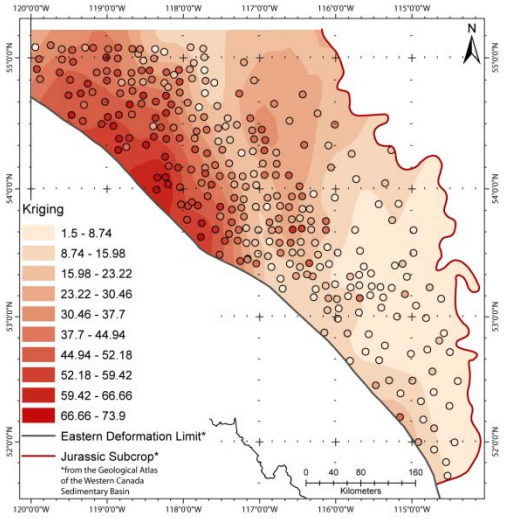
Kriging
1.5 - 8.74
8.74 - 15.98
15.98 - 23.22
23.22 - 30.46
30.46 - 37.7
37.7 - 44.94
44.94 - 52.18
52.18 - 59.42
59.42 - 66.66
66.66 - 73.9
Eastern Deformation Limit*
Jurassic Subcrop*
*from the Geological Atlas of the Western Canada Sedimentary Basin
0 40 80 160
Kilometers
N

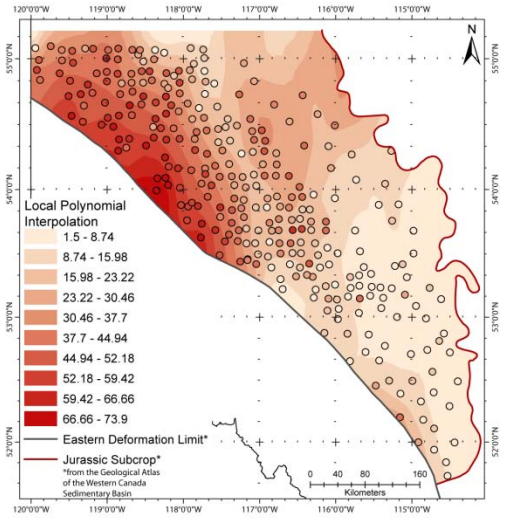
Local Polynomial Interpolation
1.5 - 8.74
8.74 - 15.98
15.98 - 23.22
23.22 - 30.46
30.46 - 37.7
37.7 - 44.94
44.94 - 52.18
52.18 - 59.42
59.42 - 66.66
66.66 - 73.9
Eastern Deformation Limit*
Jurassic Subcrop*
*from the Geological Atlas of the Western Canada Sedimentary Basin
0 40 80 160
Kilometers
N

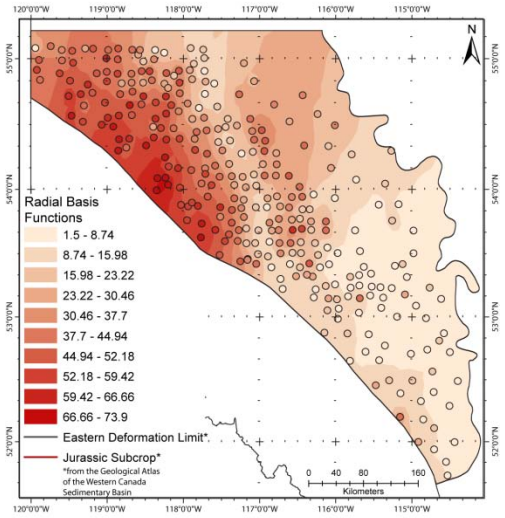
Radial Basis Functions
1.5 - 8.74
8.74 - 15.98
15.98 - 23.22
23.22 - 30.46
30.46 - 37.7
37.7 - 44.94
44.94 - 52.18
52.18 - 59.42
59.42 - 66.66
66.66 - 73.9
Eastern Deformation Limit*
Jurassic Subcrop*
*from the Geological Atlas of the Western Canada Sedimentary Basin
0 40 80 160
Kilometers
N

Chapter Four: **Sensitivity Testing**

4.1 Introduction

Quantitative subsidence analysis became possible when micropalaeontology began yielding numbers for ages and water depths (van Hinte, 1978). Subsidence analysis requires several assumptions. Some of these are inherent in all subsidence calculations and some are specific to the large-scale nature of this study. The assumptions and generalizations that are standard in subsidence calculations introduce error to the results; these errors are accounted for on subsidence curves with error bars.

The purpose for doing subsidence analysis dictates how significant the error will be to the interpretation of the results. When the subsidence profile is used as an indicator of basin tectonic styles the error is not expected to change the overall shape of the curve and therefore the model determined by the shape will not be affected (Gallagher, 1989). In this case, the margin of error can be estimated and parameters that are not available or are inaccurate can be accounted for within the error calculations and display. Similarly, the generalizations made in this study are necessary to be able to look at the overall influence of tectonics in the entire study area and not just a single point.

Using standardized constants and calculations is preferred for two reasons (Giles et al., 1998):

1. It allows for a comparison of the results, specifically the subsidence curve profiles, with those attained in other sedimentary basins (*ibid.*)
2. Within the same study, using different constants or equations will introduce additional error (*ibid*.)

4.1.1 Assumptions inherent in all subsidence calculations

The assumptions inherent in all subsidence calculations are (Angevine et al., 1990; Allen and Allen, 2005) discussed in this study. These assumptions are:

1. The sediment volume remains the same before and after compaction; porosity-loss caused by sediment loading during subsequent deposition is the sole cause of compaction (Section 4.2.1.3).
2. The pore-space in the sediments is water-filled (Section 4.2.1.3).
3. Porosity decreases with depth in an exponential relationship (Section 4.2.1.3).
4. Calculations for a unit cross-sectional area, i.e. at each point the subsidence calculations are one-dimensional (Appendix A).
5. Isostasy is achieved according to the Airy model. A unit thickness of crust is being balanced in both columns of the Airy calculations (Section **2.2.1**).
6. The maximum water depth of the basin is not more than 200m (Section 4.2.1.1).

4.1.2 Implications/generalizations in a large-scale study

In a regional study such as this one, generalizations are necessary in order to be able to complete the study in a timely manner. Simplifying sections for analysis and presentation is not unheard of in subsidence analysis (Sclater and Christie, 1980). Here, the units picked in the zone of interest were simplified, as described in Chapter 3. The best example of this is the Nordegg: Nordegg in the study area refers to the Nordegg Member, the Gordondale Member, Red Deer Member and any Red Deer Member-like lithologies. It is assumed for this study that these members are part of the same

depositional sequence. Additionally, it is assumed that any horizon used in the study was deposited synchronously. It is not practical to get exact ages at the top of each unit for more than 300 locations.

4.2 Sources of error in decompaction and backstripping equations

Ultimately, the accuracy of subsidence calculations depends on the accuracy of the input data. The two most difficult parameters to constrain are age and paleobathymetry, both of which rely on micropaleontology (van Hinte, 1978); error is also introduced by some of the generalizations and assumptions made during subsidence analysis.

The decompaction equation is derived in Appendix A and given in Section **2.2.2 (**Equation 2). The backstripping equation is also derived in Appendix A and is given in Section **2.2.3 (**Equation 6).

4.2.1 Age

Ages for the deposition of sediments are difficult to define and can actually be revised over time. Neither the decompaction equation nor the backstripping equation are time-dependent, so that even when the age assigned to a unit does change the tectonic subsidence does not need to be recalculated. Rather, the subsidence curve needs to be updated; a change in age would result in a point on the subsidence curve shifting to the left or right.

The ages used in subsidence analysis should be as accurate as possible, however this can be a challenge due to the availability and resolution of age assignments for sedimentary successions (Xie and Heller, 2009). If the margin of error in the ages

assigned to the units is known, it can be applied to the subsidence curve as horizontal error bars.

4.2.1.1 Paleobathymetry

The paleobathymetry (depositional water depth) is represented in the backstripping equation (Section 2.2.2, Equation 6) by the term *w*. The datum in subsidence calculations is present-day sea level (Angevine et al., 1990), therefore the water depth must be adjusted to account for the total change in sea-level since the time of deposition (Bond and Kominz, 1984). This means $w = w_{paleobath} - \Delta SL$, where *w* is the water depth, $w_{paleobath}$ is the water depth the layer was deposited in, and ΔSL is the change in sea level since the time of deposition. Stapel et al. (1996) show that for water depths less than 200m, the uncertainty related to the paleobathymetry term is much less than the uncertainty caused by the porosity (Figure 4-1).

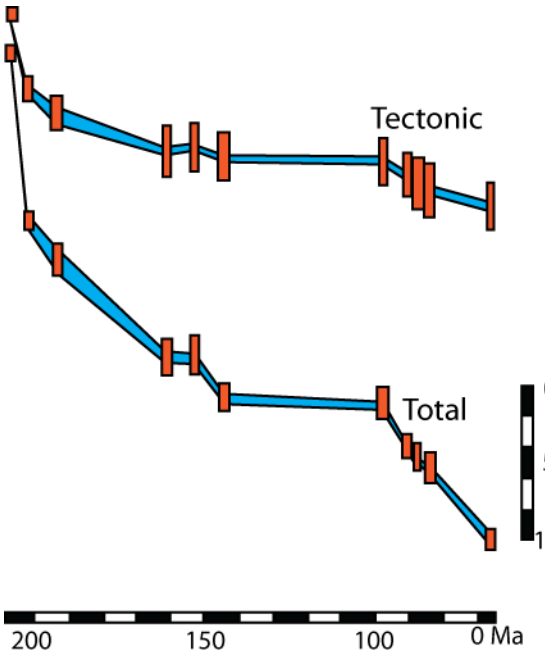

Figure 4-1: A comparison of uncertainty due to paleobathymetry (blue) and porosity (orange). Subsidence curves showing that for sedimentary units deposited in less than 200 m of water the uncertainty due to paleobathymetry is much less than that due to porosity (modified from Stapel et al., 1996).

The lower units of the Fernie Formation, the Nordegg, Poker Chip, and Rock Creek, are interpreted to be shallow shelf deposits (Marion, 1984; Stronach, 1984; Poulton et al., 1990; Riediger et al., 1990; Asgar-Deen et al., 2004), and therefore were deposited in water less than 200m deep. In the WCFB, the maximum water depth is estimated to be 200-300m (Leckie and Smith, 1992). In a foreland basin's foredeep depozone, where there is rapid subsidence, water depths greater than 200m are unavoidable. The error due to paleobathymetry will be greater in these sections of the subsidence curve.

4.2.1.2 Sea Level

Sea level is represented in the backstripping equation (Section 2.2.2, Equation 6) by the term ΔSL. In order to include the sea level term in the calculations local data must be calibrated with global sea level curves.

Eustatic sea level trends in the Jurassic record overall transgression (Hallam, 2001) however the Fernie Formation in southern Alberta records five shallowing-upward (i.e. regressive) trends (Stronach, 1984). Therefore eustatic sea level curves should not be used to correct for sea level in this study, and the change in sea level should be incorporated into the margin of error instead.

4.2.1.3 Porosity

The assumption that the pore space is water-filled has been used since the development of methods to measure porosity and determine porosity-depth relationships (Athy, 1930; Wyllie et al., 1956). The assumption that porosity decreases exponentially

with depth according to the Athy relationship was chosen for simplicity (Angevine et al., 1990).

The assumption related to porosity that leads to the most uncertainty is that porosity-loss is the sole cause of compaction. This ignores other known causes of compaction, specifically those related to changes in the solid volume (Giles et al., 1998).

The porosity on the left side of Equation 2, Section 2.2.2 is the porosity of the layer at any time during burial (Angevine et al., 1990), not the present porosity. At each time interval in the calculation process, the porosity of the layer at that time is calculated using the porosity-depth relationship given in Section 2.2.2 Equation 1. This relationship and the constants used in the relationship were empirically derived (Sclater and Christie, 1980; Angevine et al., 1990).

For a given lithology, porosity varies considerably in different locations. A compilation of porosity-depth curves for sandstones, shale and carbonates shows that porosities can vary by as much as 20% for the same lithology (Giles et al., 1998).

The accuracy of the porosity-depth relationship depends on the depths in question, and on the lithology (Gallagher, 1989; Giles et al., 1998). The exponential relationship commonly used is generally considered effective to basin depths up to 10 kilometers (Giles et al., 1998).

One reason for assuming an exponential porosity-depth relationship is that local porosity information is not always available. While porosity-depth functions can be generated using downhole porosity measurements, the initial porosity (ϕ_o) should not be extrapolated from this because this makes the initial porosity dependent on the porosity-depth function (Giles et al., 1998). Additionally, not all methods of determining porosity

from wireline logs are reliable; mixing the sources of porosities could actually generate additional sources of error (Giles et al., 1998).

4.3 Error Quantification

In order to quantify the margin of error in the calculated subsidence values for this project, a single well has been chosen as the reference well. This well, 06-36-049-23W5, is immediately west of the study area (Figure 3-1) and well was chosen because it contains a complete record of all four members identified in this study (it is far enough west for the Upper Fernie to be overlain by the Minnes Group and far enough south to contain the Rock Creek). The Upper, Middle, and Lower Monteith shown in Figure 3-1 are combined as a single unit for calculations.

4.3.1 Variation in lithologic constants

The effects of changing the lithologic constants were tested using the reference well. To see how tectonic subsidence varies with depth when the lithologic constants change the shale layers were used; the reference well has six shale layers distributed over depths ranging from 2272.1m to 3924.4m (the base of the Fernie Formation in the reference well is 3984.7m).

The change in tectonic subsidence due to a change in one of the lithologic constants varies according to depth. The percent variation was calculated by comparing the newly calculated tectonic subsidence for each of the shale layers to the tectonic subsidence calculated when using the empirically-derived lithologic constants.

The percent variations in tectonic subsidence caused by varying the lithologic constants are summarized at the end of Section 4.3.1 in Table 4.

4.3.1.1 Compaction coefficient

The compaction coefficient was changed from 0.0003 to 0.0007, in increments of 0.0001. The empirically derived value for shale is 0.0005 (Angevine et al., 1990). In Figure 4-2, it is apparent that if the empirically derived compaction coefficient is too high, the calculated tectonic subsidence will be lower than it should be and vice-versa. The uncertainty related to the compaction coefficient decreases with depth.

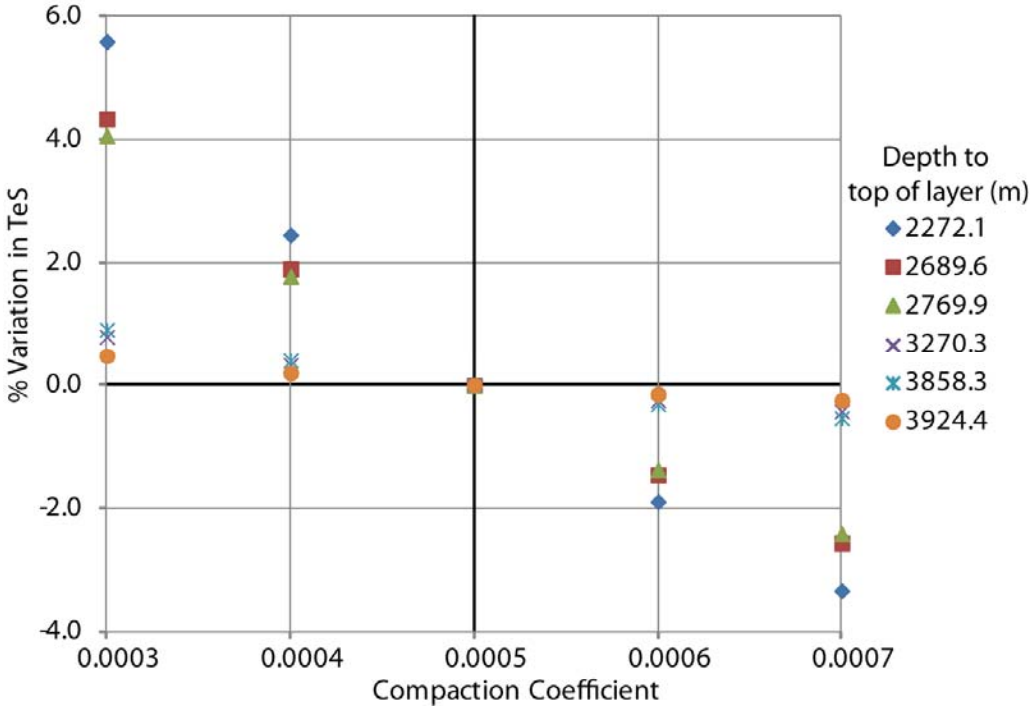

Figure 4-2: Variation in tectonic subsidence when compaction coefficient is varied. The percent variation in TeS due to changes in compaction coefficient is different at different depths. Overall, as the compaction coefficient decreases the tectonic subsidence increases. The default value for the lithology tested is 0.0005.

4.3.1.2 Porosity

The porosity was varied from 0.1 to 0.9, in increments of 0.2. The empirically derived value for shale is 0.5 (*ibid.*). Figure 4-3 shows that as porosity increases the tectonic subsidence also increases. The exception to this is 3924.4m. An examination of the porosity-depth relationship used here (Figure 4-4) shows that this is because the curves cross-over each other at approximately 3400m depth.

The maximum variation in tectonic subsidence here is 8%.

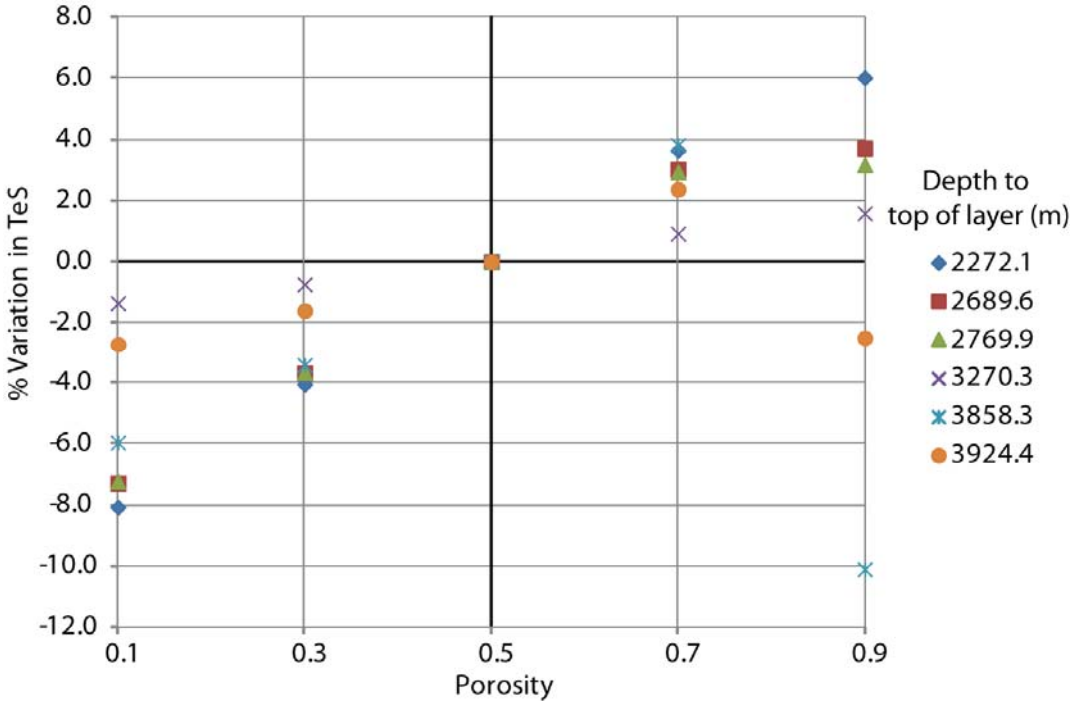

Figure 4-3: Variation in tectonic subsidence when initial porosity is varied. The percent variation in TeS due to changes in porosity is different at different depths. Overall, as the porosity increases so does the tectonic subsidence. The default value for the lithology tested is 0.5.

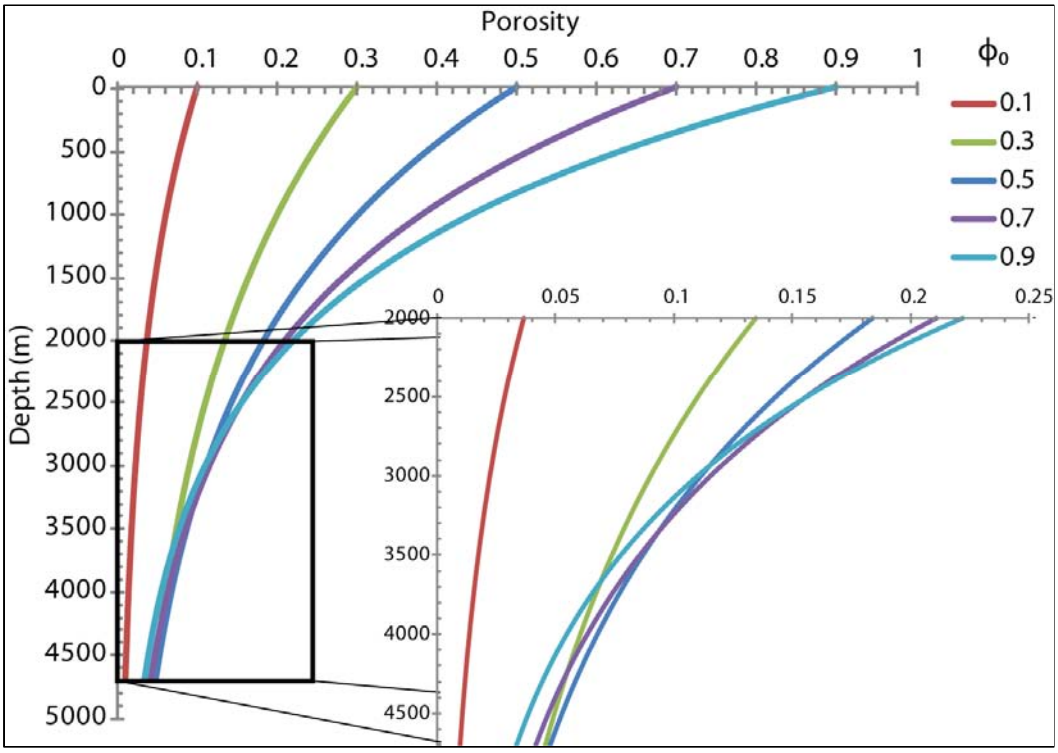

Figure 4-4: Porosity-depth relationships.

The porosity-depth curves for different initial porosities cross each other at depths greater than 2000m, as seen in the zoomed in section. This crossover results in a change in trend, i.e. from an increase to a decrease, at depths below the crossover points.

4.3.1.3 Density

The density was varied from 2.00 to 3.50, in increments of 0.5. The empirically derived value for shale is 2.72 (*ibid.*). Like the compaction coefficient, when the density decreases the tectonic subsidence increases, however the two are not related in the calculations (the compaction coefficient is a constant in the decompaction equation and the density is a constant in the backstripping equation. If the empirically derived density

is too high, the calculated tectonic subsidence will be too low, and vice versa. There is a greater change in tectonic subsidence at shallower depths when density is varied.

The density of any given lithology is unlikely to vary as much as what has been tested here. The density of a sedimentary rock will certainly not be as high as 3.5 kg/m^3, since this is higher than the density of the mantle. A density range between 2.5 and 3.0 kg/m^3 is more than reasonable for shale; this results in a tectonic subsidence variation of not more than 10%.

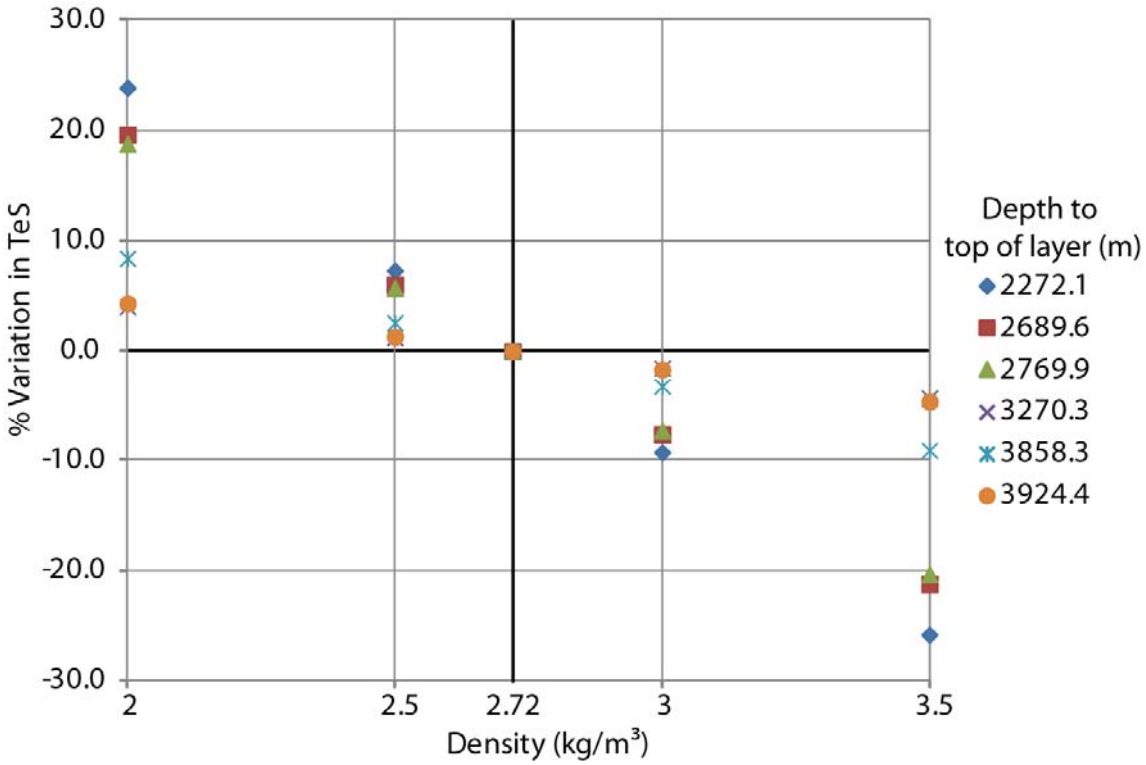

Figure 4-5: Variation in tectonic subsidence when density changes.

The percent variation in tectonic subsidence due to changes in density is different at different depths. Overall, tectonic subsidence increases as density decreases.

Table 4: Percent variation in tectonic subsidence when lithologic constants are changed

Horizon Name	Depth	Porosity	TeS	%var	CC	TeS	%var	Density (kg/m^3)	TeS	%var
Klea_park	2272.1	0.1	996.93	-8.1%	0.0003	1145.137	5.6%	2	1343.279	23.9%
Klea_park	2272.1	0.3	1040.55	-4.1%	0.0004	1111.133	2.5%	2.5	1163.571	7.3%
Klea_park	2272.1	0.5	1084.50	0.0%	0.0005	1084.5	0.0%	2.72	1084.499	0.0%
Klea_park	2272.1	0.7	1124.08	3.6%	0.0006	1064.004	-1.9%	3	983.8633	-9.3%
Klea_park	2272.1	0.9	1149.78	6.0%	0.0007	1048.347	-3.3%	3.5	804.1554	-25.9%
Kcardium	2689.6	0.1	828.44	-7.3%	0.0003	932.2672	4.3%	2	1068.858	19.6%
Kcardium	2689.6	0.3	860.72	-3.7%	0.0004	910.5454	1.9%	2.5	947.1112	6.0%
Kcardium	2689.6	0.5	893.54	0.0%	0.0005	893.5424	0.0%	2.72	893.5425	0.0%
Kcardium	2689.6	0.7	920.57	3.0%	0.0006	880.5346	-1.5%	3	825.3647	-7.6%
Kcardium	2689.6	0.9	926.73	3.7%	0.0007	870.6732	-2.6%	3.5	703.6182	-21.3%
Kkaskapau	2769.9	0.1	792.68	-7.2%	0.0003	889.2078	4.1%	2	1014.83	18.8%
Kkaskapau	2769.9	0.3	823.21	-3.7%	0.0004	869.7552	1.8%	2.5	903.4801	5.7%
Kkaskapau	2769.9	0.5	854.49	0.0%	0.0005	854.486	0.0%	2.72	854.486	0.0%
Kkaskapau	2769.9	0.7	879.64	2.9%	0.0006	842.7905	-1.4%	3	792.1298	-7.3%
Kkaskapau	2769.9	0.9	881.64	3.2%	0.0007	833.9228	-2.4%	3.5	680.7794	-20.3%
Kbfs	3270.3	0.1	516.18	-1.4%	0.0003	527.4649	0.8%	2	544.3385	4.0%
Kbfs	3270.3	0.3	519.41	-0.7%	0.0004	525.0531	0.3%	2.5	529.723	1.2%
Kbfs	3270.3	0.5	523.29	0.0%	0.0005	523.292	0.0%	2.72	523.2921	0.0%
Kbfs	3270.3	0.7	528.13	0.9%	0.0006	522.009	-0.2%	3	515.1076	-1.6%

Horizon Name	Depth	Porosity	TeS	%var	CC	TeS	%var	Density (kg/m^3)	TeS	%var
Kbfs	3270.3	0.9	531.59	1.6%	0.0007	521.0703	-0.4%	3.5	500.4922	-4.4%
Jfernie	3858.3	0.1	123.98	-6.0%	0.0003	133.0402	0.9%	2	142.8988	8.4%
Jfernie	3858.3	0.3	127.33	-3.4%	0.0004	132.365	0.4%	2.5	135.2139	2.6%
Jfernie	3858.3	0.5	131.83	0.0%	0.0005	131.8323	0.0%	2.72	131.8324	0.0%
Jfernie	3858.3	0.7	136.86	3.8%	0.0006	131.4292	-0.3%	3	127.5289	-3.3%
Jfernie	3858.3	0.9	118.51	-10.1%	0.0007	131.128	-0.5%	3.5	119.8439	-9.1%
Jpokerchp	3924.4	0.1	67.65	2.7%	0.0003	69.88476	0.5%	2	72.54121	4.3%
Jpokerchp	3924.4	0.3	68.43	-1.6%	0.0004	69.68921	0.2%	2.5	70.46272	1.3%
Jpokerchp	3924.4	0.5	69.55	0.0%	0.0005	69.54818	0.0%	2.72	69.54818	0.0%
Jpokerchp	3924.4	0.7	71.20	2.4%	0.0006	69.44833	-0.1%	3	68.38423	-1.7%
Jpokerchp	3924.4	0.9	67.81	-2.5%	0.0007	69.37826	-0.2%	3.5	66.30574	-4.7%

4.3.2 Geological Considerations

4.3.2.1 Erosion and unconformities

Unconformities are included in the sediment columns so that they can be accounted for in the subsidence curves. The presence or absence of an unconformity does not change the calculated tectonic subsidence of any of the layers (Figure 4-6); however the calculated subsidence rate between the layer above and below the unconformity will be different when the unconformity is not accounted for. This is because the age at the base of the layer above the unconformity changes when the unconformity is not accounted for.

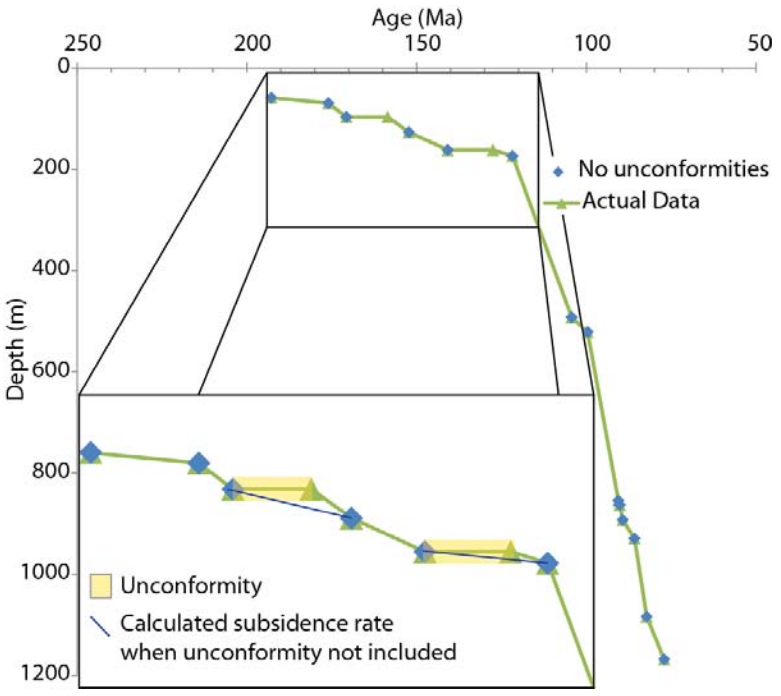

Figure 4-6: Unconformity related changes in subsidence curves. The data points do not shift with unconformities (green) or without (blue). The subsidence rate changes where the unconformity should be (inset).

When the unconformity represents an erosional event, the sediment remaining will not represent the true deposited thickness of the eroded unit, and therefore the calculated subsidence will not represent the total unit deposited.

In order to model the effect that erosion has on subsidence calculations, a comparison was made between the reference well (06-36-049-23W5), where it is assumed the Upper Fernie is fully preserved, and a well to the southeast (06-01-039-07W5) where the sub-Cretaceous unconformity sits immediately above the Upper Fernie and it is assumed that a significant portion of the Upper Fernie has been eroded (Figure 3-1).

For the model, it is assumed that the shale layers had a uniform thickness between the two wells prior to erosion. The Poker Chip Shale is 10.3m thick in 06-36-049-23W5 and 10.5m thick in 06-01-039-07W5. In 06-36-049-23W5 the Upper Fernie is 28.9m thick and in 06-36-039-07W5 it is 7.6m thick, a difference of 21.3m that amounts to removal of 73% of the Upper Fernie.

Two scenarios were tested: in the first, the thickness of the Upper Fernie in the test well was reduced to 7.6m but all other thicknesses remained the same and in the second, the thickness of the Upper Fernie was reduced to 6.6m and the Monteith was removed. In both scenarios, the thickness of the "Surface" layer increased to account for the reduced thickness of the eroded layers.

When only the thickness of the Upper Fernie is changed to reflect erosion of the layer, the layers below the Upper Fernie are not affected, but there is a change in the tectonic subsidence of all the layers above the Upper Fernie (Figure 4-7). A 73% decrease in the thickness of the Upper Fernie results in a 17.63% decrease in its calculated tectonic subsidence. The percent decrease in the calculated tectonic subsidence of the layers above the Upper Fernie decreases with depth.

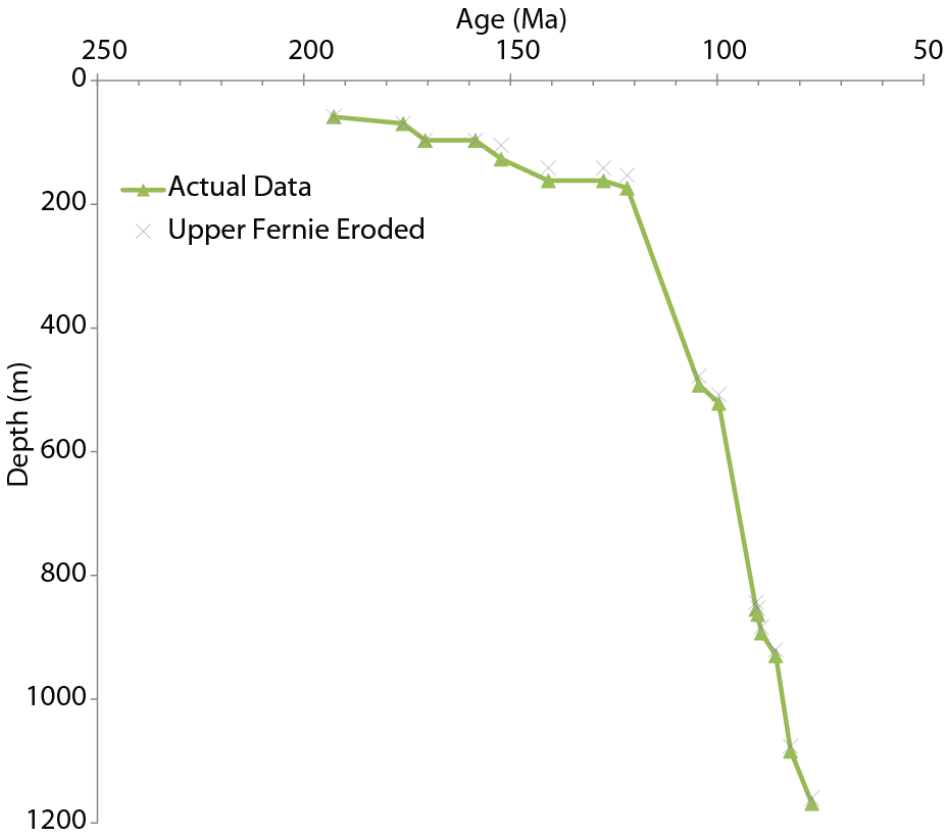

Figure 4-7: Effect of erosion of a single layer on the subsidence profile

The subsidence curve is shallower at all points younger than the eroded layer due to the missing sediment in that layer.

The most significant changes in tectonic subsidence occurred in the second scenario, when erosion removed the entire Monteith and the majority of the Upper Fernie. The tectonic subsidence of the Upper Fernie and the layers below it are the same as in scenario one; however removal of the entire Monteith results in a 35% decrease in the calculated tectonic subsidence at the base of the Cadomin (the layer immediately above the sub-Cretaceous unconformity). As the total depth of the layers decreases so does the percent decrease in the calculated tectonic subsidence of each layer (Figure 4-8).

The percent variations in tectonic subsidence are summarized in Table 5.

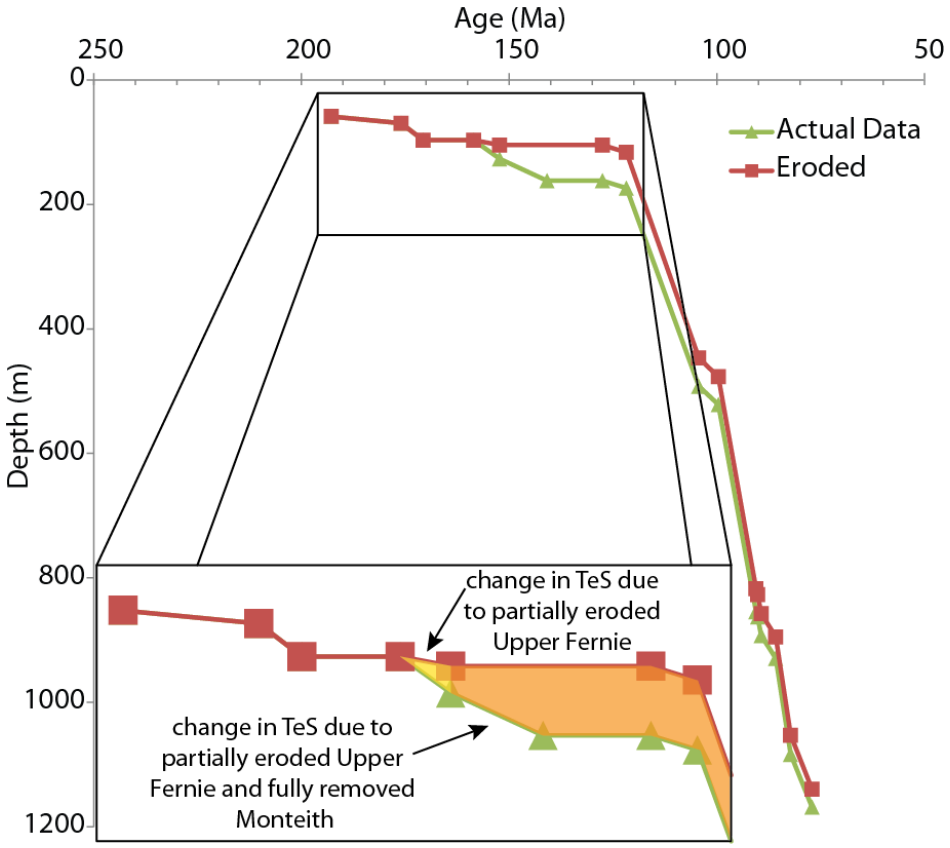

Figure 4-8: Effect of removal of one layer and partial erosion of another. The subsidence curve is shallower at all ages younger than the oldest eroded layer due to the missing sediment and the missing layer. The horizontal line representing the unconformity has a larger age range.

Table 5: Percent variation in tectonic subsidence due to erosion

		Actual Data		No unconformities			Upper Fernie Eroded			Monteith removed, Upper Fernie eroded		
Horizon	Age at Top (Ma)	TeS (m)	Tn (m)	TeS (m)	Tn (m)	% Change in TeS	TeS (m)	Tn (m)	% Change in TeS	TeS (m)	Tn (m)	% Change in TeS
Surface	0	3644.15	1992.5	3644.15	1992.5	0.00%	3666.62	2013.8	0.62%	3716.50	2064.1	1.99%
Kbelly_rv	77.05	1168.16	279.6	1168.16	279.6	0.00%	1160.10	279.6	-0.69%	1139.43	279.6	-2.46%
Klea_park	82.21	1083.55	313.1	1083.55	313.1	0.00%	1075.72	313.1	-0.72%	1052.72	313.1	-2.85%
Kbadheart	85.8	929.40	104.4	929.40	104.4	0.00%	919.96	104.4	-1.02%	894.80	104.4	-3.72%
Kcardium	89.3	892.62	55	892.62	55	0.00%	883.22	55	-1.05%	857.28	55	-3.96%
Kcard_ss	90.14	862.84	25.3	862.84	25.3	0.00%	852.55	25.3	-1.19%	826.70	25.3	-4.19%
Kkaskapau	90.56	854.49	500.4	854.49	500.4	0.00%	843.29	500.4	-1.31%	817.47	500.4	-4.33%
Kbfs	99.6	521.48	34.3	521.48	34.3	0.00%	507.63	34.3	-2.66%	476.82	34.3	-8.56%
Kmannvl	104.32	492.25	487.1	492.25	487.1	0.00%	477.48	487.1	-3.00%	446.68	487.1	-9.26%
Kcadomin	121.75	173.94	16.3	173.94	16.3	0.00%	153.43	16.3	-11.79%	116.46	16.3	-33.04%
Unconformity	127.5	162.02	0	-	-	-	141.48	0	-12.68%	104.52	0	-35.49%
Jnikanssn	140.85	162.02	50.3	162.02	50.3	0.00%	141.48	50.3	-12.68%	-	-	-
Jfernie	152.25	126.89	28.9	126.89	28.9	0.00%	104.52	7.6	-17.63%	104.52	7.6	-17.63%
Unconformity	158.5	96.69	0	-	-	-	96.69	0	0.00%	96.69	0	0.00%
Jrock_ck	170.67	96.69	37.2	96.69	37.2	0.00%	96.69	37.2	0.00%	96.69	37.2	0.00%
Jpokerchp	176	69.55	10.3	69.55	10.3	0.00%	69.55	10.3	0.00%	69.55	10.3	0.00%
Jnordegg	192.8	58.60	50	58.60	50	0.00%	58.60	50	0.00%	58.60	50	0.00%

4.3.2.2 Presence of thin beds

Formations are simplified to a single lithology in subsidence calculations. The presence of thin beds of different lithologies will influence the tectonic subsidence calculations. When a thin bed of a different lithology is present, the porosity and compaction coefficient will be different and the decompacted thickness will change. The density of the thin bed is also different, changing the total column density and the calculated tectonic subsidence for the entire column.

To quantify the effect a thin bed will have, a shale bed was inserted into the Rock Creek sandstone layer and the thickness varied. This layer is called "Thin Shale." The thickness of Thin Shale was varied from one to eighteen meters. The total present thickness of the sediment column does not change when Thin Shale is added. Instead, the Rock Creek is split into two layers, Rock Creek above Thin Shale and Rock Creek 2 below Thin Shale; the present thickness of Rock Creek 2 decreases as the thickness of Thin Shale increases (Table 6).

Table 6: Thicknesses used to quantify effect of thin beds

Thin Shale Thickness (m)	Rock Creek 2 Top (m)	Rock Creek 2 Thickness (m)
1	3907	17.4
2	3908	16.4
3	3909	15.4
4	3910	14.4
6	3912	12.4
8	3914	10.4
10	3916	8.4
14	3920	4.4
18	3924	0.4

The calculated tectonic subsidence of Rock Creek 2 decreases when a thin bed is inserted immediately above it. The maximum percent decrease in tectonic subsidence for this layer is 62.03% and the minimum is 54.92%. As Rock Creek 2 becomes thinner, the effect of a thin bed above it becomes less (Figure 4-9).

The layers below Rock Creek 2 (Nordegg and Poker Chip, at depths of 3934.7m and 3924.4m respectively) are not affected by the presence of thin beds within the layers above them.

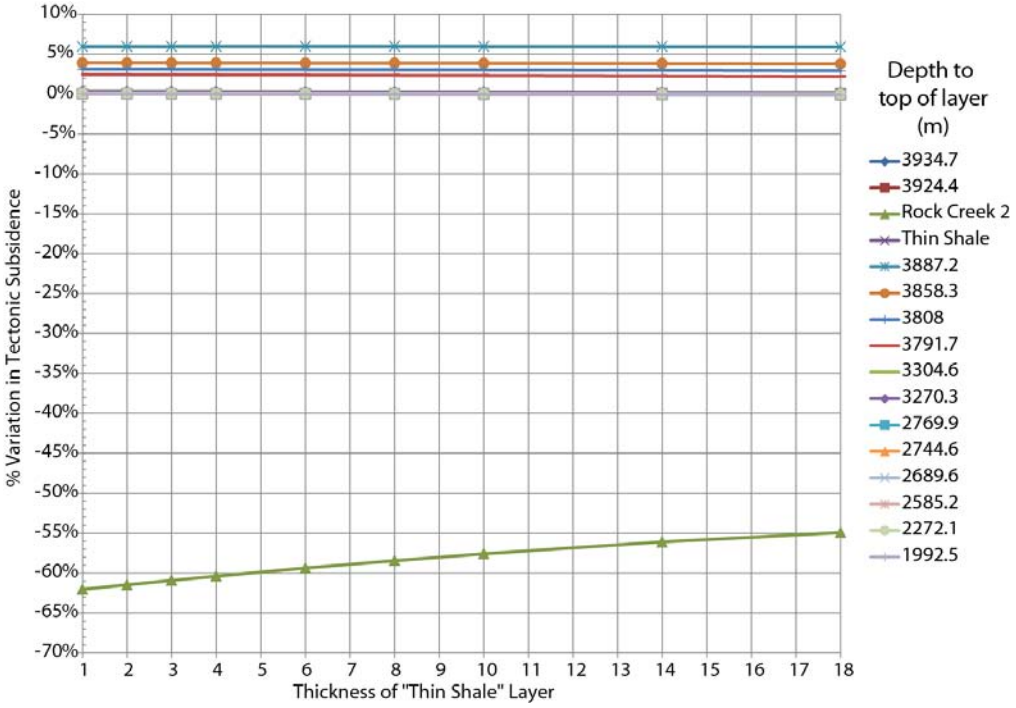

Figure 4-9: Tectonic subsidence variation caused by presence of a thin bed. Tectonic subsidence of most layers is minimally affected (i.e. less than 6% variation) by the presence of a thin bed, regardless of the thickness of that thin bed. However, the resulting decrease in thickness of the layer below the thin bed caused substantial variation in the thickness of that layer.

When a thin bed is inserted below a layer, the calculated tectonic subsidence of that layer increases. For all layers above Thin Shale, including Rock Creek, the maximum percent increase in tectonic subsidence is 5.96%. The further away from the thin bed the layer is, the smaller the variation in tectonic subsidence caused by the thin bed.

The percent variation in tectonic subsidence due to the presence of a thin bed is summarized in Table 7.

Table 7: Percent variation of tectonic subsidence caused by presence of a thin bed

Horizon Name	Top Depth (m)	Thin Shale Thickness (m)	Tectonic Subsidence (m)	Present Thickness (m)	% var
Kbelly_rv	1992.5	0	1168.16	279.6	0.00%
Kbelly_rv	1992.5	1	1168.09	279.6	-0.01%
Kbelly_rv	1992.5	2	1168.02	279.6	-0.01%
Kbelly_rv	1992.5	3	1167.96	279.6	-0.02%
Kbelly_rv	1992.5	4	1167.89	279.6	-0.02%
Kbelly_rv	1992.5	6	1167.76	279.6	-0.03%
Kbelly_rv	1992.5	8	1167.63	279.6	-0.04%
Kbelly_rv	1992.5	10	1167.50	279.6	-0.06%
Kbelly_rv	1992.5	14	1167.24	279.6	-0.08%
Kbelly_rv	1992.5	18	1166.98	279.6	-0.10%
Klea_park	2272.1	0	1083.55	313.1	0.00%
Klea_park	2272.1	1	1084.43	313.1	0.08%
Klea_park	2272.1	2	1084.37	313.1	0.08%
Klea_park	2272.1	3	1084.31	313.1	0.07%
Klea_park	2272.1	4	1084.24	313.1	0.06%
Klea_park	2272.1	6	1084.11	313.1	0.05%
Klea_park	2272.1	8	1083.98	313.1	0.04%
Klea_park	2272.1	10	1083.85	313.1	0.03%
Klea_park	2272.1	14	1083.59	313.1	0.00%
Klea_park	2272.1	18	1083.33	313.1	-0.02%
Kbadheart	2585.2	0	929.40	104.4	0.00%
Kbadheart	2585.2	1	929.34	104.4	-0.01%
Kbadheart	2585.2	2	929.27	104.4	-0.01%
Kbadheart	2585.2	3	929.21	104.4	-0.02%

Horizon Name	Top Depth (m)	Thin Shale Thickness (m)	Tectonic Subsidence (m)	Present Thickness (m)	% var
Kbadheart	2585.2	4	929.15	104.4	-0.03%
Kbadheart	2585.2	6	929.02	104.4	-0.04%
Kbadheart	2585.2	8	928.89	104.4	-0.05%
Kbadheart	2585.2	10	928.76	104.4	-0.07%
Kbadheart	2585.2	14	928.51	104.4	-0.10%
Kbadheart	2585.2	18	928.25	104.4	-0.12%
Kcardium	2689.6	0	892.62	55	0.00%
Kcardium	2689.6	1	893.48	55	0.10%
Kcardium	2689.6	2	893.42	55	0.09%
Kcardium	2689.6	3	893.35	55	0.08%
Kcardium	2689.6	4	893.29	55	0.08%
Kcardium	2689.6	6	893.16	55	0.06%
Kcardium	2689.6	8	893.04	55	0.05%
Kcardium	2689.6	10	892.91	55	0.03%
Kcardium	2689.6	14	892.66	55	0.00%
Kcardium	2689.6	18	892.40	55	-0.02%
Kcard_ss	2744.6	0	862.84	25.3	0.00%
Kcard_ss	2744.6	1	863.70	25.3	0.10%
Kcard_ss	2744.6	2	863.64	25.3	0.09%
Kcard_ss	2744.6	3	863.57	25.3	0.09%
Kcard_ss	2744.6	4	863.51	25.3	0.08%
Kcard_ss	2744.6	6	863.38	25.3	0.06%
Kcard_ss	2744.6	8	863.26	25.3	0.05%
Kcard_ss	2744.6	10	863.13	25.3	0.03%
Kcard_ss	2744.6	14	862.88	25.3	0.01%
Kcard_ss	2744.6	18	862.63	25.3	-0.02%
Kkaskapau	2769.9	0	854.49	500.4	0.00%
Kkaskapau	2769.9	1	854.42	500.4	-0.01%
Kkaskapau	2769.9	2	854.36	500.4	-0.01%
Kkaskapau	2769.9	3	854.30	500.4	-0.02%
Kkaskapau	2769.9	4	854.24	500.4	-0.03%
Kkaskapau	2769.9	6	854.11	500.4	-0.04%
Kkaskapau	2769.9	8	853.98	500.4	-0.06%
Kkaskapau	2769.9	10	853.86	500.4	-0.07%
Kkaskapau	2769.9	14	853.61	500.4	-0.10%

Horizon Name	Top Depth (m)	Thin Shale Thickness (m)	Tectonic Subsidence (m)	Present Thickness (m)	% var
Kkaskapau	2769.9	18	853.36	500.4	-0.13%
Kbfs	3270.3	0	521.48	34.3	0.00%
Kbfs	3270.3	1	523.24	34.3	0.34%
Kbfs	3270.3	2	523.18	34.3	0.33%
Kbfs	3270.3	3	523.13	34.3	0.32%
Kbfs	3270.3	4	523.07	34.3	0.30%
Kbfs	3270.3	6	522.96	34.3	0.28%
Kbfs	3270.3	8	522.85	34.3	0.26%
Kbfs	3270.3	10	522.74	34.3	0.24%
Kbfs	3270.3	14	522.51	34.3	0.20%
Kbfs	3270.3	18	522.29	34.3	0.15%
Kmannvl	3304.6	0	492.25	487.1	0.00%
Kmannvl	3304.6	1	494.00	487.1	0.36%
Kmannvl	3304.6	2	493.95	487.1	0.35%
Kmannvl	3304.6	3	493.89	487.1	0.34%
Kmannvl	3304.6	4	493.84	487.1	0.32%
Kmannvl	3304.6	6	493.73	487.1	0.30%
Kmannvl	3304.6	8	493.62	487.1	0.28%
Kmannvl	3304.6	10	493.51	487.1	0.26%
Kmannvl	3304.6	14	493.29	487.1	0.21%
Kmannvl	3304.6	18	493.07	487.1	0.17%
Kcadomin	3791.7	0	173.94	16.3	0.00%
Kcadomin	3791.7	1	178.18	16.3	2.44%
Kcadomin	3791.7	2	178.16	16.3	2.43%
Kcadomin	3791.7	3	178.14	16.3	2.41%
Kcadomin	3791.7	4	178.12	16.3	2.40%
Kcadomin	3791.7	6	178.07	16.3	2.38%
Kcadomin	3791.7	8	178.03	16.3	2.35%
Kcadomin	3791.7	10	177.98	16.3	2.32%
Kcadomin	3791.7	14	177.88	16.3	2.26%
Kcadomin	3791.7	18	177.77	16.3	2.20%
Jnikanssn	3808	0	162.02	50.3	0.00%
Jnikanssn	3808	1	167.10	50.3	3.13%
Jnikanssn	3808	2	167.08	50.3	3.12%

Horizon Name	Top Depth (m)	Thin Shale Thickness (m)	Tectonic Subsidence (m)	Present Thickness (m)	% var
Jnikanssn	3808	3	167.06	50.3	3.11%
Jnikanssn	3808	4	167.04	50.3	3.10%
Jnikanssn	3808	6	167.01	50.3	3.08%
Jnikanssn	3808	8	166.97	50.3	3.05%
Jnikanssn	3808	10	166.92	50.3	3.02%
Jnikanssn	3808	14	166.83	50.3	2.97%
Jnikanssn	3808	18	166.74	50.3	2.91%
Jfernie	3858.3	0	126.89	28.9	0.00%
Jfernie	3858.3	1	131.83	28.9	3.90%
Jfernie	3858.3	2	131.83	28.9	3.89%
Jfernie	3858.3	3	131.82	28.9	3.89%
Jfernie	3858.3	4	131.82	28.9	3.89%
Jfernie	3858.3	6	131.81	28.9	3.88%
Jfernie	3858.3	8	131.79	28.9	3.87%
Jfernie	3858.3	10	131.77	28.9	3.85%
Jfernie	3858.3	14	131.73	28.9	3.82%
Jfernie	3858.3	18	131.67	28.9	3.77%
Jrock_ck	3887.2	0	96.69	37.2	0.00%
Jrock_ck	3887.2	1	102.43	18.8	5.94%
Jrock_ck	3887.2	2	102.43	18.8	5.94%
Jrock_ck	3887.2	3	102.44	18.8	5.95%
Jrock_ck	3887.2	4	102.44	18.8	5.96%
Jrock_ck	3887.2	6	102.45	18.8	5.96%
Jrock_ck	3887.2	8	102.45	18.8	5.96%
Jrock_ck	3887.2	10	102.45	18.8	5.96%
Jrock_ck	3887.2	14	102.43	18.8	5.94%
Jrock_ck	3887.2	18	102.39	18.8	5.90%
Thin Shale	3906	1	88.04	1	0.00%
Thin Shale	3906	2	88.06	2	0.02%
Thin Shale	3906	3	88.07	3	0.03%
Thin Shale	3906	4	88.08	4	0.05%
Thin Shale	3906	6	88.10	6	0.07%
Thin Shale	3906	8	88.12	8	0.08%
Thin Shale	3906	10	88.12	10	0.09%
Thin Shale	3906	14	88.13	14	0.10%

Horizon Name	Top Depth (m)	Thin Shale Thickness (m)	Tectonic Subsidence (m)	Present Thickness (m)	% var
Thin Shale	3906	18	88.11	18	0.08%
Rock_Creek2	3906	0	153.94	28.7	0.00%
Rock_Creek2	3907	1	58.46	17.4	-62.03%
Rock_Creek2	3908	2	59.34	16.4	-61.45%
Rock_Creek2	3909	3	60.19	15.4	-60.90%
Rock_Creek2	3910	4	61.01	14.4	-60.37%
Rock_Creek2	3912	6	62.57	12.4	-59.36%
Rock_Creek2	3914	8	64.00	10.4	-58.42%
Rock_Creek2	3916	10	65.32	8.4	-57.57%
Rock_Creek2	3920	14	67.60	4.4	-56.09%
Rock_Creek2	3924	18	69.39	0.4	-54.92%
Jpokerchp	3924.4	0	69.55	10.3	0.00%
Jpokerchp	3924.4	1	69.55	10.3	0.00%
Jpokerchp	3924.4	2	69.55	10.3	0.00%
Jpokerchp	3924.4	3	69.55	10.3	0.00%
Jpokerchp	3924.4	4	69.55	10.3	0.00%
Jpokerchp	3924.4	6	69.55	10.3	0.00%
Jpokerchp	3924.4	8	69.55	10.3	0.00%
Jpokerchp	3924.4	10	69.55	10.3	0.00%
Jpokerchp	3924.4	14	69.55	10.3	0.00%
Jpokerchp	3924.4	18	69.55	10.3	0.00%
Jnordegg	3934.7	0	58.60	50	0.00%
Jnordegg	3934.7	1	58.60	50	0.00%
Jnordegg	3934.7	2	58.60	50	0.00%
Jnordegg	3934.7	3	58.60	50	0.00%
Jnordegg	3934.7	4	58.60	50	0.00%
Jnordegg	3934.7	6	58.60	50	0.00%
Jnordegg	3934.7	8	58.60	50	0.00%
Jnordegg	3934.7	10	58.60	50	0.00%
Jnordegg	3934.7	14	58.60	50	0.00%
Jnordegg	3934.7	18	58.60	50	0.00%

4.3.2.3 Lithology

The lithologies in this study have been generalized to sandstone, shale, and limestone, a common practise in subsidence analysis (Xie and Heller, 2009). The Rock Creek layer in the reference well was used to test how much this simplification changes the calculated tectonic subsidence. All three lithologic constants change when the lithology changes.

When the lithology of the Rock Creek layer is changed, the tectonic subsidence for that layer varies by up to 12.98%. This largest variation, an increase in tectonic subsidence, occurs when the lithology is changed from sandstone to limestone. The second largest variation occurs when the lithology is a mix (average) of limestone and shale, and the third largest variation is when the lithology is changed to shale. All three of these lithology changes caused a tectonic subsidence variation greater than 10% in the Rock Creek (Figure 4-10).

The change in tectonic subsidence of the Rock Creek, when its lithology is changed, propagates through the layers above it but does not affect the layers below it. The maximum change in tectonic subsidence of the other layers is 7.15%. This occurs in the layer immediately above the Rock Creek. The amount of variation in tectonic subsidence for each layer decreases the further away from the Rock Creek the layer is.

The percent variation in tectonic subsidence due to changes in the lithology of the Rock Creek is summarized in Table 8.

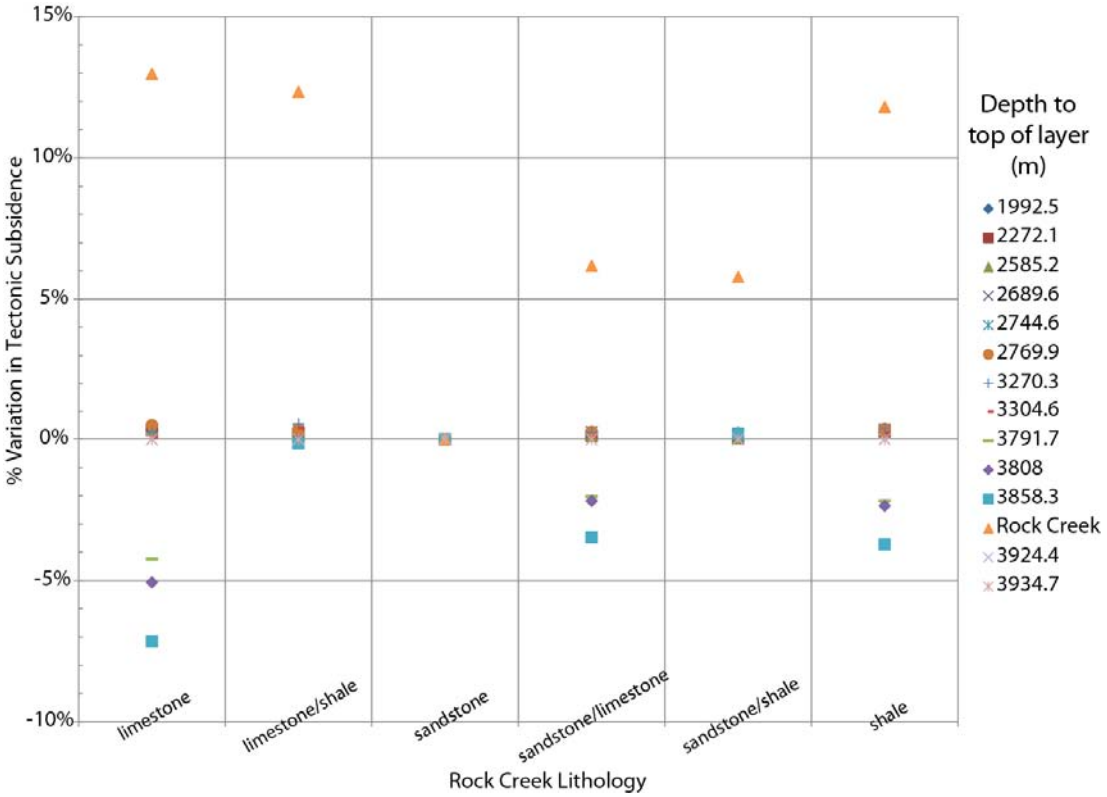

Figure 4-10: Tectonic subsidence variations when the lithology of one layer changes. Each column represents a single lithology assigned to the Rock Creek layer. The most variation in tectonic subsidence is in the Rock Creek and the layers above it.

Table 8: Percent variation in tectonic subsidence when lithology of 1 layer changes

Top Depth (m)	Rock Creek lithology	Tectonic Subsidence (m)	% var
1992.5	limestone	1168.16	0.37%
1992.5	limestone/shale	1165.73	0.16%
1992.5	sandstone	1163.83	0.00%
1992.5	sandstone/limestone	1166.12	0.20%
1992.5	sandstone/shale	1165.16	0.11%
1992.5	shale	1166.88	0.26%
2272.1	limestone	1083.55	0.31%
2272.1	limestone/shale	1082.09	0.18%

Top Depth (m)	Rock Creek lithology	Tectonic Subsidence (m)	% var
2272.1	sandstone	1080.18	0.00%
2272.1	sandstone/limestone	1081.52	0.12%
2272.1	sandstone/shale	1080.56	0.03%
2272.1	shale	1083.23	0.28%
2585.2	limestone	929.40	0.36%
2585.2	limestone/shale	927.96	0.21%
2585.2	sandstone	926.04	0.00%
2585.2	sandstone/limestone	927.39	0.15%
2585.2	sandstone/shale	926.43	0.04%
2585.2	shale	929.10	0.33%
2689.6	limestone	892.62	0.38%
2689.6	limestone/shale	891.19	0.22%
2689.6	sandstone	889.26	0.00%
2689.6	sandstone/limestone	891.54	0.26%
2689.6	sandstone/shale	890.59	0.15%
2689.6	shale	892.32	0.34%
2744.6	limestone	862.84	0.39%
2744.6	limestone/shale	862.35	0.33%
2744.6	sandstone	859.48	0.00%
2744.6	sandstone/limestone	861.76	0.27%
2744.6	sandstone/shale	860.81	0.15%
2744.6	shale	862.54	0.36%
2769.9	limestone	854.49	0.50%
2769.9	limestone/shale	853.08	0.34%
2769.9	sandstone	850.21	0.00%
2769.9	sandstone/limestone	852.49	0.27%
2769.9	sandstone/shale	851.54	0.16%
2769.9	shale	853.27	0.36%
3270.3	limestone	521.48	0.25%
3270.3	limestone/shale	523.03	0.55%
3270.3	sandstone	520.17	0.00%
3270.3	sandstone/limestone	521.45	0.25%
3270.3	sandstone/shale	521.51	0.26%

Top Depth (m)	Rock Creek lithology	Tectonic Subsidence (m)	% var
3270.3	shale	522.21	0.39%
3304.6	limestone	492.25	0.07%
3304.6	limestone/shale	493.83	0.40%
3304.6	sandstone	491.88	0.00%
3304.6	sandstone/limestone	492.24	0.07%
3304.6	sandstone/shale	492.30	0.09%
3304.6	shale	492.99	0.23%
3791.7	limestone	173.94	-4.24%
3791.7	limestone/shale	181.58	-0.03%
3791.7	sandstone	181.64	0.00%
3791.7	sandstone/limestone	177.96	-2.03%
3791.7	sandstone/shale	181.97	0.18%
3791.7	shale	177.68	-2.18%
3808	limestone	162.02	-5.07%
3808	limestone/shale	170.58	-0.05%
3808	sandstone	170.67	0.00%
3808	sandstone/limestone	166.94	-2.18%
3808	sandstone/shale	170.99	0.19%
3808	shale	166.65	-2.35%
3858.3	limestone	126.89	-7.15%
3858.3	limestone/shale	136.47	-0.14%
3858.3	sandstone	136.66	0.00%
3858.3	sandstone/limestone	131.91	-3.47%
3858.3	sandstone/shale	136.92	0.19%
3858.3	shale	131.57	-3.72%
3887.2	limestone	109.24	12.98%
3887.2	limestone/shale	108.61	12.34%
3887.2	sandstone	96.69	0.00%
3887.2	sandstone/limestone	102.66	6.18%
3887.2	sandstone/shale	102.28	5.79%
3887.2	shale	108.11	11.81%
3924.4	limestone	69.55	0.00%

Top Depth (m)	Rock Creek lithology	Tectonic Subsidence (m)	% var
3924.4	limestone/shale	69.55	0.00%
3924.4	sandstone	69.55	0.00%
3924.4	sandstone/limestone	69.55	0.00%
3924.4	sandstone/shale	69.55	0.00%
3924.4	shale	69.55	0.00%
3934.7	limestone	58.60	0.00%
3934.7	limestone/shale	58.60	0.00%
3934.7	sandstone	58.60	0.00%
3934.7	sandstone/limestone	58.60	0.00%
3934.7	sandstone/shale	58.60	0.00%
3934.7	shale	58.60	0.00%

4.3.3 Other Considerations

4.3.3.1 Overpressured formations

Overpressure can occur within the Fernie Formation, primarily in the westernmost portions of the study area (Putnam and Ward, 2001). Overpressured zones generally have higher porosities than in normally pressured zones, and this is one of several factors that causes up to a 20% variation in porosities of rocks with the same lithology, the others being composition, age, geothermal gradient, initial porosity, and packing (Giles et al., 1998). For this reason, it is simpler to account for overpressured zones in subsidence analysis by calculating the error that would result from porosity variations within each lithology.

4.3.3.2 Carbonate dissolution

Carbonate dissolution, or physiochemical compaction, will result in apparently thinner layers than were originally deposited, making the calculated tectonic subsidence

less than it should be. Carbonate dissolution also reduces the porosity of the layer, in turn changing the calculated tectonic subsidence. Some stylolites can be seen in the Nordegg (T. Poulton, pers. comm.) but they were not accounted for here. In order to account for them, an estimate of how much thickness has been removed by dissolution is needed. This can be used to create error bars or to adjust the thickness used in the tectonic subsidence calculations.

4.3.3.3 Structure (faulting) and overthickening

Subsidence analysis in faulted layers is complicated and was not attempted here. However, undetected faults in a layer will cause apparent “overthickening” of the layer resulting in more apparent tectonic subsidence than if the deposited thickness was used. This problem is avoided in this study because the study area is east of the deformation limit where overthickening in the subsurface is unlikely. Although the reference well used in this section is west of the Eastern Limit of Deformation, it is close enough to that limit that overthickening is unlikely to be a significant factor.

4.3.4 Summary

The effects of all the sources of error are cumulative; the margin of error must be large enough to account for this cumulative effect. In order to estimate the margin of error, realistic variations in the lithologic parameters should be considered.

In this study, the maximum porosity variation tested caused no more than a 10% variation in tectonic subsidence. The maximum variation caused by changing the compaction coefficient was 6%, however compaction coefficient is a constant assigned to the lithologies based on the slope of the porosity-depth curve and not a measurable

geological parameter. The maximum change in tectonic subsidence for density variations expected in sedimentary rocks is 10% however density is less variable in rocks than porosity is and is not expected to cause as much uncertainty.

Giles et al. (1998) suggest that porosity variations will cause the greatest uncertainty in subsidence calculations and that up to a 20% variation in porosity (per lithology) can be expected if a simple porosity-depth function is being used for decompaction. Bond and Kominz (1984) propose that delithification is more accurate than decompaction, however it is a complicated procedure and instead maximum and minimum limits of the porosity-depth relationship should be large enough to account for delithification. The porosity-depth curves they use to do this show that only micrite and calcisiltite will cause more than a 20% porosity variation at the surface (Figure 4-11). Below 1km depth, none of the lithologies will cause more than a 20% porosity variation (Figure 4-12).

While parameters such as erosion, the presence of thin beds, interbedded lithologies and other considerations not tested here can cause variations in tectonic subsidence calculations, these cannot be quantified in a way that will make the estimates of uncertainty more accurate.

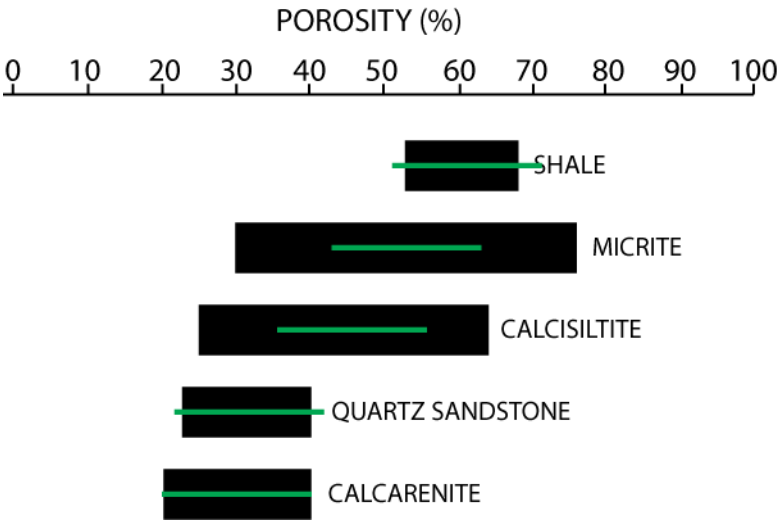

Figure 4-11: Limits of porosity variations at the surface.

Min. and max. surface porosities for different. The green bar is 20% long (adapted from Bond and Kominz, 1984)

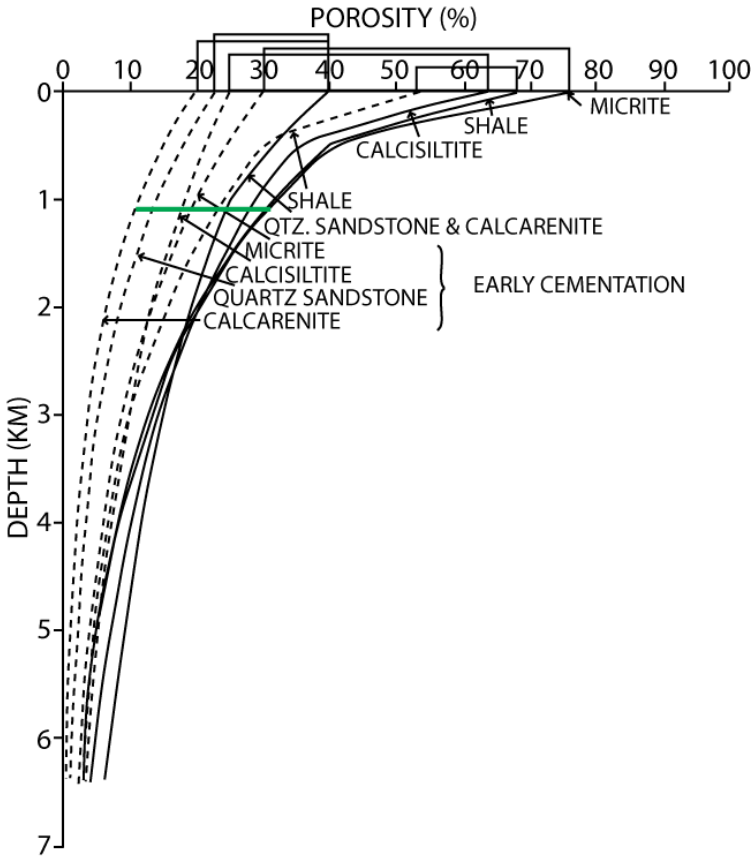

Figure 4-12: Limits of expected porosity variations at the depth.

At a depth of about 1km, the maximum porosity range for any lithology is 20% (green bar) (modified from Bond and Kominz, 1984).

The tectonic subsidence in the reference well was recalculated by increasing all of the porosities by 20% and by decreasing all of the porosities by 20% (Figure 4-13). This allows for a total porosity range of 40% per lithology error bars based on this will be large enough to account for any other sources of uncertainty but the profile of the subsidence curve, and therefore the subsidence trends being examined, are not significantly affected by this much variation. This range is also large enough to account for the fact that some micrite has been observed in the Nordegg (Collar, 1990; Poulton et al., 1990).

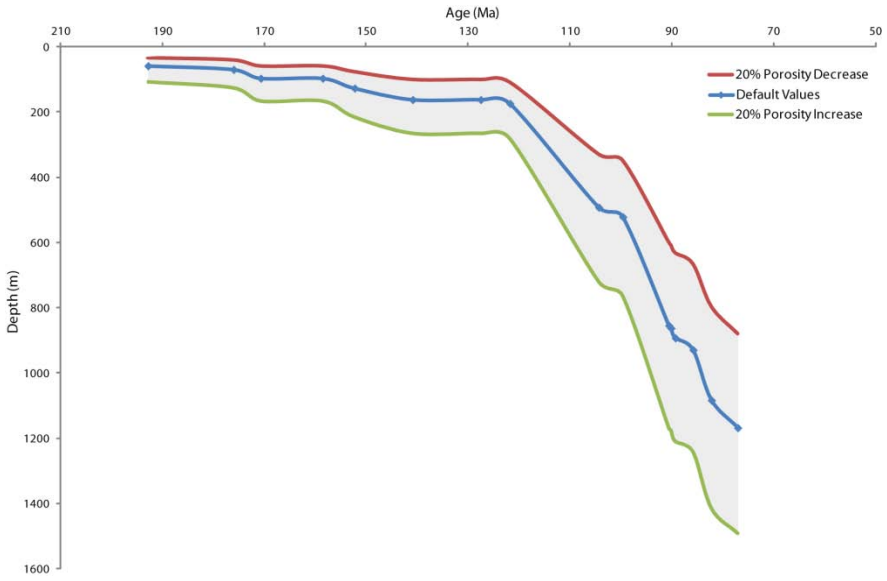

Figure 4-13: The effect of a 20% porosity variation on tectonic subsidence

The tectonic subsidence curve for the reference well (blue) and the margin of error for up to a 20% increase (green) or decrease (red) in porosity. Any tectonic subsidence values for this well that fall between the green and red profiles (grey area) are within the margin of error. The margin of error increases as total subsidence in the well increases.

Chapter Five: **Discussion**

5.1 How much does tectonic subsidence vary within the Jurassic of the Western Canada Foreland Basin?

All subsidence curves in this study display the convex-up pattern typical of a foreland basin (Xie and Heller, 2009); however, it is not practical to display 300 curves at the same time or on the same graph, which makes it difficult to compare the subsidence curves.

5.1.1 Tectonic subsidence envelope

A subsidence envelope is created by finding the maximum and minimum tectonic subsidence values for each layer. When these points are plotted on a depth vs. age chart the "envelope" is defined by outlining the minimum and maximum points at each time (Figure 5-1).

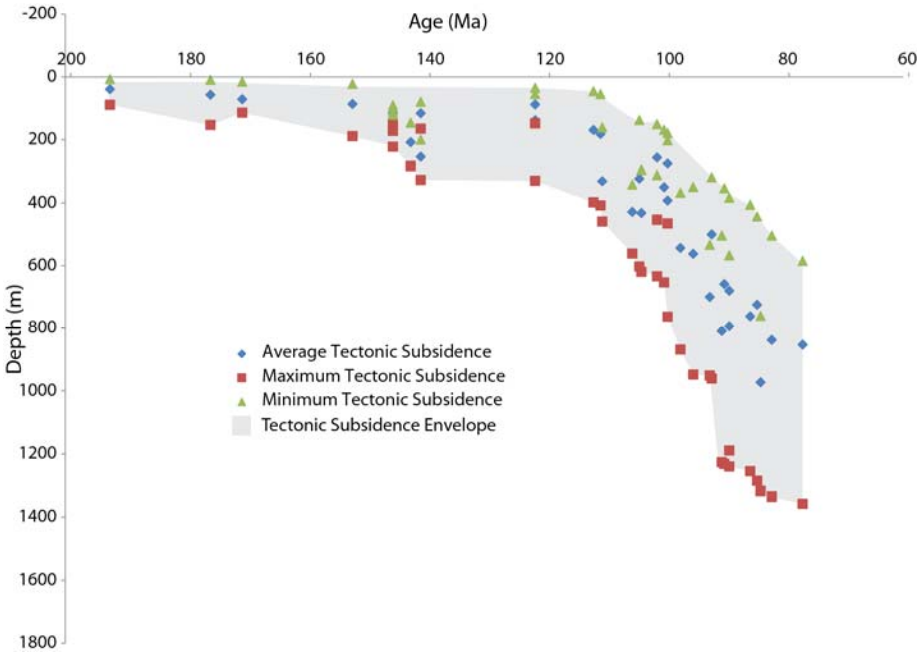

Figure 5-1: Tectonic subsidence envelope. The envelope is defined by the max. (red) and min. (green) for each layer.

5.1.2 Displaying error on the tectonic subsidence envelope

The error in tectonic subsidence, based on a 20% variation in porosity, was not calculated for all wells in the study area. Instead, the percent change in tectonic subsidence caused by a 20% variation in porosity was calculated for each layer in the reference well. This percent change in tectonic subsidence was then applied to the minimum, maximum, and average datasets used to define the envelope. Layers that do not occur in the reference well were assigned a percent change in tectonic subsidence based on age- and lithologically-equivalent formations**.** For example, the Muskiki and Cardium have been assigned the same percent variation in tectonic subsidence. The Table of Formations used is in Appendix D. Displaying the error as error bars clutters up the envelope (Figure 5-2), it is better to display the error as an extension of the envelope (Figure 5-3).

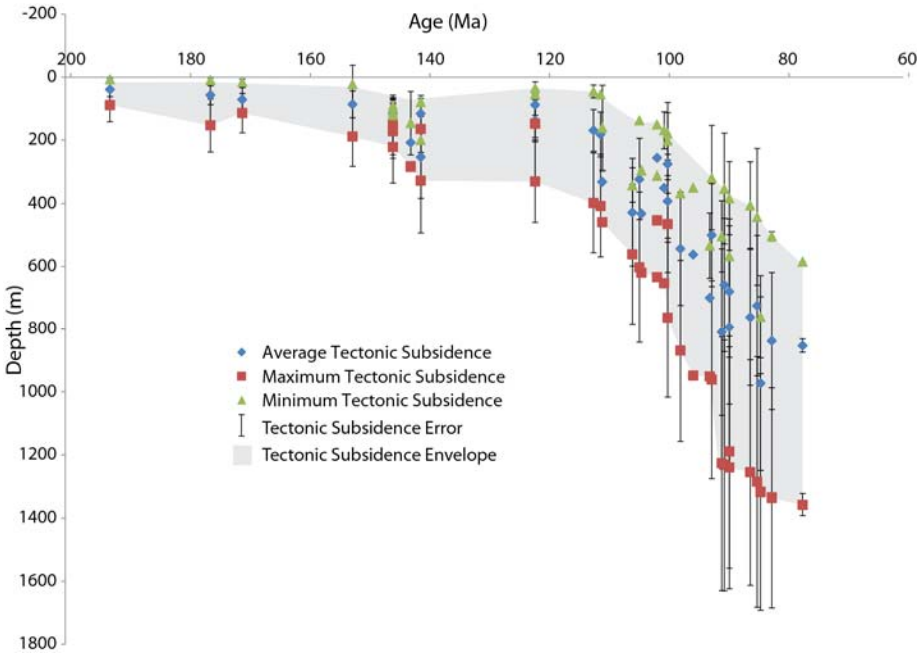

Figure 5-2: Tectonic subsidence envelope with error bars on data points.

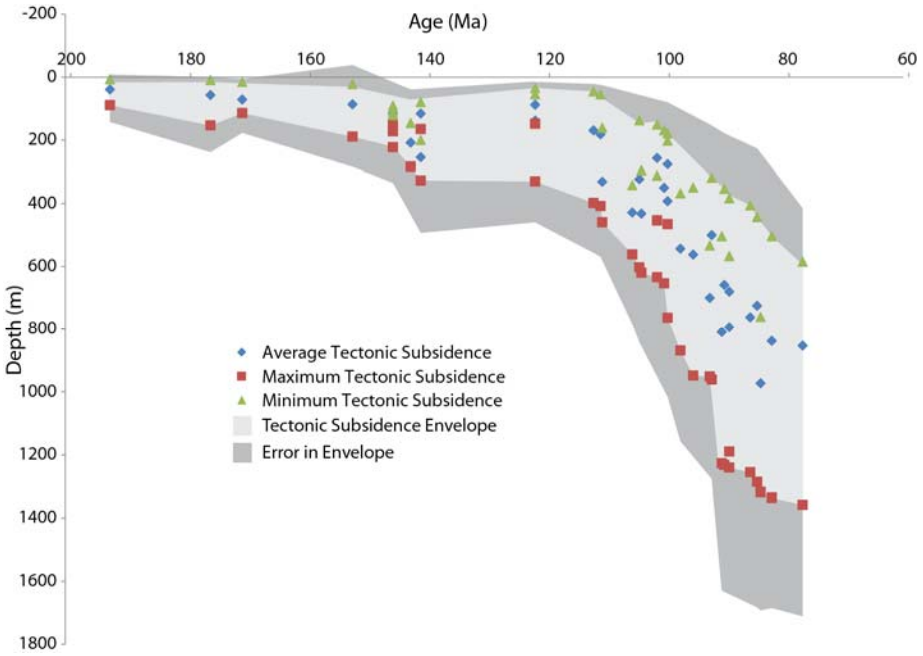

Figure 5-3: Tectonic subsidence envelope with error added to envelope.

5.1.3 Interpreting the tectonic subsidence envelope

Displaying best fit lines for each of the datasets used to create the envelope (minimum, maximum, and average tectonic subsidence) is useful for ensuring that the three datasets have similar ranges of values. The best fit lines should be approximately parallel (Figure 5-4); deviation from this could indicate significant problems in the tectonic subsidence calculated at some wells.

When the envelope deviates from the best-fit line, one possible cause is the error in the tectonic subsidence calculations; however these deviations can also be explained geologically. Before 120 Ma, the envelope deviates from the best-fit minimum and maximum lines where the sub-Cretaceous unconformity (120 Ma – 140 Ma) cuts deeper to the east than to the west. After 120 Ma there are many closely-spaced data points

and/or points with overlapping times on this chart, also leading to divergence of the envelope from the best-fit lines.

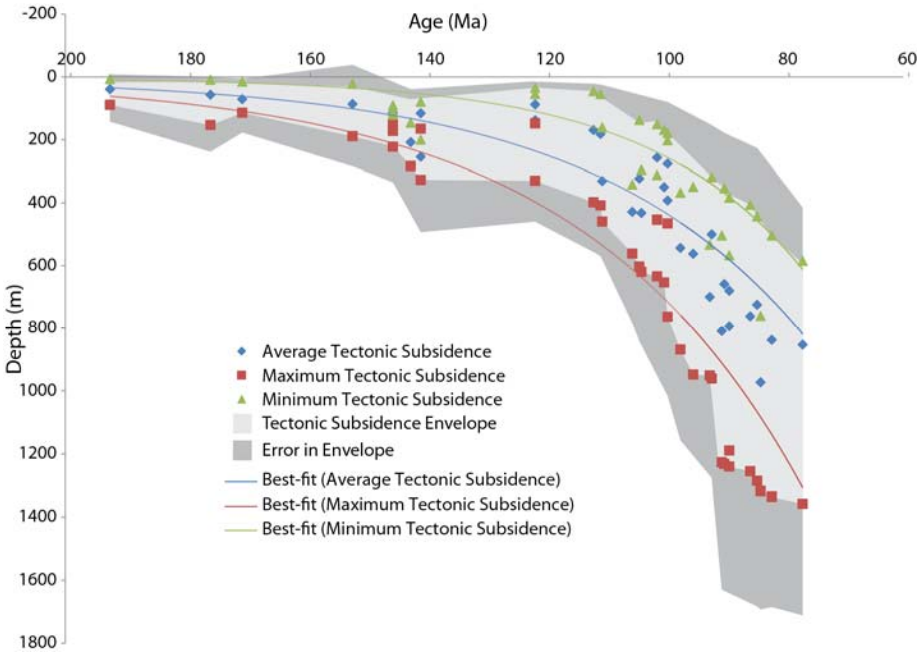

Figure 5-4: Tectonic subsidence envelope with best fit lines

Despite the geographic variation, the minimum, maximum, and average data points making up the tectonic subsidence envelope show similar regional trends. All show low subsidence rates during deposition of the Nordegg, Poker Chip Shale and Rock Creek, with a transition to more rapid subsidence (steeper slope) between 150 – 140 Ma and again between 120 – 100 Ma (Figure 5-5). The low subsidence and the rapid subsidence are broken up by a regional unconformity; this is the sub-Oxfordian unconformity (155 Ma – 170 Ma). There are two zones of rapid subsidence shown. These are broken up by the regional sub-Cretaceous unconformity. The transition from lower subsidence to rapid

subsidence following the sub-Oxfordian unconformity is not as clear on individual wells because of the effects of the sub-Cretaceous unconformity.

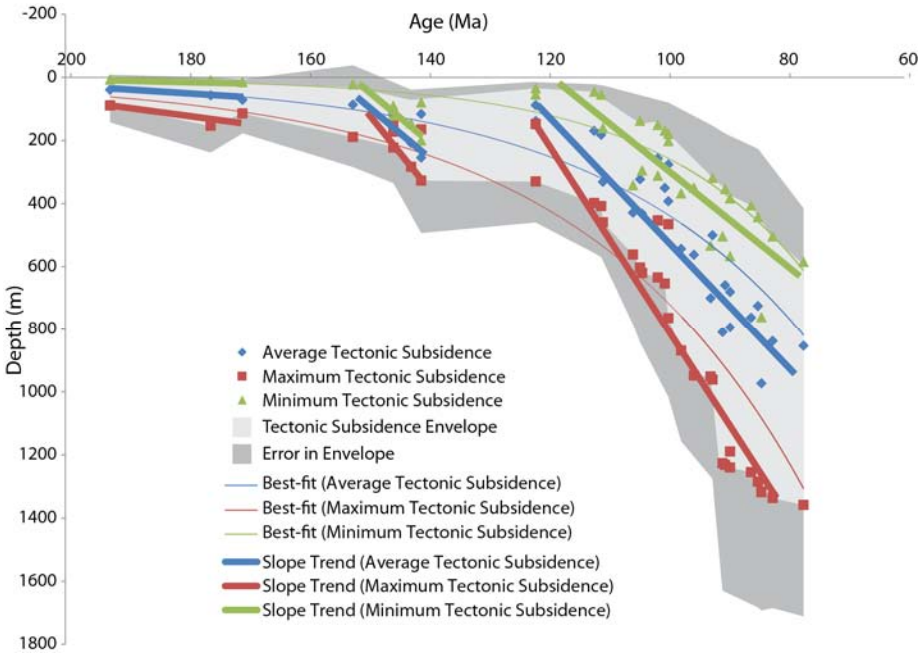

Figure 5-5: Tectonic subsidence envelope with regional subsidence trends displayed.

The tectonic subsidence envelope clearly shows that within the study area, there is a large variation in the amount of tectonic subsidence at a given time, and a single subsidence curve from a single point in the basin is not representative of the tectonic subsidence in the whole study area.

5.2 How can these tectonic subsidence variations be displayed?

It is necessary to display tectonic subsidence variations in a way that shows the variation spatially. In a smaller study area with fewer data points, it would be possible to show a subsidence curve beside each well location on a map but that is not feasible with over 300 wells in this study area.

Showing the subsidence variations on a map is the most desirable option. Tectonic subsidence maps have been used to study temporal and spatial variations in the Sirte Basin, Libya (Gumati and Nairn, 1991; Abadi et al., 2008).

Having a consistent base layer for all of the data points is necessary for mapping the data. If some of the data points have a different base layer, the calculated tectonic subsidence will be biased, appearing higher at locations where the base layer is a deeper layer.

In this study, the base layer is the Nordegg. Current structural variations do not effect tectonic subsidence calculations because they are based on thicknesses. This is particularly beneficial when the subsurface has experience post-depositional tilting (Figure 5-6).

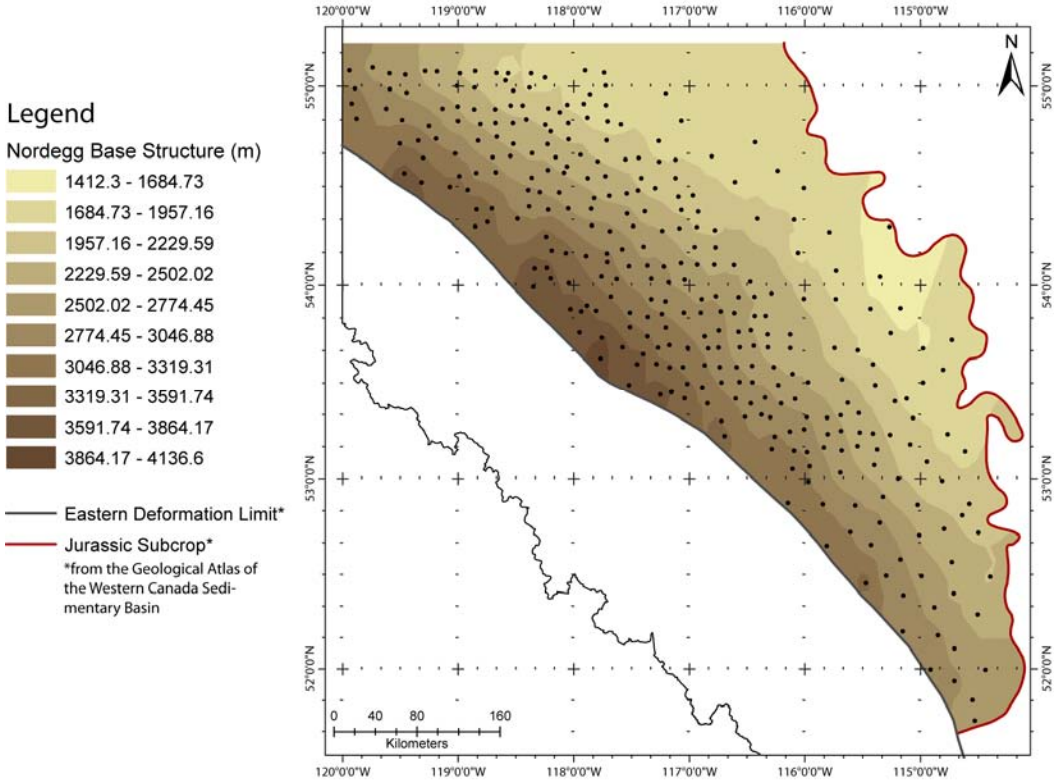

Figure 5-6: Structure map of the current depth to the base of the Nordegg

5.2.1 Relationship between tectonic subsidence and thickness

In order to be beneficial, tectonic subsidence maps must show something different than isopach maps. Before mapping any data, the tectonic subsidence and the thickness can be cross plotted to look for trends and first-order relationships between the two.

Figure 5-7 shows the cross-plots for the Nordegg, Poker Chip Shale, Rock Creek, and Upper Fernie in this study. Only the Nordegg has an R^2 value close to one, and it is the only one whose data values and best-fit line are coincident. In the Poker Chip Shale cross plot, there are two clusters of data points – one above the best-fit line and one below it. The Rock Creek and Upper Fernie cross plots are very scattered.

A further examination of the relationship between tectonic subsidence and thickness is possible by showing the residuals, the difference between each tectonic subsidence value and the corresponding point on the best fit line (Figure 5-8).

The two populations in the Poker Chip Shale can be identified in the residual. The random distribution of the Rock Creek and Upper Fernie residuals suggests that even though their cross-plots are quite scattered, a linear fit is the best fit for the datasets.

Tectonic subsidence is cumulative over time. It is directly related to thickness in the lowermost layer (here, the Nordegg), because there are no layers beneath it contributing to the tectonic subsidence. This relationship becomes less linear moving up through the layers.

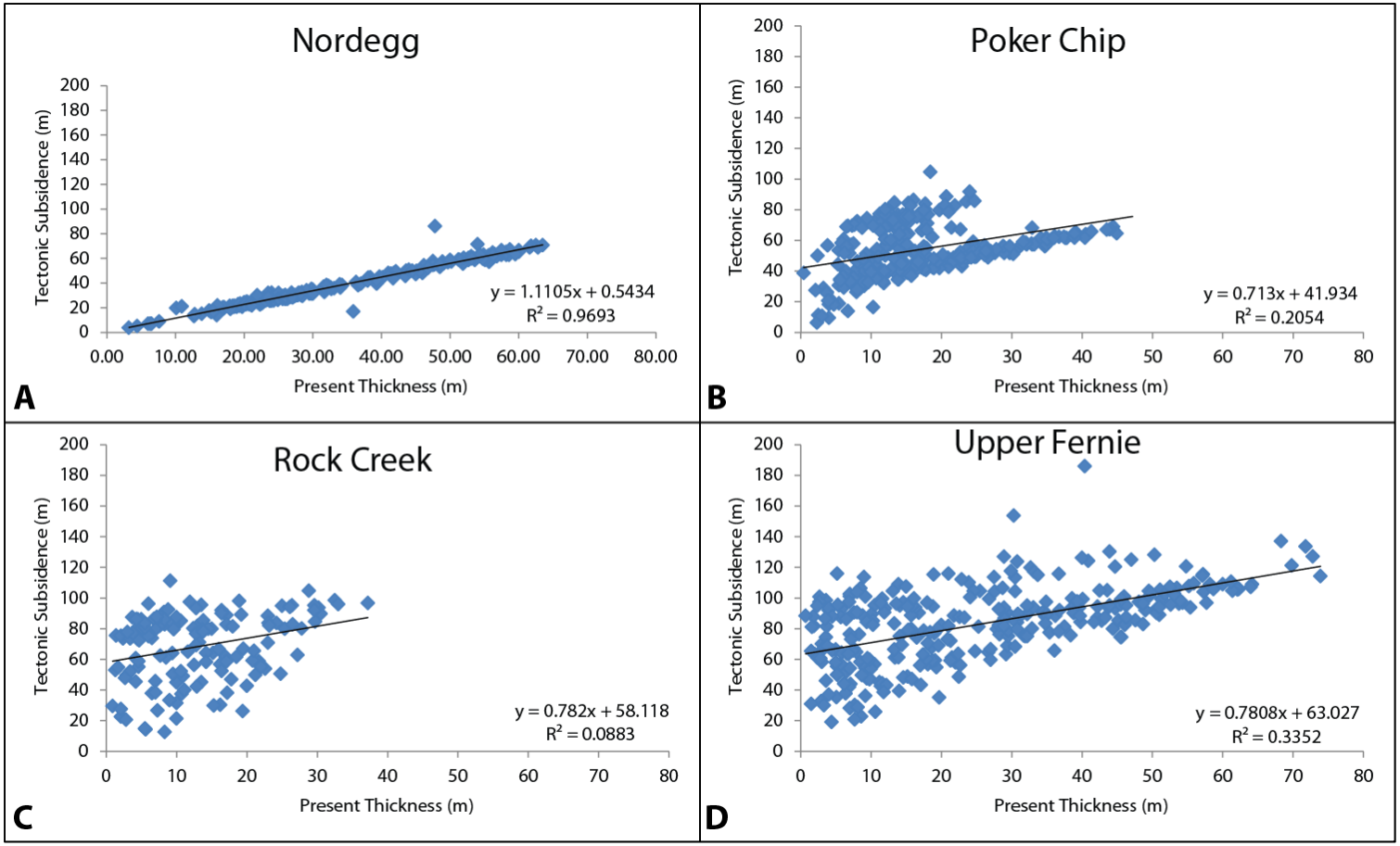

Figure 5-7: Cross plots of tectonic subsidence and thickness

A: Nordegg, B: Poker Chip Shale, C: Rock Creek, and D: Upper Fernie.

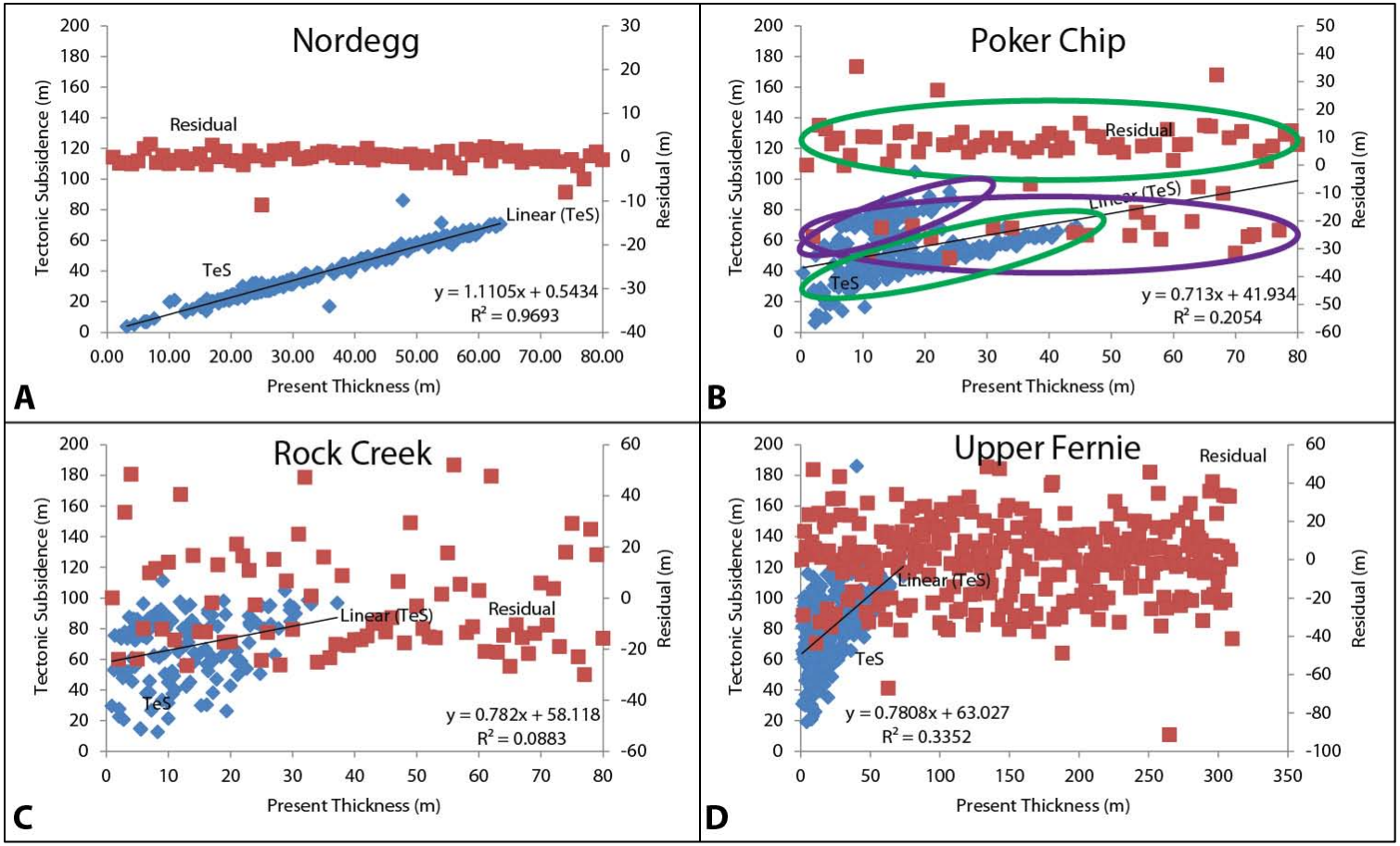

Figure 5-8: Cross plots and residuals of tectonic subsidence and thickness.

A: Nordegg, B: Poker Chip Shale, C: Rock Creek, and D: Upper Fernie.

5.2.2 Map suites

In addition to the isopach maps shown in Chapter 3, three maps were created for each of the four units of interest to create a map suite. Tectonic subsidence maps show the progression of trends throughout the basin. Residual and ratio maps provide an additional means of comparing the tectonic subsidence and the thickness.

The residual map is created by subtracting the thickness from the calculated tectonic subsidence for each layer. In these maps, a higher residual means a greater difference between tectonic subsidence and thickness. These maps show regional trends.

The ratio map shows the result when the tectonic subsidence is divided by the thickness. A higher ratio means the tectonic subsidence is considerably larger than the thickness. Regional trends are also clear on these maps.

5.2.2.1 Showing error on maps

Error calculations were not incorporated into the tectonic subsidence macros used to generate the dataset for mapping. The intent of generating the maps in this study is to examine how the subsidence varies throughout the region. Error in the calculated values is unlikely to affect the regional trends.

If this methodology was being used to tie into thermal modeling or to create paleostructure maps, the margin of error in the calculations would become more important. In that case, error could be shown using bubble shapes at each location that vary in size depending on the error. Alternately, the error could be shown on a cross-section or a separate map displayed adjacent to the tectonic subsidence map.

5.2.2.2 Nordegg

The Nordegg tectonic subsidence map (Figure 5-9B) has trends that are very similar to those in the Nordegg isopach (Figure 5-9A), with the greatest subsidence in the depocenter. There is a transition from low subsidence in the northwest to higher subsidence in the northeast that very roughly follows the Fox Creek Escarpment.

Because of the direct relationship between tectonic subsidence and thickness in the Nordegg, its residual (Figure 5-9C) is a direct measurement of where tectonic subsidence and thickness vary. The most variation between the two occurs in the west, particularly within the depocenter.

In the Nordegg, the ratio values are all close to one because of the direct relationship between tectonic subsidence and thickness. The Nordegg ratio (Figure 5-9D) increases to the west with a small low-ratio gap along the western boundary of the study area between the Fox Creek Escarpment and the southwest limit of the Nordegg depocenter.

Figure 5-9 (next page): Suite of maps for the Nordegg.

A: Isopach. B: Tectonic Subsidence. C: Residual (Tectonic Subsidence – Thickness). D: Ratio (Tectonic Subsidence/Thickness).

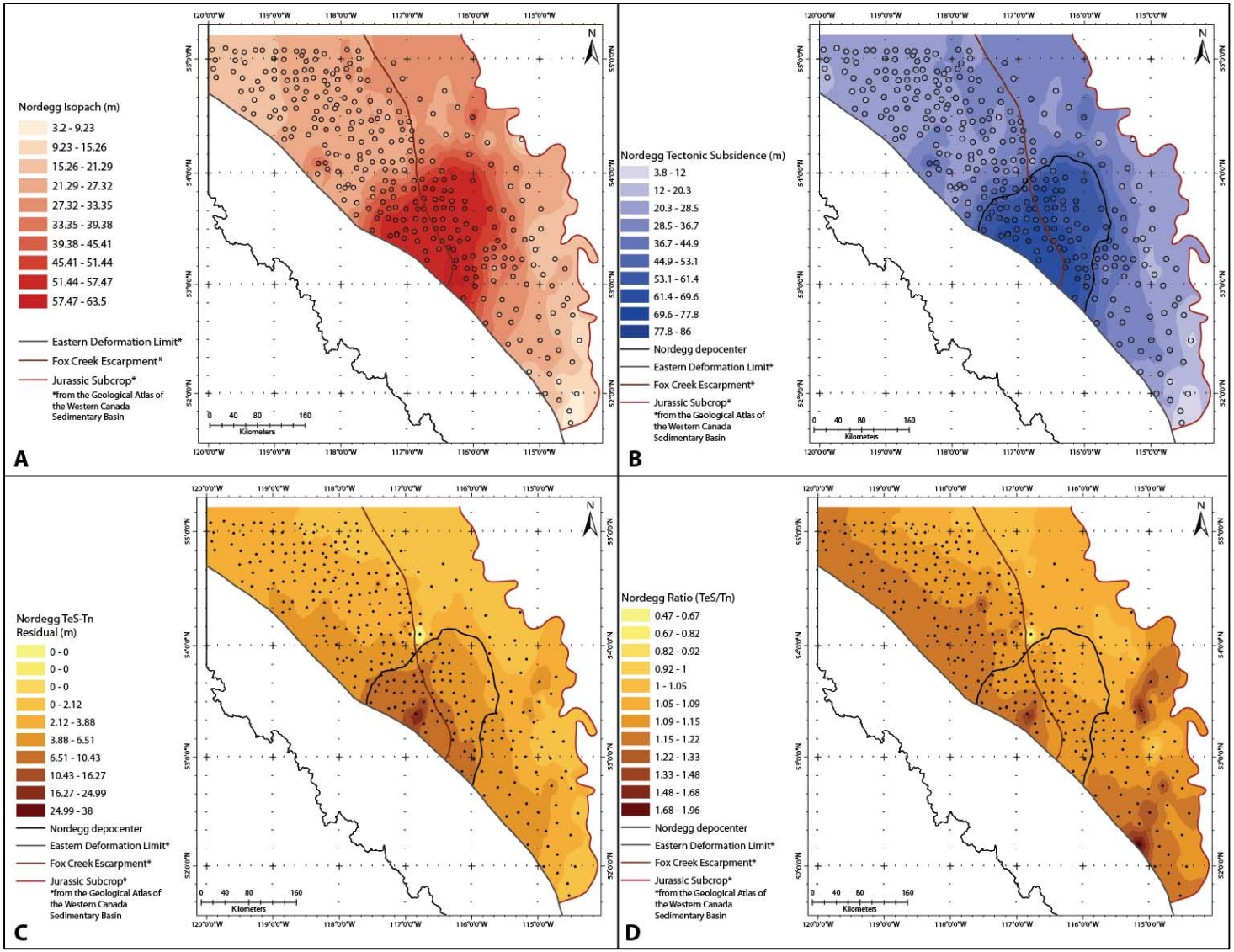
Nordegg Isopach (m)
3.2 - 9.23
9.23 - 15.26
15.26 - 21.29
21.29 - 27.32
27.32 - 33.35
33.35 - 39.38
39.38 - 45.41
45.41 - 51.44
51.44 - 57.47
57.47 - 63.5
Eastern Deformation Limit*
Fox Creek Escarpment*
Jurassic Subcrop*
*from the Geological Atlas of the Western Canada Sedimentary Basin
A
Nordegg Tectonic Subsidence (m)
3.8 - 12
12 - 20.3
20.3 - 28.5
28.5 - 36.7
36.7 - 44.9
44.9 - 53.1
53.1 - 61.4
61.4 - 69.6
69.6 - 77.8
77.8 - 86
Nordegg depocenter
Eastern Deformation Limit*
Fox Creek Escarpment*
Jurassic Subcrop*
*from the Geological Atlas of the Western Canada Sedimentary Basin
B
Nordegg TeS-Tn Residual (m)
0 - 0
0 - 0
0 - 0
0 - 2.12
2.12 - 3.88
3.88 - 6.51
6.51 - 10.43
10.43 - 16.27
16.27 - 24.99
24.99 - 38
Nordegg depocenter
Eastern Deformation Limit*
Fox Creek Escarpment*
Jurassic Subcrop*
*from the Geological Atlas of the Western Canada Sedimentary Basin
C
Nordegg Ratio (TeS/Tn)
0.47 - 0.67
0.67 - 0.82
0.82 - 0.92
0.92 - 1
1 - 1.05
1.05 - 1.09
1.09 - 1.15
1.15 - 1.22
1.22 - 1.33
1.33 - 1.48
1.48 - 1.68
1.68 - 1.96
Nordegg depocenter
Eastern Deformation Limit*
Fox Creek Escarpment*
Jurassic Subcrop*
*from the Geological Atlas of the Western Canada Sedimentary Basin
D
N
0 40 80 160
Kilometers

5.2.2.3 Poker Chip Shale

The principal features on the Poker Chip Shale tectonic subsidence map (Figure 5-10B) are the high tectonic subsidence within the limits of the Nordegg depocenter and the region of low subsidence along the northwest edge of the Fox Creek Escarpment.

The two separate trends on the Poker Chip Shale cross plot (Figure 5-10B) are linked to their locations. One trend (circled in green on Figure 5-10B) reflects that the high subsidence within the Nordegg depocenter during Nordegg deposition has not been matched by similar rates of tectonic subsidence during Poker Chip Shale subsidence. This is apparent from the Poker Chip Shale residual map (Figure 5-10C), which has the highest values within and surrounding the Nordegg depocenter boundary. The other trend shows the tectonic subsidence that occurred during the Poker Chip Shale independent of the trends associated with earlier deposition.

The Poker Chip Shale ratio map (Figure 5-10D) has the highest ratios within the limits and southeast of the Nordegg depocenter. In the north, the ratio is higher immediately to the west of the Fox Creek Escarpment.

Figure 5-10 (next page): Suite of maps for the Poker Chip Shale

A: Isopach. B: Tectonic Subsidence. C: Residual (Tectonic Subsidence – Thickness). D: Ratio (Tectonic Subsidence/Thickness).

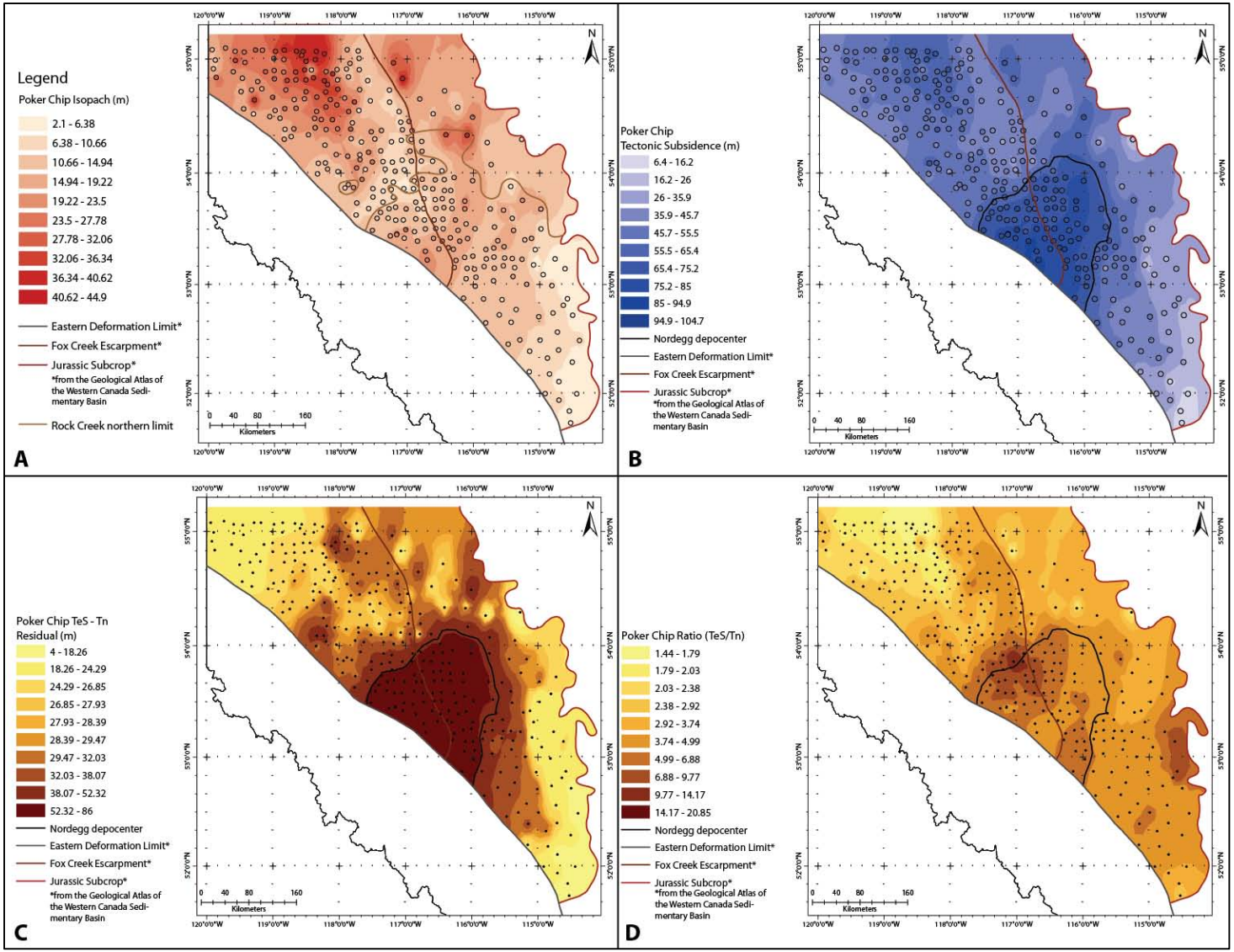
Legend
Poker Chip Isopach (m)
2.1 - 6.38
6.38 - 10.66
10.66 - 14.94
14.94 - 19.22
19.22 - 23.5
23.5 - 27.78
27.78 - 32.06
32.06 - 36.34
36.34 - 40.62
40.62 - 44.9
Eastern Deformation Limit*
Fox Creek Escarpment*
Jurassic Subcrop*
*from the Geological Atlas of the Western Canada Sedimentary Basin
Rock Creek northern limit
A
Poker Chip Tectonic Subsidence (m)
6.4 - 16.2
16.2 - 26
26 - 35.9
35.9 - 45.7
45.7 - 55.5
55.5 - 65.4
65.4 - 75.2
75.2 - 85
85 - 94.9
94.9 - 104.7
Nordegg depocenter
Eastern Deformation Limit*
Fox Creek Escarpment*
Jurassic Subcrop*
*from the Geological Atlas of the Western Canada Sedimentary Basin
B
Poker Chip TeS - Tn Residual (m)
4 - 18.26
18.26 - 24.29
24.29 - 26.85
26.85 - 27.93
27.93 - 28.39
28.39 - 29.47
29.47 - 32.03
32.03 - 38.07
38.07 - 52.32
52.32 - 86
Nordegg depocenter
Eastern Deformation Limit*
Fox Creek Escarpment*
Jurassic Subcrop*
*from the Geological Atlas of the Western Canada Sedimentary Basin
C
Poker Chip Ratio (TeS/Tn)
1.44 - 1.79
1.79 - 2.03
2.03 - 2.38
2.38 - 2.92
2.92 - 3.74
3.74 - 4.99
4.99 - 6.88
6.88 - 9.77
9.77 - 14.17
14.17 - 20.85
Nordegg depocenter
Eastern Deformation Limit*
Fox Creek Escarpment*
Jurassic Subcrop*
*from the Geological Atlas of the Western Canada Sedimentary Basin
D
0 40 80 160
Kilometers
N

The Poker Chip Shale cross plot (Figure 5-8B) shows two populations, one of which is related to subsidence that occurred in the Nordegg and the other is related to subsidence that occurred during Poker Chip Shale deposition. If the Nordegg tectonic subsidence is subtracted from the Poker Chip Shale tectonic subsidence, the resulting tectonic subsidence map (Figure 5-11B) has similar trends to the Poker Chip Shale isopach (Figure 5-11A) with highest subsidence (and thickest deposits) in the northwest corner, decreasing east to the Fox Creek Escarpment and then increasing again on the other side of it.

The residual map of the Poker Chip Shale tectonic subsidence with the Nordegg tectonic subsidence first removed (Figure 5-11C) shows higher residuals in the west. The ratio (Figure 5-11D) shows similar trends to the residual map. There are also higher residual and ratio values along the southeast edge of the study area.

Figure 5-11 (next page): Suite of maps showing the Poker Chip Shale trends (Nordegg component removed).

A: Poker Chip Shale Isopach. B: Tectonic Subsidence. C: Residual (Tectonic Subsidence – Thickness). D: Ratio (Tectonic Subsidence/Thickness).

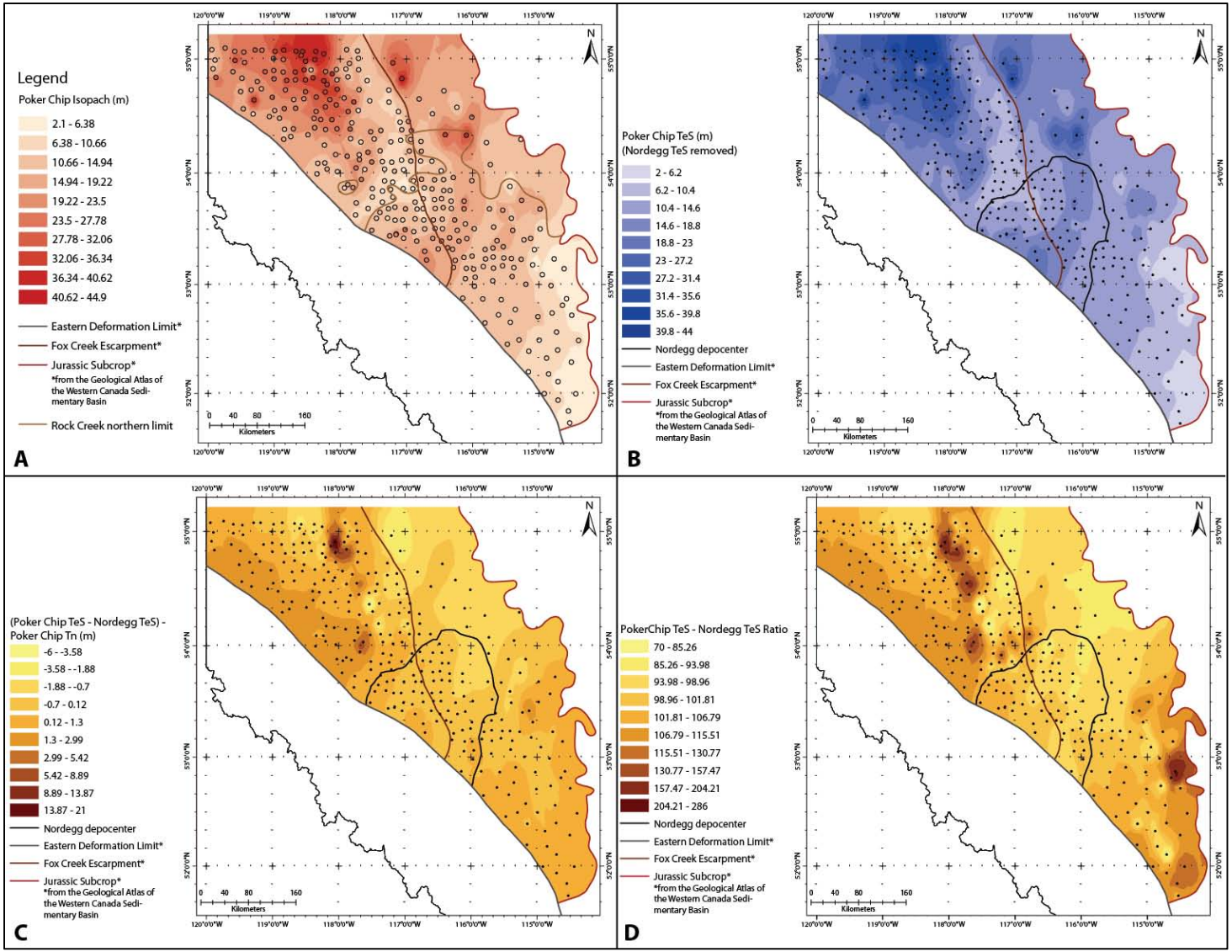
Legend
Poker Chip Isopach (m)
2.1 - 6.38
6.38 - 10.66
10.66 - 14.94
14.94 - 19.22
19.22 - 23.5
23.5 - 27.78
27.78 - 32.06
32.06 - 36.34
36.34 - 40.62
40.62 - 44.9
Eastern Deformation Limit*
Fox Creek Escarpment*
Jurassic Subcrop*
*from the Geological Atlas of the Western Canada Sedimentary Basin
Rock Creek northern limit
A
Poker Chip TeS (m)
(Nordegg TeS removed)
2 - 6.2
6.2 - 10.4
10.4 - 14.6
14.6 - 18.8
18.8 - 23
23 - 27.2
27.2 - 31.4
31.4 - 35.6
35.6 - 39.8
39.8 - 44
Nordegg depocenter
Eastern Deformation Limit*
Fox Creek Escarpment*
Jurassic Subcrop*
*from the Geological Atlas of the Western Canada Sedimentary Basin
B
(Poker Chip TeS - Nordegg TeS) - Poker Chip Tn (m)
-6 - -3.58
-3.58 - -1.88
-1.88 - -0.7
-0.7 - 0.12
0.12 - 1.3
1.3 - 2.99
2.99 - 5.42
5.42 - 8.89
8.89 - 13.87
13.87 - 21
Nordegg depocenter
Eastern Deformation Limit*
Fox Creek Escarpment*
Jurassic Subcrop*
*from the Geological Atlas of the Western Canada Sedimentary Basin
C
PokerChip TeS - Nordegg TeS Ratio
70 - 85.26
85.26 - 93.98
93.98 - 98.96
98.96 - 101.81
101.81 - 106.79
106.79 - 115.51
115.51 - 130.77
130.77 - 157.47
157.47 - 204.21
204.21 - 286
Nordegg depocenter
Eastern Deformation Limit*
Fox Creek Escarpment*
Jurassic Subcrop*
*from the Geological Atlas of the Western Canada Sedimentary Basin
D
0 40 80 160
Kilometers
N

5.2.2.4 Rock Creek

The limited distribution of the Rock Creek in this study makes it difficult to interpret the Rock Creek map suite. The tectonic subsidence (Figure 5-12B) increases to the northwest, particularly within the limits of the Nordegg depocenter.

The residual (Figure 5-12C) is highest here as well. From the limited amount of Rock Creek data northwest of the edge of the Nordegg depocenter, it appears that the tectonic subsidence and residual values decrease away from the Nordegg depocenter. The Rock Creek ratio (Figure 5-12D) has similar trends to the isopach map (Figure 5-12A**)**. Where the Rock Creek is thickest the Ratio is lowest. There is a sharp transition from thick to thin (high ratio to low ratio) immediately southeast of the southern edge of the Fox Creek Escarpment.

Figure 5-12 (next page): Suite of maps for the Rock Creek

A: Isopach. B: Tectonic Subsidence. C: Residual (Tectonic Subsidence – Thickness). D: Ratio (Tectonic Subsidence/Thickness).

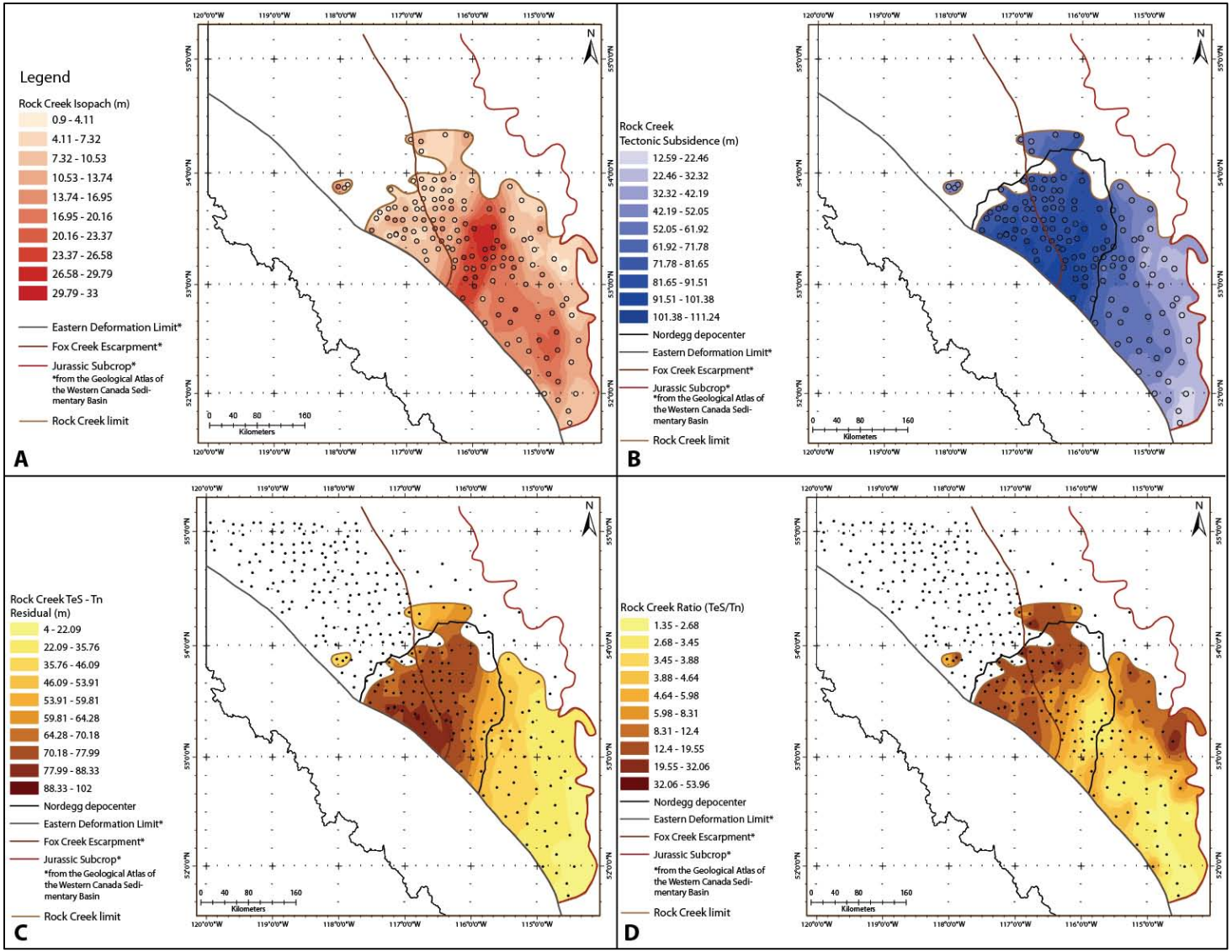
Legend
Rock Creek Isopach (m)
0.9 - 4.11
4.11 - 7.32
7.32 - 10.53
10.53 - 13.74
13.74 - 16.95
16.95 - 20.16
20.16 - 23.37
23.37 - 26.58
26.58 - 29.79
29.79 - 33
Eastern Deformation Limit*
Fox Creek Escarpment*
Jurassic Subcrop*
*from the Geological Atlas of the Western Canada Sedimentary Basin
Rock Creek limit
A
Rock Creek
Tectonic Subsidence (m)
12.59 - 22.46
22.46 - 32.32
32.32 - 42.19
42.19 - 52.05
52.05 - 61.92
61.92 - 71.78
71.78 - 81.65
81.65 - 91.51
91.51 - 101.38
101.38 - 111.24
Nordegg depocenter
Eastern Deformation Limit*
Fox Creek Escarpment*
Jurassic Subcrop*
*from the Geological Atlas of the Western Canada Sedimentary Basin
Rock Creek limit
B
Rock Creek TeS - Tn
Residual (m)
4 - 22.09
22.09 - 35.76
35.76 - 46.09
46.09 - 53.91
53.91 - 59.81
59.81 - 64.28
64.28 - 70.18
70.18 - 77.99
77.99 - 88.33
88.33 - 102
Nordegg depocenter
Eastern Deformation Limit*
Fox Creek Escarpment*
Jurassic Subcrop*
*from the Geological Atlas of the Western Canada Sedimentary Basin
Rock Creek limit
C
Rock Creek Ratio (TeS/Tn)
1.35 - 2.68
2.68 - 3.45
3.45 - 3.88
3.88 - 4.64
4.64 - 5.98
5.98 - 8.31
8.31 - 12.4
12.4 - 19.55
19.55 - 32.06
32.06 - 53.96
Nordegg depocenter
Eastern Deformation Limit*
Fox Creek Escarpment*
Jurassic Subcrop*
*from the Geological Atlas of the Western Canada Sedimentary Basin
Rock Creek limit
D
N
0 40 80 160
Kilometers

5.2.2.5 Upper Fernie

The Upper Fernie tectonic subsidence map (Figure 5-13B) shows that the highest subsidence is occurring west of the Minnes Group subcrop and within the limits of the Nordegg depocenter. Between the Minnes Group subcrop and the Fox Creek Escarpment is a zone of low subsidence, corresponding to the erosional feature identified in the Upper Fernie isopach (Figure 5-13A). East of the Fox Creek Escarpment the tectonic subsidence increases again.

The Upper Fernie residual map (Figure 5-13C) is dominated by high residual values surrounding the southern end of the Fox Creek Escarpment.

The trend in the Upper Fernie ratio map (Figure 5-13D) is for the ratio to increase to the southwest. There is a noticeable decrease in the ratio to the west of the Minnes Group Subcrop.

Figure 5-13 (next page): Suite of maps for the Upper Fernie

A: Isopach. B: Tectonic Subsidence. C: Residual (Tectonic Subsidence – Thickness). D: Ratio (Tectonic Subsidence/Thickness).

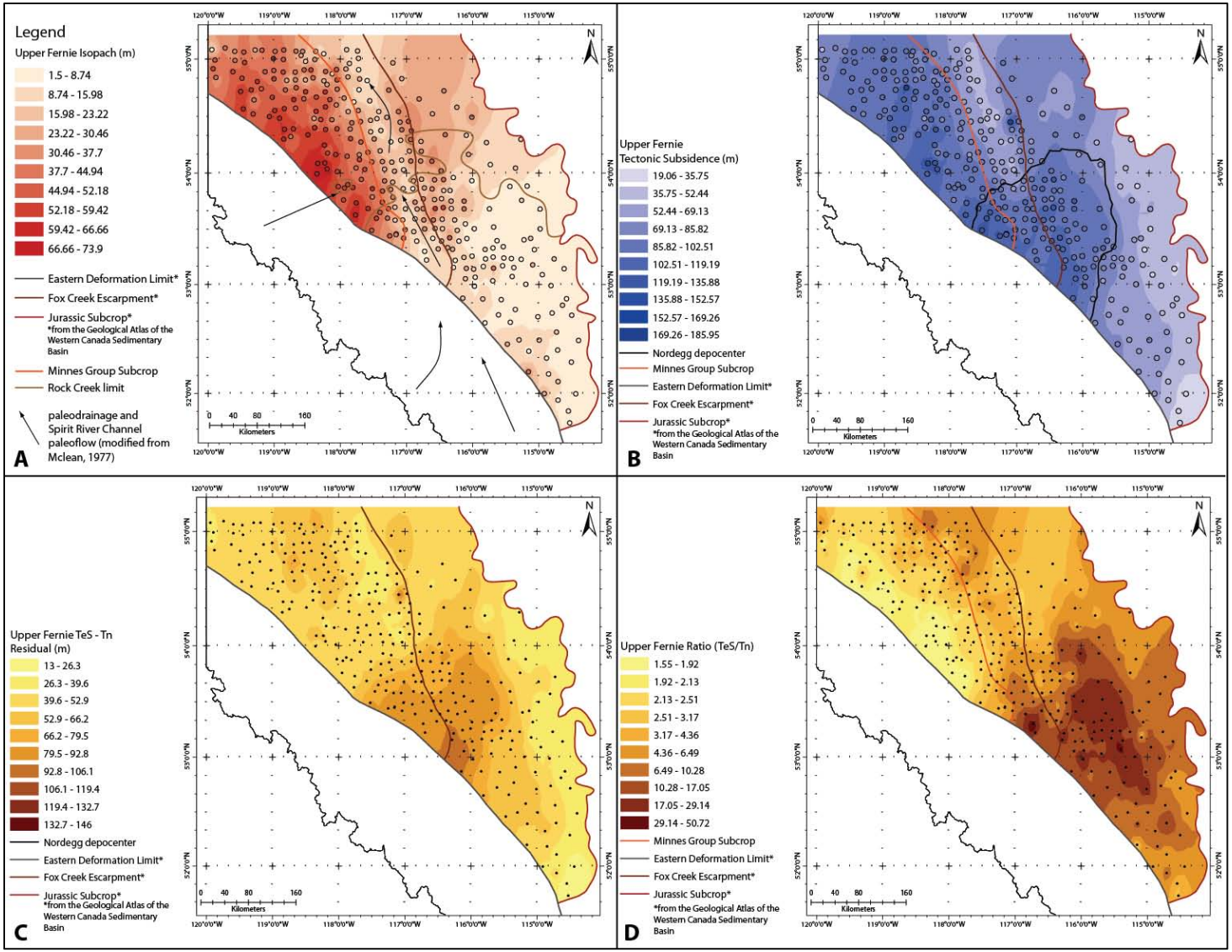
Legend
Upper Fernie Isopach (m)
1.5 - 8.74
8.74 - 15.98
15.98 - 23.22
23.22 - 30.46
30.46 - 37.7
37.7 - 44.94
44.94 - 52.18
52.18 - 59.42
59.42 - 66.66
66.66 - 73.9
Eastern Deformation Limit*
Fox Creek Escarpment*
Jurassic Subcrop*
*from the Geological Atlas of the Western Canada Sedimentary Basin
Minnes Group Subcrop
Rock Creek limit
paleodrainage and Spirit River Channel paleoflow (modified from Mclean, 1977)
A
Upper Fernie Tectonic Subsidence (m)
19.06 - 35.75
35.75 - 52.44
52.44 - 69.13
69.13 - 85.82
85.82 - 102.51
102.51 - 119.19
119.19 - 135.88
135.88 - 152.57
152.57 - 169.26
169.26 - 185.95
Nordegg depocenter
Minnes Group Subcrop
Eastern Deformation Limit*
Fox Creek Escarpment*
Jurassic Subcrop*
*from the Geological Atlas of the Western Canada Sedimentary Basin
B
Upper Fernie TeS - Tn Residual (m)
13 - 26.3
26.3 - 39.6
39.6 - 52.9
52.9 - 66.2
66.2 - 79.5
79.5 - 92.8
92.8 - 106.1
106.1 - 119.4
119.4 - 132.7
132.7 - 146
Nordegg depocenter
Eastern Deformation Limit*
Fox Creek Escarpment*
Jurassic Subcrop*
*from the Geological Atlas of the Western Canada Sedimentary Basin
C
Upper Fernie Ratio (TeS/Tn)
1.55 - 1.92
1.92 - 2.13
2.13 - 2.51
2.51 - 3.17
3.17 - 4.36
4.36 - 6.49
6.49 - 10.28
10.28 - 17.05
17.05 - 29.14
29.14 - 50.72
Minnes Group Subcrop
Eastern Deformation Limit*
Fox Creek Escarpment*
Jurassic Subcrop*
*from the Geological Atlas of the Western Canada Sedimentary Basin
D
N
0 40 80 160
Kilometers

5.3 What can these tectonic subsidence variations tell us?

5.3.1 Tectonic subsidence trends

The higher ratio and residual in the western portions of the Nordegg maps (Figure 5-9C and D) indicate that there was a western influence on subsidence during Nordegg deposition.

The presence of two trends on the Poker Chip Shale cross plot (Figure 5-8**)** show that base level movement caused by the high subsidence in the Nordegg depocenter during Nordegg deposition is not exceeded by any subsidence during deposition of the Poker Chip Shale. If the Nordegg component of tectonic subsidence is removed from the Poker Chip tectonic subsidence (Figure 5-11), the western influence on tectonic subsidence is still seen.

During Rock Creek deposition, the influence of the tectonic subsidence feature created during Nordegg deposition is not as strong as during Poker Chip Shale deposition. This means that overall tectonic subsidence in the study area has increased since deposition of the Nordegg. The low ratio in the Rock Creek (Figure 5-12D) means the thickness and tectonic subsidence values are close together, interpreted here as an indication that Rock Creek sediment deposition was keeping up with subsidence. This is consistent with the depositional environment (T. Poulton, pers. comm.).

During Upper Fernie deposition, the amount of tectonic subsidence along the western edge of the study area matches the amount of tectonic subsidence seen in the Nordegg depocenter (Figure 5-13B) showing that the loading in the west is continuing.

The high ratio in the southwest (Figure 5-13D) reflects the fact that the Rock Creek exists below this and is contributing to the cumulative tectonic subsidence.

5.3.2 Relation to underlying structure

5.3.2.1 Basement structure

The northern limit of the Rock Creek and of the Nordegg depocenter are close to the northern boundary of the Snowbird Tectonic Zone (shown in Figure 5-14) and the southern boundary of the Nordegg depocenter loosely coincides with the southern boundary of the Snowbird Tectonic Zone, suggesting a relationship between the basement structure and deposition during the Jurassic.

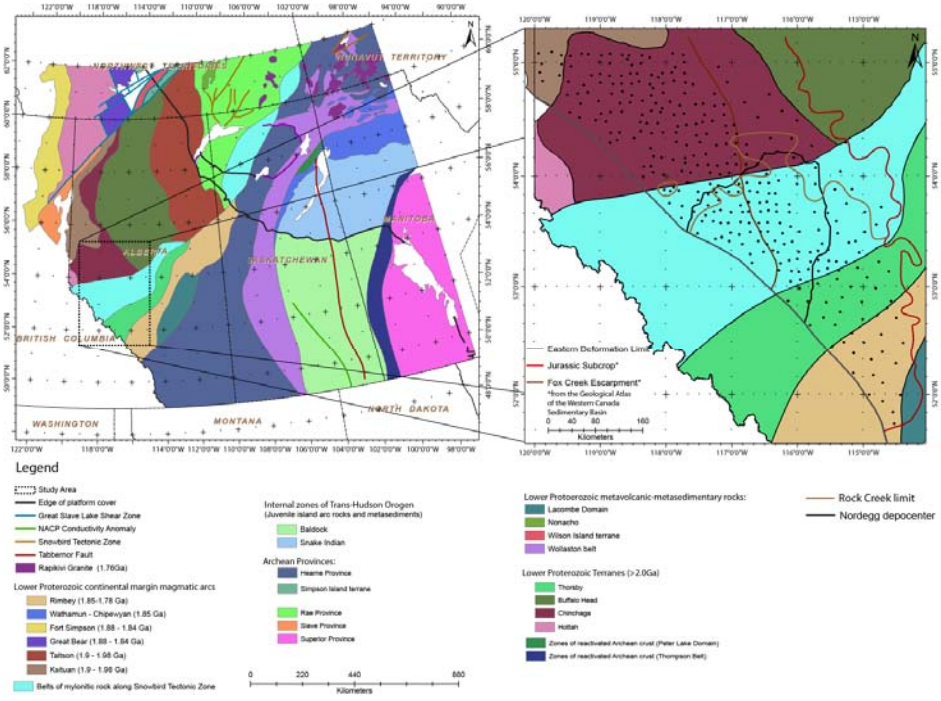

Figure 5-14: Map of basement structure showing relationship to Jurassic features The entire Western Canada Sedimentary Basin is on the left. The study area is on the right (modified from Ross et al., 1994).

5.3.2.2 Fox Creek Escarpment

The Fox Creek Escarpment was a high-relief feature in the Early Cretaceous (McLean, 1977). Uplift of the escarpment should show up on tectonic subsidence maps as a decrease in subsidence where the uplift is occurring (or an increase in subsidence adjacent to the uplift).

The transition from low subsidence to high subsidence across the Fox Creek Escarpment during Nordegg deposition (Figure 5-9B) is a direct reflection of the thicker Nordegg found on the east side of the escarpment. By contrast, the ratio and residual show that tectonic subsidence is much greater than thickness at the southern end of the escarpment (Figure 5-9C and D), suggesting that there may have been some uplift along this end of the escarpment at this time.

The Poker Chip Shale ratio (Figure 5-10D) shows that the uplift progressed north. The uplift cannot be traced during Rock Creek deposition because of the limited extent of the sands. Removal of the Upper Fernie associated with the sub-Cretaceous unconformity makes understanding the tectonic subsidence trends along the escarpment difficult, however the ratio does suggest there was more subsidence to the west of the escarpment (Figure 5-13D).

5.4 What evidence is there for an Early Jurassic initiation of the Western Canada Foreland Basin?

The Fernie Formation of west-central Alberta is interpreted to contain a nearly-complete sequence of foreland basin depozones (as described by DeCelles & Giles, 1996). The lower members identified in this study, the Nordegg, Poker Chip Shale, and

Rock Creek, are typical of a backbulge depozone (*ibid*.). The unconformity separating these from the Upper Fernie (the sub-Oxfordian unconformity) is interpreted to represent the passage of the forebulge through the study area; it is followed by deposition of the Upper Fernie in a foredeep depozone.

This interpretation extends existing models back in time using the broader definition of a foreland basin system, and as such, does not contradict existing interpretations that the Upper Fernie contains the first foredeep deposits preserved in west-central Alberta (Poulton, 1989; Miles, 2010; Miall, 2009). A critical piece of this interpretation is justifying the presence of a backbulge in the WCFB.

5.4.1 Subsidence data

All subsidence curves in this study area display the convex-up pattern typical of a foreland basin (Xie and Heller, 2009). Additionally, they all record a minor pulse of subsidence during deposition of the lower Fernie Formation (Nordegg, Poker Chip Shale, and Rock Creek), indicated by the gentle slope of the subsidence curve during deposition of these units. Following this is a period of erosion/non-deposition represented on the subsidence curve by a horizontal line. This represents passage of a forebulge through the study area. Finally, rapid subsidence began during deposition of the Upper Fernie and continued into the Cretaceous, shown by the steeply sloping section of the subsidence curve. In the northwestern portion of the study area, this rapid subsidence is interrupted by the regional sub-Cretaceous unconformity event. The same event has removed too much of the Upper Jurassic strata to pinpoint when the rapid subsidence begins in the

eastern portions of the study area. These same trends can be identified on the tectonic subsidence envelope (Figure 5-15).

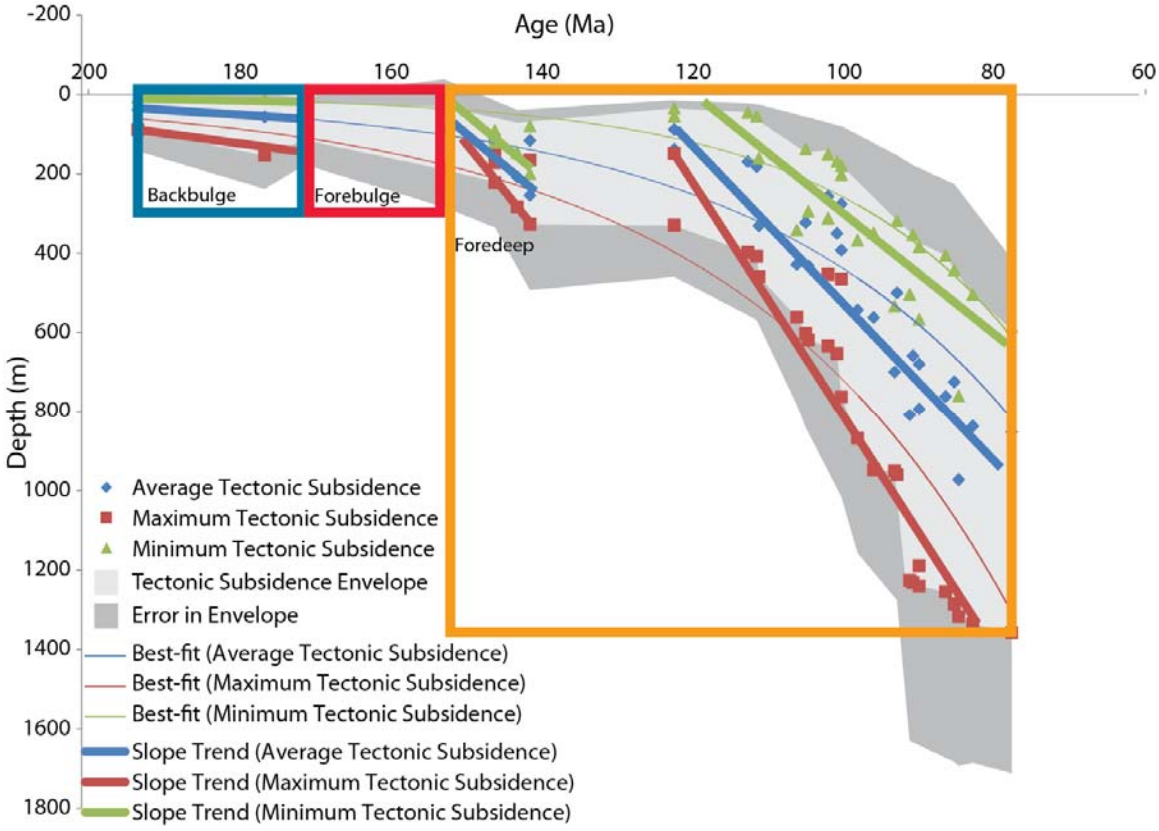

Figure 5-15: Interpreted tectonic subsidence envelope for WCFB.

The tectonic subsidence envelope shows the low subsidence rates expected in a backbulge depozone (blue rectangle), the unconformity associated with the passage of a forebulge (red rectangle) and the rapid subsidence during deposition in the foredeep (yellow rectangle).

The low rate of subsidence in the lower Jurassic deposits is typical of a backbulge. Here, the subsidence is minor because of the distance from the orogenic load. The rapid subsidence seen on the tectonic subsidence curves during deposition of the

Upper Fernie and continuing into the Cretaceous is also typical of deposition in a foredeep. The Nordegg ratio and residual maps both indicate that subsidence was higher to the west, where the developing orogeny was creating a tectonic load.

5.4.2 Isopach Maps

A combined, regional, isopach map of the lower Fernie members (Nordegg, Poker Chip Shale, and Rock Creek) thins to the northwest, northeast, and southeast away from a depocenter that has a maximum thickness of 114.6m (Figure 5-16). This depocenter developed during Nordegg deposition and well log facies indicate that it correlates to the carbonate platform/ramp facies identified in the Nordegg Member (Asgar-Deen et al., 2003; Asgar-Deen et al., 2004). The Nordegg thins to the northwest and southeast away from the depocenter (Figure 3-3). This is consistent with deposition in a backbulge (DeCelles and Giles, 1996; Currie, 1997) where accommodation space is restricted toward the orogeny by the forebulge and in the other direction by the craton.

The Upper Fernie thickens to the west (Figure 3-7). East of the Minnes Group subcrop the preserved thickness is partially controlled by erosion associated with the sub-Cretaceous unconformity, however the thickening to the west is still evident west of this subcrop limit. This westward thickening is interpreted to be controlled by rapid subsidence in the foredeep.

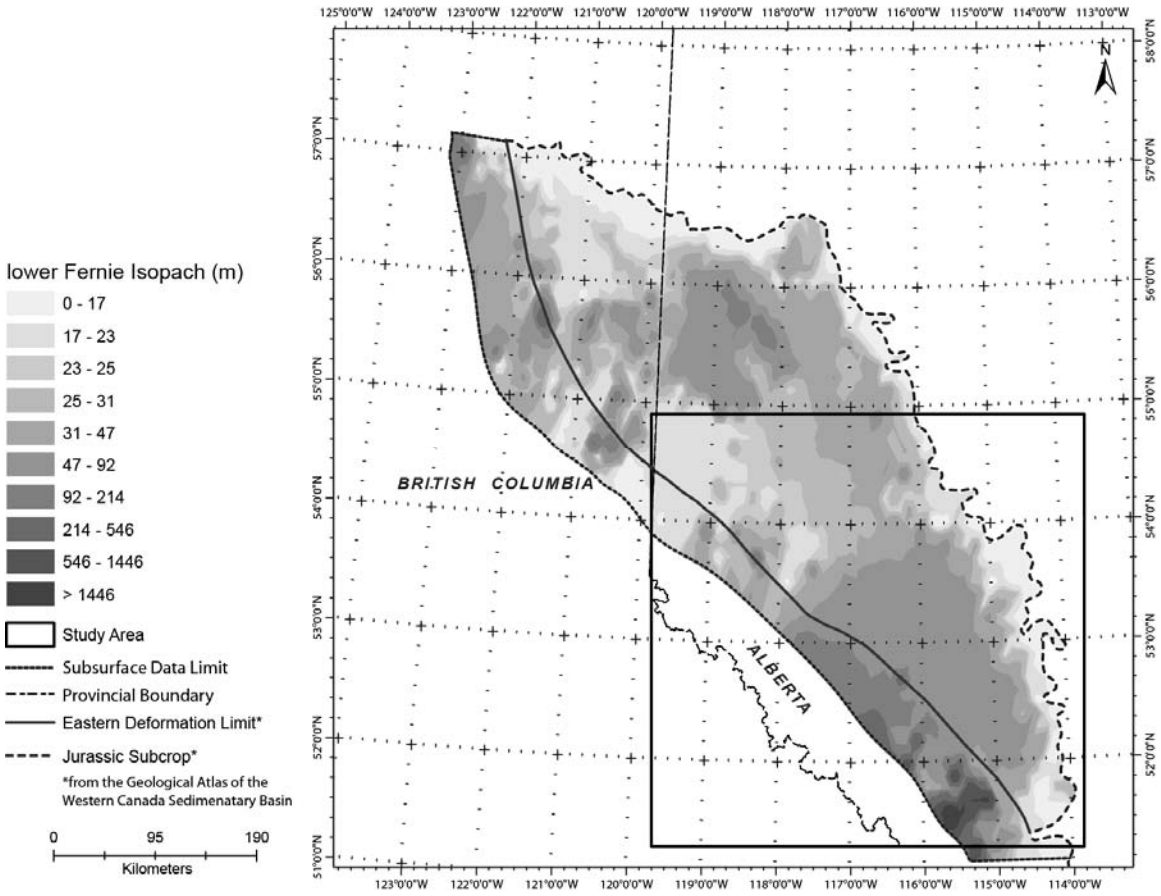

Figure 5-16: Regional isopach of the lower Fernie Formation.

5.4.3 Sedimentological Data

Haddad and Watts (1999) identified two loading stages for marine foreland basins. In the first stage, associated with terrane accretion, carbonates are deposited in the foreland basin. These shelfal carbonates are eventually replaced by terrigenous clastics as the basin first deepens then fills (*ibid.*). This pattern is consistent with the "underfilled trinity" identified by Sinclair (1997) and with what was deposited in the WCFB during the Jurassic.

The lower Fernie members (Nordegg, Poker Chip Shale, and Rock Creek) are fine-grained and shallow-marine (Marion, 1984; Stronach, 1984; Putnam and Moore, 1993; Poulton et al., 1994; Asgar-Deen et al., 2004). This is expected in backbulge basins; similar deposits have been identified in the Appalachian foreland basin (Filer, 2003). The maximum combined thickness of the Nordegg, Poker Chip Shale and Rock Creek in the study area is 114.6m and the average combined thickness is 46.29m. Flexural modeling predicts that backbulge basins are approximately 10m thick (Flemings and Jordan, 1989; DeCelles and Giles, 1996) however Filer (2003) identified several parameters that would increase the accommodation space in a backbulge basin up to 400m or more.

These interpretations are consistent with previously established models involving restricted ocean circulation during deposition of the lower Fernie Formation. Asgar-Deen (2003) and Riediger and Coniglio (1992) both interpreted the presence of a “sill” in west-central Alberta during Early-Middle Jurassic times, consistent with a forebulge that must exist west of the study area if the Lower Jurassic units in this study were deposited in a backbulge basin.

Passage of a forebulge through the study area is marked by the unconformities between deposition of the Rock Creek and Upper Fernie Members (represented as the sub-Oxfordian unconformity in this study). Poulton et al. (1990) also noted the presence of a significant unconformity beneath the foredeep deposits and associated it with forebulge migration. A cross-section flattened on this unconformity (**FIGURE3-20**) suggests this unconformity may control the extent of the Rock Creek sands. In other

words, their distribution is limited by passage of the forebulge through the region during that time.

The sub-Cretaceous unconformity is not interpreted to be the forebulge unconformity because of the rapid subsidence seen in the Minnes Group in the northwest, before the timing of this unconformity and occurrences of westerly-derived sediments below the sub-Cretaceous unconformity (Marion, 1984; Poulton, 1984).

This interpretation is in agreement with previous authors who have established that the Upper Fernie deposits are westerly-derived foreland basin deposits (Poulton, 1989; Miles, 2010; Miall, 2009), however, given the Walther's Law-type relationship of the foreland basin system depozones described in **SECTION2-2**, these cannot be the first foreland basin deposits in the WCFB.

5.4.4 Implications of an Early Jurassic initiation of the WCFB

5.4.4.1 Phantom foredeep and missing flysch

The interpretation of the presence of a backbulge indicates a flexural response to crustal loading began earlier than previously documented, as there must have been a corresponding foredeep further to the west. The earlier timing corresponds to the deformation and convergence of terranes in the "Intermontane" belt of the Canadian Cordillera in the Early Jurassic (Ghosh, 1995; Murphy et al., 1995; Dickinson, 2004).This initial foredeep was subsequently reworked by the advancing orogeny (Royse Jr, 1993). The presence of an earlier foredeep to the west of the study area is a likely

location for the “missing” flysch (Stockmal et al., 1992) to have been deposited prior to being reworked by the fold-thrust belt.

5.4.4.2 The timing discrepancies related to initiation of the WCFB

This interpretation helps to resolve the timing problems identified in Section 1.2. It reduces the time between the onset of Cordilleran deformation and the initiation of the WCFB and it reduces the time between initiation of the foreland basins in western Canada and Montana (Figure 5-17).

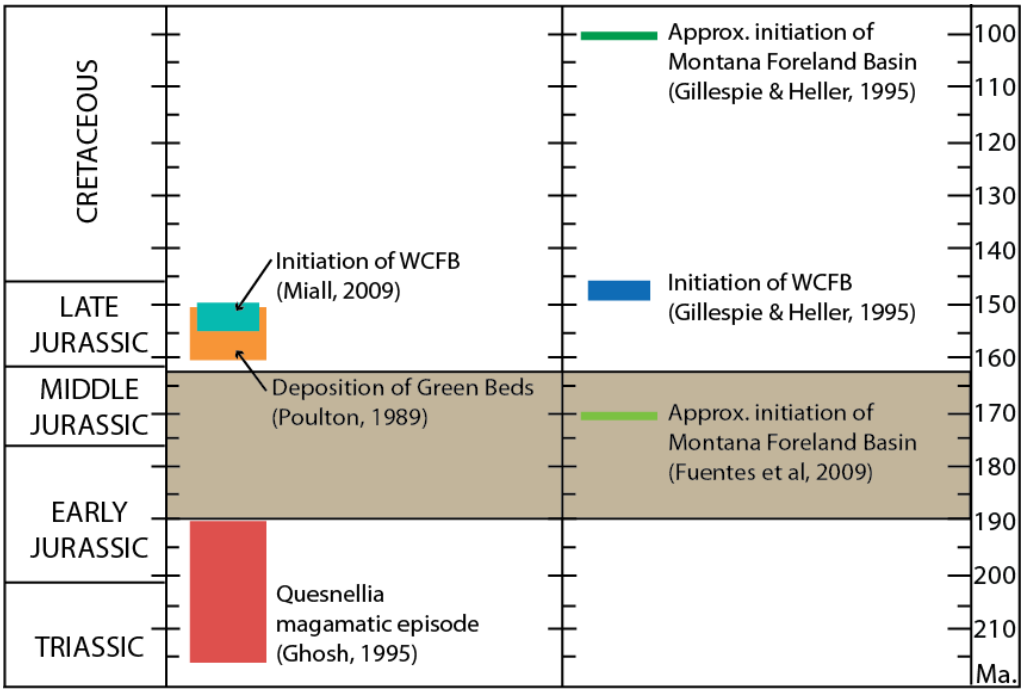

Figure 5-17: Chronological chart of foreland basin initiation.

The foreland basin initiation coincides with the onset of deposition in the backbulge, which happened from Early to Middle Jurassic (brown box). This timing fits better with the timing of Cordilleran deformation and the initiation of the Montana Foreland Basin.

5.4.4.2.1 Foreland basin initiation along the axis of western North America

The timing of the development of the foreland basins along the axis of western North America is not clear. This problem stems from the different ways the initiation of the foreland basin is defined (Miall, 2009). Initially, it was proposed that the initiation of the foreland basin in Canada occurred much earlier than in the northern United States(Gillespie and Heller, 1995), then it was argued that very little time passed between the initiation of these two foreland basins (Fuentes et al., 2009).

This interpretation finds a middle ground. The WCFB is slightly older than the corresponding foreland basin in the United States, but not by as many years as Gillespie and Heller (1995) proposed.

5.4.4.2.2 Timing of Cordilleran deformation and foreland basin initiation

The lack of evidence for Early Jurassic Cordilleran deformation in the western Canada sedimentary deposits was a significant factor in the development of the idea that the accretionary events were not occurring on the western margin of North America, but on a ribbon continent that existed west of North America (Johnston, 2008; Hildebrand, 2009). In this model, accretion of the ribbon continent during the Cretaceous caused the initiation of the WCFB. The data presented in this study indicate that there was enough crustal loading on the western margin of Canada during the Early Jurassic to create a flexural response.

Chapter Six: **Conclusions and Future Work**

6.1 Conclusions

The purpose of this study was to investigate two problems. First, recent studies in the United States used subsidence analysis to constrain the initiation of the foreland basin there; no similar studies existed in Canada. Second, the practice of using a small number of subsidence curves to represent the subsidence profile of the entire basin did not account for the variation of tectonic subsidence within the basin.

A study of the error inherent in subsidence calculations showed that the largest numerical source of error is porosity. Error bars created based on estimates of up to a 20% variation in porosity can be applied to subsidence curves and all other sources of error, including accounting for paleobathymetry and sea level changes, will fall within this margin of error.

The objectives of this study were addressed by answering four questions:

1. How much does tectonic subsidence vary within the Jurassic of the Western Canada Foreland Basin? Subsidence curves from over 300 wells in west-central Alberta were generated. The distribution of minimum and maximum values for each horizon formed a tectonic subsidence envelope that illustrated there is considerable local variation in the tectonic subsidence throughout the study area. However, regional trends, such as initially low rates of subsidence followed by a transition to rapid subsidence, are very clear in the envelope. Regional unconformities appear as gaps between data points on the subsidence envelope.

2. How can these tectonic subsidence variations be displayed? The relationship between tectonic subsidence and thickness can be compared in cross plots and in maps. Three types of maps were used to interpret tectonic subsidence variations within the Fernie Formation: tectonic subsidence, the residual (thickness subtracted from tectonic subsidence), and a ratio of tectonic subsidence to thickness.
3. What can these tectonic subsidence variations tell us about regional and local tectonics? The linear relationship between the thickness and the tectonic subsidence (once the cumulative trends have been removed from layers above the base) is interpreted to mean tectonics are the most significant control on subsidence within the study area.

   Tectonic subsidence maps are a proxy for paleostructure maps; they show how the position of the base layer changes after deposition of each unit. The base layer here is the starting base layer chosen for the study and does not account for structural features inherited from deeper in the basin.

   Tectonic subsidence residual maps, created by subtracting the thickness from the tectonic subsidence, can be used to show regional trends. In the case of the Fernie Formation, they are interpreted to show a western tectonic influence in the lower units and where tectonic subsidence outpaced sediment deposition. Like the residual maps, tectonic subsidence ratio maps compare the tectonic

subsidence and the thickness. Both can be used to look for regional and local trends in the tectonic subsidence variations.

4. What evidence is there for an Early Jurassic initiation of the Western Canada Foreland Basin? A lower Jurassic initiation of the WCFB is supported using the foreland basin system model proposed by DeCelles and Giles (1996). Evidence of a backbulge in the study area at the times the Nordegg, Poker Chip and Rock Creek units were deposited is found in isopach patterns, sedimentological and geochemical indications of a restricted basin, and low subsidence rates typical in regions distal to crustal loading. Tectonic subsidence maps from this study show that tectonic subsidence increases to the west as early as the Nordegg. The sub-Oxfordian unconformity (between the Rock Creek and the Upper Fernie) represents passage of a forebulge through the area, and the Upper Fernie deposits are the first foredeep deposits in west-central Alberta.

6.2 Relevance

The spreadsheet macros developed as part of this study can be customized to include as much detail as required to perform subsidence analysis. As such, it is useful for performing calculations at a single location, but even more so for performing calculations at multiple locations because of the time saved and the error reduced by automation.

The tectonic subsidence envelope can be used to show variation in subsidence curve profiles within a study area once subsidence analysis is complete and it has been

shown that maps of the tectonic subsidence give a visual, spatial representation of the relationship between sedimentation and tectonics.

The evidence for an Early Jurassic initiation of the WCFB provides better constraints on the two main timing issues inherent in the traditional model that the initiation of the foreland basin did not occur until the late-Middle to early-Late Jurassic. The timing of the initiation of the WCFB proposed here fits better with the onset of deformation in the Canadian Cordillera and with the timing of foreland basin initiation along the axis of the western margin of North America.

6.3 Framework for new studies and unresolved questions

This study provides a framework for future studies of the Fernie Formation in west-central Alberta. Flexural modeling in the Early Jurassic on palinspastically restored datasets would indicate if the lateral position of the study area along the axis of the orogeny is in the right place for a backbulge to have formed during the Early Jurassic.

Biostratigraphy is needed in the Fernie Formation to refine the dates of the deposits and the positions of unconformities. Better resolution of the boundary between the Poker Chip Shale and the Upper Fernie, where the Rock Creek sands are not present, would provide further constraints for the subsidence analysis. A more detailed examination of the Nordegg carbonate platform with a focus on looking for evidence to confirm or dispute platform drowning similar to that found at the base of modern marine foreland basin successions (Pigram et al., 1989; Galewsky et al., 2000), would be useful in resolving the fact that the high tectonic subsidence observed over this platform is not consistent with platform/shelf deposition.

A more detailed synthesis of the entire foreland basin in Western Canada during the Jurassic is needed, including a study of the relationship between sedimentology and underlying structural features. This would include the Peace River Arch area to the north and the Sweetgrass Arch area in southern Alberta. This study was not continued further south because the stratigraphy changes significantly and there are structural complications both in the Fernie Basin (Stronach, 1982) and associated with the Sweetgrass Arch (Michener, 1934). This work remains to be done in the future.

Finally, a study of Jurassic deposits within the fold-thrust belt is needed to extend the dataset to the west and look for any remaining evidence of the forebulge and foredeep, sometimes referred to as the "phantom foredeep" (Royse Jr, 1993), that existed in the Early Jurassic.

References

Abadi, A.M., van Wees, J.-D., van Dijk, P.M., and Cloetingh, S. a. P.L., 2008, Tectonics and subsidence evolution of the Sirt Basin, Libya: Bulletin of the American Association of Petroleum Geologists, v. 92, no. 8, p. 993-1027, doi: 10.1306/03310806070.

Allen, P., and Allen, J., 2005, Basin analysis: principles and applications: Blackwell Publishing.

Angevine, C.L., Heller, P.L., and Paola, C., 1990, Quantitative sedimentary basin modeling: AAPG.

Asgar-Deen, M., 2003, Stratigraphy, Sedimentology and Paleogeography of the Lower Jurassic Nordegg Member (Gordondale Member), west-central Alberta, Canada: University of Calgary.

Asgar-Deen, M., Hall, R.R., Craig, J., and Riediger, C., 2003, New biostratigraphic data from the Lower Jurassic Fernie Formation in the subsurface of west-central Alberta and their stratigraphic implications: Canadian Journal of Earth Sciences,.

Asgar-Deen, M., Riediger, C., Hall, R., Laboratories, H., By, C., and Ottawa, D., 2004, The Gordondale Member: designation of a new member in the Fernie Formation to replace the informal“ Nordegg Member” nomenclature of the subsurface of west-central Alberta: Bulletin of Canadian Petroleum Geology, v. 52, no. 3, p. 201.

Athy, L.F., 1930, Density, Porosity, and Compaction of Sedimentary Rocks: Bulletin of the American Association of Petroleum Geologists, v. 14, no. 1, doi: 10.1126/science.51.1323.468.

Beaumont, C., 1981, Foreland basins: Geophysical Journal of the Royal Astronomical Society, v. 65, p. 291-329.

Berman, R.G., Davis, W.J., and Pehrsson, S., 2007, Collisional Snowbird tectonic zone resurrected: Growth of Laurentia during the 1.9 Ga accretionary phase of the Hudsonian orogeny: Geology, v. 35, no. 10, p. 911, doi: 10.1130/G23771A.1.

Bond, G., and Kominz, M., 1984, Construction of tectonic subsidence curves for the early Paleozoic miogeocline, southern Canadian Rocky Mountains: Implications for subsidence mechanisms, age of breakup, and crustal thinning: Bulletin of the Geological Society of America, v. 95, no. 2, p. 155.

Collar, I., 1990, Stratigraphy and sedimentology of the Jurassic Fernie Formation in the Sylvan Lake, Medicine River and Gilby Fields, south-central Alberta.: University of Alberta.

Colpron, M., and Price, R., 1995, Tectonic significance of the Kootenay terrane, southeastern Canadian Cordillera: An alternative model: Geology, v. 23, no. 1, p. 25, doi: 10.1130/0091-7613(1995)023<0025:TSOTKT>2.3.CO;2.

Colpron, M., Warren, M.J., and Price, R., 1998, Selkirk fan structure, southeastern Canadian Cordillera: Tectonic wedging against an inherited basement ramp: Geological Society of America Bulletin, v. 110, no. 8, p. 1060-1074.

Core Laboratories Geological Sciences Department Stratigraphic Correlation Chart: Stratigraphic Correlation Chart,.

Crampton, S., and Allen, P., 1995, Recognition of forebulge unconformities associated with early stage foreland basin development: example from the North Alpine foreland basin: Bulletin of the American Association of Petroleum Geologists, v. 79, no. 10, p. 1495–1514.

Currie, B., 1997, Sequence stratigraphy of nonmarine Jurassic–Cretaceous rocks, central Cordilleran foreland-basin system: Geological Society of America Bulletin, v. 109, no. 9, p. 1206.

DeCelles, P., and Giles, K., 1996, Foreland basin systems: Basin Research, v. 8, no. 2, p. 105–123.

Dickinson, W., 2009, Anatomy and global context of the North American Cordillera: Backbone of the Americas: shallow subduction, plateau uplift, and ridge and terrane collision,, p. 1-29, doi: 10.1130/2009.1204(01).For.

Dickinson, W., 2004, Evolution of the North American Cordillera: Annual, v. 32, no. 1, p. 13-45, doi: 10.1146/annurev.earth.32.101802.120257.

Dickinson, W., 1974, Plate Tectonics and Sedimentation, *in* Dickinson, W. ed., Tectonics and Sedimentation, Society of Economic Paleontologists and Mineralogists, p. 1-27.

Dickinson, W., 1976, Sedimentary basins developed during evolution of Mesozoic-Cenozoic arc-trench system in western North America: Canadian Journal of Earth Sciences, v. 13, no. 9, p. 1268–1287.

Edwards, D., Brown, R., Devonian, U., Formation, L., Leduc, A., Cambrian, M., Cambrian, U., and Homeglen-rimbey, T., 1999, Understanding the influence of

Precambrian crystalline basement on Upper Devonian carbonates in central Alberta from a geophysical perspective: Bulletin of Canadian Petroleum Geology, v. 47, no. 4, p. 412-438.

Filer, J.K., 2003, Stratigraphic evidence for a Late Devonian possible back-bulge basin in the Appalachian basin , United States: Basin Research, v. 15, p. 417-429.

Flemings, P., and Jordan, T., 1989, A synthetic stratigraphic model of foreland basin development: Journal of Geophysical Research, v. 94, no. B4, p. 3851-3866.

Fuentes, F., DeCelles, P., and Gehrels, G., 2009, Jurassic onset of foreland basin deposition in northwestern Montana, USA: Implications for along-strike synchroneity of Cordilleran orogenic activity: Geology, v. 37, no. 4, p. 379-382.

Gabrielse, H., Monger, J., Wheeler, J., and Yorath, C., 1991, Part A. Morphogeological belts, tectonic assemblages, and terranes, *in* Gabrielse, H. and Yorath, C. eds., Geology of the Cordilleran Orogen in Canada, p. 15–28.

Galewsky, J., Silver, E.A., Gallup, C.D., Edwards, R.L., and Potts, D.C., 2000, Foredeep tectonics and carbonate platform dynamics in the Huon Gulf , Papua New Guinea: Geology, v. 24, no. 9, p. 819 - 822.

Gallagher, K., 1989, An examination of some uncertainties associated with estimates of sedimentation rates and tectonic subsidence: Basin Research, v. 2, no. 2, p. 97–114.

Ghosh, D., 1995, Nd-Sr isotopic constraints on the interactions of the Intermontane Superterrane with the western edge of North America in the southern Canadian Cordillera: Canadian Journal of Earth Sciences, v. 32, no. 10, p. 1740–1758.

Giles, M., Indrelid, S., and James, D., 1998, Compaction–the great unknown in basin modelling: Geological Society London Special Publications, v. 141, no. 1, p. 15, doi: 10.1144/GSL.SP.1998.141.01.02.

Gillespie, J.M., and Heller, P.L., 1995, Beginning of foreland subsidence in the Columbian-Sevier belts, southern Canada and northwest Montana:: Geology, v. 23, no. 8, p. 723-726.

Gumati, Y., and Nairn, A., 1991, Tectonic subsidence of the Sirte Basin, Libya: Journal of Petroleum Geology, v. 14, no. January, p. 93-102.

Haddad, D., and Watts, A., 1999, Subsidence history, gravity anomalies, and flexure of the northeast Australian margin in Papua New Guinea: Tectonics, v. 18, no. 5, p. 827, doi: 10.1029/1999TC900009.

Hall, R., 1984, Lithostratigraphy and biostratigraphy of the Fernie Formation (Jurassic) in the southern Canadian Rocky Mountains: The Mesozoic of middle North America: Canadian Society of Petroleum Geologists Memoir, v. 9, p. 233–248.

Hallam, A., 1988, A re-evaluation of Jurassic eustasy in the light of new data and the revised Exxon curve, *in* Wilgus, C., Hastings, B., Kendall, Cgs., Posamentier, H., Ron, C., and van Wagner, J. eds., Sea-Level Changes - An Integrated Apporach. SEPM Special Publication 42, p. 261-273.

Hallam, A., 2001, A review of the broad pattern of Jurassic sea-level changes and their possible causes in the light of current knowledge: Palaeogeography, Palaeoclimatology, Palaeoecology, v. 167, no. 1-2, p. 23-37, doi: 10.1016/S0031-0182(00)00229-7.

Haq, B., Hardenbol, J., and Vail, P., 1987, Chronology of fluctuating sea levels since the Triassic (250 million years ago to present): Science, v. 235, p. 1156-1167.

Hildebrand, R.S., 2009, Did westward subduction cause Cretaceous-Tertiary orogeny in the North American Cordillera?: Geological Society of America Special Paper 457, v. 457.

van Hinte, J., 1978, Geohistory analysis—application of micropaleontology in exploration geology: Bulletin of the American Association of Petroleum Geologists, v. 62, p. 201-222.

Höy, T., and Dunne, K., 1998, Early Jurassic Rossland Group, Southern British Columbia. Part 1: Stratigraphy and Tectonics: Geological Survey, British Columbia Bulletin No. 102,, doi: 10.1038/423007a.

Johnston, S.T., 2008, The Cordilleran Ribbon Continent of North America: Annual Review of Earth and Planetary Sciences,.

Jones, A.G., Snyder, D., Hanmer, S., Asudeh, I., White, D., Eaton, D., and Clarke, G., 2002, Magnetotelluric and teleseismic study across the Snowbird Tectonic Zone, Canadian Shield: A Neoarchean mantle suture?: Geophysical Research Letters, v. 29, no. 17, p. 17-20, doi: 10.1029/2002GL015359.

Jordan, T., 1981, Thrust loads and foreland basin evolution, Cretaceous, western United States: Bulletin of the American Association of Petroleum Geologists, v. 12, no. 12, p. 2506-2520.

Kukulski, R., 2009, Applied stratigraphy and sedimentology of the Late Jurassic to Earliest Cretaceous Monach Formation, Nikanassin Group, Northwest Alberta: University of Calgary.

Larrieu, T., 1995, Basin analysis with a spreadsheet: Journal of Geological Education, v. 43, p. 107-113.

Leckie, D., and Smith, D., 1992, Regional setting, evolution, and depositional cycles of the Western Canada Foreland Basin: American Association of Petroleum Geologists Memoir, v. 55, p. 9–46.

Losert, J., 1986, Jurassic Rock Creek Member in the subsurface of the Edson area (west-central Alberta): Alberta Research Council Open File Report, , no. 1986-3.

Mahan, K.H., and Williams, M.L., 2005, Reconstruction of a large deep-crustal terrane: Implications for the Snowbird tectonic zone and early growth of Laurentia: Geology, v. 33, no. 5, p. 385, doi: 10.1130/G21273.1.

Marion, D., 1984, The Middle Jurassic Rock Creek Member and associated units in the subsurface of west-central Alberta: The Mesozoic of middle North America: Canadian Society of Petroleum Geologists Memoir, v. 9, p. 319–344.

McLean, J., 1977, The Cadomin Formation; stratigraphy, sedimentology, and tectonic implications: Bulletin of Canadian Petroleum Geology, v. 25, no. 4, p. 792.

Miall, A.D., 2009, Initiation of the Western Interior foreland basin: Geology, v. 37, no. 4, p. 383.

Miall, A.D., Catuneanu, O., Vakarelov, B.K., and Post, R., 2009, The Western Interior Basin, *in* The Sedimentary Basins of the World, Volume 5, Elsevier Science Ltd, p. 329-362.

Michener, C.E., 1934, The northward extension of the Sweetgrass Arch: The Journal of Geology, v. 42, no. 1, p. 45–61.

Miles, B., 2010, Unraveling the stratigraphic architecture of the Jurassic-Cretaceous Nikanassin Group, northwestern Alberta, Canada: UNIVERSITY OF CALGARY.

Monger, J., and Price, R., 2002, The Canadian Cordillera: geology and tectonic evolution: CSEG Recorder, v. 27, no. 2, p. 17-36.

Murphy, D.C., van Der Heyden, P., Parrish, R.R., Klepacki, D.W., McMillan, W., Struik, L.C., and Gabites, J., 1995, New geochronological constraints on Jurassic

deformation of the western edge of North America, southeastern Canadian Cordillera, *in* Miller, D.M. and Busby, C. eds., Jurassic Magmatism and Tectonics of the North American Cordillera, Geological Society of America, Boulder, Colorado, p. 159-171.

Naylor, M., and Sinclair, H., 2008, Pro- vs. retro-foreland basins: Basin Research, v. 20, no. 3, p. 285-303, doi: 10.1111/j.1365-2117.2008.00366.x.

Osborn, G., Stockmal, G.S., and Haspel, R., 2006, Emergence of the Canadian Rockies and adjacent plains: A comparison of physiography between end-of-Laramide time and the present day: Geomorphology, v. 75, p. 450–477, doi: 10.1016/j.geomorph.2005.07.032.

O'Connell, S.C., Dix, G.R., and Barclay, J.E., 1990, The origin , history , and regional structural development of the Peace River Western Canada: Bulletin of Canadian Petroleum Geology, v. 38, p. 4-24.

Petersen, N.T., Smith, P.L., Mortensen, J.K., Creaser, R.A., and Tipper, H.W., 2004, Provenance of Jurassic sedimentary rocks of south-central Quesnellia, British Columbia: implications for paleogeography: Canadian Journal of Earth Sciences, v. 41, no. 1, p. 103–125.

Pigott, J.D., and Sattayarak, N., 1993, Aspects of sedimentary basin evolution assessed through tectonic subsidence analysis . Example : northern Gulf of Thailand: Journal of Southeast Asian Earth Sciences, v. 8, no. 1983, p. 407-420.

Pigram, C., Davies, P., Feary, D., and Symonds, P., 1989, Tectonic controls on carbonate platform evolution in southern Papua New Guinea: passive margin to foreland basin: Geology, v. 17, no. 3, p. 199-202.

Poulton, T., 1984, The Jurassic of the Canadian Western Interior, from 49N latitude to Beaufort Sea: The Mesozoic of Middle North America, Canadian Society of Petroleum Geologists Memoir 9,, p. 15-41.

Poulton, T., 1989, Upper Absaroka to Lower Zuni: the transition to the foreland basin (B. D. Ricketts, Ed.): Western Canada Sedimentary Basin: a case history,, p. 233.

Poulton, T., Christopher, J., Hayes, B., Losert, J., Tittemore, J., and Gilchrist, R., 1994, Jurassic and lowermost Cretaceous strata of the Western Canada sedimentary basin, *in* Shetsen, I. and Mossop, G.D. eds., Geological Atlas of the Western Canada Sedimentary Basin, Canadian Society of Petroleum Geologists and the Alberta Research Council, Calgary.

Poulton, T., Tittemore, J., and Dolby, G., 1990, Jurassic strata of northwestern (and west-central) Alberta and northeastern British Columbia: Bulletin of Canadian Petroleum Geology, v. 38, no. 34190, p. 159–175.

Price, R., 1994, Cordilleran Tectonics and the Evolution of the Western Canada Sedimentary Basin, *in* Shetsen, I. and Mossop, G.D. eds., Geological Atlas of the Western Canada Sedimentary Basin, Canadian Society of Petroleum Geologists and the Alberta Research Council, Calgary.

Price, R., 1973, Large-scale gravitational flow of supracrustal rocks, southern Canadian Rockies: Gravity and tectonics,, p. 491–502.

Price, R., and Monger, J., 2000, A transect of the southern Canadian Cordillera from Calgary to Vancouver: Geological Association of Canada, Cordilleran Section, Vancouver, BC, Field Trip Guidebook,, p. 165 pp.

Putnam, P., and Moore, S., 1993, The Jurassic (Bajocian) Rock Creek Member of West-Central Alberta, *in* Carboniferous to Jurassic: Pangea: Calgary Alberta, Canada, August 15-17, 1993: core workshop: guidebook, Wednesday, August l8, 1993, ERCB Core Research Centre, Canadian Society of Petroleum Geologists, p. 162.

Putnam, P., and Ward, G.S., 2001, The relation between stragtigraphic elements, pressure regime, and hydrocarbons in the Alberta deep basin (with emphasis on select Mesozoic units): Bulletin of the American Association of Petroleum Geologists, v. 85, no. 4, p. 691-714.

Raines, K., 2011, Stratigraphy and provenance of early foreland basin deposits, Minnes Group, British Columbia and Alberta: University of Calgary.

Ricketts, B.D., 2009, Cordilleran sedimentary basins of Western Canada record 180 million years of terrane accretion, *in* The Sedimentary Basins of the United States and Canada, Elsevier Science Ltd, p. 363-394.

Riediger, C., 2002, Hydrocarbon source rock potential and comments on correlation of the Lower Jurassic Poker Chip Shale, west-central Alberta: Bulletin of Canadian Petroleum Geology, v. 50, no. 2, p. 263-276, doi: 10.2113/50.2.263.

Riediger, C., and Coniglio, M., 1992, Early diagenetic calcites and associated bitumens in the“ Nordegg Member”; implications for Jurassic paleogeography of the Western Canada Sedimentary Basin: Bulletin of Canadian Petroleum Geology, v. 40, no. 4, p. 381.

Riediger, C., Fowler, M., Snowdon, L., and Goodarzi, F., 1990, Source rock analysis of the Lower Jurassic “Nordegg Member” and oil-source rock correlations, northwestern Alberta and northeastern British Columbia: Bulletin of Canadian, v. 38, no. 33290, p. 236-249.

Root, K.G., 2001, Devonian Antler fold and thrust belt and foreland basin development in the southern Canadian Cordillera : implications for the Western Canada Sedimentary Basin: Bulletin of Canadian Petroleum Geology, v. 49, no. 1, p. 7-36.

Rosenthal, L., 1989, The stratigraphy, sedimentology and petrography of the Jurassic-Early Cretaceous clastic wedge in western Alberta: University of Manitoba.

Ross, G., 1989, Crystalline basement: the foundations of the Western Canada Sedimentary Basin: Western Canada Sedimentary Basin: a case history,.

Ross, G., Broome, J., and Miles, W., 1994, Potential Fields and Basement Structure - Western Canada Sedimentary Basin, *in* Shetsen, I. and Mossop, G.D. eds., Geological Atlas of the Western Canada Sedimentary Basin, Canadian Society of Petroleum Geologists and the Alberta Research Council, Calgary.

Ross, G., Patchett, P.J., Hamilton, M., Heaman, L., DeCelles, P., Rosenberg, E., and Giovanni, M.K., 2005, Evolution of the Cordilleran orogen (southwestern Alberta, Canada) inferred from detrital mineral geochronology, geochemistry, and Nd isotopes in the foreland basin: Geological Society of: Geological Society of America Bulletin, v. 117, no. 5/6, p. 747-763.

Royse Jr, F., 1993, Case of the phantom foredeep: Early Cretaceous in west-central Utah: Geology, v. 21, no. 2, p. 133-136.

Sclater, J., and Christie, P., 1980, Continental Stretching: An explanation of the post-mid-Cretaceous subsidence of the central North Sea Basin: Journal of Geophysical Research, v. 85, no. B7, p. 3711-3739.

Sinclair, H., 1997, Tectonostratigraphic model for underfilled peripheral foreland basins : An Alpine perspective: Geological Society of America Bulletin, v. 109, no. 3, p. 324-346.

Sinclair, H., and Naylor, M., 2011, Foreland basin subsidence driven by topographic growth versus plate subduction: Geological Society of America Bulletin, , no. November, doi: 10.1130/B30383.1.

Stapel, G., Cloetingh, S., and Pronk, B., 1996, Quantitative subsidence analysis of the Mesozoic evolution of the Lusitanian basin (western Iberian margin): Tectonophysics, v. 266, no. 1-4, p. 493–507.

Stockmal, G.S., Cant, D.J.D., and Bell, J.S., 1992, Relationship of the stratigraphy of the Western Canada foreland basin to Cordilleran tectonics: insights from geodynamic models: Foreland Basins and Fold Belts: American Association of Petroleum Geologists Memoir, v. 55, no. 1, p. 107–124.

Stronach, N., 1984, Depositional environments and cycles in the Jurassic Fernie Formation, southern Canadian Rocky Mountains: The Mesozoic of middle North America: Canadian Society of Petroleum Geologists Memoir, v. 9, p. 43–67.

Stronach, N., 1982, Sedimentology and paleoecology of a shale basin: the Fernie Formation of the southern Rocky Mountains, Canada: University of Calgary.

Tittemore, J., 1991, Jurassic lithologies and some factors affecting sediment distribution in northwestern Alberta:.

Trabucho-Alexandre, J., Dirkx, R., and Veld, H., 2012, Toarcian Black Shales In the Dutch Central Graben: Record of Energetic, Variable Depositional Conditions During An Oceanic Anoxic Event: Journal of Sedimentary, v. 81, no. 1, p. 64-79, doi: 10.2110/jsr.2011.5.

Turer, D., and Maynard, J.B., 2003, Combining Subsidence Analysis and Detrital Modes of Sandstones to Constrain Basin History: An Example from the Eastern Pontides of Turkey: International Geology Review, v. 45, no. 4, p. 329-345, doi: 10.2747/0020-6814.45.4.329.

Unterschutz, J., Creaser, R. a., Erdmer, P., Thompson, R.I., and Daughtry, K.L., 2002, North American margin origin of Quesnel terrane strata in the southern Canadian Cordillera: Inferences from geochemical and Nd isotopic characteristics of Triassic metasedimentary rocks: Geological Society of America Bulletin, v. 114, no. 4, p. 462-475, doi: 10.1130/0016-7606(2002)114<0462:NAMOOQ>2.0.CO;2.

Wright, G., McMechan, M., and Potter, D., 1994, Structure and architecture of the Western Canada sedimentary basin, *in* Shetsen, I. and Mossop, G.D. eds., Geological Atlas of the Western Canada Sedimentary Basin, Canadian Society of Petroleum Geologists and the Alberta Research Council, Calgary.

Wyllie, M., Gregory, A.R., and Gardner, L., 1956, Elastic wave velocities in heterogeneous and porous media: Geophysics, v. 21, no. 1, p. 41.

Xie, X., and Heller, P.L.L., 2009, Plate tectonics and basin subsidence history: Geological Society of America Bulletin, v. 121, no. 1-2, p. 55, doi: 10.1130/B26398.1.

Zubin-Stathopoulos, K., 2011, Tectonic Evolution, Paleogeography and Paleoclimate of Pennsylvanian-Permian Strata in East-Central British Columbia: Implications from Conodont Biostratigraphy and Carbonate Sedimentology: University of Calgary.

APPENDIX A: TECTONIC SUBSIDENCE DERIVATIONS

A.1. Decompaction Equation

The decompaction equation calculates the thickness of a layer at the end of its deposition, before it was buried and compacted by subsequent layers (Figure A-1).

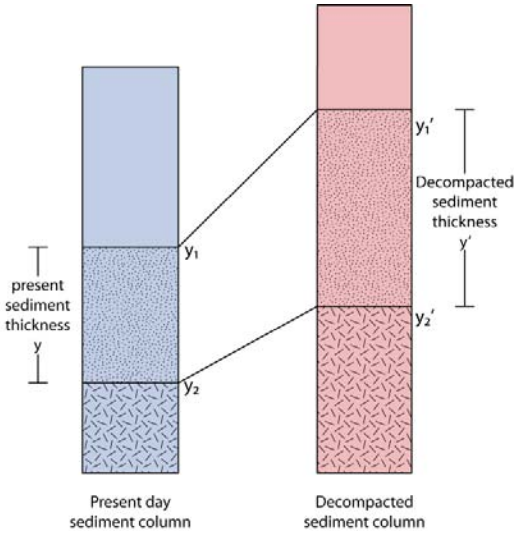

Figure A-1: Decompaction

The depths and thicknesses of the decompacted sediment column (right) are different from those of the present day sediment column (left). Modified from Gallagher, 1989.

There are two assumptions required for this equation (Angevine et al., 1990):

1. The sediment volume remains the same before and after compaction; porosity-loss caused by sediment loading during subsequent deposition is the sole cause of compaction
2. Porosity decreases with depth in an exponential relationship.

We will derive the decompaction equation for a unit cross-sectional area whose length, *l*, and width, *w*, are both one (Figure A-2). By doing this, volume and thickness of the layer are interchangeable.

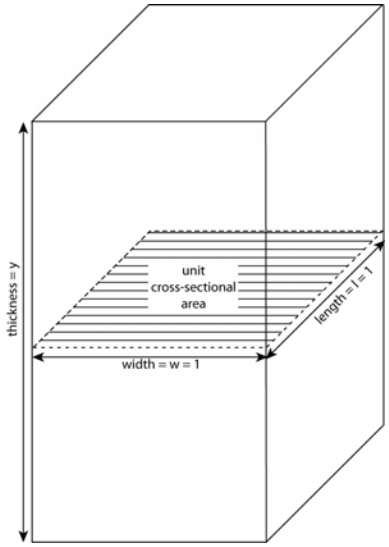

Figure A-2: A unit cross-sectional area

A sedimentary layer of thickness *y* with a length and width of 1. By assuming a unit cross-sectional area, the calculations can be carried out in terms of one dimension, the thickness, because the area is 1.

The total present volume, *V*, of a sediment layer is given by $V = l \times w \times y$, where *l* is the length, *w* is the width and *y* is the thickness of the layer. The total volume of a sediment layer can also be written as

(1) $\boldsymbol{V = V_s + V_w}$

where V_s is the volume of sediment grains in the layer and V_w is the volume of water-filled pore space in the layer. For a unit cross-sectional area **(1)** becomes

(2) $\boldsymbol{y = y_s + V_w}$

where y is the total thickness of the layer and y_s is the thickness of just the sediment grains.

To calculate the thickness of the layer before compaction, y', **(2)** becomes

(3) $y' = y_s' + V_w'$

where y_s' is the thickness of the sediment grains before compaction and V_w' is the volume of water-filled pore space before compaction. Since the volume of the sediment grains remains unchanged before and after compaction, **(3)** can be rewritten as

(4) $\boldsymbol{y' = y_s + V_w'.}$

The exponential relationship between porosity and depth is given by

(5) $\boldsymbol{\phi = \phi_0 e^{-cy}}$

where ϕ is the porosity at depth, ϕ_0 is the original porosity of the layer when it was deposited, and c is the compaction coefficient. The present volume of water-filled pore space in the layer can be found by taking the integral of **(5)** between the bottom of the layer, y_2, and the top of the layer, y_1:

(6) $\boldsymbol{V_w = \int_{y_1}^{y_2} \phi_0 e^{-cy} dy}$

Integrating, **(6)** becomes

(7) $\boldsymbol{V_w = \frac{\phi_0}{c}\{\exp(-cy_1) - \exp(-cy_2)\}}$

Similarly, the volume of water-filled pore space in the layer before compaction can be found by integrating over the bottom of the decompacted layer, y_2', and the top of the decompacted layer, y_1':

(8) $$\boldsymbol{V_w' = \frac{\phi_0}{c}\{\exp(-cy_1') - \exp(-cy_2')\}}$$

Plugging **(8)** into **(4)**, we get

(9) $$\boldsymbol{y' = y_s' + \frac{\phi_0}{c}\{\exp(-cy_1') + \exp(-cy_2')\}}$$

In order to solve for *y'*, we still need to solve for y_s'. Since the sediment volume does not change during compaction, $y_s' = y_s$, we can replace y_s in **(3)** and solve for y_s':

(10) $$\boldsymbol{y_s' = y - V_w}$$

Here, *y* is the current thickness of the sediments, $y = y_2 - y_1$, and *Vw* is given by **(7)** so that **(10)** becomes

(11) $$\boldsymbol{y_s' = y_2 - y_1 - \frac{\phi_0}{c}\{\exp(-cy_1) - \exp(-cy_2)\}}$$

The decompacted thickness is given by

(12) $$\boldsymbol{y' = y_2' - y_1'.}$$

Substituting **(11)** and **(12)** into **(9)** gives the decompaction equation:

(13)

$$\boxed{\boldsymbol{y_2' - y_1' = y_2 - y_1 - \frac{\phi_0}{c}\{\exp(-cy_1) - \exp(-cy_2)\} + \frac{\phi_0}{c}\{\exp(-cy_1') + \exp(-cy_2')\}}}$$

A.2. Backstripping Equations

Density, ρ, is the mass, m, per unit volume; mass is given by $m = \rho \times l \times w \times y$. For a unit cross-sectional area, this becomes

(14) $\boldsymbol{m = \rho y}$

Weight, W, is the mass times the gravitational force, g, so using **(14)**,

(15) $\boldsymbol{W = \rho g y}$

Assuming Airy isostasy, the total weight of a column in the sediment-filled basin must equal the total weight of a column of a water-filled basin of the same depth (Figure A-3). The sediment-filled column has four layers: the water at the top of the basin, the sediment, the crust, and the portion of the mantle above the depth of compensation (left side of Figure A-3). The water-filled column has three layers: the water, the crust, and the portion of the mantle above the depth of compensation (right side of Figure A-3). The total weight of each column is the sum of the weights of each layer within the column.

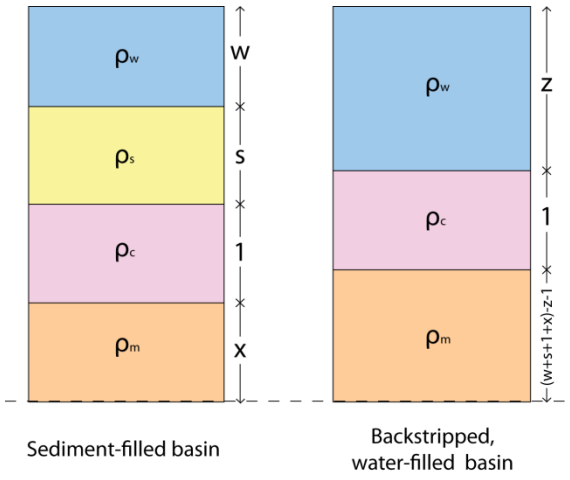

Figure A-3: Balanced columns in Airy Isostasy

Schematic illustration of the sediment columns that must be balanced in order to derive the tectonic subsidence equation. Modified from (Angevine et al., 1990).

For these calculations, we assume the thickness of the crust is equal in both columns and is a unit thickness. The height of the mantle in the water-filled column is the total thickness of the sediment-filled column less the thickness of the water and crust in the water-filled column: $(w + s + 1 + x) - z - 1$. Therefore,

(16)

$$\boldsymbol{\rho_w w g + \rho_s s g + \rho_c g + \rho_m x g = \rho_w z g + \rho_c g + \rho_m [(w + s + 1 + x) - z - 1] g}$$

where ρ_w is the density of water, w is the thickness of the water layer in the sediment-filled column, z is the thickness of the water layer in the backstripped (water-filled) column, ρ_s is the density of the sediment layer, s is the thickness of the sediment layer, ρ_c is the density of the crust, ρ_m is the density of the mantle, x is the thickness of the mantle layer and g is the acceleration of gravity.

Since g occurs in each term it can be removed from **(16)** which can then be simplified as follows:

(17) $$\boldsymbol{\rho_w w + \rho_s s + \rho_c + \rho_m x = \rho_w z + \rho_c + \rho_m w + \rho_m s + \rho_m + \rho_m x - \rho_m z - \rho_m}$$

The terms ρ_c and $\rho_m x$ can be subtracted from both sides of **(17)** and the two occurrences of ρ_m on the right side cancel each other out, leaving:

(18) $$\boldsymbol{\rho_w w + \rho_s s = \rho_w z + \rho_m w + \rho_m s - \rho_m z}$$

Rearranging **(18)** so that all of the terms containing z are on the left side and all the terms containing w and s are on the right side, we have:

(19) $\boldsymbol{\rho_m z - \rho_w z = \rho_m w - \rho_w w + \rho_m s - \rho_s s}$

This becomes:

(20) $\boldsymbol{z(\rho_m - \rho_w) = w(\rho_m - \rho_w) + s(\rho_m - \rho_s)}$

Divide both sides of **(20)** by $(\rho_m - \rho_w)$ to get

(21) $\boldsymbol{z = \frac{w(\rho_m - \rho_w)}{(\rho_m - \rho_w)} + \frac{s(\rho_m - \rho_s)}{(\rho_m - \rho_w)}}$

Finally, we get

(22) $\boxed{\boldsymbol{z = w + s\left(\frac{\rho_m - \rho_s}{\rho_m - \rho_w}\right)}}$

If the water depth (i.e. paleobathymetry) is not known, *w* is removed from this equation and accounted for with error bars on subsidence curves instead. An additional term, to account for sea level changes, is also customarily accounted for with error bars on the subsidence curves. When included, this term is also added to the right side of **(22)**.

Before we can solve for *z* we must determine the density of the sediment layer. Recall from Figure A-3 that s is the decompacted thickness of the sediment layer at a given time interval. Since the density of the sediment layer, ρ_s, changes with compaction it must be recalculated for each layer in the sediment column at each time interval.

The sediment layer consists of two parts: the grains, with density ρ_g, and the pore space, which we assume is water-filled and has a density ρ_w (Figure A-4).

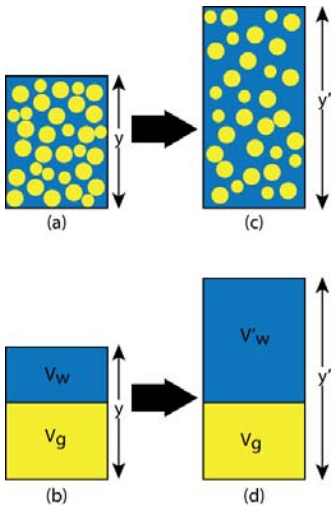

Figure A-4: Decompaction of a sediment layer

A sediment layer (a) of thickness y consists of grains (yellow) and water-filled pore space (blue). The total volume of the sediment layer (b) is the volume of the water-filled pore space, Vw, plus the volume of the sediment grains, Vg. The change in thickness of the layer when it is decompacted (b), y, is due to the change in volume of the pore space, V`(d). Modified from (Angevine et al., 1990).

Density is the mass per unit volume so the density of the sediment, ρ_s, is the total mass of the sediment (the mass of the grains, m_g, plus the mass of the water-filled pore space, m_w) divided by the volume, V.

(23) $$\boldsymbol{\rho_s = \frac{m_g + m_w}{V} = \frac{m_g}{V} + \frac{m_w}{V}}$$

The grain density, ρ_g, is the mass of the grains divided by the volume of the grains

(24) $$\boldsymbol{\rho_g = \frac{m_g}{V_g}}$$

The total volume of the layer, V, is the volume of the grains, V_g, plus the volume of the water-filled pore space, V_w: $V = V_g + V_w$, therefore $V_g = V - V_w$ and **(24)** becomes

(25) $\boldsymbol{\rho_g = \frac{m_g}{V - V_w}}$

Porosity is the ratio between the volume of the void space and the total volume, but we are assuming the void spaces are filled with water, so that

(26) $\boldsymbol{\phi = \frac{V_w}{V}}$

and

(27) $\boldsymbol{V_w = \phi V}$

Therefore **(25)** becomes

(28) $\boldsymbol{\rho_g = \frac{m_g}{V - \phi V} = \frac{m_g}{V(1 - \phi)}}$

which can be rearranged as:

(29) $\boldsymbol{\frac{m_g}{V} = \rho_g(1 - \phi)}$

The water density, ρ_w, is given by

(30) $\boldsymbol{\rho_w = \frac{m_w}{V_w}}$

where m_w is the mass of the water filling the pore spaces and V_w is the volume of the water-filled pore spaces. Substituting in **(27)**, **(30)** becomes

(31) $\boldsymbol{\rho_w = \frac{m_w}{\phi V}}$

Substituting **(29)** and **(31)** into **(23)** we get the density of the sediment grains, i.e. the bulk density of the layer:

(32) $\boxed{\boldsymbol{\rho_s = \phi \rho_w + (1 - \phi)\rho_g}}$

The porosity of a layer **(26)** after decompaction can be written as

(33) $$\boldsymbol{\phi' = \frac{V'_w}{V'}}$$

where V'_w is given by **(8)** and $V^{'}$ is the decompacted volume. For a unit cross-sectional area it is equal to the decompacted thickness **(12)**. Substituting **(8)** and **(12)** into **(33)**, we get:

(34) $$\boxed{\boldsymbol{\phi' = \frac{\phi_0}{c}\frac{\left(exp(-cy'_1)-exp(-cy'_2)\right)}{y'_2-y'_1}}}$$

For a column with *i* layers, each layer's contribution to the total density of the column, ρ_{S^*}, is proportional to that layers percentage of the total column thickness. The total column density for a column of *i* layers can be written as:

(35) $$\boxed{\boldsymbol{\rho_{S^*} = \frac{\sum_1^i\{[\phi'_i\rho_w+(1-\phi'_i)\rho_s]T_i\}}{S^*}}}$$

where T_i is the decompacted thickness of each layer and S^* is the total decompacted thickness of the sediment column. The expression in brackets on the right-hand side is **(32**) so that **(35)** can be written as:

(36) $$\boldsymbol{\rho_{S^*} = \frac{\sum_1^i(\rho_{S_i}T_i)}{S^*}}$$

APPENDIX B: EXCEL MACROS

B.1. Background Information

The macros used for the subsidence calculations are listed below, with comments about the macro listed to the right. Comments within the macro are shown in green and Visual Basic commands are shown in blue.

B.2. Definition of variables

Option Explicit Dim myCell Dim myNum Dim i As Integer Dim j As Integer Dim k As Integer Dim Rng As Range	The option explicit command means that all variables used in the macros must be defined before they can be used. The Dim command names the variables.

B.3. Start

Sub Start() 'Define the number of horizons for the well, fill in the No. column, copy column headers to well	
Worksheets("Data").Activate Set myCell = Application.InputBox(prompt:="Select the first cell in the first (left-most) column for this well", Type:=8) myNum = Application.InputBox("How many horizons does this well have?") myCell.Value = 1	Sets the reference cell (**myCell**) and the number of layers(**myNum**) in the sediment column
For i = 1 To myNum - 1 myCell.Offset(i, 0).Value = i + 1 Next	Gives each layer a sequential number in the first column of the worksheet

myCell.Offset(-1, 0).Value = "No." myCell.Offset(-1, 0).HorizontalAlignment = xlCenter myCell.Offset(-1, 0).VerticalAlignment = xlCenter	Labels the sequential number column
myCell.Offset(-1, 1).Value = "Well ID" myCell.Offset(-1, 1).HorizontalAlignment = xlCenter myCell.Offset(-1, 1).VerticalAlignment = xlCenter	Labels the location column
myCell.Offset(-1, 2).Value = "Horizon" & Chr(10) & "Name" myCell.Offset(-1, 2).HorizontalAlignment = xlCenter myCell.Offset(-1, 2).VerticalAlignment = xlCenter	Labels the layer name column
myCell.Offset(-1, 3).Value = "Present Upper" & Chr(10) & "Burial Depth" & Chr(10) & "(m)" myCell.Offset(-1, 3).HorizontalAlignment = xlCenter myCell.Offset(-1, 3).VerticalAlignment = xlCenter	Labels the top depth column
myCell.Offset(-1, 4).Value = "Present Lower" & Chr(10) & "Burial Depth" & Chr(10) & "(m)" myCell.Offset(-1, 4).HorizontalAlignment = xlCenter myCell.Offset(-1, 4).VerticalAlignment = xlCenter	Labels the bottom depth column
myCell.Offset(-1, 5).Value = "Lithology" & Chr(10) & "Type" myCell.Offset(-1, 5).HorizontalAlignment = xlCenter myCell.Offset(-1, 5).VerticalAlignment = xlCenter	Labels the lithology column
myCell.Offset(-1, 6).Value = "Compaction" & Chr(10) & "Coefficient" myCell.Offset(-1, 6).HorizontalAlignment = xlCenter myCell.Offset(-1, 6).VerticalAlignment = xlCenter	Labels the compaction coefficient column
myCell.Offset(-1, 7).Value = "Porosity" myCell.Offset(-1, 7).HorizontalAlignment = xlCenter myCell.Offset(-1, 7).VerticalAlignment = xlCenter	Labels the porosity column
myCell.Offset(-1, 8).Value = "Density" & Chr(10) & "(kg/m^3)" myCell.Offset(-1, 8).HorizontalAlignment = xlCenter myCell.Offset(-1, 8).VerticalAlignment = xlCenter	Labels the density column
myCell.Offset(-1, 9).Value = "Age" & Chr(10) & "(Ma)" myCell.Offset(-1, 9).HorizontalAlignment = xlCenter myCell.Offset(-1, 9).VerticalAlignment = xlCenter	Labels the age column
myCell.Offset(-1, 10).Value = "Total" & Chr(10) &	Labels the thickness

"Thickness" & Chr(10) & "(m)" myCell.Offset(-1, 10).HorizontalAlignment = xlCenter myCell.Offset(-1, 10).VerticalAlignment = xlCenter	column
myCell.Offset(-1, 11).Value = "Total" & Chr(10) & "Subsidence" & Chr(10) & "(m)" myCell.Offset(-1, 11).HorizontalAlignment = xlCenter myCell.Offset(-1, 11).VerticalAlignment = xlCenter	Labels the total subsidence column
myCell.Offset(-1, 12).Value = "Tectonic" & Chr(10) & "Subsidence" & Chr(10) & "(m)" myCell.Offset(-1, 12).HorizontalAlignment = xlCenter myCell.Offset(-1, 12).VerticalAlignment = xlCenter	Labels the tectonic subsidence column
myCell.Offset(-1, 13).Value = "Total" & Chr(10) & "Column" & Chr(10) & "Density" & Chr(10) & "(kg/m^3)" myCell.Offset(-1, 13).HorizontalAlignment = xlCenter myCell.Offset(-1, 13).VerticalAlignment = xlCenter	Labels the total density column
myCell.Offset(-1, 14).Value = "Present" & Chr(10) & "Thickness" & Chr(10) & "(m)" myCell.Offset(-1, 14).HorizontalAlignment = xlCenter myCell.Offset(-1, 14).VerticalAlignment = xlCenter	Labels the present thickness column
myCell.Offset(-1, 15).Value = "Porosity" myCell.Offset(-1, 15).HorizontalAlignment = xlCenter myCell.Offset(-1, 15).VerticalAlignment = xlCenter	Labels the calculated porosity column
myCell.Offset(-1, 16).Value = "Density" & Chr(10) & "(kg/m^3)" myCell.Offset(-1, 16).HorizontalAlignment = xlCenter myCell.Offset(-1, 16).VerticalAlignment = xlCenter	Labels the calculated density column
myCell.Offset(-1, 17).Value = "Proportional" & Chr(10) & "Density" & Chr(10) & "(kg/m^3)" myCell.Offset(-1, 17).HorizontalAlignment = xlCenter myCell.Offset(-1, 17).VerticalAlignment = xlCenter	Labels the proportional density column
Range((myCell.Offset(-2, 15)), (myCell.Offset(-2, 17))).Select Selection.Merge myCell.Offset(-2, 15).Value = "T= 0Ma" myCell.Offset(-2, 15).HorizontalAlignment = xlCenter	Groups the porosity, density and proportional densities at T=0Ma together

End Sub	

B.4. Bottom depth

Sub pLBD() 'Calculate the present Lower Burial Depth for each horizon	Fills in the bottom depth of each layer (top of layer below it)
For i = 0 To myNum - 1 myCell.Offset(i, 4).Value = "=R[1]C[-1]" Next End Sub	

B.5. Autofilling the constants

The spreadsheet is designed so that all of the constants used are in separate worksheets. First, the layer name is matched to the Table of Formations worksheet, which contains the list of layers with their lithologies and ages. Then the lithology is used to find the correct values from the Lithologic Constants worksheet.

B.5.1. Lithology Information

Sub autoLith() 'Autofill the Lithology Information for the well	Uses the value in the horizon column to find and fill in the lithology from the Table of Formations
For i = 0 To myNum - 1 myCell.Offset(i, 5).Value = "=VLOOKUP(RC[-3],'Table of Formations'!C[-5]:C[-2],2,FALSE)" Next End Sub	

B.5.2. Compaction Coefficient

Sub autoCC() 'Autofill the Compaction Coefficient for the well	Uses the value in the lithology column to find and fill in the compaction coefficient from the Lithologic Constants
For i = 0 To myNum - 2 myCell.Offset(i, 6).Value = "=VLOOKUP(RC[-1],'Lithologic Constants'!C[-6]:C[-3],2,FALSE)" Next End Sub	Unconformities and the surface layer are given lithologies of NA

B.5.3. Porosity

Sub autoPHI() 'Autofill the Porosity for the well	Uses the value in the lithology column to find and fill in the porosity from the Lithologic Constants
For i = 0 To myNum - 2 myCell.Offset(i, 7).Value = "=VLOOKUP(RC[-2],'Lithologic Constants'!C[-7]:C[-4],3,FALSE)" Next End Sub	

B.5.4. Density

Sub autoRHO() 'Autofill the Density for the well	Uses the value in the lithology column to find and fill in the density from the Lithologic Constants
For i = 0 To myNum - 2 myCell.Offset(i, 8).Value = "=VLOOKUP(RC[-3],'Lithologic Constants'!C[-8]:C[-5],4,FALSE)" Next End Sub	

B.5.5. Age

Sub autoAge() 'Autofill the Age for the well	Uses the value in the lithology column to find and fill in the Age at the top of the layer from the Table of Formations.
For i = 0 To myNum - 2 myCell.Offset(i, 9).Value = _ "=IF(horiz=""Unconformity"",VLOOKUP(R[-1]C[-7],'Table of Formations'!C[-9]:C[-6],4,FALSE),VLOOKUP(RC[-7],'Table of Formations'!C[-9]:C[-6],3,FALSE))" 'myCell.Offset(i, 9).Value = "=VLOOKUP(RC[-7],'Table of Formations'!C[-9]:C[-2],3,FALSE)" Next End Sub	If the layer is an unconformity, the age used is the age at the bottom of the horizon above it.

B.6. Present Thickness

Sub pThick() 'Calculate the Present Thickness of each horizon	Calculates the present thickness of the layer using the equation: y_2-y_1
For i = 0 To myNum - 2 myCell.Offset(i, 14).Formula = "=IF(horiz=""Unconformity"",0,y2_-y1_)" Next End Sub	If the layer is an unconformity, a thickness of zero is assigned.

B.7. Total Thickness

Sub tThick() 'Complete Total Thickness Column	Calculates the cumulative present thickness of the column
For i = 0 To myNum - 2 Set Rng = Range(myCell.Offset(i, 14), myCell.Offset(myNum - 2, 14)) myCell.Offset(i, 10).Formula = _ "=SUM(" & Rng.Address() & ")" Next	
'Fill in first entry of Total Subsidence Column Set Rng = Range(myCell.Offset(0, 14), myCell.Offset(myNum - 2, 14)) myCell.Offset(0, 11).Formula = _ "=SUM(" & Rng.Address() & ")" End Sub	The total subsidence at T=0Ma is the cumulative present thickness of the column

B.8. Porosity and density at current time

Sub Time_0MA() 'Calculate Porosity at T=0Ma	Calculates the current porosity of each layer using the equation: $\frac{\phi}{c}\frac{e^{-cy_1}-e^{-cy_2}}{y_2-y_1}$

For i = 0 To myNum - 2
  myCell.Offset(i, 15).Formula = _
  "=IF(lith=""NA"",0,(phi/cc)*((EXP(-cc*y1_)-EXP(-cc*y2_))/(y2_-y1_)))"
  myCell.Offset(i, 15).NumberFormat = "0.000"
Next
	If the layer is assigned a lithology of "NA," (i.e. an unconformity), porosity is set to zero.

'Calculate Density at T=0Ma
For i = 0 To myNum - 2
  myCell.Offset(i, 16).Formula = _
  "=(RC[-1]*rho_h2o)+((1-RC[-1])*rho)"
  myCell.Offset(i, 16).NumberFormat = "0.000"
Next
	Calculates the current density of each layer at T=0Ma using the equation:
	$\rho_s = \phi\rho_w + (1-\phi)\rho_g$

'Calculate Proportional Density at T=0Ma
For i = 0 To myNum - 2
  myCell.Offset(i, 17).Formula = "=(RC[-1]*RC[-3])/" & myCell.Offset(0, 10) & ""
  myCell.Offset(i, 17).NumberFormat = "0.000"
Next
	Calculates the proportional density of each layer at T=0Ma using the equation:
	$\rho_{S^*} = \frac{\rho_S y}{S^*}$

Set Rng = Range(myCell.Offset(0, 17), myCell.Offset(myNum - 2, 17)) myCell.Offset(0, 13).Formula = _ "=SUM(" & Rng.Address() & ")" End Sub	Sums the proportional densities and enters in the Total Column Density for T=0Ma

B.9. Calculations at each time interval

Because the number of time intervals depends on the number of layers, the number of calculations needed varies for each sediment column. The number of time intervals is determined from the number of layers in each sediment column. This section sets up the blank columns to fill with calculations.

Sub D_TS_col() 'Set up columns for Decompaction and Tectonic Subsidence Calculations at each time	
For i = 0 To myNum - 3 myCell.Offset(-1, 17 + ((6 * i) + 1)).Formula = "Depth" & Chr(10) & "to Top" & Chr(10) & "(m)" myCell.Offset(-1, 17 + ((6 * i) + 1)).HorizontalAlignment = xlCenter myCell.Offset(-1, 17 + ((6 * i) + 1)).VerticalAlignment = xlCenter	Labels the Depth to the Top column at each time interval.
myCell.Offset(-1, 17 + ((6 * i) + 2)).Formula = " Depth" & Chr(10) & "to Bottom" & Chr(10) & " (m)" myCell.Offset(-1, 17 + ((6 * i) + 2)).HorizontalAlignment = xlCenter myCell.Offset(-1, 17 + ((6 * i) + 2)).VerticalAlignment = xlCenter	Labels the Depth to the Bottom column at each time interval.
myCell.Offset(-1, 17 + ((6 * i) + 3)).Formula = "Decompacted" & Chr(10) & "Thickness" & Chr(10) & "(m)" myCell.Offset(-1, 17 + ((6 * i) + 3)).HorizontalAlignment = xlCenter myCell.Offset(-1, 17 + ((6 * i) + 3)).VerticalAlignment = xlCenter myCell.Offset(-1, 17 + ((6 * i) + 3)).ColumnWidth = 13.29	Labels the Decompacted Thickness column at each time interval.
myCell.Offset(-1, 17 + ((6 * i) + 4)).Formula = "Porosity" myCell.Offset(-1, 17 + ((6 * i) + 4)).HorizontalAlignment = xlCenter	Labels the calculated porosity column at each time interval.

myCell.Offset(-1, 17 + ((6 * i) + 4)).VerticalAlignment = xlCenter	
myCell.Offset(-1, 17 + ((6 * i) + 5)).Formula = "Density" & Chr(10) & "(kg/m^3)" myCell.Offset(-1, 17 + ((6 * i) + 5)).HorizontalAlignment = xlCenter myCell.Offset(-1, 17 + ((6 * i) + 5)).VerticalAlignment = xlCenter	Labels the calculated density column at each time interval.
myCell.Offset(-1, 17 + ((6 * i) + 6)).Formula = "Proportional" & Chr(10) & "Density" & Chr(10) & "(kg/m^3)" myCell.Offset(-1, 17 + ((6 * i) + 6)).HorizontalAlignment = xlCenter myCell.Offset(-1, 17 + ((6 * i) + 6)).VerticalAlignment = xlCenter myCell.Offset(-1, 17 + ((6 * i) + 6)).ColumnWidth = 12.29	Labels the proportional density column at each time interval.
Range((myCell.Offset(-2, 17 + ((6 * i) + 1))), (myCell.Offset(-2, 17 + ((6 * i) + 6)))).Select Selection.Merge myCell.Offset(-2, 17 + ((6 * i) + 1)).Value = "T=" & myCell.Offset(i + 1, 9) & "Ma" myCell.Offset(-2, 17 + ((6 * i) + 1)).HorizontalAlignment = xlCenter	Groups the depth to the top, depth to the bottom, decompacted thickness, porosity, density and proportional densities together at each time interval.
Next End Sub	

B.9.1. Decompacted depths and thicknesses

Sub NewDepths() 'Calculate decompacted depths and thicknesses	Calculates the depth to the top and bottom of each layer and the thickness of each layer at the given time interval.
For i = 0 To myNum - 1 For j = i + 1 To myNum - 2 myCell.Offset(j, 17 + ((6 * i) + 1)).Formula = "=IF(horiz=""Surface"",0,IF(horiz=""Unconformity"",R[-1]C[1],R[-1]C+R[-1]C[2]))" myCell.Offset(j, 17 + ((6 * i) + 1)).NumberFormat = "0.00"	The depth to the top of the surface layer is 0. For unconformities it is the top depth of the layer above. For all other layers it is the depth to the top of the layer above plus the thickness of that layer.
myCell.Offset(j, 17 + ((6 * i) + 2)).Formula = _ "=IF(horiz=""Surface"",0,IF(horiz=""Unconformity"",R[-1]C[1],Tn+RC[-1]+((phi/cc)*(EXP(-cc*RC[-1])-EXP(-cc*RC)-EXP(-cc*y1_)+EXP(-cc*y2_)))))" myCell.Offset(j, 17 + ((6 * i) + 2)).NumberFormat = "0.00"	The depth to the bottom of the surface layer is 0. For unconformities it is the bottom depth of the layer above. For all other layers it is calculated iteratively using the equation: $y_2' = y + y_1' + \frac{\phi_0}{c}\{\exp(-cy_1') - \exp(-cy_2') - \exp(-cy_1) + \exp(-cy_2)\}$
myCell.Offset(j, 17 + ((6 * i) + 3)).Formula = "=IF(lith=""NA"",0,RC[-1]-RC[-2])" myCell.Offset(j, 17 + ((6 * i) + 3)).NumberFormat = "0.00" Next j Next i End Sub	The thickness of each layer at the given time interval is calculated using the equation: $y' = y_2' - y_1'$

B.9.2. Decompacted porosity and density

Sub NewDensity() 'Calculate decompacted porosity and density	

For i = 0 To myNum - 1
  For j = i + 1 To myNum - 2
  myCell.Offset(j, 17 + ((6 * i) + 4)).Formula = _
  "=IF(lith=""NA"",0,(phi/cc)*((EXP(-cc*RC[-3])-EXP(-cc*RC[-2]))/(RC[-2]-RC[-3])))"
  myCell.Offset(j, 17 + ((6 * i) + 4)).NumberFormat = "0.000"
 	
  myCell.Offset(j, 17 + ((6 * i) + 5)).Formula = "=(RC[-1]*rho_h2o)+((1-RC[-1])*rho)"
  myCell.Offset(j, 17 + ((6 * i) + 5)).NumberFormat = "0.000"
  Next j
Next i
End Sub
	Calculates the decompacted porosity and density for each layer at the given time interval.
	
	The porosity of layers with the lithology NA it is 0. For all other layers it is calculated using the equation:
	$\phi' = \frac{\phi_0}{c}\frac{\left(exp(-cy_1')-exp(-cy_2')\right)}{y_2'-y_1'}$
	
	The density of each layer at the given time is calculated using the equation:
	$\rho_s = \phi'\rho_w + (1-\phi')\rho_g$

B.9.3. Total Subsidence

Sub ToSub() 'Fill in Total Subsidence	Adds entry to the total subsidence column for the given time interval

For i = 1 To myNum - 2
  Set Rng = Range(myCell.Offset(0, 11 + ((6 * i) + 3)), (myCell.Offset(myNum - 2, 11 + ((6 * i) + 3))))
  myCell.Offset(i, 11).Formula = _
  "=SUM(" & Rng.Address() & ")"
  myCell.Offset(i, 11).NumberFormat = "0.00"
Next
End Sub
	The total subsidence at the given time interval is the sum of the decompacted thicknesses of each layer at that time interval.

B.9.4. Proportional density

Sub PropDens() 'Calculate proportional densities and fill in total column density	
Dim total As Long	
For i = 0 To myNum - 1 total = myCell.Offset(i + 1, 11) For j = i + 1 To myNum - 2 myCell.Offset(j, 17 + ((6 * i) + 6)).Formula = "=RC[-1]*RC[-3]/" & total & "" myCell.Offset(j, 17 + ((6 * i) + 6)).NumberFormat = "0.000" If IsError(myCell.Offset(j, 17 + ((6 * i) + 6)).Value) Then myCell.Offset(j, 17 + ((6 * i) + 6)).Value = 0 Else Next j Next i	Calculates the proportional density of each layer at the given time interval using the equation: $\rho_{S^*} = \frac{\rho_S y}{S^*}$
For i = 1 To myNum - 2 Set Rng = Range(myCell.Offset(0, 12 + ((6 * i) + 5)), (myCell.Offset(myNum - 2, 12 + ((6 * i) + 5)))) myCell.Offset(i, 13).Formula = _ "=SUM(" & Rng.Address() & ")" myCell.Offset(i, 13).NumberFormat = "0.000" Next End Sub	Sums the proportional densities and enters in the Total Column Density for the given time interval.

B.9.5. Tectonic Subsidence

Sub TeSub() 'Calculate Tectonic Subsidence	
For i = 0 To myNum - 2 myCell.Offset(i, 12).Formula = "=(ToS*(rho_mantle-TCD))/(rho_mantle-rho_h2o)" myCell.Offset(i, 12).NumberFormat = "0.00" Next End Sub	Calculates the tectonic subsidence of the sediment column at the given time interval using the equation: $z = w + s\left(\frac{\rho_m - \rho_s}{\rho_m - \rho_w}\right)$

APPENDIX C: ARCGIS COORDINATE SYSTEMS

C.1. Coordinate Systems

Layer Name	Coordinate System
Well locations	UTM Zone 11 (CM=117), NAD 27, latitude/longitude
Shapefiles from the Geological Atlas of the Western Canada Sedimentary Basin	GCS_NorthAmerican_1983
Township grid exported as shapefile from GeoScout	UTM Zone 11 (CM=117), NAD 27, latitude/longitude
Fernie Type Locations (exported from Google Earth in a kml file)	GCS_WGS_1984

APPENDIX D: TABLE OF FORMATIONS AND LITHOLOGIC CONSTANTS

D.1. Table of Formations

Formation Name	Lithology	Age at Top (Ma)	Age at Base (Ma)
Surface	NA	0	
Kbelly_rv	sandstone	77.05	82.21
Klea_park	shale	82.21	84.08
Kchinook	sandstone	84.08	84.65
Kcolorado	shale	84.65	90.56
Kbadheart	sandstone	85.8	89.3
Kcardium	shale	89.3	90.14
Kmuskiki	shale	89.3	90.14
Kcard_ss	sandstone	90.14	90.56
Kkaskapau	shale	90.56	95.33
K2nd_ws	shale	92.24	97.77
Kdoe_ck	sandstone	92.57	93.03
Kdunvegan	sandstone	95.33	97.47
Kshftbury	shale	97.47	100.19
Kbfs	shale	99.6	99.6
Kviking	shale	99.6	100.19
Kvik_ss	sandstone	100.19	101.37

Formation Name	Lithology	Age at Top (Ma)	Age at Base (Ma)
Kcadotte	sandstone	101.37	103.98
Kjoli_fou	shale	101.37	102.55
Kharmon	shale	103.98	104.03
Kmannvl	sandstone	104.32	121.75
Kfalher	sandstone	105.5	110.52
Kwilrich	shale	110.52	110.82
Kbluesky	sandstone	110.82	112
Kgething	sandstone	112	121.75
Kcadomin	sandstone	121.75	127.5
Kellrslie	sandstone	121.75	127.5
Jnikanssn	sandstone	140.85	158.25
Kmonach	sandstone	140.85	142.54
Monach	sandstone	140.85	142.54
Beattie_Peaks	shale	142.54	145.5
Lower_Monteith	sandstone	145.5	152.25
Middle_Monteith	sandstone	145.5	152.25
Upper_Monteith	sandstone	145.5	152.25
Jfernie	shale	152.25	158.5
Jrock_ck	sandstone	170.67	172

Formation Name	Lithology	Age at Top (Ma)	Age at Base (Ma)
Jpokerchp	shale	176	183
Jnordegg	limestone	192.8	198.84
Trbaldnnl	limestone	216.5	228.7
TRchly_lk	limestone	229.75	235
TRhalfway	sandstone	235	238
TRdoig	shale	238	243
TRiassic	shale	243	250
TRmontney	shale	243	250
PRbelloy	sandstone	260	284
Mdebolt	limestone	324	340.78
Melkton	limestone	330.22	340.78
Mturner_v	limestone	330.22	340.78
Mshunda	limestone	340.78	346.56
Mpekisko	limestone	346.56	350.44
Mbanff	limestone	350.44	357.44
Mbakken	shale	357.44	359.94
Mexshaw	shale	357.44	359.94
Jgray_bds	shale		
Jgrn_bds	sandstone		

Formation Name	**Lithology**	**Age at Top (Ma)**	**Age at Base (Ma)**
Kbickfrd	shale		
Miss_sys	NA		
Unconformity	NA		

(Core Laboratories Geological Sciences Department)

D.2. Lithologic Constants

Lithology	Compaction coefficient	Porosity	Density
shale	0.0005	0.5	2.72
sandstone	0.0003	0.4	2.65
dolostone	0.0007	0.5	2.71
limestone	0.0007	0.5	2.71
sandstone/limestone	0.0005	0.45	2.68
limestone/shale	0.0006	0.5	2.715
NA	0	0	0
rho_h2o	1.03		
rho_mantle	3.33		

(Angevine et al., 1990)

APPENDIX E: WELL LIST

This table contains a list of wells used in this study, as well as the name of the spreadsheet the subsidence calculations for that well are located.

Latitude	Longitude	UWI	Containing File
53.45474N	-117.15021	100/01-03-052-22W5/00	30/07/2010
53.73333N	-117.75342	100/02-11-055-26W5/00	30/07/2010
53.75977N	-117.94826	100/02-21-055-27W5/00	30/07/2010
53.54449N	-116.10624	100/03-02-053-15W5/00	30/07/2010
53.50012N	-116.7206	100/03-22-052-19W5/00	30/07/2010
53.58649N	-116.45394	100/04-21-053-17W5/00	30/07/2010
53.76247N	-116.57127	100/04-23-055-18W5/00	30/07/2010
53.50184N	-116.45197	100/05-21-052-17W5/00	30/07/2010
53.29926N	-116.71919	100/06-09-050-19W5/00	30/07/2010
53.48753N	-116.22875	100/06-13-052-16W5/00	30/07/2010
53.74969N	-116.12442	100/06-14-055-15W5/00	30/07/2010
53.74937N	-116.32165	100/06-16-055-16W5/00	30/07/2010
53.83770N	-117.35813	100/06-16-056-23W5/00	30/07/2010
53.85239N	-117.23584	100/06-20-056-22W5/00	30/07/2010
53.41484N	-116.59639	100/06-21-051-18W5/00	30/07/2010
53.41630N	-117.03847	100/06-21-051-21W5/02	30/07/2010
53.67910N	-117.01231	100/06-22-054-21W5/00	30/07/2010
53.64779N	-117.39828	100/07-12-054-24W5/00	30/07/2010
53.48759N	-117.5211	100/07-18-052-24W5/00	30/07/2010
53.50344N	-116.56371	100/07-22-052-18W5/00	30/07/2010
53.67872N	-116.83445	100/07-23-054-20W5/00	30/07/2010
53.69178N	-116.44162	100/07-28-054-17W5/00	30/07/2010
53.86554N	-116.72702	100/08-27-056-19W5/00	30/07/2010
53.68090N	-117.2694	100/09-23-054-23W5/00	30/07/2010
53.69381N	-117.17148	100/09-28-054-22W5/00	30/07/2010
53.78352N	-117.2016	100/09-28-055-22W5/00	30/07/2010
53.39070N	-116.46522	100/10-08-051-17W5/00	30/07/2010
53.58028N	-116.26771	100/10-15-053-16W5/00	30/07/2010
53.57932N	-116.58849	100/10-16-053-18W5/00	30/07/2010
53.57981N	-117.05417	100/10-17-053-21W5/00	30/07/2010
53.84262N	-116.33834	100/10-17-056-16W5/00	30/07/2010
53.41991N	-116.34164	100/10-19-051-16W5/00	30/07/2010
53.85735N	-116.60793	100/10-21-056-18W5/00	30/07/2010

Latitude	Longitude	UWI	Containing File
53.67963N	-116.12498	100/10-22-054-15W5/00	30/07/2010
53.44923N	-117.15445	100/10-34-051-22W5/00	30/07/2010
53.73999N	-117.36118	100/11-09-055-23W5/00	30/07/2010
53.39062N	-116.83961	100/11-11-051-20W5/00	30/07/2010
53.73984N	-116.86699	100/11-11-055-20W5/00	30/07/2010
53.68158N	-116.74551	100/11-21-054-19W5/00	30/07/2010
53.76908N	-116.7427	100/11-22-055-19W5/00	30/07/2010
53.87023N	-117.80647	100/11-28-056-26W5/00	30/07/2010
53.57802N	-117.16849	100/12-15-053-22W5/00	30/07/2010
53.49432N	-117.01657	100/13-15-052-21W5/00	30/07/2010
53.86023N	-117.51233	100/13-21-056-24W5/00	30/07/2010
53.85907N	-117.04603	100/13-22-056-21W5/00	30/07/2010
53.77138N	-116.4661	100/14-21-055-17W5/00	30/07/2010
53.59682N	-117.28197	100/14-23-053-23W5/00	30/07/2010
53.68307N	-117.57566	100/14-23-054-25W5/00	30/07/2010
53.78472N	-117.51191	100/14-28-055-24W5/00	30/07/2010
53.68291N	-116.31859	100/15-20-054-16W5/00	30/07/2010
53.59557N	-117.45113	100/15-22-053-24W5/02	30/07/2010
53.62576N	-117.76691	100/15-33-053-26W5/00	30/07/2010
53.32018N	-116.51602	100/16-14-050-18W5/00	30/07/2010
53.84324N	-116.43192	100/16-15-056-17W5/00	30/07/2010
53.86033N	-116.90047	100/16-21-056-20W5/00	30/07/2010
53.68336N	-116.56094	100/16-22-054-18W5/00	30/07/2010
53.43764N	-117.2486	100/16-25-051-23W5/00	30/07/2010
53.58945N	-116.867	102/06-22-053-20W5/00	30/07/2010
53.47534N	-116.88434	102/07-09-052-20W5/00	30/07/2010
53.58039N	-116.73484	102/10-16-053-19W5/00	30/07/2010
53.99229N	-118.34752	100/01-10-058-03W6/02	09/08/2010
54.18166N	-117.5781	100/01-18-060-24W5/00	09/08/2010
53.87854N	-118.0265	100/01-35-056-01W6/00	09/08/2010
54.29954N	-117.4844	100/02-26-061-24W5/00	09/08/2010
54.09528N	-117.21824	100/03-15-059-22W5/00	09/08/2010
54.09727N	-117.51925	100/04-15-059-24W5/00	09/08/2010
54.38831N	-118.04684	100/04-26-062-01W6/00	09/08/2010
54.38816N	-117.84642	100/04-28-062-26W5/00	09/08/2010
54.11218N	-117.06935	100/05-22-059-21W5/00	09/08/2010
53.86639N	-117.93405	100/05-27-056-27W5/00	09/08/2010
53.89610N	-117.88217	100/06-01-057-27W5/00	09/08/2010

Latitude	Longitude	UWI	Containing File
54.08426N	-118.3364	100/06-11-059-03W6/00	09/08/2010
54.01115N	-118.03913	100/06-14-058-01W6/00	09/08/2010
54.02760N	-117.03995	100/06-22-058-21W5/02	09/08/2010
54.30224N	-117.84222	100/06-28-061-26W5/00	09/08/2010
54.24484N	-118.23561	100/07-04-061-02W6/00	09/08/2010
54.09965N	-117.36098	100/07-15-059-23W5/00	09/08/2010
54.27285N	-117.68559	100/07-16-061-25W5/00	09/08/2010
54.36232N	-117.53625	100/07-16-062-24W5/00	09/08/2010
54.28863N	-117.08471	100/07-21-061-21W5/00	09/08/2010
54.37491N	-117.38291	100/07-21-062-23W5/00	09/08/2010
53.94088N	-116.43469	100/07-22-057-17W5/00	09/08/2010
54.27427N	-117.23068	100/08-16-061-22W5/00	09/08/2010
54.08816N	-118.22892	100/09-09-059-02W6/00	09/08/2010
54.01477N	-117.17699	100/09-15-058-22W5/00	09/08/2010
54.16045N	-117.71086	100/10-05-060-25W5/00	09/08/2010
53.94202N	-117.6778	100/10-20-057-25W5/00	09/08/2010
54.11853N	-117.70767	100/10-20-059-25W5/00	09/08/2010
54.03083N	-117.62585	100/10-22-058-25W5/00	09/08/2010
54.16202N	-118.06644	100/11-03-060-01W6/00	09/08/2010
54.17584N	-118.18949	100/11-11-060-02W6/00	09/08/2010
53.92890N	-116.89025	100/11-15-057-20W5/00	09/08/2010
53.94425N	-116.76686	100/11-21-057-19W5/00	09/08/2010
54.14754N	-117.89195	100/11-31-059-26W5/00	09/08/2010
54.32100N	-118.74396	100/12-31-061-05W6/00	09/08/2010
54.38177N	-118.21907	100/13-22-062-02W6/00	09/08/2010
54.03354N	-118.19572	100/13-23-058-02W6/00	09/08/2010
54.04426N	-117.75663	100/13-26-058-26W5/00	09/08/2010
54.19484N	-117.39354	100/14-16-060-23W5/00	09/08/2010
53.91795N	-117.20451	100/15-09-057-22W5/00	09/08/2010
54.10547N	-116.78066	100/16-16-059-19W5/00	09/08/2010
54.10538N	-116.93075	100/16-16-059-20W5/00	09/08/2010
54.03211N	-117.32596	100/16-22-058-23W5/00	09/08/2010
53.93834N	-116.57255	102/05-23-057-18W5/00	09/08/2010
53.92864N	-117.32569	102/09-15-057-23W5/00	09/08/2010
54.29721N	-118.85135	1S0/01-29-061-06W6/02	09/08/2010
54.51860N	-119.3136	100/01-08-064-09W6/00	24/08/2010
54.63300N	-117.11765	100/03-21-065-21W5/00	24/08/2010
54.82489N	-117.70446	100/03-26-067-25W5/00	24/08/2010

Latitude	Longitude	UWI	Containing File
54.49004N	-117.29271	100/03-32-063-22W5/00	24/08/2010
54.73596N	-118.04408	100/04-26-066-01W6/00	24/08/2010
54.71163N	-118.22475	100/05-15-066-02W6/00	24/08/2010
54.58002N	-118.22136	100/05-34-064-02W6/00	24/08/2010
54.44826N	-117.09084	100/06-15-063-21W5/00	24/08/2010
54.54997N	-117.72322	100/06-21-064-25W5/00	24/08/2010
54.56634N	-118.84349	100/06-28-064-06W6/00	24/08/2010
54.65130N	-118.54542	100/06-28-065-04W6/00	24/08/2010
54.47836N	-117.44192	100/06-29-063-23W5/00	24/08/2010
54.66550N	-119.02425	100/06-32-065-07W6/00	24/08/2010
54.84158N	-117.88192	100/06-34-067-26W5/00	24/08/2010
54.62426N	-117.79057	100/07-13-065-26W5/00	24/08/2010
54.62242N	-117.2592	100/07-16-065-22W5/00	24/08/2010
54.54980N	-118.9888	100/07-21-064-07W6/00	24/08/2010
54.46353N	-117.54075	100/07-22-063-24W5/00	24/08/2010
54.38958N	-118.70647	100/07-29-062-05W6/00	24/08/2010
54.73893N	-119.19003	100/07-30-066-08W6/00	24/08/2010
54.66616N	-118.35897	100/07-34-065-03W6/00	24/08/2010
54.56411N	-119.46264	100/08-29-064-10W6/00	24/08/2010
54.59841N	-118.05559	100/09-03-065-01W6/00	24/08/2010
54.33658N	-118.48369	100/10-02-062-04W6/00	24/08/2010
54.45247N	-117.68997	100/10-15-063-25W5/00	24/08/2010
54.53986N	-117.41245	100/10-16-064-23W5/00	24/08/2010
54.72957N	-119.34157	100/10-19-066-09W6/00	24/08/2010
54.64189N	-117.43714	100/10-20-065-23W5/00	24/08/2010
54.48215N	-118.9159	100/10-25-063-07W6/00	24/08/2010
54.65767N	-117.9397	100/10-25-065-27W5/00	24/08/2010
54.56788N	-118.08134	100/10-28-064-01W6/00	24/08/2010
54.49694N	-119.0683	100/10-36-063-08W6/00	24/08/2010
54.54026N	-117.11742	100/11-16-064-21W5/00	24/08/2010
54.71523N	-119.50342	100/11-18-066-10W6/00	24/08/2010
54.64280N	-119.30032	100/11-21-065-09W6/00	24/08/2010
54.56989N	-118.67077	100/11-27-064-05W6/00	24/08/2010
54.48057N	-118.39285	100/11-28-063-03W6/00	24/08/2010
54.71306N	-118.52121	100/12-15-066-04W6/00	24/08/2010
54.54041N	-117.87753	100/12-16-064-26W5/00	24/08/2010
54.72887N	-118.82626	100/12-22-066-06W6/00	24/08/2010
54.81605N	-118.04648	100/12-23-067-01W6/00	24/08/2010

Latitude	Longitude	UWI	Containing File
54.77656N	-118.19779	100/13-02-067-02W6/00	24/08/2010
54.46934N	-118.12269	100/13-20-063-01W6/00	24/08/2010
54.64538N	-118.69944	100/13-21-065-05W6/00	24/08/2010
54.44099N	-117.82164	100/14-11-063-26W5/00	24/08/2010
54.47035N	-118.29205	100/14-19-063-02W6/00	24/08/2010
54.38472N	-118.83931	100/14-21-062-06W6/00	24/08/2010
54.54199N	-118.36015	100/15-15-064-03W6/00	24/08/2010
54.73097N	-117.71281	100/15-21-066-25W5/00	24/08/2010
54.74820N	-118.66241	100/15-27-066-05W6/00	24/08/2010
54.39808N	-118.38348	100/15-28-062-03W6/00	24/08/2010
54.64546N	-118.15363	100/16-24-065-02W6/00	24/08/2010
53.05029N	-116.10473	100/02-15-047-15W5/00	09/09/2010
53.06475N	-115.95807	100/02-22-047-14W5/00	09/09/2010
53.23785N	-115.52255	100/02-22-049-11W5/00	09/09/2010
54.37221N	-116.92191	100/04-22-062-20W5/00	09/09/2010
54.63430N	-117.55107	100/04-22-065-24W5/00	09/09/2010
53.34115N	-115.53101	100/04-27-050-11W5/00	09/09/2010
53.41464N	-116.08324	100/05-24-051-15W5/00	09/09/2010
53.40130N	-115.21943	100/06-14-051-09W5/00	09/09/2010
53.48737N	-115.38982	100/06-15-052-10W5/00	09/09/2010
53.15347N	-116.28472	100/06-21-048-16W5/00	09/09/2010
53.41577N	-115.11969	100/06-21-051-08W5/00	09/09/2010
53.50259N	-115.97234	100/07-22-052-14W5/00	09/09/2010
53.51633N	-115.67829	100/07-27-052-12W5/00	09/09/2010
53.16876N	-115.54263	100/07-28-048-11W5/00	09/09/2010
53.31604N	-115.805	100/08-15-050-13W5/02	09/09/2010
53.32958N	-115.68874	100/08-21-050-12W5/00	09/09/2010
53.25525N	-116.0041	100/08-29-049-14W5/00	09/09/2010
54.27882N	-116.77678	100/09-16-061-19W5/00	09/09/2010
53.24686N	-115.68674	100/09-21-049-12W5/00	09/09/2010
54.10291N	-116.61051	100/10-15-059-18W5/00	09/09/2010
53.31878N	-115.98283	100/10-16-050-14W5/00	09/09/2010
53.31767N	-116.29839	100/10-17-050-16W5/00	09/09/2010
52.98336N	-115.96789	100/10-21-046-14W5/00	09/09/2010
53.24361N	-116.12822	100/10-21-049-15W5/00	09/09/2010
53.59467N	-115.40843	100/10-21-053-10W5/00	09/09/2010
54.29367N	-116.93213	100/10-21-061-20W5/00	09/09/2010
54.72752N	-117.2636	100/10-21-066-22W5/00	09/09/2010

Latitude	Longitude	UWI	Containing File
53.33235N	-116.37424	100/10-23-050-17W5/00	09/09/2010
53.95849N	-116.28735	100/10-27-057-16W5/00	09/09/2010
53.39087N	-116.2039	100/11-07-051-15W5/00	09/09/2010
53.21615N	-116.25836	100/11-10-049-16W5/02	09/09/2010
53.66786N	-115.54053	100/11-15-054-11W5/00	09/09/2010
53.75525N	-115.25646	100/11-15-055-09W5/00	09/09/2010
54.45337N	-116.96618	100/11-16-063-20W5/00	09/09/2010
54.38032N	-117.06725	100/11-22-062-21W5/00	09/09/2010
53.14418N	-116.09229	100/12-14-048-15W5/00	09/09/2010
53.23078N	-115.80079	100/12-14-049-13W5/00	09/09/2010
54.19164N	-116.76971	100/12-15-060-19W5/00	09/09/2010
53.92823N	-115.73084	100/12-16-057-12W5/00	09/09/2010
53.67989N	-115.74213	100/12-20-054-12W5/00	09/09/2010
53.14550N	-115.6799	100/13-15-048-12W5/00	09/09/2010
53.23356N	-115.40836	100/13-16-049-10W5/00	09/09/2010
54.01787N	-116.47182	100/13-16-058-17W5/00	09/09/2010
53.21929N	-116.69124	100/15-10-049-19W5/00	09/09/2010
53.39370N	-115.62725	100/16-12-051-12W5/00	09/09/2010
53.93063N	-116.00816	100/16-16-057-14W5/00	09/09/2010
54.19367N	-116.9534	100/16-17-060-20W5/00	09/09/2010
53.16214N	-115.83449	100/16-21-048-13W5/00	09/09/2010
53.15111N	-115.37226	102/02-22-048-10W5/00	09/09/2010
53.22605N	-115.26024	102/06-16-049-09W5/00	09/09/2010
53.13808N	-115.98037	102/08-16-048-14W5/00	09/09/2010
54.81041N	-117.59027	100/01-21-067-24W5/00	15/09/2010
55.05683N	-119.45503	100/02-16-070-10W6/00	15/09/2010
54.80805N	-118.2427	100/03-21-067-02W6/00	15/09/2010
54.98484N	-119.58831	100/03-22-069-11W6/00	15/09/2010
55.04309N	-118.24751	100/04-09-070-02W6/00	15/09/2010
54.96763N	-119.4449	100/04-15-069-10W6/00	15/09/2010
54.91223N	-117.91011	100/04-28-068-26W5/00	15/09/2010
54.83829N	-119.87664	100/04-35-067-13W6/00	15/09/2010
54.88433N	-118.85795	100/05-16-068-06W6/00	15/09/2010
54.86924N	-118.11848	100/06-08-068-01W6/00	15/09/2010
54.95921N	-117.85794	100/06-11-069-26W5/00	15/09/2010
54.88451N	-118.67769	100/06-15-068-05W6/00	15/09/2010
54.88673N	-119.61938	100/06-16-068-11W6/00	15/09/2010
55.07415N	-119.18188	100/06-20-070-08W6/00	15/09/2010

Latitude	Longitude	UWI	Containing File
55.07549N	-118.85185	100/06-21-070-06W6/00	15/09/2010
55.07498N	-119.28522	100/06-22-070-09W6/00	15/09/2010
54.81167N	-118.80498	100/06-23-067-06W6/00	15/09/2010
54.91340N	-119.91979	100/06-28-068-13W6/00	15/09/2010
55.00128N	-119.00623	100/06-28-069-07W6/00	15/09/2010
54.98807N	-119.89183	100/07-22-069-13W6/00	15/09/2010
55.00274N	-117.72172	100/07-27-069-25W5/00	15/09/2010
54.82563N	-118.99769	100/07-28-067-07W6/00	15/09/2010
55.02889N	-118.58928	100/08-06-070-04W6/00	15/09/2010
54.80282N	-119.25191	100/10-14-067-09W6/00	15/09/2010
55.06381N	-118.56695	100/10-17-070-04W6/00	15/09/2010
54.90296N	-118.44032	100/10-19-068-03W6/00	15/09/2010
55.07774N	-119.93935	100/10-20-070-13W6/00	15/09/2010
54.90329N	-118.54246	100/10-21-068-04W6/00	15/09/2010
55.07783N	-117.90111	100/10-21-070-26W5/00	15/09/2010
55.09337N	-119.73592	100/10-27-070-12W6/00	15/09/2010
54.83127N	-119.48181	100/10-29-067-10W6/00	15/09/2010
54.88839N	-118.22011	100/11-15-068-02W6/00	15/09/2010
54.88735N	-119.13363	100/11-15-068-08W6/00	15/09/2010
54.97662N	-118.52065	100/11-15-069-04W6/00	15/09/2010
55.06311N	-118.36818	100/11-15-070-03W6/00	15/09/2010
55.06353N	-118.98146	100/11-15-070-07W6/00	15/09/2010
55.06416N	-119.59291	100/11-15-070-11W6/00	15/09/2010
54.81614N	-118.52336	100/11-22-067-04W6/00	15/09/2010
54.81601N	-118.67595	100/11-22-067-05W6/00	15/09/2010
55.06683N	-117.73385	100/13-15-070-25W5/00	15/09/2010
54.99283N	-118.85606	100/14-21-069-06W6/00	15/09/2010
54.90523N	-117.71838	100/15-22-068-25W5/00	15/09/2010
55.06552N	-118.66598	100/16-15-070-05W6/00	15/09/2010
54.99279N	-118.38113	100/16-21-069-03W6/00	15/09/2010
54.90600N	-118.05265	100/16-22-068-01W6/00	15/09/2010
54.83406N	-118.40873	100/16-29-067-03W6/00	15/09/2010
54.89895N	-119.00223	102/07-21-068-07W6/00	15/09/2010
54.65026N	-116.80283	100/01-28-065-19W5/00	20/01/2011
51.72275N	-114.52935	100/02-08-032-04W5/00	20/01/2011
52.45313N	-115.47128	100/02-23-040-11W5/00	20/01/2011
54.72181N	-116.42912	100/02-24-066-17W5/00	20/01/2011
52.86107N	-115.5641	100/03-08-045-11W5/00	20/01/2011

Latitude	Longitude	UWI	Containing File
52.87421N	-116.14484	100/03-17-045-15W5/00	20/01/2011
53.50071N	-114.97477	100/03-21-052-07W5/00	20/01/2011
54.57762N	-116.23466	100/03-32-064-15W5/00	20/01/2011
52.77061N	-115.34959	100/04-11-044-10W5/02	20/01/2011
52.70435N	-115.00969	100/05-18-043-07W5/00	20/01/2011
52.32567N	-114.87724	100/06-01-039-07W5/00	20/01/2011
54.33232N	-116.09087	100/06-06-062-14W5/00	20/01/2011
52.17777N	-114.84631	100/06-18-037-06W5/00	20/01/2011
52.10748N	-114.70361	100/06-19-036-05W5/00	20/01/2011
53.67851N	-114.9766	100/06-21-054-07W5/00	20/01/2011
52.90618N	-115.32262	100/06-25-045-10W5/00	20/01/2011
54.82775N	-117.06601	100/06-25-067-21W5/00	20/01/2011
54.49143N	-116.00791	100/06-35-063-14W5/00	20/01/2011
54.52060N	-116.60397	100/07-11-064-18W5/00	20/01/2011
52.86393N	-115.02457	100/07-12-045-08W5/00	20/01/2011
54.04257N	-115.34665	100/07-25-058-10W5/00	20/01/2011
53.72042N	-114.72552	100/08-06-055-05W5/00	20/01/2011
53.14062N	-114.61163	100/08-14-048-05W5/00	20/01/2011
54.07276N	-115.72672	100/09-04-059-12W5/00	20/01/2011
52.86787N	-115.84195	100/09-08-045-13W5/00	20/01/2011
51.83315N	-114.54696	100/09-18-033-04W5/00	20/01/2011
54.33654N	-116.40959	100/10-01-062-17W5/00	20/01/2011
51.99414N	-114.43516	100/10-12-035-04W5/00	20/01/2011
53.07164N	-115.39743	100/10-21-047-10W5/00	20/01/2011
52.81044N	-114.6373	100/10-22-044-05W5/00	20/01/2011
52.19818N	-115.15081	100/10-24-037-09W5/00	20/01/2011
52.72145N	-115.605	100/10-24-043-12W5/00	20/01/2011
52.64910N	-115.80822	100/10-28-042-13W5/00	20/01/2011
53.88281N	-115.17226	100/10-31-056-08W5/00	20/01/2011
52.48739N	-114.39483	100/10-32-040-03W5/00	20/01/2011
51.93540N	-114.70402	100/12-19-034-05W5/00	20/01/2011
52.86955N	-114.57535	100/13-07-045-04W5/00	20/01/2011
54.96445N	-117.20066	100/13-07-069-21W5/00	20/01/2011
52.73894N	-114.79277	100/13-27-043-06W5/00	20/01/2011
52.38894N	-115.14627	100/13-30-039-08W5/02	20/01/2011
52.49256N	-115.29493	100/13-31-040-09W5/00	20/01/2011
52.57785N	-115.17068	100/13-36-041-09W5/00	20/01/2011
52.98811N	-114.81098	100/14-21-046-06W5/00	20/01/2011

Latitude	Longitude	UWI	Containing File
54.29539N	-115.26521	100/14-22-061-09W5/00	20/01/2011
53.03214N	-115.69211	100/15-04-047-12W5/00	20/01/2011
54.16363N	-116.0581	100/15-05-060-14W5/00	20/01/2011
54.26786N	-115.78647	100/15-07-061-12W5/00	20/01/2011
52.65385N	-115.42491	100/15-30-042-10W5/00	20/01/2011
51.99592N	-114.91025	100/16-10-035-07W5/00	20/01/2011
52.28799N	-114.50358	100/16-21-038-04W5/00	20/01/2011
52.56316N	-114.72617	100/16-25-041-06W5/00	20/01/2011
52.49080N	-114.98926	100/16-31-040-07W5/00	20/01/2011
53.31437N	-115.06232	102/06-14-050-08W5/00	20/01/2011
52.71893N	-114.49778	102/06-22-043-04W5/02	20/01/2011
52.39880N	-114.70931	102/06-31-039-05W5/00	20/01/2011
53.88011N	-115.43041	102/06-33-056-10W5/00	20/01/2011
53.22970N	-114.76458	102/10-14-049-06W5/00	20/01/2011
53.56701N	-114.80237	102/14-10-053-06W5/00	20/01/2011
53.08745N	-114.94316	102/14-27-047-07W5/00	20/01/2011
53.00031N	-115.19037	102/16-26-046-09W5/00	20/01/2011
53.17722N	-115.08625	104/14-27-048-08W5/00	20/01/2011

APPENDIX F: LIST OF FILES IN DIGITAL APPENDIX

The attached digital appendix contains the following files:

F.1. AllResults.xlsx

This is an excel spreadsheet containing the final calculated results for all wells. The intermediate steps are not included in this spreadsheet.

F.2. BlankSpreadhseet.xlsm

This is a blank, macro-enabled, spreadsheet containing the macros and worksheets needed to run subsidence calculations.

F.3. SpreadsheetSetup.avi

This is a video (without sound) showing the steps for setting up the spreadsheet in Excel 2007 and how it runs.

F.4. Data Spreadsheets (folder)

This folder contains the macro-enabled spreadsheets with all of the data calculations and all of the subsidence curves. An index of which wells are in each file is found in Appendix E.

F.4.1. Aug 9 2010.xlsm

F.4.2. August 24 2010.xlsm

F.4.3. Jan 20 2011.xlsm

F.4.4. July 30 2010.xlsm

F.4.5. Sept 8 2010.xlsm

F.4.6. Sept 15 2010.xlsm

F.5. Macro modules (folder)

This folder contains the modules that must be imported to visual basic in any spreadsheet to enable subsidence calculations.